

Bor-Stickstoff-Analoga Reaktiver Organischer Moleküle

1,2-Azaborinin, Phenylborylen und das Dewar-Valenzisomer des 1,2-Dihydro-1,2-azaborinins

Eine Matrixisolationstudie

Dissertation

der Mathematisch-Naturwissenschaftlichen Fakultät
der Eberhard Karls Universität Tübingen
zur Erlangung des Grades eines
Doktors der Naturwissenschaften
(Dr. rer. nat.)

vorgelegt von
Klara Edel
aus Kupino/Russland

Tübingen
2018

Gedruckt mit Genehmigung der Mathematisch-Naturwissenschaftlichen Fakultät der
Eberhard Karls Universität Tübingen.

Tag der mündlichen Qualifikation:	24.01.2018
Dekan:	Prof. Dr. Wolfgang Rosenstiel
1. Berichterstatter:	Prof. Dr. Holger F. Bettinger
2. Berichterstatter:	Prof. Dr. Lars Wesemann

meinen Eltern

Danksagung

Meinen größten Dank möchte ich Herrn Prof. Dr. Holger F. Bettinger für die Bereitstellung des Themas, Betreuung meiner Doktorarbeit, die anregenden Diskussionen und für seine Hilfe und Unterstützung während der gesamten Zeit aussprechen.

Prof. Dr. Shih-Yuan Liu und seiner Gruppe danke ich für die Zusammenarbeit an dem 1,2-Azaborinin- und dem Dewar-Projekt und die Bereitstellung mehrerer Verbindungen. Prof. Dr. Reinhold Fink danke ich für die Zusammenarbeit bei computerchemischen Rechnungen. Prof. Dr. Günter Gauglitz danke ich für die hilfreiche Beratung bei der Bestimmung einer Quantenausbeute. Bei Dr. Dirk Grote bedanke ich mich für die ESR-Messungen unter Matrixisolationsbedingungen und Dr. Klaus Merz für den Versuch eine Kristallstrukturanalyse durchzuführen.

Mein Dank gilt den Mitarbeitern der Glasbläserei, Elektrowerkstatt und der Metallwerkstatt, vor allem Herrn Eberhard Braun. Sie waren in der Lage jede noch so komplizierte Spezialanfertigung für mich zu machen.

Bei der NMR-Abteilung bedanke ich mich für die zeitintensiven Kinetikmessungen, bei Cäcilia Maichle-Mössmer für die Kristallstrukturanalyse und bei Petra Krüger für die Elementaranalysen. Weiterhin gilt mein Dank der Abteilung Massenspektrometrie.

Dem Arbeitskreis Bettinger danke ich herzlich für die schöne gemeinsame Zeit. Ich möchte mich für die Hilfe bei großen und kleinen Problemen bei allen derzeitigen und ehemaligen Mitgliedern, vor allem bei Matthias Krieg, Florian Reicherter und bei Thomas Geiger bedanken.

Bei meiner Familie und meinen Freunden möchte ich mich für die Unterstützung während der Doktorarbeit und Studienzeit bedanken, vor allem bei meinen Eltern, die mir alles ermöglicht haben. Meinen Freunden Helene Knecht und Marc Stickel bedanke ich mich für ihre Hilfe während des Studiums und für eine tolle gemeinsame Studienzeit.

Meinem Freund Robin Frauenlob danke ich für seine Unterstützung und dass er immer für mich da ist.

Inhaltsverzeichnis

Abkürzungen und Symbole	3
Zusammenfassung	4
Abstract	5
Liste der Publikationen	6
Eigenanteil	7
1. Einleitung	9
<i>1.1 BN/CC Analogie</i>	<i>9</i>
1.1.1 Iminoborane	10
<i>1.2 1,2-Azaborinin</i>	<i>10</i>
1.2.2 1,2-Azaborinin	11
1.2.3 Gesättigte cyclische Iminoborane	11
1.2.4 Aromatische cyclische Iminoborane	12
1.2.5 Matrixisolationsversuche	14
<i>1.3 Dewar-Valenzisomere von 1,2-Dihydro-1,2-azaborininen</i>	<i>16</i>
1.3.2 Dewar-Benzol	16
1.3.3 Dewar-Valenzisomer des 1,2-Dihydro-1,2-azaborinins	17
<i>1.4 Borylene</i>	<i>18</i>
1.4.1 Matrixisolationsversuche	18
2. Zielsetzung	20
3. Matrixisolationsmethoden	21
<i>3.1 Blitzvakuumpyrolyse</i>	<i>21</i>
4. Ergebnisse und Diskussion	23
<i>4.1 1,2-Azaborinin</i>	<i>23</i>
<i>4.2 Mögliche Isomerisierungsreaktionen von 1,2-Azaborinin</i>	<i>26</i>
4.2.1 Ringkontraktion	26
4.2.2 Ringöffnung zu BN-substituierten Endiinen	27
4.2.3 Fragmentierung von 1,2-Azaborinin	30
<i>4.3 Dewar-Valenzisomer des 1,2-Dihydro-1,2-azaborinins</i>	<i>32</i>
4.3.1 Matrixisolationsstudie	32
4.3.2 Photochemie in Lösung	34
<i>4.4 Phenylborylen</i>	<i>38</i>
4.4.1 UV/Vis-Spektroskopie	38
4.4.2 IR-Spektroskopie	41
4.4.3 ESR-Spektroskopie	43
5. Literaturverzeichnis	46

Anhang

Publikation 1
Publikation 2
Publikation 3
Publikation 4

Erklärung

Für die Publikationen 1-4 wurde eine Zustimmung der jeweiligen Verlage eingeholt.

Abbildung 1 und die Abbildungen 3-16 entstammen den Publikationen 1-4 und wurden teilweise, hauptsächlich aufgrund geänderter Nummerierung der jeweiligen Verbindungen, leicht verändert.

Abkürzungen und Symbole

Å	Ångström
A	Absorption
° C	Grad Celsius
cm ⁻¹	Wellenzahl
E _a	Aktivierungsenergie
ESR	Elektronenspinresonanz
f	Oszillatorstärke
ΔH [‡]	Aktivierungsenthalpie
FVP	Blitzvakuumpyrolyse
GC-MS	Gaschromatographie- Massenspektrometrie
HOMO	höchstes besetztes Molekülorbital
IR	Infrarot
K	Kelvin
KHMDS	Kaliumhexamethyldisilazid
λ	Wellenlänge
LiTMP	Lithium-2,2,6,6,-tetramethylpiperidid
LUMO	niedrigstes unbesetztes Molekülorbital
Mes	Mesityl
NBO	Natürliche Bindungssorbitale
NHC	N-heterocyclische Carbene
nm	Nanometer
NMR	Kernspinresonanzspektroskopie
ν	Frequenz, Stretschwiegung
ω	Quantenmechanisch berechnete Frequenz
PAH	Polycyclische aromatische Kohlenwasserstoffe
Ph	Phenyl
TCE	Tetrachlorethan
TBS	<i>tert</i> -Butyldimethylsilyl
TS	Übergangszustand
ZPVE	Nullpunktsschwingungsenergie

Zusammenfassung

Mit Hilfe von Matrixisolationstechniken ist es möglich reaktive Zwischenstufen, die unter normalen Laborbedingungen nicht direkt nachgewiesen werden können, zu generieren und zu isolieren. Diese Arbeit handelt hauptsächlich über Untersuchungen von Borverbindungen mit Hilfe der Matrixisolationstechnik und lässt sich in drei Teilbereiche unterteilen.

1. Matrixisolation von 1,2-Azaborinin: 1,2-Azaborinin, ein BN-Analogon von *ortho*-Benzin, konnte mit Hilfe von Matrixisolationstechniken in einer Argonmatrix bei 4 K isoliert und mit Hilfe von Infrarotspektroskopie charakterisiert werden. Quantenchemische Rechnungen lassen eine hohe Lewis-Acidität des Bor-Zentrums erwarten und dies konnte durch die Reaktion mit Stickstoff bestätigt werden.

Um Nebenprodukte bei der Generierung von 1,2-Azaborinin zu identifizieren bzw. auszuschließen wurden mögliche Isomerisierungs- und Fragmentierungsmechanismen mit Hilfe von quantenmechanischen Rechnungen untersucht.

2. Dewar-Valenzisomer von 1,2-Dihydro-1,2-azaborinin: Die Photochemie von Derivaten des 1,2-Dihydro-1,2-azaborinins wurden sowohl unter Matrixisolationsbedingungen als auch in Lösung bei Zimmertemperatur untersucht. Es zeigte sich ausschließlich die Bildung des Dewar-Valenzisomers als einzigem Reaktionsprodukt. Die Isomerisierung ist thermisch reversibel und Aktivierungsparameter wurden bestimmt. Bei einer Änderung der eingestrahlten Wellenlänge ist eine Cycloreversion der Dewar-Verbindung zum Cyclobutadien und dem entsprechenden Iminoboran zu beobachten.

3. Reaktionen von Phenylborylen: Borylene sind Analoga der Carbene und Nitrene. Doch im Vergleich zu den Carbenen und Nitrenen sind Borylene bisher kaum untersucht worden. In dieser Arbeit konnte die Reaktion zwischen Phenylborylen mit Stickstoff und mit Kohlenstoffmonoxid unter Matrixisolationsbedingungen mit Hilfe mehrerer Spektroskopiemethoden (IR, UV und ESR) gezeigt werden.

Abstract

Matrix isolation techniques enable generation and isolation of reactive intermediates which usually cannot be detected under conventional laboratory conditions. This thesis is mainly focused on investigation of boron containing compounds using the matrix isolation technique, and is based on three main projects.

1. Matrix isolation of 1,2-azaborinine: 1,2-Azaborinine, the BN analogue of *ortho*-benzyne, could be generated and isolated by matrix isolation techniques and characterized by IR spectroscopy. A strong Lewis acidic character at the boron center was predicted by computational chemistry and could be supported by the spontaneous reaction with dinitrogen under matrix isolation conditions.

To identify the byproducts, which are formed during the generation of 1,2-azaborinine, possible isomerization and fragmentation pathways were investigated by computational chemistry techniques.

2. Dewar valence isomer of 1,2-dihydro-1,2-azaborinine: The photochemistry of 1,2-dihydro-1,2-azaborinine derivatives was investigated in cryogenic matrices and in solution at room temperature. In both media, full conversion exclusively to the Dewar valence isomer was found upon irradiation with UV light. This reaction was observed to be thermally reversible and activation parameters were determined. Changing the wavelength of the UV light results into cycloreversion of the Dewar compound to cyclobutadien and the corresponding iminoborane.

3. Reactions of Phenyl borylene: Borylenes are analogues of carbenes and nitrenes. In contrast to carbenes and nitrenes little is known about borylenes. In this study the reactivity of phenyl borylene was investigated towards dinitrogen and carbon monoxide under matrix isolation conditions using various spectroscopic techniques (IR, UV and ESR).

Liste der Publikationen

Publikation 1

1,2-Azaborine: The Boron-Nitrogen Derivative of *ortho*-Benzyne

K. Edel, S. A. Brough, A. N. Lamm, S.-Y. Liu, H. F. Bettinger, *Angew. Chem. Int. Ed.* **2015**, *54*, 7819.

Publikation 2

Isomerization and Fragmentation Pathways of 1,2-Azaborine

K. Edel, R. F. Fink, H. F. Bettinger, *J. Comput. Chem.* **2016**, *37*, 110.

Publikation 3

Photoreactions of Phenylborylene with Dinitrogen and Carbon Monoxide

K. Edel, M. Krieg, D. Grote, H. F. Bettinger, *J. Am. Chem. Soc.* **2017**, *139*, 15151.

Publikation 4

The Dewar isomer of 1,2-dihydro-1,2-azaborinines: Isolation, fragmentation, and energy storage

K. Edel, X. Yang, J. S. A. Ishibashi, A. N. Lamm, C. Maichle-Mössmer, Z. X. Giustra, S.-Y. Liu, H. F. Bettinger, *Angew. Chem. Int. Ed.* **2018**, *57*, 5296.

Eigenanteil

Publikation 1

1,2-Azaborine: The Boron-Nitrogen Derivative of *ortho*-Benzyne

K. Edel, S. A. Brough, A. N. Lamm, S.-Y. Liu, H. F. Bettinger, *Angew. Chem. Int. Ed.* **2015**, 54, 7819.

Sarah A. Brough führte die ersten Matrixisolationsversuche mit Kohlenstoffdioxid durch, die einen Hinweis auf die Bildung von 1,2-Azaborinin in der Gasphase lieferten. Daraufhin optimierte ich die Versuche mit Kohlenstoffdioxid und führte Matrixexperimente mit isotopenmarkiertem Kohlenstoffdioxid, Argon und Stickstoff durch. Ich habe die IR-Spektren ausgewertet, Abbildungen erstellt und am Verfassen des Manuskripts mitgearbeitet.

Ashley N. Lamm und Shih-Yuan Liu stellten die Ausgangsverbindung zu Verfügung. Holger F. Bettinger hatte die Projektidee, führte quantenchemische Rechnungen durch und verfasste das Manuskript.

Publikation 2

Isomerization and Fragmentation Pathways of 1,2-Azaborine

K. Edel, R. F. Fink, H. F. Bettinger, *J. Comput. Chem.* **2016**, 37, 110.

Holger F. Bettinger hatte die Projektidee und führte Rechnungen zu den angeregten Zuständen des Nitrenoborols durch, Reinhold F. Fink untersuchte diese mittels der MCCEPA-Methode. Alle weiteren quantenchemischen Rechnungen wurden von mir durchgeführt. Das Manuskript wurde zu 70 % von mir verfasst.

Publikation 3

Photoreactions of Phenylborylene with Dinitrogen and Carbon Monoxide

K. Edel, M. Krieg, D. Grote, H. F. Bettinger, *J. Am. Chem. Soc.* **2017**, *139*, 15151.

Holger F. Bettinger hatte die Projektidee und führte die ersten IR- und UV/Vis-Matrixexperimente mit von Matthias Krieg synthetisierten Ausgangsverbindung durch. Darauf aufbauend optimierte ich die IR- und UV/Vis-Matrixexperimente und führte Versuche mit isotopenmarkiertem Stickstoff und Kohlenstoffmonoxid durch. Ich wertete die Versuche aus, synthetisierte die Ausgangsverbindung, berechnete die IR-Spektren, erstellte Abbildungen und habe am Verfassen des Manuskripts mitgearbeitet.

Ich und Holger F. Bettinger sind an die Ruhr-Universität Bochum gereist, um ESR-Matrixisolationsexperimente mit Dirk Grote durchzuführen. Die ESR-Spektren wertete Dirk Grote aus.

Holger F. Bettinger führte quantenchemische Rechnungen durch und verfasste das Manuskript.

Publikation 4

The Dewar isomer of 1,2-dihydro-1,2-azaborinines: Isolation, fragmentation, and energy storage

K. Edel, X. Yang, J. S. A. Ishibashi, A. N. Lamm, C. Maichle-Mössmer, Z. X. Giustra, S.-Y. Liu, H. F. Bettinger, *Angew. Chem. Int. Ed.* **2018**, *57*, 5296.

Holger F. Bettinger hatte die Projektidee und arbeitete am Verfassen des Manuskripts mit. Ich führte bis auf die katalysierte Rückreaktion alle Experimente und quantenchemischen Rechnungen durch und wertete die Ergebnisse aus. Das Manuskript habe ich zu 70 % verfasst. Jacob S. A. Ishibashi, Ashley N. Lamm und Shih-Yuan Liu stellten die Ausgangsverbindungen zur Verfügung. Xinyu Yang, Zachary X. Giustra und Shih-Yuan Liu untersuchten die katalysierte Rückreaktion und werteten deren Ergebnisse aus. Shih-Yuan Liu arbeitete am Verfassen des Manuskripts mit.

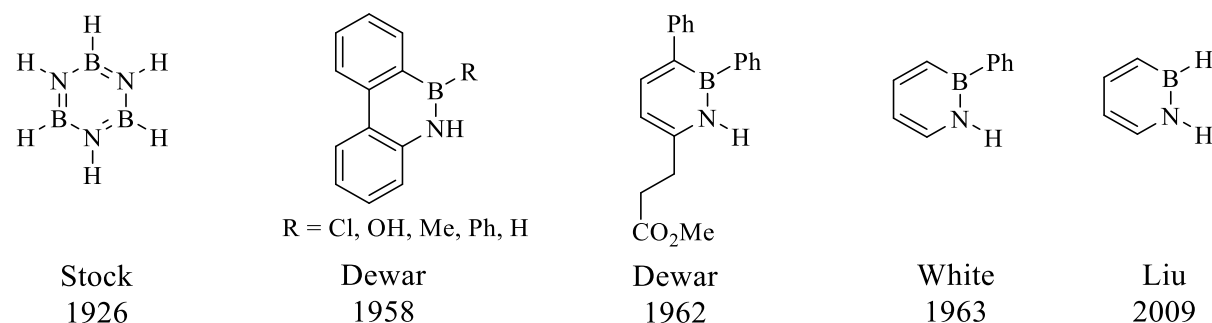
Cäcilia Maichle-Mössmer führte die Kristallstrukturanalyse durch.

1. Einleitung

1.1 BN/CC Analogie

Der formale Austausch von CC-Bindungen durch isoelektronische BN-Bindungen ermöglicht die Veränderung der elektronischen Eigenschaften von Molekülen. Dadurch ist eine Variation von chemischen und physikalischen Stoffeigenschaften möglich, die für eine Vielzahl von Anwendungen von Interesse ist.^[1] BN-Bindungen haben in Gegensatz zu CC-Bindungen ein Dipolmoment,^[2] wodurch die Reaktivität der Verbindung meist erhöht ist. Durch den Einbau von BN-Einheiten in polycyclische aromatische Kohlenwasserstoffe (PAH, engl.: polycyclic aromatic hydrocarbons) kann gezielt die HOMO-LUMO-Lücke der PAH modifiziert werden.^[1d, 3] Dadurch stoßen Heteroaromaten mit einer oder mehreren BN-Einheiten auf ein großes Interesse in den Materialwissenschaften und in der biomedizinischen Forschung.^[2, 4]

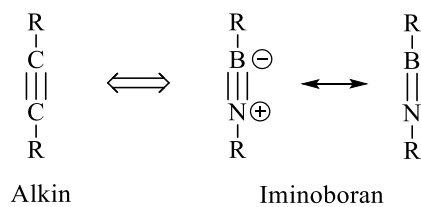
Das bekannteste Beispiel für eine BN/CC-Analogie ist wohl das Borazin (Schema 1), das auch als „anorganisches Benzol“ bekannt ist,^[5] und 1926 von Alfred Stock synthetisiert wurde.^[6] Der erste Heteroaromat mit nur einer BN-Einheit wurde 1958 von Dewar beschrieben (Schema 1).^[7] Daraufhin entwickelten in den 1960er Jahren Dewar und White die ersten Synthesen für 1,2-Dihydro-1,2-azaborinin, die nur aus einem sechsgliedrigen Ring bestehen (Schema 1).^[8] In den letzten Jahrzehnten ist das Interesse an 1,2-Dihydro-1,2-azaborininen neu entfacht und mehrere Gruppen, wie die von Ashe,^[9] Yamaguchi,^[3c] Liu^[10] und Braunschweig^[11] erzielten große Fortschritte auf diesem Gebiet. Die Gruppe von Liu entwickelte 2009 die erste Synthese für das Stammsystem des 1,2-Dihydro-1,2-azaborinins (Schema 1).^[10a]



Schema 1. Beispiele für BN-substituierte Heteroaromaten.

1.1.1 Iminoborane

Eine weitere gut untersuchte Klasse von BN-substituierten Verbindungen sind die Iminoborane, die isoelektronisch zu den Alkinen sind. Im Gegensatz zu den Alkinen, die kinetisch inert sind, neigen Iminoborane aufgrund des Dipolmoments der BN-Bindung^[12] dazu Ringe bzw. Polymere zu bilden.^[13] Um Iminoborane zu isolieren und handzuhaben, sind tiefere Temperaturen, hohe Verdünnungen und sterisch anspruchsvolle Reste notwendig.^[13] Weiterhin können Iminoborane durch N-Heterocyclische Carbene (NHCs) stabilisiert werden.^[14] Das erste Iminoboran F₅C₆-BN-*t*Bu wurde von Paetzold et al. isoliert.^[15] Zahlreiche weitere Beispiele folgten,^[13, 14b, 16] darunter (Me₃Si)₃C-BN-SiMe₃ und (Me₃Si)₃Si-BN-SiMe₃ von Haase und Klingebiel,^[17] welche bei Zimmertemperatur stabil sind.

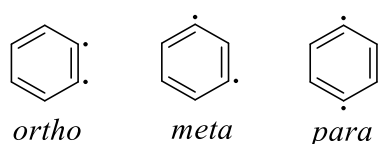


Schema 2. Isoelektronische Beziehung zwischen Alkinen und Iminoboranen.

1.2 1,2-Azaborinin

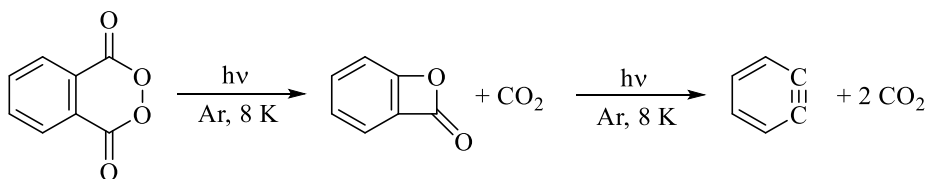
1.2.1 Arine

Arine sind hochreaktive aromatische Verbindungen, die formal durch Abstraktion zweier Wasserstoffatome gebildet werden, mit Didehydrobenzol (Benzin) als einfachstem Vertreter. Unter den drei möglichen Isomeren *ortho*-, *meta*-, und *para*-Benzin (Schema 3) ist das *ortho*-Benzin energetisch am stabilsten^[18] und in der organischen Synthese am häufigsten vertreten.^[19] Die Reaktivität resultiert aus der gewinkelten und damit gespannten CC-Dreifachbindung und der reduzierten Überlappung der p-Orbitale, die sich in der Ringebene befinden.^[19d, 19h]



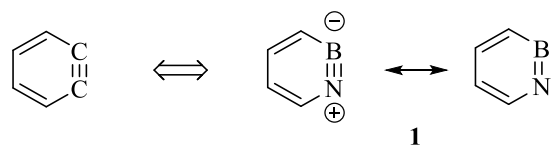
Schema 3. Die drei Isomere des Didehydrobenzols.

Das Auftreten von Arinen als reaktive Zwischenstufen wurde erstmals 1902 von Stoermer und Kahlert postuliert.^[20] Bedeutende Beweise für die Existenz und Struktur von *ortho*-Benzin wurden von Wittig^[21] und Roberts^[22] geliefert. Der direkte spektroskopische Nachweis erfolgte 1973 durch Chapman^[23] mit Hilfe von Matrixisolationstechniken (Schema 3). Warmuth^[24] konnte 1997 *ortho*-Benzin in einem molekularen Container erzeugen und isolieren und somit NMR-Spektren von *ortho*-Benzin in Lösung messen. Seit der Entdeckung der Arine vor über hundert Jahren gab es große Fortschritte in der Darstellung von Arinen. Dadurch ist es möglich, Arine in einer Vielzahl von organischen Synthesen einzusetzen.^[19]



Schema 4. Erzeugung von *ortho*-Benzin unter Matrixisolationsbedingungen nach Chapman et al.^[23]

1.2.2 1,2-Azaborinin



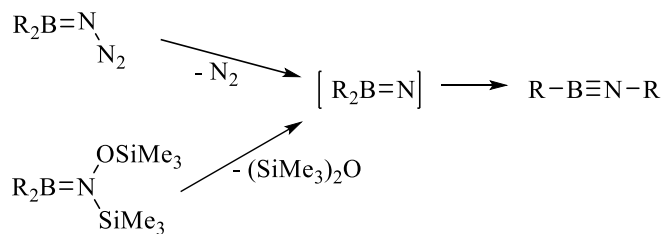
Schema 5. Isoelektronische Beziehung zwischen *ortho*-Benzin und 1,2-Azaborinin.

Das Austauschen der CC-Dreifachbindung in *ortho*-Benzin durch eine BN-Einheit, führt zum 1,2-Azaborinin (**1**) (Schema 5), einem cyclischen Iminoboran. Durch die Einbindung einer BN-Einheit in einen Sechsring können die Reste des Iminoborans nicht die bevorzugte lineare Ausrichtung einnehmen, wodurch eine höhere Reaktivität, wie im Falle des *ortho*-Benzins, im Vergleich zu acyclischen Iminoboranen zu erwarten ist. Im Gegensatz zum *ortho*-Benzin erfährt der Sechsring des 1,2-Azaborinins starke strukturelle Verzehrung.^[25] Der Singulett-Grundzustand ist mit 53.0 kcal mol⁻¹ [CCSD(T)/6-311++G**] gegenüber dem Triplettzustand stark begünstigt.^[25a] Einen direkten Nachweis für die Existenz von **1** gab es bisher noch nicht.

1.2.3 Gesättigte cyclische Iminoborane

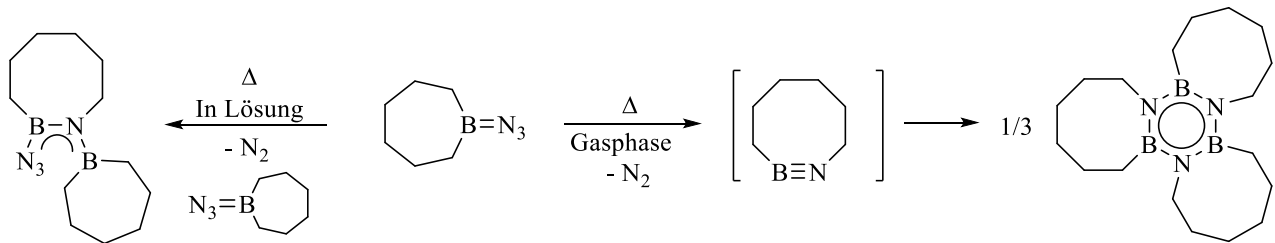
Die einzige Untersuchung zu gesättigten cyclischen Iminoboranen wurde 2004 von Paetzold et al.^[26] veröffentlicht. Cyclische Iminoborane verschiedener Ringgrößen (6- 9-Ringe) werden

dabei durch eine von Paetzold schon früher ausgiebig untersuchte Umlagerung dargestellt.^[13] Erhitzen von Azidodiorganylboranen oder Dialkyl[trimethylsilyl-(trimethylsilyloxy)]boranen führt unter Abspaltung der Abgangsgruppe N₂ bzw. (SiMe₃)₂O formal zum Borylnitren, welches zum Iminoboran umlagert (Schema 6). Experimentelle Befunde zeigen, dass der Verlust der Abgangsgruppe und die Wanderung eines Restes zum N-Atom konzertiert ablaufen. Dies ist im Einklang mit quantenchemischen Untersuchungen, die zeigen, dass Borylnitrene mit Alkylresten am B-Atom kein Minimum auf der Potentialenergiefläche besitzen.^[13, 25b, 27]



Schema 6. Synthese von Iminoboranen.

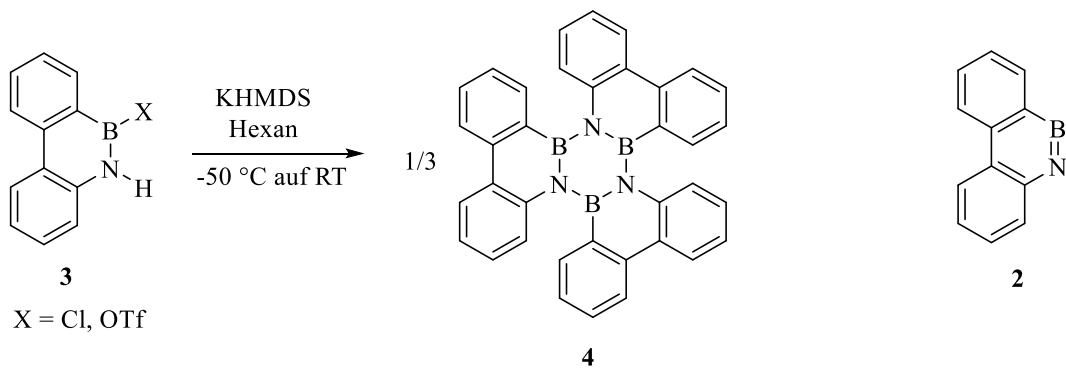
Die gesättigten cyclischen Iminoborane konnten nicht direkt nachgewiesen werden. Ihr Auftreten wurde durch Abfangreaktion (z.B. mit einem nicht reagierten Azidodiorganylboran) oder durch Trimerisierung bzw. Dimerisierung nachgewiesen (Schema 7).



Schema 7. Beispiel eines gesättigten cyclischen Iminoborans als reaktive Zwischenstufe nach Paetzold et al.^[26]

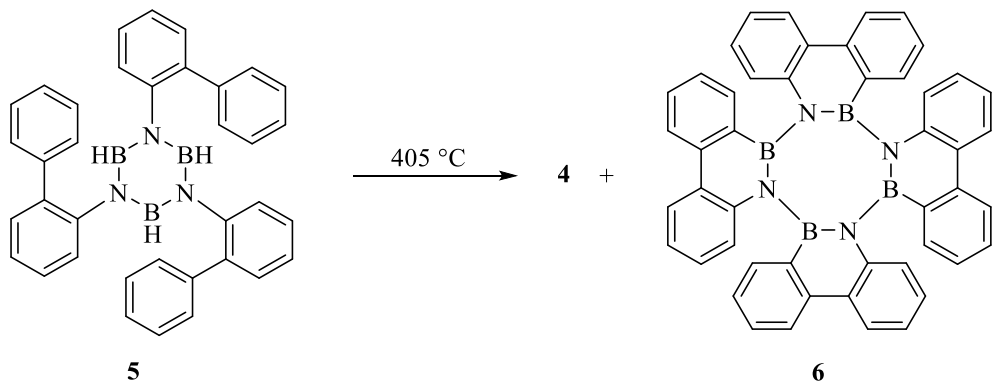
1.2.4 Aromatische cyclische Iminoborane

Die Gruppe von Bettinger untersuchte als erste die Bildung von 1,2-Azaborininen als reaktive Zwischenstufe. Dabei wurden intensiv die Abfangreaktionen des Dibenzo[c,e][1,2]azaborinins (**2**),^[25b, 28] einem Derivat von **1**, untersucht. Wird z.B. die Vorstufe **3** (Schema 8) mit einer sterisch anspruchsvollen Base, wie Kaliumhexamethyldisilazid (KHMDS) oder Lithium-2,2,6,6,-tetramethylpiperidid (LiTMP), behandelt, so entsteht die Verbindung **4**, ein Trimer von **2** (Schema 8).^[28] Jedoch ist das Auftreten von **2** als Zwischenstufe unwahrscheinlich.^[28a]



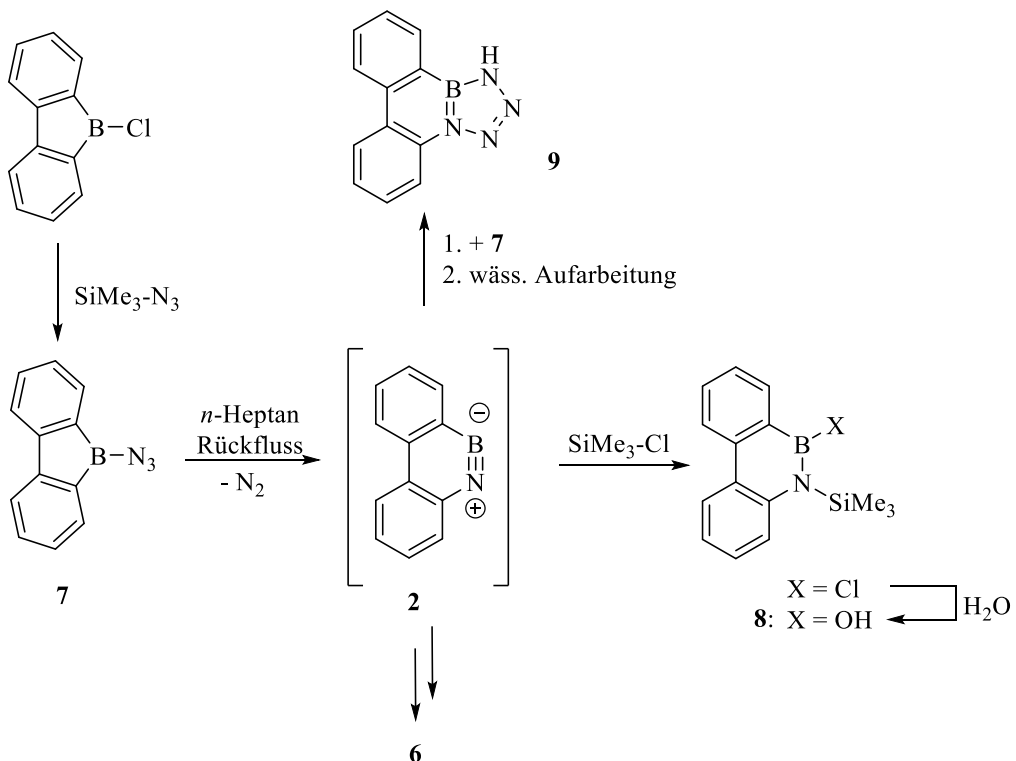
Schema 8. Dehydrohalogenierungsreaktion von **3** nach Biswas et al.^[28b]

Die Synthese von **4** wurde 1965 von Köster^[29] durch eine thermische Dehydrierung von **5** beschrieben (Schema 9). Als Biswas et al.^[28b] die literaturbekannte Synthese wiederholte, wurde zusätzlich die Verbindung **6**, ein Tetramer von **2**, in 3 % Ausbeute isoliert.



Schema 9. Thermolyse von N,N',N''-Tris-(2-biphenyl)borazin (**5**) nach Biswas et al.^[28b]

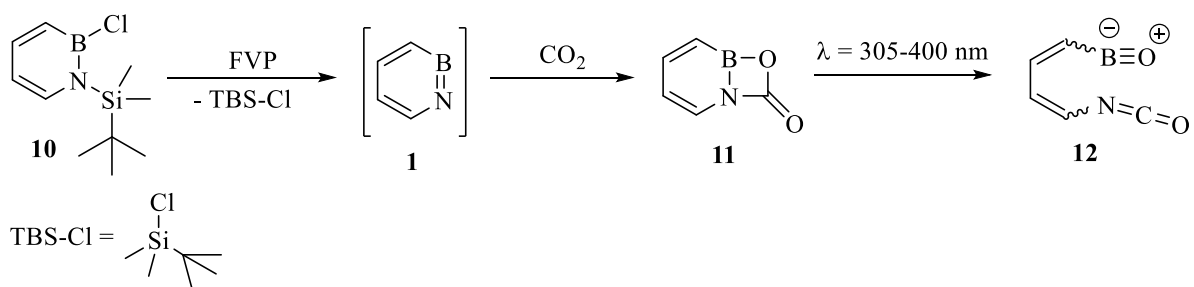
Ausgehend von der Chemie der cyclischen und acyclischen Azidodiorganylboranen R₂BN₃, die von Paetzold et al.^[13, 26] beschrieben wurde, untersuchten Müller et al. die thermische Zersetzung von 9-Azido-9-borafluoren (**7**).^[25b] Beim Erhitzen von **7** in einer *n*-Heptanlösung entsteht das Tetramer **6** in 8-10 % Ausbeute (Schema 10). Dieser Befund deutet stark auf die Entstehung von **2** als Zwischenstufe hin. Nach einer wässrigen Aufarbeitung des Reaktionsgemisches konnte mittels GC-MS-Analytik die Verbindungen **8** und **9** nachgewiesen werden, die als Abfangprodukte von **2** interpretiert werden können.



Schema 10. Thermische Zersetzungsreaktion von Azidoborol 7 nach Müller et al.^[25b]

1.2.5 Matrixisolationsversuche

Während meiner Diplomarbeit untersuchte ich, ob **1** als Zwischenstufe bei der Blitzvakuumpyrolyse (FVP, engl.: flash vacuum pyrolysis) von 1,2-Dihydro-1-*tert*-butyldimethylsilyl-2-chloro-1,2-azaborinin (**10**) auftritt und mit CO_2 abgefangen werden kann (Schema 11). Die Versuche erwiesen sich als erfolgreich.^[30] Das resultierende IR-Spektrum zeigte eine neue Bande bei $1874/79\text{ cm}^{-1}$, welche mit Hilfe von quantenchemischen Rechnungen und dem Einsatz von isotopenmarkiertem Kohlenstoffdioxid ($^{13}\text{CO}_2$ und $\text{C}(^{18}\text{O})_2$) sich der Carbonylschwingung der Verbindung **11** (Schema 11), einem cyclischen Carbamat, zuordnen ließ. Durch anschließende Photolyse mit UV-Licht ($\lambda = 305\text{-}400\text{ nm}$) ging **11** eine [2+2]- Cycloreversion zu der offenkettigen Verbindung **12** mit einer Isocyanat- und einer BO-Einheit ein, welche charakteristischen Schwingungen im IR-Spektrum (Abbildung 1) zeigen. Das Auftreten dieser funktionellen Gruppen konnte ebenfalls durch Isotopenmarkierung und quantenchemischen Rechnungen bestätigt werden.^[30]



Schema 11. Matrixisolationsexperiment: Bei der Blitzvakuumpyrolyse (FVP) von **10** entsteht **1** in der Gasphase und reagiert beim Ausfrieren mit CO_2 zu **11**.^[30]

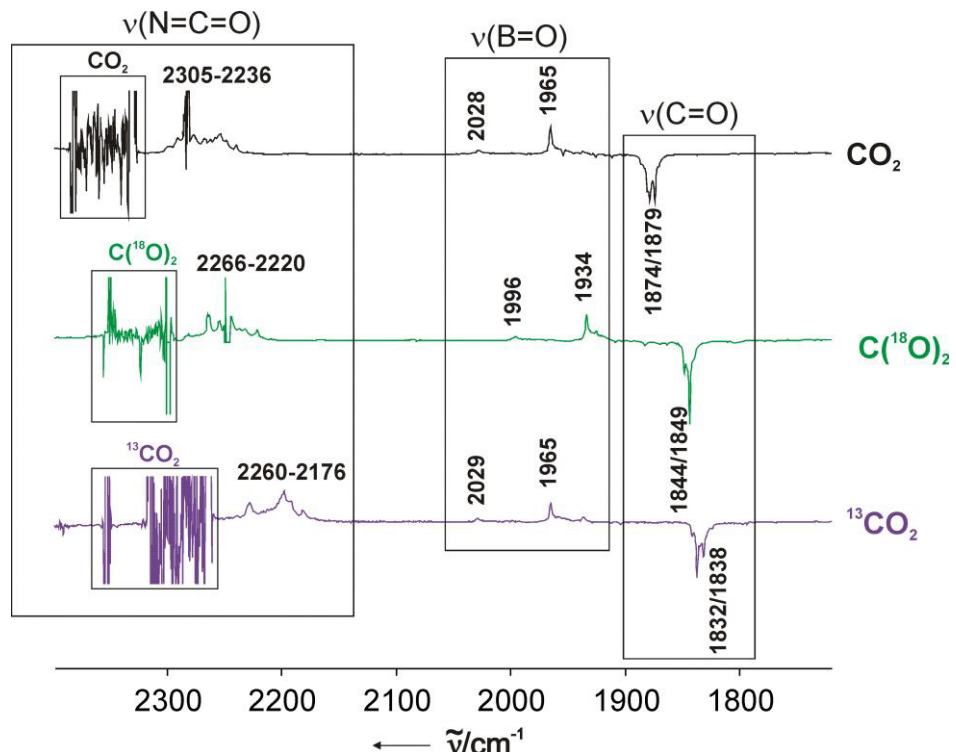
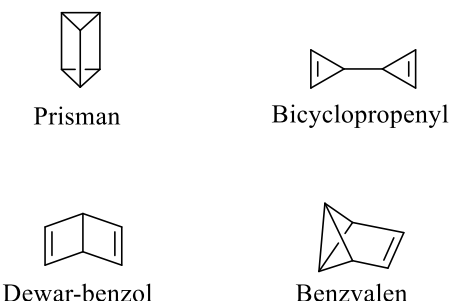


Abbildung 1. IR-Differenzspektren zeigen die Photoisomerisierung von **11** zu **12**. Differenzspektren nach Photolyse mit $\lambda = 305\text{-}400 \text{ nm}$: Signale der Carbonylgruppe von **11** nehmen ab, während neue Signale von **12** entstehen. Vor der Photolyse: Abfangreaktion von **1**, welches durch FVP (740°C) von **10** entsteht und mit reinem Kohlenstoffdioxid zu **11** reagiert und anschließend bei 52 K ausgefroren wird.

1.3 Dewar-Valenzisomere von 1,2-Dihydro-1,2-azaborininen

1.3.1 Valenzisomere des Benzols

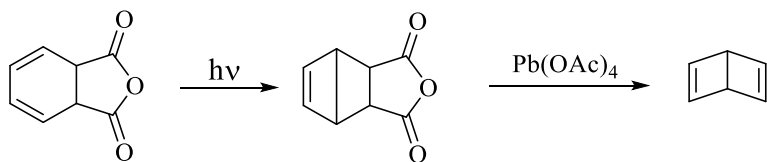
Mit der Summenformel des Benzols C_6H_6 sind 217 denkbare Valenzisomere möglich.^[31] Diese sind jedoch instabiler als die aromatische Ringstruktur des Benzols, die von Kekulé 1865 vorgeschlagen wurde.^[32] Bevor die tatsächliche Struktur des Benzols erwiesen war, gab es einige alternative Vorschläge, wie z. B. das Dewar-Benzol^[33] oder das Prisman,^[34] welches auch als Ladenburg-Benzol bekannt ist (Schema 12). Heute sind vier Valenzisomere des Benzols bekannt: Prisman,^[35] Dewar-Benzol,^[36] Benzvalen^[37] und Bicycloprenyl^[38] (Schema 12).



Schema 12. Bekannte Valenzisomere des Benzols.

1.3.2 Dewar-Benzol

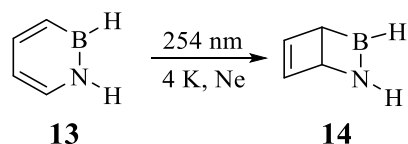
Dewar-Benzol entsteht unter bestimmten Umständen bei der Photolyse des Benzols als Nebenprodukt.^[39] Die Hauptprodukte dabei sind Fulven und Benzvalen. Die Photochemie des Benzols zeigt eine starke Abhängigkeit von der Bestrahlungswellenlänge und vom Aggregatzustand.^[37, 39-40] Die erste direkte Synthese von Dewar-Benzol wurde erstmals von van Tamelen und Pappas 1963 veröffentlicht (Schema 13).^[36] Dewar-Benzol isomerisiert zum Benzol mit einer Halbwertszeit von zwei Tagen und mit einer Aktivierungsenthalpie von $\Delta H^\ddagger = 25.1 \pm 2 \text{ kcal mol}^{-1}$.^[41] Laut Woodward-Hoffmann-Regeln ist die disrotatorische Ringöffnung nicht erlaubt und die konrotatorische Ringöffnung würde zum sogenannten „trans-Benzol“ führen.^[42] Quantenchemische Rechnungen bestätigen jedoch eine konrotatorische Ringöffnung mit entsprechend hoher Aktivierungsenthalpie.^[43]



Schema 13. Synthese von Dewar-Benzol nach van Tamelen und Pappas.^[36]

1.3.3 Dewar-Valenzisomer des 1,2-Dihydro-1,2-azaborinins

Im Jahr 2012 untersuchten Brough et al.^[44] die Photochemie des 1,2-Dihydro-1,2-azaborinins (**13**) unter Matrixisolationsbedingungen (Schema 14). Im Gegensatz zu der Photochemie des Benzols,^[39b] entsteht bei der Belichtung von **13** in festem Neon ausschließlich das entsprechende Dewar-Valenzisomer **14** bei vollständigem Umsatz.

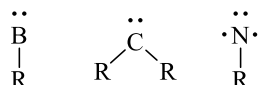


Schema 14. Photoisomerisierung von **13** zu **14** nach Brough et al.^[44]

Daraufhin untersuchten Bettinger und Hauler^[45] die Rückreaktion von **14** mit Hilfe von quantenchemischen Rechnungen. Neben der klassischen konrotatorischen und der disrotatorischen Ringöffnung wurden zwei weitere Ringöffnungen mit jeweils zwei Übergangszuständen gefunden. Diese sind energetisch günstiger, als die konrotatorische Ringöffnung. Die berechnete Aktivierungsenergie von 22 kcal mol⁻¹ bedeutet, dass **14** in Lösung für kurze Zeit detektiert werden könnte. Jedoch würde **14** in Lösung zur Dimerisierung oder Oligomerisierung neigen, da die entsprechenden Energiebarrieren (3 kcal mol⁻¹) als sehr gering berechnet wurden.^[45]

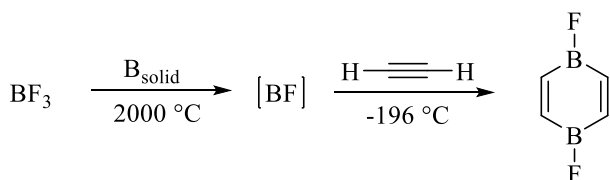
1.4 Borylene

Borylene sind als Analoga der Carbene und Nitrene hochreaktive Spezies (Schema 15). Sie haben, wie Nitrene, nur einen Substituenten und besitzen ein nichtgebundenes Elektronenpaar in einem sp-Orbital und zwei leere p-Orbitale. Dadurch werden sie als elektrophil eingestuft.^[46]



Schema 15. Vergleich von Borylenen mit Carbenen und Nitrenen.

Im Vergleich zu der gut untersuchten Chemie der Carbene^[47] und Nitrene^[48] gibt es für Borylene nur wenige Beispiele in der Literatur. Die meisten davon beruhen auf Abfangreaktionen der Borylene. Timms^[49] zum Beispiel berichtete die Bildung von BF und BCl durch Komproportionierung von BF_3 bzw. BCl_3 über festem Bor bei 1800-2000 °C und nach dem Abfangen mit Acetylen konnte 1,4-Diboracyclohexadien isoliert werden (Schema 16). Weitere Beispiele von West,^[50] Power^[51] und Tokitoh^[52] folgten. In den letzten Jahrzehnten konnten vor allem Braunschweig und Bertrand Borylene mit Hilfe von N-Heterocyclischen Carbenen (NHC) als Zwischenstufe stabilisieren und sogar isolieren.^[46] Zudem wurden Borylene als Liganden an Übergangsmetallen intensiv untersucht.^[53]

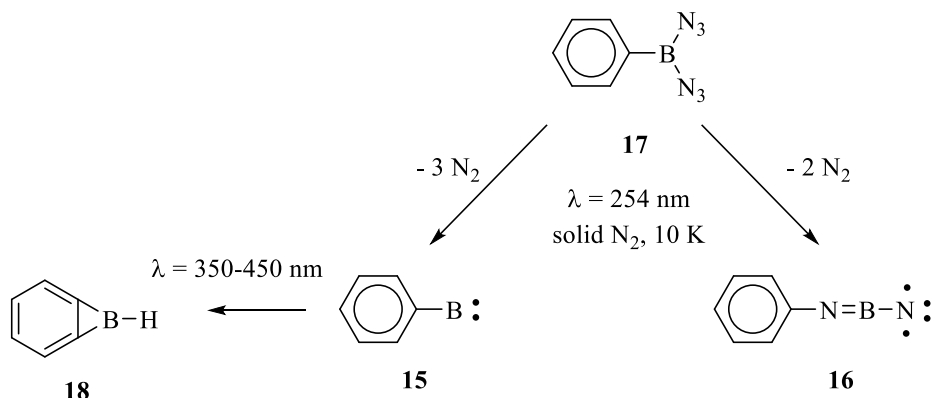


Schema 16. Bildung und Abfangreaktion von BF nach Timms et al.^[49]

1.4.1 Matrixisolationsversuche

Einen direkten spektroskopischen Nachweis von Borylenen mit kleinen Resten am B-Atom (z.B. FB, ClB, H_2NB und HC_2B) konnte Andrews mit Hilfe von Matrixisolationstechniken zeigen.^[54] Dafür wurden Boratome, die durch Laserablation entstehen, mit verschiedenen kleinen Molekülen (z.B. F₂, Cl₂, NH₃ und C₂H₂) co-kondensiert und in einer Argonmatrix isoliert. Dabei entsteht eine Vielzahl von Verbindungen, darunter auch Borylene. Deren IR-Banden konnten mit Hilfe von quantenchemischen Rechnungen und den Einsatz isotopenmarkierter Verbindungen zugeordnet werden.

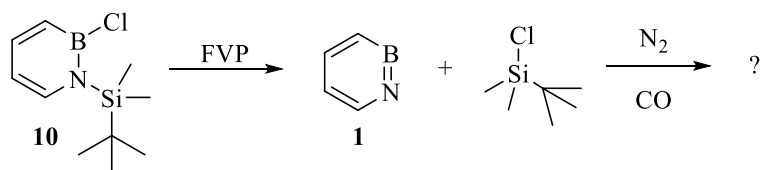
2006 zeigte Bettinger, dass Phenylborylen (**15**) neben dem Nitren **16** durch die Photolyse ($\lambda = 254$ nm) von Phenyldiazidoboran (**17**) in einer Stickstoffmatrix bei 10 K entsteht (Schema 17).^[55] Borylen **15** geht eine intramolekulare C-H-Insertion zum Benzoboriren (**18**) ein, wenn es mit Licht der Wellenlängen $\lambda = 350\text{-}450$ nm belichtet wird.^[55] Unter den gleichen Photolysebedingungen entstehen im Bereich $1417\text{-}1387\text{ cm}^{-1}$ neue IR-Banden, die nicht zu der Verbindung **18** gehören und es sich vermutlich um ein Produkt zwischen **15** und N_2 handelt. Um diese Annahme zu stützen bedarf es jedoch weiterer Untersuchungen.



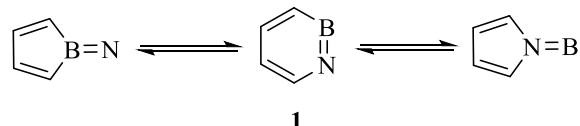
Schema 17. Photochemische Zersetzung von **17** unter Matrixisolationsbedingungen nach Bettinger.^[55]

2. Zielsetzung

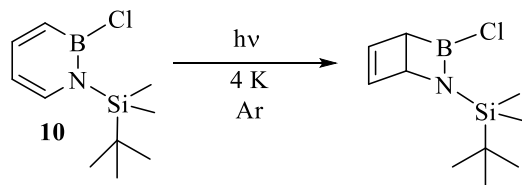
Das Ziel dieser Doktorarbeit war es, mit Hilfe von Matrixisolationsmethoden einen direkten spektroskopischen Nachweis von 1,2-Azaborinin (**1**) zu erzielen und Abfangreaktionen mit kleinen Molekülen, wie z.B. mit N₂ und CO, zu untersuchen.



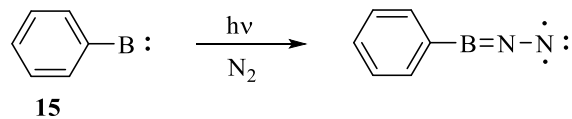
Es soll zudem mit Hilfe von quantenchemischen Rechnungen untersucht werden, ob **1** unter den FVP-Bedingungen isomerisieren und fragmentieren kann. Dabei sollen verschiedene Reaktionsmechanismen betrachtet werden.



Die Photoisomerisierung von weiteren Derivaten des 1,2-Dihydro-1,2-azaborinins (**13**) zu den entsprechenden Dewar-Valenzisomeren soll untersucht werden. Zunächst wird die Photochemie von **10**, da es die Vorstufe von **1** ist (siehe oben), unter Matrixisolationsbedingungen betrachtet. Anschließend soll die Photoisomerisierung von weiteren Derivaten auch in Lösung untersucht werden.



Die Matrixexperimente mit Phenylborylen (**15**) sollen fortgesetzt werden und mögliche Reaktionen von **15** mit kleinen Molekülen, wie N₂ und CO, mit verschiedenen Spektroskopiemethoden (IR, UV/Vis und ESR) untersucht werden.



3. Matrixisolationstechniken

Mit Hilfe von Matrixisolationstechniken^[56] können reaktive Zwischenstufen erzeugt und isoliert und mit spektroskopischen Methoden (IR, UV/Vis und ESR) nachgewiesen werden. Dabei werden reaktive Zwischenstufe oder deren Vorläufer mit einem Überschuss eines Matrixgases auf einem optischen Fenster, dessen Temperatur 4 K oder mehr ist, aufgedampft. Die tiefen Temperaturen werden mit Hilfe eines Kryostaten mit einem geschlossenen Heliumkreislauf (engl.: closed cycle helium cryostat) erreicht. Als Matrixgase kommen inerte Gase, wie Stickstoff, Neon oder Argon in Frage. Die Matrixgase können jedoch bewusst mit reaktiven Gasen, wie z.B. CO, CO₂, H₂ oder HCl, dotiert werden, um die Reaktivität der Verbindungen zu untersuchen. Die optischen Fenster sind je nach Spektroskopiemethode CsI (IR), Saphir (UV/Vis) oder ein Kupferdraht (ESR) und sind durchlässig für IR-Strahlung (CsI) bzw. für UV-Licht (Saphir).

Das äußere Matrixgehäuse (Abbildung 2) enthält zwei parallele Fenster, die durchlässig für IR-Strahlung (KBr) oder für UV-Licht (Quarz) sind. Das äußere Gehäuse ist zudem frei drehbar, d.h. die beiden äußeren Fenster und das kalte Matrixfenster können parallel ausgerichtet werden und in einem Spektrometer für die Aufnahme eines Spektrums positioniert werden. Des Weiteren ist im äußeren Gehäuse ein Quarzfenster eingebaut, durch welches die Matrix mit Licht geeigneter Wellenlängen bestrahlt werden kann, um Photochemie der isolierten Verbindungen zu untersuchen. Als Lichtquellen für diese Dissertation wurden hauptsächlich eine Quecksilberhochdrucklampe bzw. eine Quecksilberniedrigdrucklampe (PenRay, 254 nm) verwendet. Während eines Matrixexperiments muss ein Hochvakuum (10^6 - 10^5 mbar) gewährleistet sein, damit das kalte Fenster thermisch isoliert ist und sich z.B. Wasser aus der Luft nicht auf dem kalten Fenster abscheiden kann.

3.1 Blitzvakuumpyrolyse

Bei der Blitzvakuumpyrolyse (FVP, engl.: flash vacuum pyrolysis) wird eine geeignete Verbindung durch das Anlegen eines Hochvakuums (10^6 - 10^5 mbar) verdampft und durch ein heißes Rohr (Ofen), in dem thermische Reaktion stattfinden können, geleitet. Teilchen, die aus dem Ofen austreten, werden mit einem Überschuss des gewünschten Matrixgases gemischt und auf das kalte Matrixfenster aufgedampft (Abbildung 2).

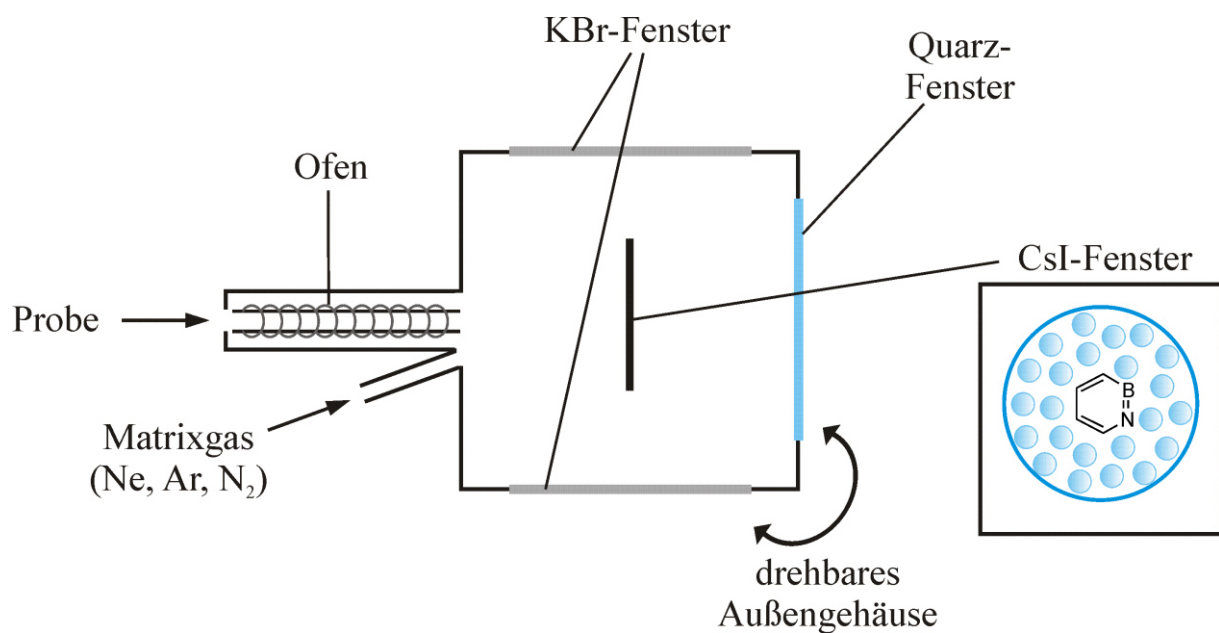


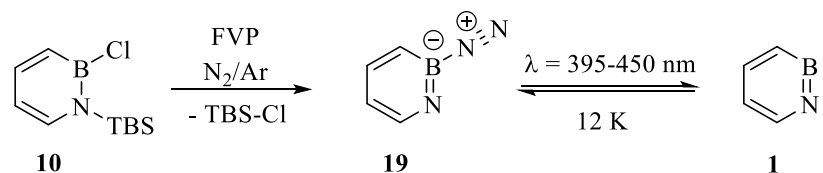
Abbildung 2. Vereinfachte Skizze eines Matrixprobenkopfes (hier: für IR-Spektroskopie).

4. Ergebnisse und Diskussion

4.1 1,2-Azaborinin

Nach der erfolgreichen Abfangreaktion des 1,2-Azaborinins (**1**) mit Kohlenstoffdioxid war die Überlegung nahe, **1** direkt in einer Argonmatrix zu isolieren und spektroskopisch nachzuweisen. Rechnungen zeigen jedoch, dass die Rückreaktion mit *tert*-Butyldimethylsilylchlorid (TBS-Cl) kaum einer Aktivierungsenergie bedarf und stark exotherm ist. Das bedeutet, wenn **1** in der Gasphase nicht abgefangen wird, kann es beim Ausfrieren mit TBS-Cl zurück zu der Ausgangsverbindung **10** reagieren. Und in der Tat, wenn die FVP und anschließendes Ausfrieren mit Argon unter den gleichen Bedingungen durchgeführt wird, wie bei den CO₂-Versuchen, sind im resultierenden IR-Spektrum nur Signale der Ausgangsverbindung zu sehen. Wird allerdings die Pyrolysetemperatur um 70-80 °C erhöht, sind Signale von TBS-Cl und weitere neue Signale im resultierenden IR-Spektrum zu sehen. Der Vergleich der neuen IR-Signale mit quantenchemischen Rechnungen zeigte jedoch nur teilweise Übereinstimmung. Somit ließ es sich nicht sagen, ob **1** tatsächlich isoliert werden kann.

Um die neuen IR-Signale eindeutig zuordnen zu können, wurde Stickstoff als Matrixgas verwendet. Maier et al. hat unter ähnlichen Versuchsbedingungen das Borabenzol-Stickstoff-Addukt hergestellt.^[57] In unseren Versuchen bildet sich dabei das Stickstoff-Addukt **19** (Schema 18). Dieses lässt sich mit Licht der Wellenlänge $\lambda = 395\text{-}450 \text{ nm}$ zu **1** und N₂ spalten. Diese Reaktion ist reversibel: indem die Matrix vorsichtig von 4 auf 12 K erwärmt wird (Abbildung 3), bildet sich **19** zurück. Nach einigen Experimenten stellte sich heraus, dass die Verwendung einer Mischung aus Stickstoff und Argon (30:70) vorteilhaft ist. Einerseits läuft die photolytische Spaltung von **19** besser ab, je weniger Stickstoff in der Gasmischung ist. Dies kann dadurch erklärt werden, dass das gebildete **1** wieder mit N₂ reagieren kann, wenn genug N₂-Moleküle in der unmittelbaren Nähe sind. Umgekehrt läuft die Rückreaktion mit N₂ schlechter ab, je weniger Stickstoff in der Gasmischung vorhanden ist.



Schema 18. Bildung von **19** durch FVP von **10** und anschließende Co-Kondensation mit einer N₂/Ar-Mischung.

Die $\nu(\text{NN})$ Strettschwingung von **19** liegt bei 2266 cm^{-1} und erinnert an die $\nu(\text{NN})$ Strettschwingung bei 2197.6 cm^{-1} des Borabenzol- N_2 -Addukts, über welches Maier et al. berichtete.^[57] Um die Bildung von **19** zu belegen, wurden Matrixexperimente mit isotopenmarkiertem Stickstoff ($^{15}\text{N}_2$) durchgeführt. Der Isotopenshift von 75 cm^{-1} stimmt mit einem berechneten Isotopenshift von 77 cm^{-1} (CCSD(T)/TZ2P) und dem berichteten Isotopenshift für das Borabenzol- N_2 -Addukt (73.3 cm^{-1})^[57] überein.

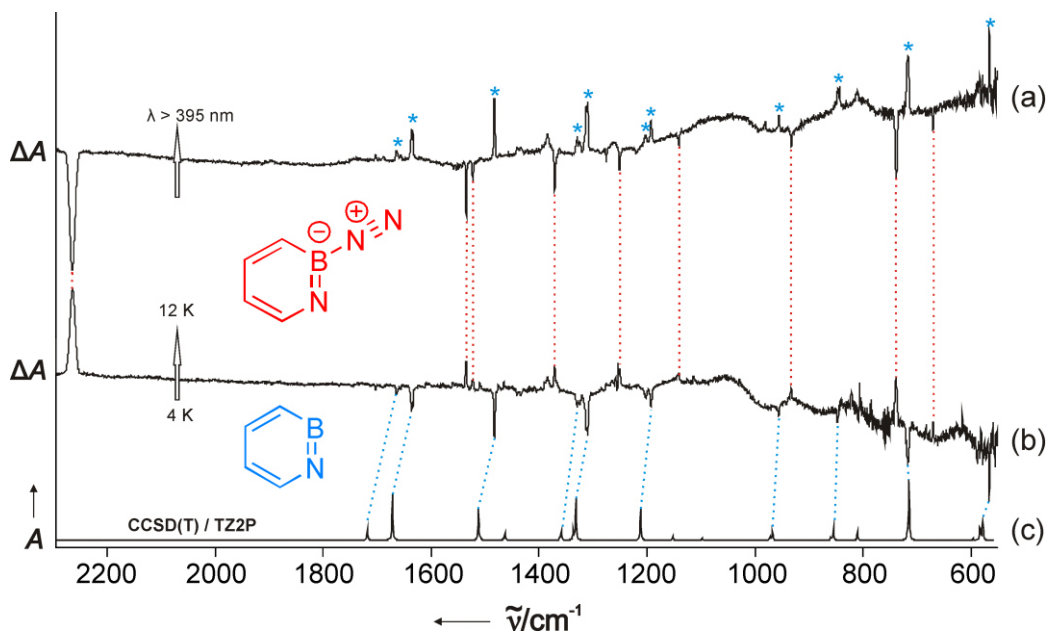


Abbildung 3. IR-Differenzspektren zeigen reversible Reaktion zwischen **1** und **19**. (a) Matrix, die durch FVP von **10** und anschließendes Ausfrieren bei 6 K mit einem Überschuss einer N_2/Ar -Mischung (3:7) entsteht, wird für 1 h mit $\lambda = 395\text{-}400 \text{ nm}$ belichtet. Differenzspektrum zeigt den Unterschied vor und nach der Photolyse. Abnehmende Signale gehören zu **19** und zunehmende Signale gehören zu **1**. (b) IR-Differenzspektrum zeigt den Unterschied vor und nach dem Tempern ($4 \text{ K} \rightarrow 12 \text{ K}$), welches nach der Photolyse stattfand. (c) Theoretisches Spektrum [CCSD(T)/TZ2P] von **1**.

Erst durch den Versuch mit Stickstoff war es möglich die IR-Signale von **1** eindeutig zuzuordnen. Diese stimmen gut mit quantenchemischen Rechnungen (Abbildung 3) überein. Der gleiche Satz von Signalen ist auch in den IR-Spektren der Agron-Versuche vorhanden. Quantenchemische Untersuchungen zeigen, dass **1** und N_2 ohne Barriere zu einem van der Waals Komplex mit einer Bindungsenergie von $6.0 \text{ kcal mol}^{-1}$ [CCSD(T)/TZ2P+ZPVE] reagieren. Dies ist auch durch die spontane Reaktion bei bereits 12 K ersichtlich.

Die quantenchemische Analyse der Struktur von **1** zeigt eine stark von regelmäßigen Sechsring abweichende Struktur. Der Winkel am B-Atom beträgt 142.5° , der Winkel am N-

Atom 108.4° und der BN-Bindungsabstand 1.318 \AA [CCSD(T)/TZ2P]. Eine Analyse der natürlichen Bindungssorbitale (NBOs, engl.: natural bond orbitals) [B3LYP/6-311+G**] zeigt, dass das N-Atom ein freies Elektronenpaar in der Molekülebene besitzt (HOMO-1) und das B-Atom ein leeres Orbital mit einem starken p-Charakter (LUMO) (Abbildung 4). Die Besetzungszahlen der beiden Orbitale betragen jeweils 1.80e^- und 0.22e^- . Die Partialladungen sind groß und betragen am N-Atom -0.79 und am B-Atom $+0.97$. Der Wiberg-Bindungsindex zwischen dem B- und dem N-Atom hat einen Wert von 1.46 und entspricht nicht einer BN-Dreifachbindung sondern eher den beiden Resonanzstrukturen in Schema 19. Diese Ergebnisse zeigen, dass das Borzentrum eine starke Lewis-Acidität besitzt und somit eine Reaktion mit einer schwachen Lewis-Base wie N_2 erklärt.

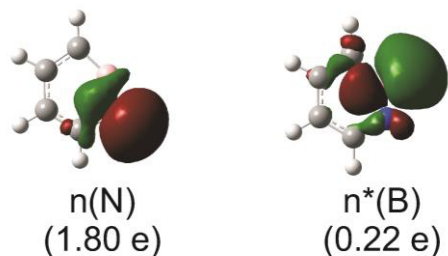
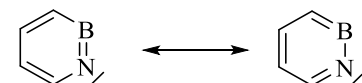


Abbildung 4. NBOs und deren Besetzungszahlen [B3LYP/6-311+G**] von **1**.



Schema 19. Resonanzstrukturen von **1**.

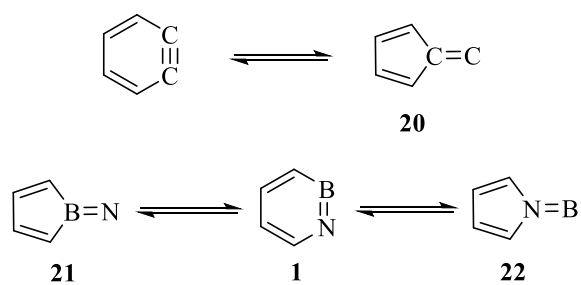
4.2 Mögliche Isomerisierungsreaktionen von 1,2-Azaborinin

Bei den Versuchen mit Argon ist **1** nicht die einzige Verbindung, die entsteht. Mindestens zwei IR-Signalsätze von unbekannten Produkten können unterschieden werden. Dies kann durch das Ausfrieren bei unterschiedlichen Temperaturen festgestellt werden. Bei einer Matrixtemperatur von 30 K ist Argon nicht ganz fest und die Pyrolyseprodukte können sich darin bewegen und miteinander reagieren. Mögliche Produkte können z.B., wie beim *ortho*-Benzin,^[23] das Dimer oder das Trimer von **1** sein. Der Vergleich mit den berechneten Spektren lässt jedoch keine eindeutigen Schlüsse zu.

Weiterhin könnte es im 820 °C heißen Ofen zu Isomerisierungs- und Fragmentierungsreaktionen von **1** kommen. Eine theoretische Untersuchung von Isomerisierungs- und Fragmentierungsmechanismen soll zeigen, ob diese Mechanismen unter den FVP-Bedingungen möglich sind.

4.2.1 Ringkontraktion

Die Isomerisierung von *ortho*-Benzin zum Cyclopentadienylidencarben (**20**) (Schema 19) wurde kontrovers diskutiert.^[58] Computerchemische Untersuchungen zeigen, dass **20** 30 kcal mol⁻¹ höher in Energie als *ortho*-Benzin ist und sich in einem flachen Minimum auf der Potentialenergiefläche befindet.^[59] Würde es zur ähnlichen Ringkontraktion von **1** kommen, so wären die beiden Strukturisomere **21** und **22** möglich (Schema 20). In Tabelle 1 sind die relativen Energien von **21** und **22**, die auf verschiedenen Theorieniveaus berechnet wurden, zu sehen. Es ist zu erkennen, dass **22** ca. 32 kcal mol⁻¹ über **1**, ähnlich wie **20** über *ortho*-Benzin, liegt. Die Bildung von **22** ist jedoch unwahrscheinlich, da die Energie des Übergangszustand **1** → **22** ca. 65 kcal mol⁻¹ beträgt.



Schema 20. Ringkontraktionsreaktionen von *ortho*-Benzin und **1**.

Tabelle 1. Relative Energien mit Korrektur der Nullpunktsschwingungsenergie (ΔE_{ZPVE} in kcal mol⁻¹) der Strukturisomere **1**, **21** und **22** und dem Übergangszustand zwischen **1** und **22** (TS **1 → 22**)

	1	21 (1A₁)	21 (3A₂)	22	TS (1 → 22)
B3LYP/3-611+G**	0	68.5	71.4	39.6	70.6
MP2/3-611+G**	0	85.2	80.5	36.9	68.0
MP2/cc-pVTZ	0	87.3	83.6	36.4	66.4
CCSD(T)/cc-pVTZ// B3LYP/6-311+G**	0	66.9	68.7	31.5	65.2

21 besitzt einen antiaromatischen Borolring und ist mit der relativen Energie von ca. 67 kcal mol⁻¹ zu hoch, um unter den Versuchsbedingungen beobachtet zu werden. Die Struktur von **21** wurde genauer untersucht, da Borylnitrene als mögliche Zwischenstufen bei der Bildung von 1,2-Azaborinen, auftreten können (Schema 6, 10).^[25b] Die angeregten Zustände wurden auf hohen Theorieniveaus bestimmt (Tabelle 2). Zusammenfassend lässt sich sagen, dass die Zustände ¹A₁, ¹B₁ und ³A₂ energetisch nahe beieinander liegen, wobei der Triplett-Zustand ³A₂ energetisch etwas bevorzugt ist. Auf dem B3LYP- und dem CASPT2-Niveau entspricht der ¹A₁-Zustand einem Sattelpunkt 1. Ordnung und nicht einem Minimum auf der Potentialenergiefläche.

Tabelle 2. Relative Energien (in kcal mol⁻¹) der energetisch niedrig liegenden Zustände von **6**, berechnet auf verschiedenen Theorieniveaus.

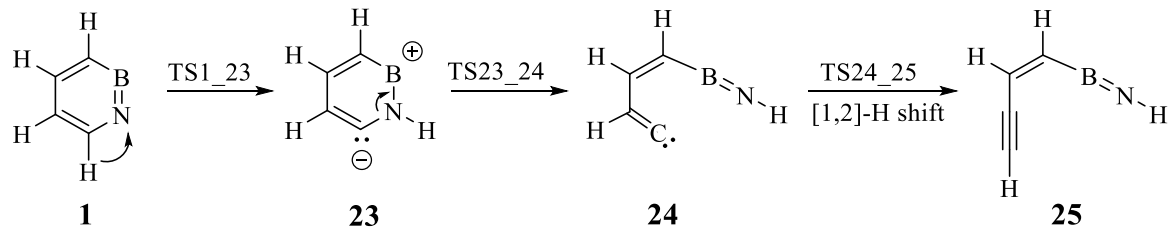
	¹ A ₁	¹ A ₂	¹ B ₁	³ A ₂	³ B ₁
CASPT2 ^a	0	+20.4	-6.3	-11.1	-5.4
MRCI+Q//CASPT2 ^b	0	+26.2	+6.3	-4.2	+7.5
B3LYP ^c	0	-	-	+2.9	-
CCSD(T)//B3LYP ^b	0	-	-	+1.8	-
ACPF//CASPT2	0	29.0	11.4	-1.7	12.5
MCCEPA//CASPT2	0	25.0	12.8	-5.4	11.4

^a 6-31G* Basissatz; ^b cc-pVTZ Basissatz für die Einzelpunktsberechnung; ^c 6-311+G** Basissatz.

4.2.2 Ringöffnung zu BN-substituierten Endiinen

Die Isomerisierung von *ortho*-Benzin zum *meta*- und *para*-Benzin und anschließender Ringöffnung zum Endiin wurde mit quantenchemischen Rechnungen untersucht.^[59c, 60] Die Ringöffnung von *meta*- und *para*-Benzin zum Endiin ist auch experimentell bekannt.^[59c, 60-61] Im Falle von **1** sind aufgrund der BN-Einheit zwei Ringöffnungsmechanismen möglich. Beim ersten Mechanismus (Schema 21, Abbildung 5) wird zunächst ein Proton auf das benachbarte N-Atom übertragen (**23**). Dieser Schritt hat eine Aktivierungsenergie von 77 kcal mol⁻¹ und ist der energetisch höchste in dieser Ringöffnungsreaktion. Anschließend folgt eine C-N-

Bindungsspaltung zum Vinyliden **24**, welches sich in einem sehr flachen Minimum auf der Potentialenergiefläche befindet und durch eine [1,2]-H Wanderung zum BN-Endiin **25** umwandelt. Eine geringe Aktivierungsenergie für die Umlagerung von Vinyliden zum Acetylen ist experimentell und quantenchemisch bekannt.^[62]



Schema 21. Mechanismus zur Ringöffnung von **1** zum BN-Endiin **25**.

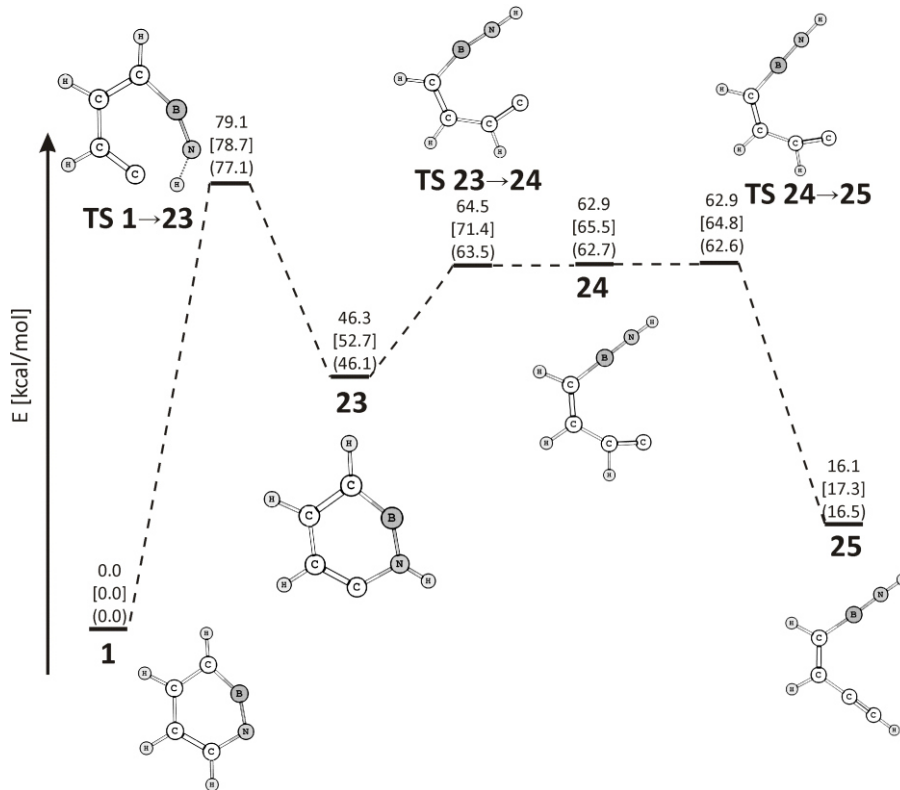
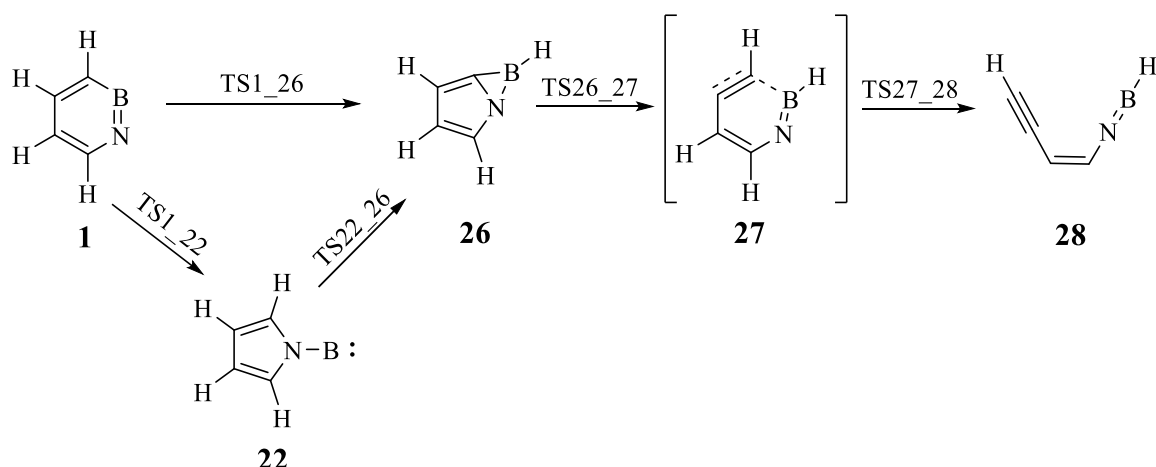


Abbildung 5. Potentialenergiendiagramm für die Ringöffnung von **1** zum BN-Endiin **25** berechnet auf den Theorieniveaus: B3LYP/6-311+G**, [MP2/cc-pVTZ], and (CCSD(T)/cc-pVTZ//B3LYP/6-311+G**).

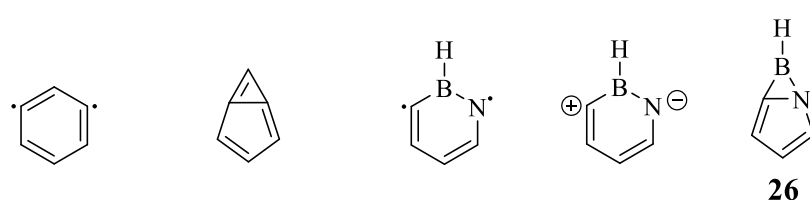
Beim zweiten Reaktionsmechanismus (Schema 22, Abbildung 6) kommt es zunächst zu einer Hydridübertragung zum benachbarten B-Atom. Es entsteht der anti-Bredt Bicyclus **26**,

der energetisch nur 10 kcal mol⁻¹ über **1** liegt. Die Barriere für die Bildung von **26** ist jedoch mit 79 kcal mol⁻¹ sehr hoch. Für die Bildung von **26** wurde ein weiterer zweistufiger Mechanismus gefunden. Dabei kommt es zuerst zur Ringkontraktion zum Borylen **22** und anschließend zu einer C-H-Insertion des Borylens, ähnlich wie beim Phenylborylen (**15**) (Schema 17),^[55] zur Verbindung **26**. Die zweistufige Bildung von **26** ist energetisch fast so hoch, wie der einstufige Prozess. Die Struktur von **26** ist isoelektronisch zu *meta*-Benzin. Die tatsächliche Struktur von *meta*-Benzin (Schema 23) war bis 2002 unklar, da je nach Theorieniveau die bicyclische Struktur bzw. das monocyclische Biradikal begünstigt sind (Schema 22).^[63] Erst durch ein IR-Spektrum von matrixisoliertem *meta*-Benzin konnte die monocyclische Struktur bestätigt werden.^[61a] Verschiedene Theorieniveaus (B3LYP, MP2 und CASSCF(8,8)) schlagen die bicyclische Struktur von **26** vor. Dies ist durch die Elektronegativitätsdifferenz des C- und N-Atoms zu erklären.

Durch eine [1,2]-H-Wanderung und gleichzeitige Ringöffnung von **26** entsteht die Zwischenstufe **27**, aus welcher mit einer geringen Aktivierungsenergie von 2 kcal mol⁻¹ das BN-substituierte Endiin **28** entsteht.



Schema 22. Mechanismus zur Ringöffnung von **1** zum BN-Endiin **28**.



Schema 23. Mögliche Strukturen von *meta*-Benzin und **26**.

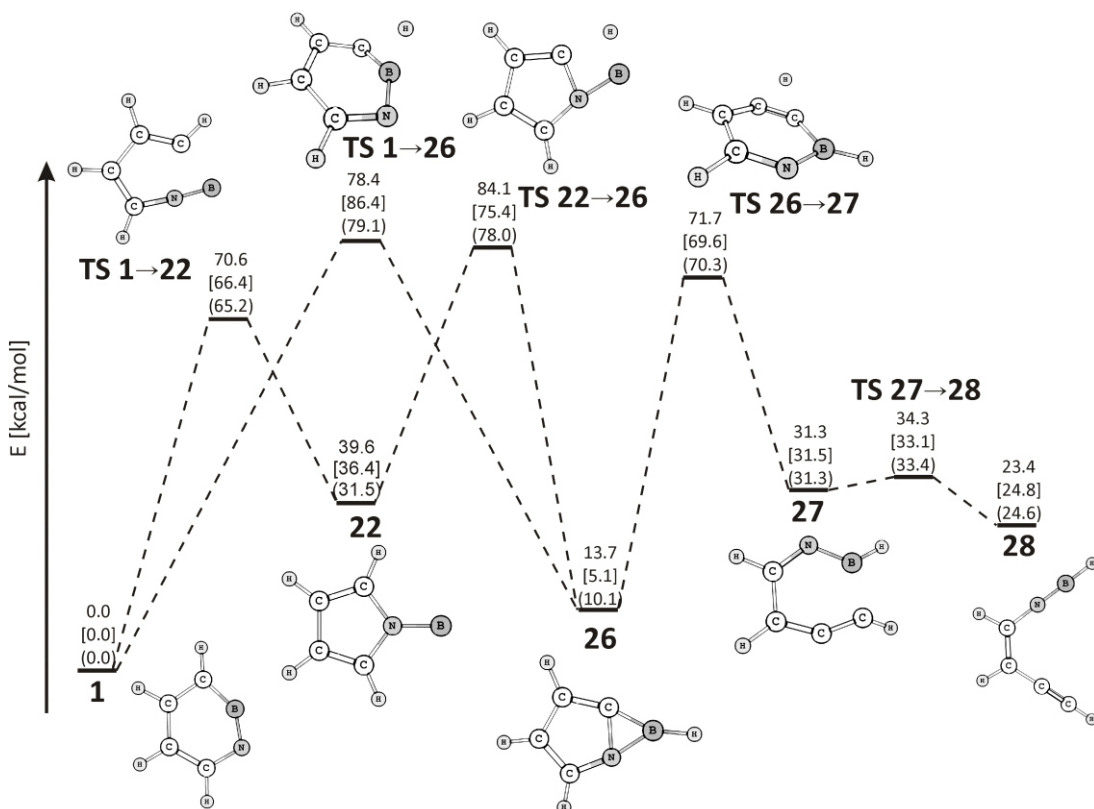
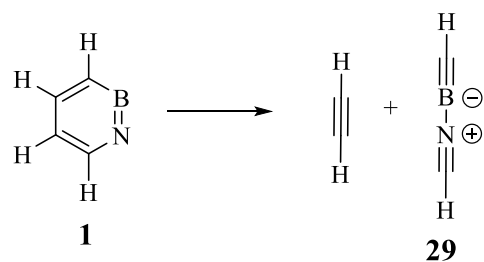


Abbildung 6. Potentialenergiendiagramm für die Ringöffnung von **1** zum BN-Endiin **28** berechnet auf den Theorieebenen: B3LYP/6-311+G**, [MP2/cc-pVTZ], and (CCSD(T)/cc-pVTZ//B3LYP/6-311+G**).

4.2.3 Fragmentierung von 1,2-Azaborinin

Weiterhin wurde die konzertierte Fragmentierung von **1** zu Acetylen und zum BN-substituierten Diacetylen (**29**) (Schema 24) berechnet. Zhang berichtete die Fragmentierung von *ortho*-Benzin zu Acetylen und Diacetylen bei Temperaturen über 1200 K.^[64] Die Fragmentierungsprodukte sind 52 kcal mol⁻¹ höher in Energie als *ortho*-Benzin und der Übergangszustand beträgt 88 kcal mol⁻¹.^[64-65] Die Fragmentierung von **1** ist energetisch deutlich ungünstiger als die Fragmentierung von *ortho*-Benzin. Die beiden Produkte sind 113 kcal mol⁻¹ höher in Energie als **1** und die Energie des Übergangszustands liegt bei 120 kcal mol⁻¹.



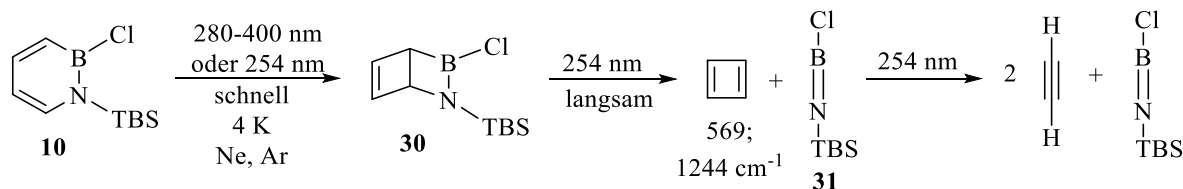
Schema 24. Fragmentierung von **1**.

Zusammenfassend lässt sich sagen, dass die beiden Ringöffnungsmechanismen und der Fragmentierungsmechanismus hohe Aktivierungsenergien benötigen, die bei den FVP-Bedingungen nicht gegeben sind. Die resultierenden IR-Spektren zeigen keine Signale der beiden Endiine **25** und **28** und anderer berechneter Strukturen. Bei **25** und **28** wäre eine $\nu(\text{BN})$ Stretschwung und eine $\nu(\text{NH})$ bzw. eine $\nu(\text{BH})$ Schwingung im IR-Spektrum zu erwarten, die nicht vorhanden sind.

4.3 Dewar-Valenzisomer des 1,2-Dihydro-1,2-azaborinins

4.3.1 Matrixisolationsstudie

Wie das Stammsystem **13** zeigt auch **10** eine Photoisomerisierung zum Dewar-Valenzisomer **30** (Schema 25). Diese Reaktion zeigt einen vollständigen Umsatz, und beim Belichten mit Licht der Wellenlänge $\lambda = 280\text{-}400 \text{ nm}$ ist **30** das einzige Photoprodukt. Dies ist nicht der Fall bei der Photolyse mit Licht der Wellenlänge $\lambda = 254 \text{ nm}$. Hier wird, nachdem sich **30** gebildet hat, eine langsame Cycloreversion von **30** zum Cyclobutadien und dem entsprechenden Iminoboran **31** beobachtet (Schema 25). Cyclobutadien geht dann eine weitere Cycloreversion zu zwei Äquivalenten Acetylen ein. Iminoboran **31** zeigt eine ausgeprägte Iminoboranschwingung (Abbildung 6) bei $1968 \text{ cm}^{-1} v(^{11}\text{BN})$ und bei $2022 \text{ cm}^{-1} v(^{10}\text{BN})$ mit einem Intensitätsverhältnis von 4:1, was dem natürlichen Isotopenverhältnis von ^{11}B zu ^{10}B entspricht. Die experimentellen Werte stimmen gut mit berechneten Werten überein (Abbildung 7).



Schema 25. Photochemie von **10** unter Matrixisolationsbedingungen.

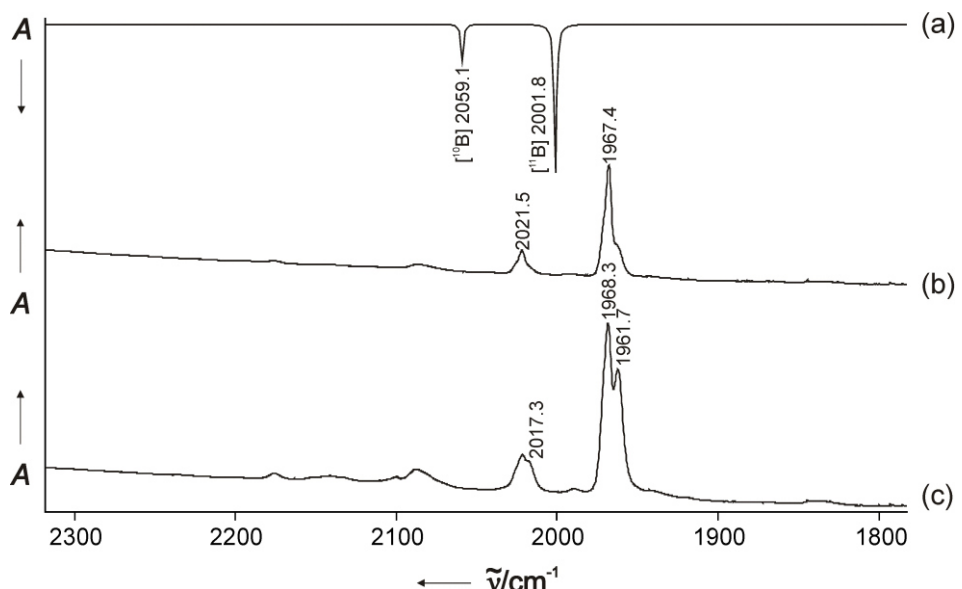
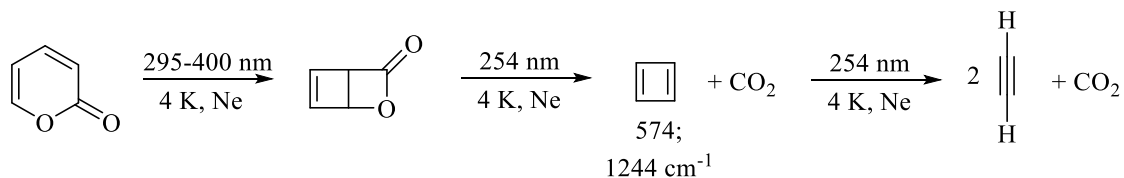


Abbildung 7. Berechnetes (B3LYP/6-311+G**) IR-Spektrum (a) und experimentelle (Ne, 4 K) IR-Spektren von **31** nach 3.5 Stunden (b) und 27 Stunden (c) Photolyse von **10** mit $\lambda = 254 \text{ nm}$.

Um die IR-Signale von Cyclobutadien eindeutig zuordnen zu können, wurden die literaturbekannten Matrixisolationsexperimente von Chapman et al. wiederholt (Schema 26).^[66] Der Vergleich beider Versuche zeigt, dass bei der Photolyse von **10** tatsächlich Cyclobutadien entsteht.



Schema 26. Literaturbekannte Darstellung von Cyclobutadien unter Matrixisolationsbedingungen von Chapman et al.^[66]

Mit diesen Erkenntnissen wurden die Belichtungsversuche mit dem Stammsystem **13** wiederholt und auch erstmals die Photochemie von 1,2-Dideuterio-1,2-azaborinin (**32**) untersucht (Tabelle 3). Bei der Photolyse beider Verbindungen entsteht tatsächlich Cyclobutadien und Acetylen. Jedoch konnte die Bildung des Iminoborans HBNH bzw. DBND nicht eindeutig belegt werden.^[54c, 67] Das Dewar-Valenzisomer des 1,2-Dideuterio-1,2-azaborinins (**33**) zeigt die entsprechende Isotopenverschiebung der beiden Strettschwingungen $\nu(\text{B-H/D})$ und $\nu(\text{N-H/D})$ (Tabelle 4).

Tabelle 3. Experimentelle und berechnete Schwingungsfrequenzen, berechnete Intensitäten und Isotopenverschiebung der beiden Strettschwingungen $\nu(\text{B-H/D})$ und $\nu(\text{N-H/D})$ von **13** und **32**.

13	32	13	32			
ν_{exp} [cm ⁻¹]	ν_{exp} [cm ⁻¹]	ω_{theor} [cm ⁻¹]	Intensity [km mol ⁻¹]	ω_{theor} [cm ⁻¹]	Intensity [km mol ⁻¹]	Assignment
3463.1	2564.1	3604.84	35.9	2640.91	25.4	$\nu(\text{N-H,D})$
2547.8- 2527.0	1926.8- 1892.4	2620.92	181.8	1949.49	136.7	$\nu(\text{B-H,D})$
$\Delta \nu_{\text{exp}}$ [cm ⁻¹]				$\Delta \omega_{\text{theor}}$ [cm ⁻¹]		
899				963.93		$\nu(\text{N-H,D})$
621-634				671.43		$\nu(\text{B-H,D})$

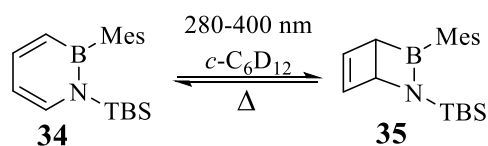
Tabelle 4. Experimentelle und berechnete Schwingungsfrequenzen, berechnete Intensitäten und Isotopenverschiebung der beiden Strettschwingungen $\nu(\text{B-H/D})$ und $\nu(\text{N-H/D})$ von **14** und **33**.

14	33	14		33		
ν_{exp} [cm $^{-1}$]	ν_{exp} [cm $^{-1}$]	ω_{theor} [cm $^{-1}$]	Intensity [km mol $^{-1}$]	ω_{theor} [cm $^{-1}$]	Intensity [km mol $^{-1}$]	Assignment
3482.2	2585.0	3618.22	16.6	2655.65	15.3	$\nu(\text{N-H,D})$
2602.3- 2566.5	1913.2- 1948.0	2653.43	177.8	1980.26	129	$\nu(\text{B-H,D})$
$\Delta \nu_{\text{exp}}$ [cm $^{-1}$]				$\Delta \omega_{\text{theor}}$ [cm $^{-1}$]		
897.2				962.57	$\nu(\text{N-H,D})$	
619-689				673.17	$\nu(\text{B-H,D})$	

4.3.2 Photochemie in Lösung

Durch die erfolgreiche Matrixisolationsstudie waren wir ermutigt die Photochemie von Azaborininen in Lösung zu untersuchen. Dies erwies sich als erfolgreich. Die Belichtung von 1,2-Dihydro-1-*tert*-butyldimethylsilyl-2-mesityl-1,2-azaborinin (**34**) mit $\lambda = 280\text{-}400$ nm in deuterierten Cyclohexan (*c*-C₆D₁₂) zeigte einen vollständigen Umsatz zum entsprechenden Dewar-Valenzisomer **35** (Schema 27, Abbildung 8). Die Quantenausbeute der Photoreaktion wurde in *n*-Hexan bei einer Wellenlänge von 284 nm bestimmt und beträgt $\Phi(284\text{ nm}) = 0.46 \pm 0.8$.

Die NMR-Signale von **35** konnten mit Hilfe von 2D-NMR-Spektroskopie und durch den Vergleich mit quantenchemischen Rechnungen (B3LYP/6-311+G**) zugeordnet werden. Im ¹¹B-NMR entstand durch die Belichtung ein neues Signal bei 52.9 ppm (*c*-C₆D₁₂). Dies ist im Einklang mit der berechneten Tieffeldverschiebung von 13.0 ppm im Vergleich zum Signal von **34** bei 40.3 ppm (*c*-C₆D₁₂). Die Protonen an den beiden Brückenkopfatomen haben, wie erwartet für nichtaromatische Methingruppen, eine Verschiebung von 3.00 und 4.75 ppm (Abbildung 8) und zeigen eine entsprechende Kopplung im ¹H,¹H-COSY-NMR. Die beiden Methylgruppen der TBS-Gruppe sind, durch die fehlende Molekülsymmetrie, diastereotop.



Schema 27. Isomerisierung von **34** zu **35**.

Unter inerten Bedingungen ist **35** stabil und reagiert nur langsam zurück zu **34**. Auch ist **35** für kurze Zeit stabil an Luft und kann sogar säulenchromatographisch aufgereinigt werden, hydrolysiert jedoch langsam zum Trimesitylboroxin.

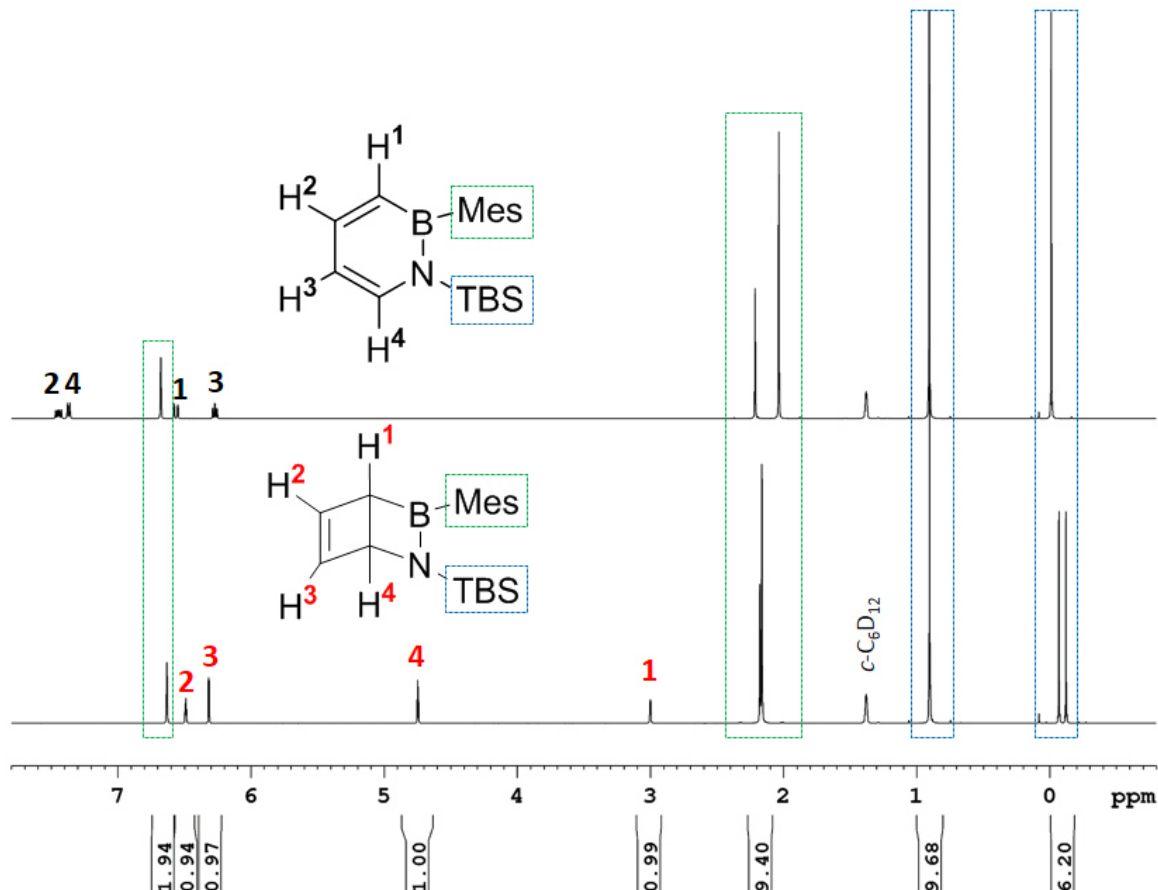


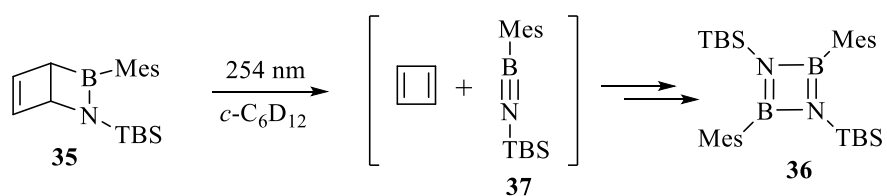
Abbildung 8. ¹H NMR-Spektren in *c*-C₆D₁₂ von **34** (oben) und **35** (unten) nach Photolyse mit $\lambda = 280\text{--}400\text{ nm}$.

Die Aktivierungsenergie der Rückreaktion zu **34** wurde nach Arrhenius mit Hilfe von ¹H-NMR bestimmt. Die nötigen kinetischen Konstanten wurden in einem Temperaturbereich von 358 – 373 K gemessen. Als Lösungsmittel wurde deuteriertes 1,1,2,2-Tetrachlorethan ($[\text{D}_2]\text{TCE}$) verwendet, da es einen hohen Siedepunkt hat. Die Aktivierungsenergie E_a beträgt $27.0 \pm 1.2 \text{ kcal}\cdot\text{mol}^{-1}$ und der präexponentielle Faktor $\log A = 12.5 \pm 0.7 \text{ s}^{-1}$. Der Wert für die Aktivierungsenergie ist viel höher, als der berechnete Wert für das Stammsystem **14**. Daher wurde die Rückreaktion nochmals für die substituierten Systeme quantenchemisch (B3LYP/6-311+G**) untersucht. Für **35** wurde ein Übergangszustand für die Ringöffnung gefunden, der der günstigsten Ringöffnung von **14** entspricht, jedoch ist die Cycloreversion im Vergleich zu

14 einstufig und die Aktivierungsenergie ist höher und beträgt 26.0 kcal mol⁻¹. Dies ist im Einklang mit dem experimentell gefundenem Wert.

Weiterhin wurde die thermische Rückreaktion katalytisch untersucht. In einer Testreihe mit verschiedenen Metallkatalysatoren zeigte als einziger der Wilkinson-Katalysator (3 mol %) einen vollständigen Umsatz in weniger als einer Stunde. Die Reaktionsenthalpie dieser katalysierten Rückreaktion wurde in einem Reaktionskalorimeter auf $\Delta H = (48 \pm 1)$ kcal mol⁻¹ bestimmt. Dieser Wert stimmt gut mit dem berechneten Wert von $\Delta E_{ZPVE} = -51.9$ kcal mol⁻¹ (B3LYP/6-311+G**) überein.

Da unter Matrixisolationsbedingungen eine Cycloreversion von **30** zum Cyclobutadien und Iminoboran **31** beobachtet wurde, untersuchten wir die Photochemie von **30** mit Licht der Wellenlänge $\lambda = 254$ nm. Die Verfolgung mittels ¹H-NMR zeigte eine Abnahme der Signale von **30** und die Zunahme neuer Signale. Bei einer der Verbindungen, die aus der Reaktionsmischung isoliert werden konnte, handelt es sich um 1,3,2,4-Diazadiboretidin **36**, ein Dimer des Iminoborans **37** (Schema 28). Von Verbindung **36** konnte auch eine Kristallstrukturanalyse durchgeführt werden (Abbildung 9). Die Bildung von **37** konnte mittels ¹H- und ¹¹B-NMR festgestellt werden. Im ¹¹B-NMR entsteht ein Signal bei 17.4 ppm, das im typischen Bereich der N-Silyl substituierten Iminoborane (16-22 ppm)^[13, 16b, 17] liegt und mit dem berechneten Wert von 17.2 ppm (B3LYP/6-311+G**) übereinstimmt. Die NMR-Signale von **37** nehmen langsam über mehrere Stunden ab, wobei gleichzeitig die Signale von **36** zunehmen. Diese Befunde lassen vermuten, dass die Photochemie in der Lösung ähnlich der unter Matrixisolationsbedingungen verläuft.



Schema 28. Cycloreversion von **35** durch Photolyse mit $\lambda = 254$ nm in Lösung.

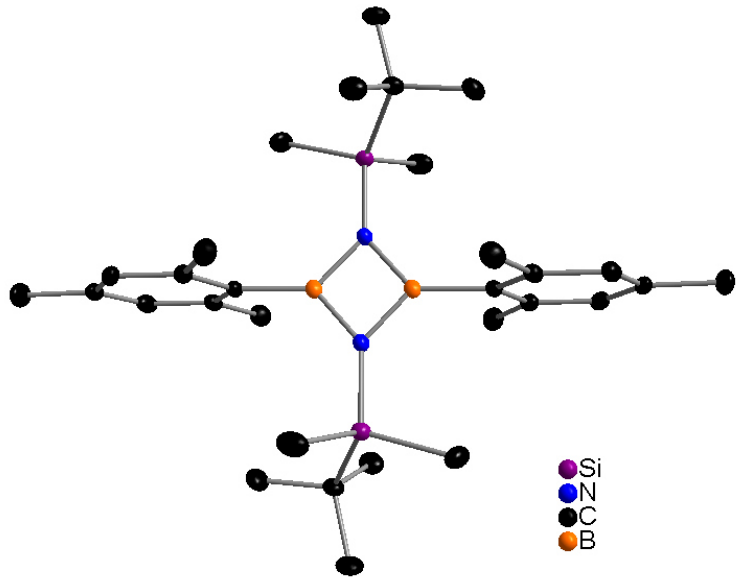
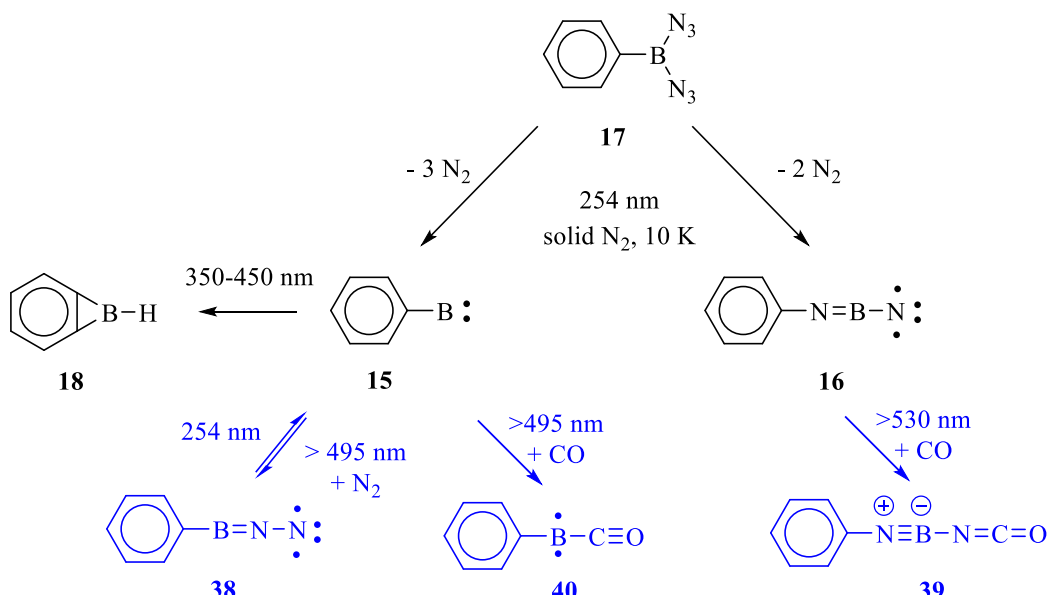


Abbildung 9. Kristallstruktur von **36**.

4.4 Phenylborylen

4.4.1 UV/Vis-Spektroskopie

Um photochemische Reaktionen von **15** gezielt zu untersuchen, wurde zunächst die bekannte Photochemie von **17**, die sich auf IR- und ESR-Spektroskopie beschränkte, mit UV/Vis-Spektroskopie untersucht. Eine Stickstoffmatrix von **17**, dessen Absorptionsmaximum bei 250 nm ist, wurde mit Licht der Wellenlänge $\lambda = 254$ nm belichtet. Das resultierende UV/Vis-Spektrum (Abbildung 10) zeigt Banden des Nitrens **16** und ein Signal bei 375 nm, das **15** zugeordnet werden konnte. Die Zuordnung der einzelnen Banden erfolgte durch einen Vergleich mit quantenchemischen Rechnungen, unterschiedlichem Verhalten der Banden bei Photolyse mit Licht unterschiedlicher Wellenlängen und durch den Vergleich mit den Ergebnissen der IR- und ESR-Versuche.



Schema 29. Bildung von Borylen **15** und Nitren **16** durch die photochemische Zersetzung von **17** und Reaktionen von **15** mit N₂ und CO und von **16** mit CO unter Matrixisolationsbedingungen. Reaktion und Reaktionsprodukte, die blau markiert sind, wurden in dieser Arbeit untersucht.

Wird nun diese Matrix mit Licht der Wellenlängen $\lambda = 350\text{-}450$ nm bestrahlt, so nimmt nur die Bande 375 nm ab, während die anderen Banden unverändert bleiben. Aus früheren Versuchen ist bekannt, dass unter diesen Bedingungen **15** zu **18** reagiert (Schema 29).^[55] Wird die Matrix stattdessen längerwellig ($\lambda = 530\text{-}630$ nm) bestrahlt, so nehmen die Signale von **16** leicht ab (Abbildung 11a). Das Signal von **15** bleibt dabei unverändert. Bei einer anschließenden Photolyse mit Licht der Wellenlängen $\lambda = 495\text{-}630$ nm nimmt das Signal von

15 ab (Abbildung 11b). In unserer Gruppe wurden kürzlich die angeregten Zustände von **15** untersucht.^[68] Es wurde gezeigt, dass für **15** zwei Absorptionsbanden im UV/Vis-Spektrum zu erwarten sind. Die intensive Absorption ist für 392 nm (TD-B3LYP, $f=0.041$) und die deutlich schwächere für 529 nm berechnet.^[68] In den UV/Vis-Versuchen ist die Zuordnung der schwachen Bande aufgrund der geringen Intensität schwierig. Sie liegt vermutlich bei 518 nm (Abbildung 11). In einer anschließenden Photolyse mit $\lambda = 254$ nm nimmt die Bande von **15** wieder zu. Aus den IR-Versuchen (siehe unten) ist bekannt, dass bei der Photolyse mit $\lambda = 495\text{--}630$ nm **15** mit N₂ zum Ph-BNN (**38**) reagiert. Diese Reaktion ist reversibel, wenn mit $\lambda = 254$ nm belichtet wird (Schema 29).

Die eben beschriebenen Versuche wurden mit einer CO-dotierten (5% CO) Stickstoffmatrix wiederholt, um Reaktionen von **15** und **16** mit CO zu untersuchen. Bei der Photolyse mit $\lambda = 530\text{--}630$ nm ist eine starke Abnahme der Banden von **16** zu sehen. Durch den Vergleich mit den IR-Versuchen ist ersichtlich, dass dabei das Isocyanat **39** (Schema 29) entsteht. (Ob bei den Versuchen mit N₂ unter den gleichen Bedingungen das Azid Ph-NB-N₃ entsteht, konnte nicht eindeutig belegt werden.) Weiterhin nimmt auch hier das Signal von **15** durch das Bestrahlen mit $\lambda = 495\text{--}630$ nm ab und eine neue Bande bei 303 nm nimmt zu. Dabei entsteht das Photoprodukt **40** (Schema 29).

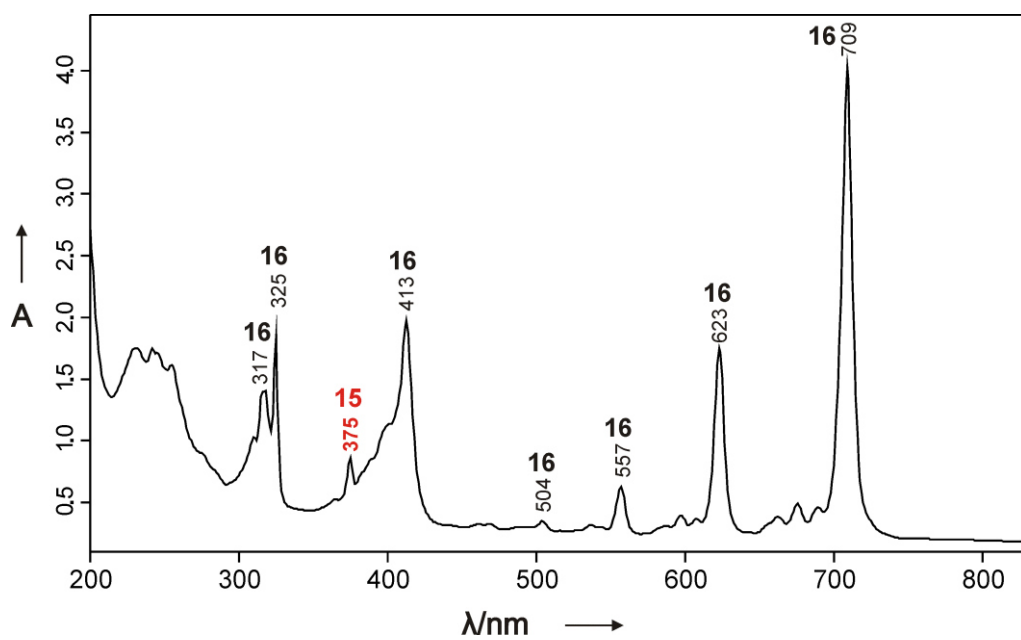


Abbildung 10. UV/Vis-Spektrum nach der Photolyse von **17** in einer Stickstoffmatrix bei 7 K für 35 min mit $\lambda = 254$ nm. Die Signale der dabei gebildeten Verbindungen **15** und **16** sind markiert.

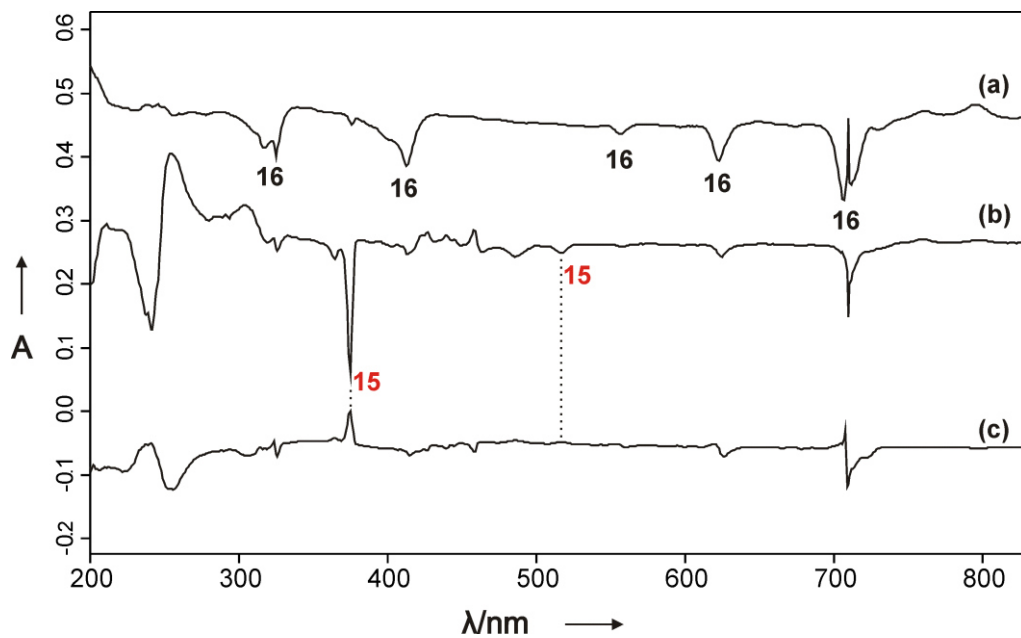


Abbildung 11. UV/Vis-Differenzspektren zeigen Veränderungen in den UV/Vis-Spektren (die nach der Photolyse mit $\lambda = 254$ nm von **17** in einer N_2 -Matrix aufgenommen wurden, siehe Abbildung 10) nach der Photolyse mit (a) $\lambda = 530-630$ nm für 2h , (b) $\lambda = 495-630$ nm für 1h und (c) mit $\lambda = 254$ nm für 25min. Signale, die nach unten zeigen nehmen ab und Signale die nach oben zeigen zunehmen zu.

4.4.2 IR-Spektroskopie

Aufgrund der UV/Vis-Versuche konnten die IR-Versuche optimiert werden, da nun die Absorptionen von **15** und **16** bekannt waren. Wie bereits früher beschrieben,^[55] wurde **17** in einer Stickstoffmatrix bei 4 K isoliert und photochemisch (mit $\lambda = 254$ nm) zu den Verbindungen **15** und **16** zersetzt. Auch hier wurde anschließend zunächst mit $\lambda = 530\text{-}630$ nm belichtet. Dabei nahmen die Signale von **16** leicht ab. Die anschließende Photolyse mit $\lambda = 495\text{-}630$ nm zeigte eine Abnahme von **15** und Zunahme neuer Signale im Bereich von $1417\text{-}1387$ cm^{-1} (Abbildung 12). Eine Bildung von **18** wurde dabei nicht beobachtet. Der Vergleich mit dem berechneten Wert von 1433.0 cm^{-1} [B3LYP/6-311+G**] lässt die Bildung von **38** vermuten. Der Einsatz von isotopenmarkiertem Stickstoff ($^{15}\text{N}_2$) zeigt eine Isotopenverschiebung von ca. $25\text{-}28$ cm^{-1} und stimmt mit der berechneten Isotopenverschiebung von 24.9 cm^{-1} für **38** überein. Die anschließende Photolyse mit $\lambda = 254$ nm zeigt die reversible Reaktion (Signale von **15** nehmen zu und Signale von **38** nehmen ab, Abbildung 12).

In einer CO-dotierten Stickstoffmatrix (5% CO) wird die Reaktion zwischen **16** und CO zu **39** durch die Photolyse mit $\lambda = 530\text{-}630$ nm beobachtet (Schema 29). Die Isocyanat-Bande zeigt die erwarteten Isotopenverschiebungen, die mit berechneten Werten (B3LYP/6-311+G**) übereinstimmen, wenn ^{13}CO und C^{18}O verwendet werden (Abbildung 13). Die Signale der Iminoboranschwingung zeigen dabei, wie erwartet, keine Isotopenverschiebungen. Bei der anschließenden Photolyse mit $\lambda = 495\text{-}630$ nm nehmen die Signale von **15** ab und neue Signale von **40** nehmen zu (Abbildung 14). Die gleichen Signale entstehen bereits bei der Photolyse mit $\lambda = 254$ nm. Auch diese zeigen die erwartete Isotopenverschiebung. Es entsteht ein weiteres neues Signal bei 1980 cm^{-1} durch die Photolyse mit $\lambda = 495\text{-}630$ nm, das eine Isotopenverschiebung in der ^{13}CO - bzw. C^{18}O -dotierten Matrix zeigt (Abbildung 14). Vermutlich gehört es zu der zweifach koordinierten Verbindung $\text{PhB}(\text{CO})_2$.

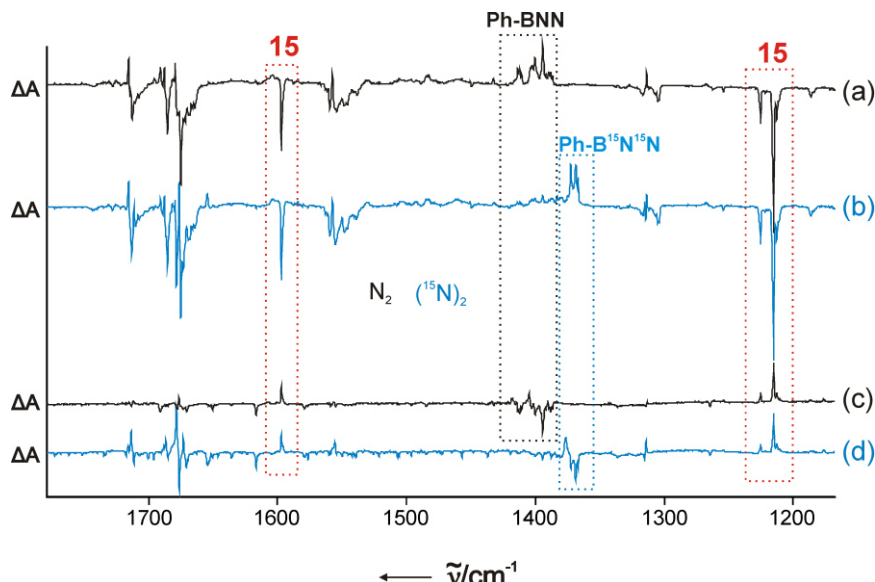


Abbildung 12. IR-Differenzspektren zeigen die reversible Reaktion zwischen **15** und N_2 . In schwarz sind die Differenzspektren einer N_2 -Matrix und in blau einer $(^{15}\text{N})_2$ -Matrix. Vor der Photolyse mit $\lambda = 495\text{-}630 \text{ nm}$ wurde eine Matrix, die **17** enthält, mit $\lambda = 254 \text{ nm}$ und anschließend mit $\lambda = 530\text{-}630 \text{ nm}$ belichtet. Differenzspektren (a) und (b) sind nach der Photolyse mit $\lambda = 495\text{-}630 \text{ nm}$ und Differenzspektren (c) und (d) nach der Photolyse mit $\lambda = 254 \text{ nm}$. Signale, die nach unten zeigen nehmen ab und Signale die nach oben zeigen nehmen zu.

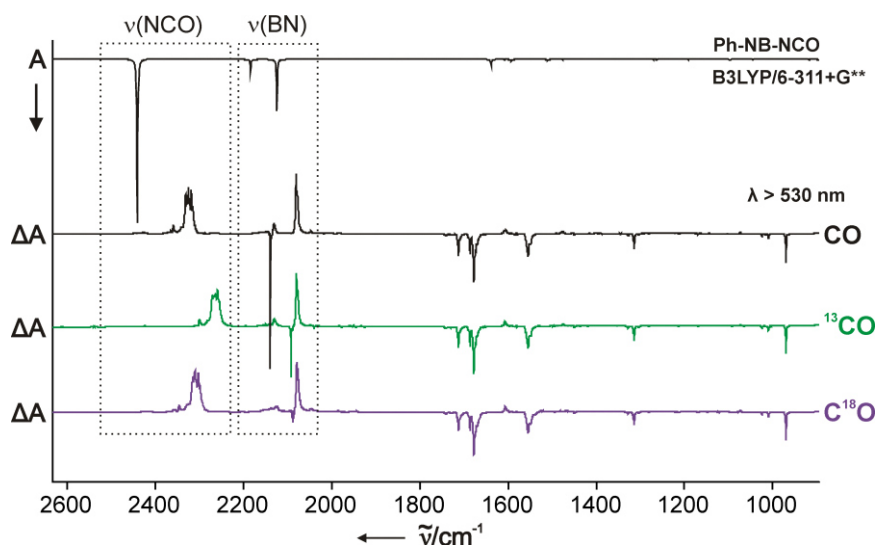


Abbildung 13. IR-Differenzspektren zeigen die Reaktion zwischen **16** und Kohlenstoffmonoxid durch Photolyse mit $\lambda = 530\text{-}630 \text{ nm}$. Vor der Photolyse mit $\lambda = 530\text{-}630 \text{ nm}$ wurde **17** in einer 5% $\text{CO}/^{13}\text{CO}/\text{C}^{18}\text{O}$ -dotierten N_2 -Matrix mit $\lambda = 254 \text{ nm}$ belichtet. Signale, die nach unten zeigen nehmen ab und Signale die nach oben zeigen nehmen zu. Oben befindet sich ein theoretisches Spektrum [B3LYP/6-311+G**] von **39**.

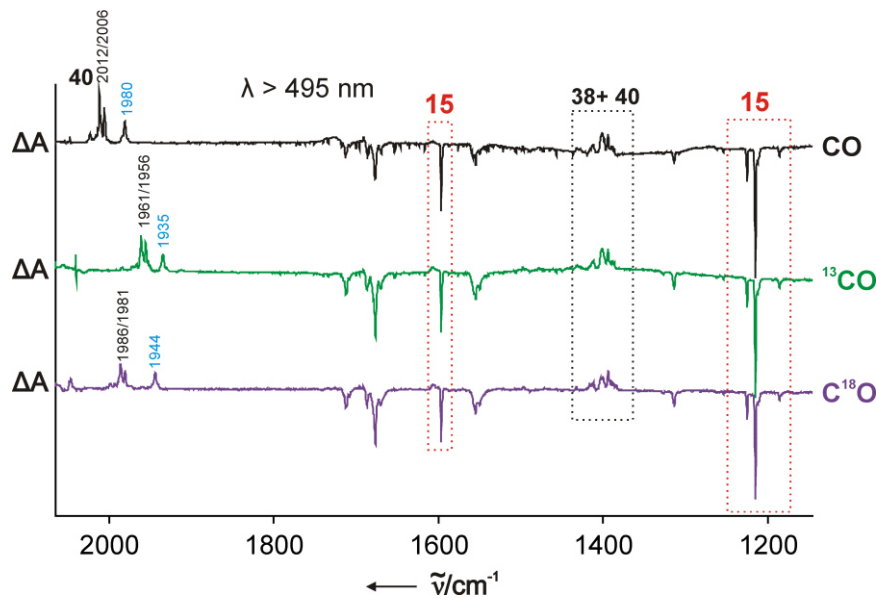


Abbildung 14. IR-Differenzspektren zeigen die Reaktion zwischen **15** und Kohlenstoffmonoxid durch Photolyse mit $\lambda = 495\text{-}630\text{ nm}$. Vor der Photolyse mit $\lambda = 495\text{-}630\text{ nm}$ wurde **17** in einer 5% CO/ ^{13}CO /C ^{18}O -dotierten N $_2$ -Matrix mit $\lambda = 254\text{ nm}$ und anschließend mit $\lambda = 530\text{-}630\text{ nm}$ belichtet. Signale, die nach unten zeigen nehmen ab und Signale die nach oben zeigen zu.

4.4.3 ESR-Spektroskopie

Ergänzend zur UV/Vis- und IR-Spektroskopie wurden ESR-Messungen der matrixisolierten Spezies durchgeführt. Frühere Berechnungen auf dem MRMP2-Theorieniveau sagen für **16** und **38** einen Triplet-Grundzustand ($^3\text{A}_2$) voraus.^[69] **40** besitzt ebenfalls einen Triplet-Grundzustand ($^3\text{A}_2$), der 10.1 kcal mol $^{-1}$ in Energie niedriger ist als der $^1\text{A}_2$ -Zustand und 12.0 kcal mol $^{-1}$ niedriger als der $^1\text{A}_1$ -Zustand [CASPT2-CAS(12,12)/cc-pVTZ//B3LYP/6-311+G**]. Ein Triplet-Grundzustand für **16** wurde bereits früher gezeigt^[55] und konnte in unseren Versuchen reproduziert werden ($|D/hc| = 1.247\text{ cm}^{-1}$ und $|E/hc| = 0.002\text{ cm}^{-1}$ in einer N $_2$ -Matrix). Es ist jeweils das intensivste Signal, das in unseren Experimenten gemessen wurde (Abbildung 15). Der kleine E-Wert zeigt, dass die (NBN)-Einheit zylindrisch ist. Dies bestätigt eine lineare Struktur, die quantenchemisch berechnet wurde.^[69] Daneben wurde ein schwaches Signal mit den Werten $|D/hc| = 0.882\text{ cm}^{-1}$ und $|E/hc| = 0.001\text{ cm}^{-1}$ gemessen (Abbildung 15a-c). Dieses nimmt an Intensität zu, wenn die Matrix mit $\lambda = 505\text{ nm}$ belichtet wird und nimmt durch Photolyse mit $\lambda = 254\text{ nm}$ ab. Aus den UV/Vis- und IR-Ergebnissen ist bereits bekannt, dass unter diesen Bedingungen Verbindung **38** entsteht und wieder abgebaut wird. In der CO-dotierten N $_2$ -Matrix entsteht neben den Signalen von **16** und **38** ein weiteres Signal ($|D/hc| = 0.525\text{ cm}^{-1}$ und $|E/hc| = 0.005\text{ cm}^{-1}$, Abbildung 15d-f), das der Verbindung **40** zugeordnet wird. Dieses entsteht bereits nach der ersten Belichtung mit $\lambda = 254\text{ nm}$ und nimmt mit der Photolyse

mit $\lambda = 505$ nm zu. Gleichzeitig wächst das Signal von **38**. Die gleichzeitige Zunahme von **38** und **40** wurde bereits in den IR-Spektren beobachtet (Abbildung 14). Verbindung **16** nimmt in der CO-dotierten N₂-Matrix ab, wenn die Matrix mit $\lambda = 630$ nm belichtet wird. Dies ist ersichtlich, da aus den IR-Versuchen bekannt ist, dass aus **16** und CO sich das Isocyanat **39** bildet. Die D-Werte in unseren Versuchen nehmen in der Reihenfolge **16** > **38** > **40** ab. Abbildung 16 zeigt die berechneten Spindichten von **16**, **38** und **40**. Darin ist zu erkennen, dass die Spindichten am terminalen N-Atom in **16** und **38** bzw. am O-Atom in **40** von links nach rechts abnehmen. **16** hat einen ähnlichen D-Wert wie Borylnitrene, die eine geringe Delokalisierung besitzen.^[27a, 70] Das B-Atom in **40** ist isoelektronisch zu dem C-Atom in Carbenen. Dies wird durch ähnliche D-Werte von **40** und Phenylcarben ($|D/hc| = 0.518 \text{ cm}^{-1}$)^[71] bestätigt.

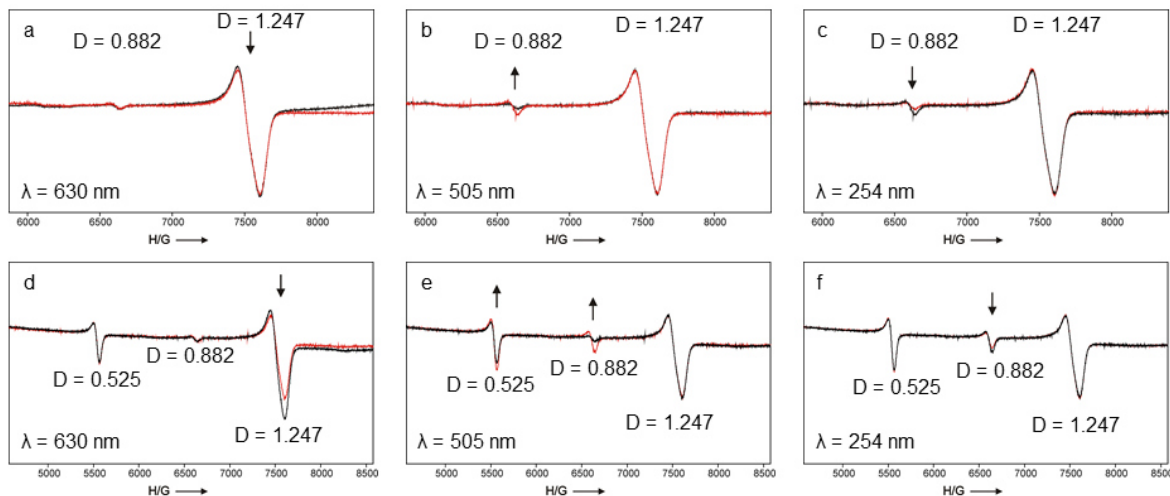
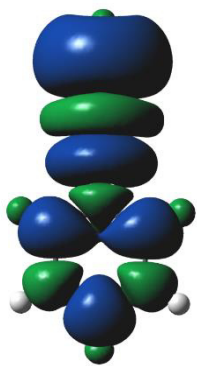
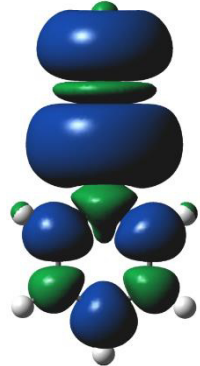


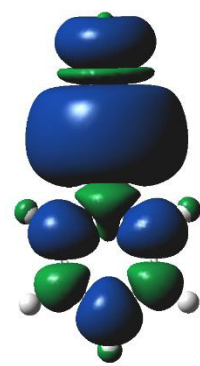
Abbildung 15. ESR-Spektren (4 K) nach der Photolyse ($\lambda = 254$ nm) von **17** in N₂ (Bilder a-c) und in N₂ dotiert mit 5% CO (Bilder d-f). Spektren vor (schwarz) und nach (rot) der Belichtung mit der jeweils angezeigten Wellenlänge im Bild. Pfeile deuten auf eine Zunahme oder Abnahme eines Signals.



PhNBN (**16**)



PhBNN (**38**)



PhBCO (**40**)

Abbildung 16. Theoretisch berechnete Spindichten (UB3LYP/6-311+G**).

Durch Kombination verschiedener Spektroskopiemethoden (UV/Vis-, IR- und ESR-Spektroskopie) in Verbindung mit Matrixisolationstechniken konnten die Reaktionen von **15** und **16** mit N₂ und CO untersucht werden. Dadurch war es möglich die Absorptionsbanden von **15** und **16** zuzuordnen. Borylen **15** besitzt eine Absorptionsbande bei 375 nm und eine sehr schwache Bande vermutlich bei 518 nm. Die Verbindungen **16**, **38** und **40** besitzen eine lineare Struktur, sowie einen Triplett-Grundzustand. **38** und **40** können als die ersten Bor-Analoga von Diazoalkanen (R₂CNN) und Ketenen (R₂CCO) angesehen werden.

5. Literaturverzeichnis

- [1] a) T. Hatakeyama, S. Hashimoto, S. Seki, M. Nakamura, *J. Am. Chem. Soc.* **2011**, *133*, 18614; b) C. A. Jaska, D. J. H. Emslie, M. J. D. Bosdet, W. E. Piers, T. S. Sorensen, M. Parvez, *J. Am. Chem. Soc.* **2006**, *128*, 10885; c) S. M. Mansell, N. C. Norman, C. A. Russell, *Dalton Trans.* **2010**, *39*, 5084; d) X.-Y. Wang, H.-R. Lin, T. Lei, D.-C. Yang, F.-D. Zhuang, J.-Y. Wang, S.-C. Yuan, J. Pei, *Angew. Chem. Int. Ed.* **2013**, *52*, 3117; e) E. R. Abbey, A. N. Lamm, A. W. Baggett, L. N. Zakharov, S.-Y. Liu, *J. Am. Chem. Soc.* **2013**, *135*, 12908; f) E. R. Abbey, L. N. Zakharov, S.-Y. Liu, *J. Am. Chem. Soc.* **2011**, *133*, 11508.
- [2] P. G. Campbell, A. J. Marwitz, S. Y. Liu, *Angew. Chem. Int. Ed.* **2012**, *51*, 6074.
- [3] a) M. J. D. Bosdet, W. E. Piers, T. S. Sorensen, M. Parvez, *Angew. Chem. Int. Ed.* **2007**, *46*, 4940; b) M. Lepeltier, O. Lukyanova, A. Jacobson, S. Jeeva, D. F. Perepichka, *Chem. Commun. (Cambridge, U. K.)* **2010**, *46*, 7007; c) T. Taniguchi, S. Yamaguchi, *Organometallics* **2010**, *29*, 5732; d) J. Dosso, J. Tasserouf, F. Fasano, D. Marinelli, N. Biot, A. Fermi, D. Bonifazi, *Angew. Chem. Int. Ed.* **2017**, *56*, 4483.
- [4] a) X.-Y. Wang, J.-Y. Wang, J. Pei, *Chem. - Eur. J.* **2015**, *21*, 3528; b) M. J. D. Bosdet, W. E. Piers, *Can. J. Chem.* **2009**, *87*, 8; c) Z. Liu, T. B. Marder, *Angew. Chem. Int. Ed.* **2008**, *47*, 242.
- [5] E. Wiberg, A. Bolz, *Ber. Dtsch. Chem. Ges. B* **1940**, *73B*, 209.
- [6] A. Stock, E. Pohland, *Ber. Dtsch. Chem. Ges.* **1926**, *59*, 2215.
- [7] M. J. S. Dewar, V. P. Kubba, R. Pettit, *J. Chem. Soc. (Res.)* **1958**, 3073.
- [8] a) M. J. S. Dewar, P. A. Marr, *J. Am. Chem. Soc.* **1962**, *84*, 3782; b) D. G. White, *J. Am. Chem. Soc.* **1963**, *85*, 3634.
- [9] a) A. J. Ashe, Fang, *Org. Lett.* **2000**, *2*, 2089; b) A. J. Ashe, X. Fang, X. Fang, J. W. Kampf, *Organometallics* **2001**, *20*, 5413.
- [10] a) A. J. V. Marwitz, M. H. Matus, L. N. Zakharov, D. A. Dixon, S.-Y. Liu, *Angew. Chem. Int. Ed.* **2009**, *48*, 973; b) E. R. Abbey, L. N. Zakharov, S.-Y. Liu, *J. Am. Chem. Soc.* **2008**, *130*, 7250.
- [11] a) H. Braunschweig, C. Hörl, L. Mailänder, K. Radacki, J. Wahler, *Chem. Eur. J.* **2014**, *20*, 9858; b) H. Braunschweig, A. Gackstatter, T. Kupfer, T. Scheller, F. Hupp, A. Damme, N. Arnold, W. C. Ewing, *Chem. Sci.* **2015**, *6*, 3461.
- [12] a) P. Paetzold, C. V. Pllotho, G. Schmid, R. Boese, B. Schrader, D. Bougeard, U. Pfeiffer, R. Gleiter, W. Schüfer, *Chem. Ber.* **1984**, *117*, 1089; b) N. C. Baird, R. K. Datta, *Inorg. Chem.* **1972**, *11*, 17; c) V. M. Rosas-Garcia, *Comp. Theor. Chem.* **2011**, 967, 160.
- [13] P. Paetzold, *Adv. Inorg. Chem.* **1987**, *31*, 123.
- [14] a) F. Dahcheh, D. Martin, D. W. Stephan, G. Bertrand, *Angew. Chem. Int. Ed.* **2014**, *53*, 13159; b) F. Dahcheh, D. W. Stephan, G. Bertrand, *Chem. - Eur. J.* **2015**, *21*, 199; c) H. Braunschweig, W. C. Ewing, K. Geetharani, M. Schäfer, *Angew. Chem. Int. Ed.* **2015**, *54*, 1662; d) A. K. Swarnakar, C. Hering-Junghans, K. Nagata, M. J. Ferguson, R. McDonald, N. Tokitoh, E. Rivard, *Angew. Chem. Int. Ed.* **2015**, *54*, 10666; e) A. K. Swarnakar, C. Hering-Junghans, M. J. Ferguson, R. McDonald, E. Rivard, *Chem. Sci.* **2017**, *8*, 2337.
- [15] P. Paetzold, A. Richter, T. Thijssen, S. Wuertenberg, *Chem. Ber.* **1979**, *112*, 3811.

- [16] a) P. Paetzold, *Pure Appl. Chem.* **1991**, *63*, 345; b) H. Nöth, *Angew. Chem. Int. Ed.* **1988**, *27*, 1603; c) E. v. Steuber, G. Elter, M. Noltemeyer, H.-G. Schmidt, A. Meller, *Organometallics* **2000**, *19*, 5083.
- [17] M. Haase, U. Klingebiel, *Angew. Chem. Int. Ed.* **1985**, *24*, 324.
- [18] P. G. Wenthold, R. R. Squires, *J. Am. Chem. Soc.* **1994**, *116*, 6401.
- [19] a) J.-A. Garcia-Lopez, M. F. Greaney, *Chem. Soc. Rev.* **2016**, *45*, 6766; b) D. Pérez, D. Peña, E. Guitián, *Eur. J. Org. Chem.* **2013**, *2013*, 5981; c) A. V. Dubrovskiy, N. A. Markina, R. C. Larock, *Org. Biomol. Chem.* **2013**, *11*, 191; d) C. M. Gampe, E. M. Carreira, *Angew. Chem. Int. Ed.* **2012**, *51*, 3766; e) P. M. Tadross, B. M. Stoltz, *Chem. Rev.* **2012**, *112*, 3550; f) H. Yoshida, K. Takaki, *Synlett* **2012**, *23*, 1725; g) A. Bhunia, S. R. Yetra, A. T. Biju, *Chem. Soc. Rev.* **2012**, *41*, 3140; h) C. Wentrup, *Aust. J. Chem.* **2010**, *63*, 979; i) R. Sanz, *Org. Prep. Proced. Int.* **2008**, *40*, 215; j) H. H. Wenk, M. Winkler, W. Sander, *Angew. Chem. Int. Ed.* **2003**, *42*, 502; k) H. Pellissier, M. Santelli, *Tetrahedron* **2003**, *59*, 701.
- [20] R. Stoermer, B. Kahlert, *Ber. Dtsch. Chem. Ges.* **1902**, *35*, 1633.
- [21] a) G. Wittig, *Naturwissenschaften* **1942**, *30*, 696; b) G. Wittig, G. Harborth, *Ber. Dtsch. Chem. Ges.* **1944**, *77*, 306; c) G. Wittig, L. Pohmer, *Chem. Ber.* **1956**, *89*, 1334.
- [22] a) J. D. Roberts, H. E. Simmons, Jr., L. A. Carlsmith, W. C. Vaughan, *J. Am. Chem. Soc.* **1953**, *75*, 3290; b) J. D. Roberts, D. A. Semenow, H. E. Simmons, Jr., L. A. Carlsmith, *J. Am. Chem. Soc.* **1956**, *78*, 601; c) M. Panar, J. D. Roberts, *J. Am. Chem. Soc.* **1960**, *82*, 3629.
- [23] O. L. Chapman, K. Mattes, C. L. McIntosh, J. Pacansky, G. V. Calder, G. Orr, *J. Am. Chem. Soc.* **1973**, *95*, 6134.
- [24] a) R. Warmuth, *Angew. Chem. Int. Ed.* **1997**, *36*, 1347; b) R. Warmuth, *Eur. J. Org. Chem.* **2001**, *2001*, 423.
- [25] a) P. J. Fazen, L. A. Burke, *Inorg. Chem.* **2006**, *45*, 2494; b) M. Müller, C. Maichle-Mössmer, H. F. Bettinger, *Angew. Chem. Int. Ed.* **2014**, *53*, 9380.
- [26] J. Münster, P. Paetzold, E. Schröder, H. Schwan, T. von Bennigsen-Mackiewicz, *Z. Anorg. Allg. Chem.* **2004**, *630*, 2641.
- [27] a) M. Filthaus, L. Schwertmann, P. Neuhaus, R. W. Seidel, I. M. Oppel, H. F. Bettinger, *Organometallics* **2012**, *31*, 3894; b) M. T. Nguyen, *J. Chem. Soc., Chem. Commun.* **1987**, 342.
- [28] a) J. Hahn, Dissertation Universität Tübingen **2017**; b) S. Biswas, M. Müller, C. Tönshoff, K. Eichele, C. Maichle-Mössmer, A. Ruff, B. Speiser, H. F. Bettinger, *Eur. J. Org. Chem.* **2012**, *2012*, 4634.
- [29] R. Köster, S. Hattori, Y. Morita, *Angew. Chem. Int. Ed.* **1965**, *4*, 695.
- [30] K. Edel, Diplomarbeit Universität Tübingen **2013**.
- [31] G. Nagendrappa, *Resonance* **2001**, *6*, 74.
- [32] a) A. Kekulé, *Bull. Soc. Chim. Fr.* **1865**, *3*, 98; b) A. Kekulé, *Liebigs Ann. Chem.* **1866**, *137*, 129.
- [33] J. Dewar, *Proc. R. Soc. Edinb.* **1867**, *6*, 82.
- [34] A. Ladenburg, *Ber. Dtsch. Chem. Ges.* **1869**, *2*, 140.
- [35] T. J. Katz, N. Acton, *J. Am. Chem. Soc.* **1973**, *95*, 2738.
- [36] E. E. van Tamelen, S. P. Pappas, *J. Am. Chem. Soc.* **1963**, *85*, 3297.
- [37] K. E. Wilzbach, J. S. Ritscher, L. Kaplan, *J. Am. Chem. Soc.* **1967**, *89*, 1031.
- [38] W. E. Billups, M. M. Haley, *Angew. Chem. Int. Ed.* **1989**, *28*, 1711.
- [39] a) H. R. Ward, J. S. Wishnok, *J. Am. Chem. Soc.* **1968**, *90*, 5353; b) D. E. Johnstone, J. R. Sodeau, *J. Phys. Chem.* **1991**, *95*, 165.

- [40] L. Kaplan, K. E. Wilzbach, *J. Am. Chem. Soc.* **1967**, *89*, 1030.
- [41] a) R. Breslow, J. Napierski, A. H. Schmidt, *J. Am. Chem. Soc.* **1972**, *94*, 5906; b) P. Lechkten, R. Breslow, A. H. Schmidt, N. J. Turro, *J. Am. Chem. Soc.* **1973**, *95*, 3025.
- [42] a) E. E. van Tamelen, *Angew. Chem. Int. Ed.* **1965**, *4*, 738; b) E. E. Van Tamelen, *Acc. Chem. Res.* **1972**, *5*, 186; c) R. B. Woodward, R. Hoffmann, *Angew. Chem., Int. Ed. Engl.* **1969**, *8*, 781.
- [43] R. W. A. Havenith, L. W. Jenneskens, J. H. van Lenthe, *J. Mol. Struct. (Theochem)* **1999**, *492*, 217.
- [44] S. A. Brough, A. N. Lamm, S.-Y. Liu, H. F. Bettinger, *Angew. Chem. Int. Ed.* **2012**, *51*, 10880.
- [45] H. F. Bettinger, O. Hauler, *Beilstein J. Org. Chem.* **2013**, *9*, 761.
- [46] M. Soleilhavoup, G. Bertrand, *Angew. Chem. Int. Ed.* **2017**, *56*, 10282.
- [47] a) D. Bourissou, O. Guerret, F. P. Gabbaï, G. Bertrand, *Chem. Rev.* **2000**, *100*, 39; b) K. Hirai, T. Itoh, H. Tomioka, *Chem. Rev.* **2009**, *109*, 3275; c) J. Vignolle, X. Cattoën, D. Bourissou, *Chem. Rev.* **2009**, *109*, 3333.
- [48] a) M. S. Platz, in *Reactive Intermediate Chemistry*, John Wiley & Sons, Inc., **2005**, pp. 501; b) N. P. Gritsan, M. S. Platz, *Chem. Rev.* **2006**, *106*, 3844; c) G. Dequirez, V. Pons, P. Dauban, *Angew. Chem. Int. Ed.* **2012**, *51*, 7384.
- [49] a) P. L. Timms, *J. Am. Chem. Soc.* **1968**, *90*, 4585; b) P. L. Timms, *Acc. Chem. Res.* **1973**, *6*, 118.
- [50] B. Pachaly, R. West, *Angew. Chem. Int. Ed.* **1984**, *23*, 454.
- [51] W. J. Grigsby, P. P. Power, *J. Am. Chem. Soc.* **1996**, *118*, 7981.
- [52] M. Ito, N. Tokitoh, T. Kawashima, R. Okazaki, *Tetrahedron Lett.* **1999**, *40*, 5557.
- [53] a) H. Braunschweig, R. D. Dewhurst, A. Schneider, *Chem. Rev.* **2010**, *110*, 3924; b) H. Braunschweig, R. D. Dewhurst, V. H. Gessner, *Chem. Soc. Rev.* **2013**, *42*, 3197.
- [54] a) L. Andrews, P. Hassanzadeh, J. M. L. Martin, P. R. Taylor, *J. Phys. Chem.* **1993**, *97*, 5839; b) P. Hassanzadeh, L. Andrews, *J. Phys. Chem.* **1993**, *97*, 4910; c) C. A. Thompson, L. Andrews, *J. Am. Chem. Soc.* **1995**, *117*, 10125; d) C. A. Thompson, L. Andrews, J. M. L. Martin, J. El-Yazal, *J. Phys. Chem.* **1995**, *99*, 13839; e) L. Andrews, D. V. Lanzisera, P. Hassanzadeh, Y. Hannachi, *J. Phys. Chem. A* **1998**, *102*, 3259.
- [55] H. F. Bettinger, *J. Am. Chem. Soc.* **2006**, *128*, 2534.
- [56] I. R. Dunkin, *Matrix-Isolation Techniques*, Oxford University Press, Oxford, **1998**.
- [57] G. Maier, H. P. Reisenauer, J. Henkelmann, C. Kliche, *Angew. Chem. Int. Ed.* **1988**, *27*, 295.
- [58] a) M. Barry, R. F. C. Brown, F. W. Eastwood, D. A. Gunawardana, C. Vogel, *Aust. J. Chem.* **1984**, *37*, 1643; b) C. Wentrup, R. Blanch, H. Briehl, G. Gross, *J. Am. Chem. Soc.* **1988**, *110*, 1874; c) R. F. C. Brown, F. W. Eastwood, *Synlett* **1993**, *1993*, 9.
- [59] a) N. A. Burton, G. E. Quelch, M. M. Gallo, H. F. Schaefer, *J. Am. Chem. Soc.* **1991**, *113*, 764; b) E. W.-G. Diau, J. Casanova, J. D. Roberts, A. H. Zewail, *Proc. Natl. Acad. Sci. U.S.A.* **2000**, *97*, 1376; c) M. Winkler, B. Cakir, W. Sander, *J. Am. Chem. Soc.* **2004**, *126*, 6135; d) M. Winkler, *J. Phys. Chem. A* **2005**, *109*, 1240.

- [60] a) M. Winkler, W. Sander, *Aust. J. Chem.* **2010**, *63*, 1013; b) L. V. Moskaleva, L. K. Madden, M. C. Lin, *Phys. Chem. Chem. Phys.* **1999**, *1*, 3967.
- [61] a) W. Sander, M. Exner, M. Winkler, A. Balster, A. Hjerpe, E. Kraka, D. Cremer, *J. Am. Chem. Soc.* **2002**, *124*, 13072; b) R. R. Jones, R. G. Bergman, *J. Am. Chem. Soc.* **1972**, *94*, 660; c) R. G. Bergman, *Acc. Chem. Res.* **1973**, *6*, 25.
- [62] a) Y. Osamura, H. F. Schaefer, S. K. Gray, W. H. Miller, *J. Am. Chem. Soc.* **1981**, *103*, 1904; b) K. M. Ervin, J. Ho, W. C. Lineberger, *J. Chem. Phys.* **1989**, *91*, 5974; c) M. M. Gallo, T. P. Hamilton, H. F. Schaefer, *J. Am. Chem. Soc.* **1990**, *112*, 8714; d) N.-Y. Chang, M.-Y. Shen, C.-H. Yu, *J. Chem. Phys.* **1997**, *106*, 3237; e) J. Levin, H. Feldman, A. Baer, D. Ben-Hamu, O. Heber, D. Zajfman, Z. Vager, *Phys. Rev. Lett.* **1998**, *81*, 3347; f) J. F. Stanton, J. Gauss, *J. Chem. Phys.* **1999**, *110*, 1831; g) S. Zou, J. M. Bowman, *Chem. Phys. Lett.* **2003**, *368*, 421; h) S. Joseph, A. J. C. Varandas, *J. Phys. Chem. A* **2010**, *114*, 13277.
- [63] a) M. Winkler, W. Sander, *J. Phys. Chem. A* **2001**, *105*, 10422; b) B. A. Hess Jr, *Eur. J. Org. Chem.* **2001**, 2185; c) E. Kraka, J. Anglada, A. Hjerpe, M. Filatov, D. Cremer, *Chem. Phys. Lett.* **2001**, *348*, 115.
- [64] X. Zhang, A. T. Maccarone, M. R. Nimlos, S. Kato, V. M. Bierbaum, G. B. Ellison, B. Ruscic, A. C. Simmonett, W. D. Allen, H. F. Schaefer, *J. Chem. Phys.* **2007**, *126*, 044312.
- [65] G. Ghigo, A. Maranzana, G. Tonachini, *Phys. Chem. Chem. Phys.* **2014**, *16*, 23944.
- [66] O. L. Chapman, C. L. McIntosh, J. Pacansky, *J. Am. Chem. Soc.* **1973**, *95*, 614.
- [67] E. R. Lory, R. F. Porter, *J. Am. Chem. Soc.* **1973**, *95*, 1766.
- [68] M. Krasowska, M. Edelmann, H. F. Bettinger, *J. Phys. Chem. A* **2016**, *120*, 6332.
- [69] H. F. Bettinger, *J. Organomet. Chem.* **2006**, *691*, 4480.
- [70] a) H. F. Bettinger, H. Bornemann, *J. Am. Chem. Soc.* **2006**, *128*, 11128; b) H. F. Bettinger, M. Filthaus, H. Bornemann, I. M. Oppel, *Angew. Chem. Int. Ed.* **2008**, *47*, 4744.
- [71] A. M. Trozzolo, R. W. Murray, E. Wasserman, *J. Am. Chem. Soc.* **1962**, *84*, 4990.

Publikation 1

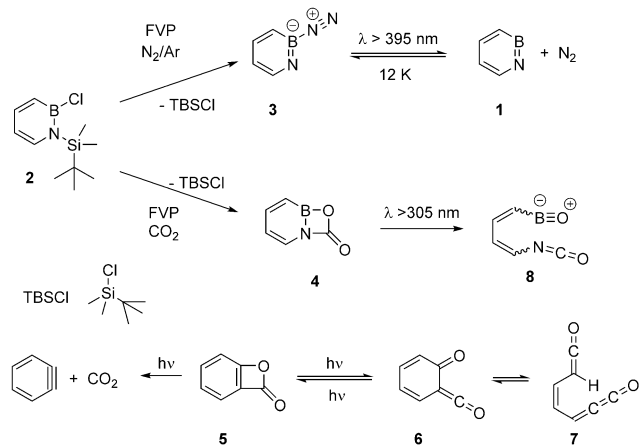
1,2-Azaborine: The Boron-Nitrogen Derivative of *ortho*-Benzyne**

Klara Edel, Sarah A. Brough, Ashley N. Lamm, Shih-Yuan Liu, and Holger F. Bettinger*

Dedicated to Professor Wolfram Sander on the occasion of his 60th birthday

Abstract: The BN analogue of *ortho*-benzyne, 1,2-azaborine, is generated by flash vacuum pyrolysis, trapped under cryogenic conditions, and studied by direct spectroscopic techniques. The parent BN aryne spontaneously binds N_2 and CO_2 , thus demonstrating its highly reactive nature. The interaction with N_2 is photochemically reversible. The CO_2 adduct of 1,2-azaborine is a cyclic carbamate which undergoes photocleavage, thus resulting in overall CO_2 splitting.

The chemistry of arynes, aromatic compounds that lack two hydrogen atoms, can be traced back to 1902.^[1] Since then, significant progress has turned *ortho*-benzyne, benzene derivatives that feature a highly strained triple bond, into invaluable reactive intermediates in all branches of organic synthesis.^[2] Formal substitution of the triply bonded carbon atoms of *ortho*-benzyne by an isoelectronic boron–nitrogen (BN) unit results in the unknown 1,2-azaborine (**1**; Scheme 1).^[3] The similarity of carbon and its BN derivatives is well documented in chemistry, including the graphite/hexagonal boron nitride and benzene/1,2-dihydro-1,2-azaborine pairs, as well as the Dewar forms of the latter.^[4] However, evidence for the existence of BN arynes is scarce and indirect as it comes from a self-trapping experiment.^[5] Here we show by direct spectroscopic techniques that **1** can exist as a reactive intermediate. We found that **1** can be generated by flash vacuum pyrolysis (FVP) from the precursor **2** by thermal elimination of *tert*-butyldimethylsilylchloride, and isolated in cryogenic matrices. 1,2-Azaborine spontaneously binds dinitrogen N_2 (adduct **3**) in a photochemically reversible trans-



Scheme 1. Generation and trapping of 1,2-azaborine (**1**) with N_2 and CO_2 by flash vacuum pyrolysis (FVP) of **2** at 800–850°C.

formation. The reaction of 1,2-azaborine with carbon dioxide (CO_2) and subsequent irradiation results in CO_2 splitting via a cyclic carbamate (**4**) intermediate. In contrast, the cyclic CO_2 adduct of the *ortho*-benzyne, benzoxet-2-one (**5**) undergoes, among other reactions, photodecarboxylation (Scheme 1).^[6] Our results show that the two heteroelements, boron and nitrogen, increase and modulate the reactivity compared to the all-carbon analogue. Our research introduces a novel class of reactive intermediates to chemistry. It may prove useful in materials and medicinal chemistry where the boron–nitrogen isoelectronic substitution is sought in order to modify the properties of electronic materials^[7] or biologically active compounds.^[8]

The thermally induced elimination of trialkylsilyl chlorides from suitable precursors has proven to be a reliable method for the synthesis of iminoboranes.^[9] Likewise, FVP of compound **2**^[10] (Scheme 1) at oven temperatures of 800–850°C, and isolation of pyrolysis products in a large excess of argon at 6 K yielded the corresponding silyl chloride as demonstrated by comparison with the infrared spectrum of an authentic sample. Besides the silyl chloride and the unconverted precursor, at least two sets of additional signals were observed (see Figure S1 in the Supporting Information). One set of signals decreased in intensity if increasingly larger amounts of N_2 were included into the argon matrix gas, and at the same time a set of new signals appeared. The most prominent signal among them is a band at 2266 cm^{-1} . This band is reminiscent of the dinitrogen stretching vibration $\nu(NN)$ observed previously by Maier et al. for the boraben-

[*] K. Edel, S. A. Brough, H. F. Bettinger
Institut für Organische Chemie, Universität Tübingen
Auf der Morgenstelle 18, 72076 Tübingen (Germany)
E-mail: Holger.Bettinger@uni-tuebingen.de

A. N. Lamm, S.-Y. Liu
Department of Chemistry and Biochemistry, University of Oregon
Eugene, OR 97403-1253 (USA)
S.-Y. Liu
Department of Chemistry, Boston College
Chestnut Hill, MA 02467-3860 (USA)

[**] The research was supported by the Deutsche Forschungsgemeinschaft and the National Institutes of Health (Grant R01-GM094541). We are grateful to the bwGRid project [<http://www.bwgrid.de>, member of the German D-Grid initiative, funded by Bundesministerium für Bildung und Forschung and Ministerium für Wissenschaft, Forschung und Kunst, Baden-Württemberg] for the computational resources. S.-Y.L. thanks the Camille Dreyfus Teacher-Scholar Awards Program for a Teacher Scholar award.

Supporting information for this article is available on the WWW under <http://dx.doi.org/10.1002/anie.201502967>.

zene-dinitrogen adduct. When employing $^{15}\text{N}_2$, the isotopic shift is 75 cm^{-1} , which is in good agreement with Maier et al.^[11] (73.3 cm^{-1}) for borabenzene-dinitrogen, and with computations at the CCSD(T)/TZ2P level of theory. The remaining signals of **3** have, at most, slight isotopic shifts which are in agreement with theoretical calculations (see Table S1 in the Supporting Information). The computations support assignment of the structure as **3**, having end-on coordinated dinitrogen (Scheme 1).

The adduct **3** was found to be photolabile. Irradiation of **3** with the output of a high-pressure mercury lamp ($\lambda > 395\text{ nm}$) resulted in disappearance of the set of signals assigned to **3** and the concomitant growth of a set of signals which are assigned to the parent 1,2-azaborine (**1**; Figure 1). This set of

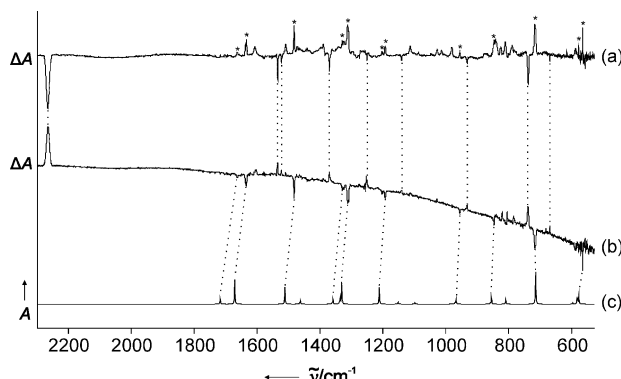


Figure 1. Generation of **1** through irradiation of **3** in Ar/N₂ (70:30). a) IR difference spectrum obtained from the pyrolysis products of **2** frozen at 6 K after two hours of irradiation with visible light ($\lambda > 395\text{ nm}$, 4 K). The decreasing signals (pointing downwards) belong to the dinitrogen adduct **3**, and the increasing signals belong to **1** (*). b) Difference spectrum after subsequent annealing for 30 min at 12 K (starting from 4 K), thus showing reversibility of the reaction **3** \rightleftharpoons **1** + N₂. c) Computed IR spectrum of **1** at the CCSD(T)/TZ2P level of theory.

signals is the same as that observed after thermolysis of **2** in the absence of dinitrogen. After photogenerating **1** from **3**, the latter could be regenerated by careful annealing of the matrix from 4 K to 12 K (Figure 1), thus indicating that the reaction of **1** + N₂ is essentially without a barrier. Both **3** and [$^{15}\text{N}_2$]-**3** behaved identically during photolysis and subsequent annealing. As expected, the bands assigned to **1** (see Table S2 in the Supporting Information) do not show any shifts in the presence of $^{15}\text{N}_2$.

After the successful generation of **1** and trapping with N₂, we used CO₂ as another small molecule for studying the reactivity of **1**. FVP of **2** and deposition with neat CO₂ at 52 K gave new signals in the IR absorption spectrum. The new signals which result from the reaction with CO₂ (Figure 2) can be attributed to the new species **4** by comparison with the computed spectrum (B3LYP/6-311 + G***) (see Figure S2 in the Supporting Information). Very prominent is the split band at $1874/79\text{ cm}^{-1}$ which is associated with the carbonyl stretching vibration $\nu(\text{CO})$ of the cyclic carbamate. Using isotopically labelled carbon dioxide, C(^{18}O)₂ and $^{13}\text{CO}_2$, isotopic shifts (Figure 2), which are in good agreement with

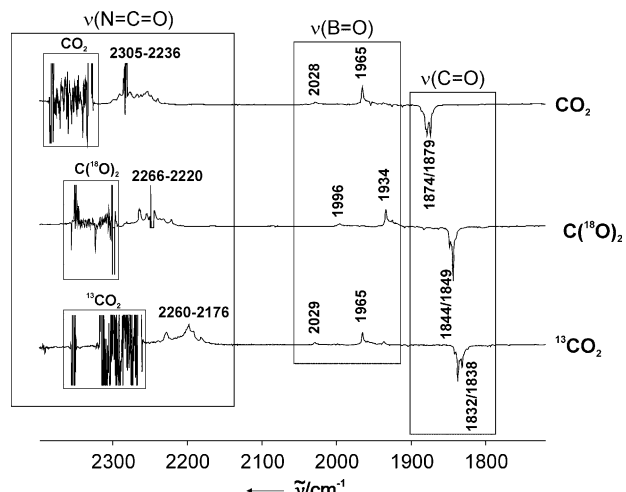


Figure 2. Difference spectra obtained upon irradiation ($\lambda > 305\text{ nm}$, 4 K) of **4**, which was generated by trapping of **1** with neat carbon dioxide at a deposition temperature of 52 K after FVP of **2** at 800°C . Carbonyl stretching of **4** disappears (bands pointing downwards) upon irradiation with UV light, while new bands for **8** are appearing (bands pointing upwards) for natural (top), C(^{18}O)₂ (center), and $^{13}\text{CO}_2$ (bottom) isotopomers.

calculations (B3LYP/6-311 + G**), were observed (see Figure S3 and Table S3 in the Supporting Information).

The carbon analogue of **4** is benzoxetone (**5**), which is known to be in a photochemical equilibrium with the α -oxoketene **6** (Scheme 1). Prolonged irradiation of **5** leads to *ortho*-benzyne.^[6a,b] Recently the reversible rearrangement of **6** into the ketene **7** was reported to proceed at high temperatures.^[6d] Irradiation of **4** with UV light ($\lambda > 305\text{ nm}$) did not result in loss of CO₂. Rather, **4** underwent ring opening through a retro [2+2] cycloaddition to give **8**, that is, a boron-nitrogen analogue of **7** (Scheme 1).

All signals of **4** disappeared simultaneously while new signals in the range 2303–2236 cm⁻¹ of the isocyanate group of **8** and the signals 1965 and 2208 cm⁻¹ of the BO unit^[12] appeared (Figure 2). The structure of **8** could be confirmed again through the use of isotopically labelled carbon dioxide and is in excellent agreement with the corresponding computed isotopic shifts (B3LYP/6-311 + G***; see Table S4 in the Supporting Information). Further irradiation with $\lambda = 254\text{ nm}$ leads to decomposition of **8** to an unknown product.

The most remarkable structural feature of **1** is the distortion of the hexagon with a small angle at N and a wide angle at boron in the singlet ground state, as noted previously.^[3,5] This feature can be rationalized by the difference in electronegativity: the more electronegative N atom prefers to have a lone pair (HOMO-1) in the molecular plane, while the more electropositive B atom prefers an empty in-plane orbital (LUMO) which has a strong p character (Figure 3a). The natural bond orbital (NBO) analysis arrives at occupancies of 1.80 e^- and 0.22 e^- for the lone pair and empty orbitals, respectively, and a pronounced $n(\text{N}) \rightarrow n^*(\text{B})$ interaction [$E(2) = 27.6\text{ kcal mol}^{-1}$] according to the second-order perturbation estimate of the donor-acceptor interaction in the NBO basis. The natural charges obtained from the NBO

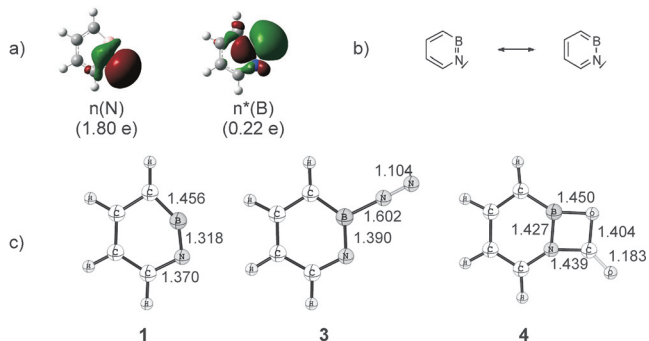


Figure 3. a) Natural bond orbitals (NBOs) and their occupation numbers which describe the in-plane part of the BN linkage as computed at the B3LYP/6-311+G** level of theory. b) Resonance forms of 1,2-azaborine. c) Structures and selected bond lengths in Å of molecules **1**, **3**, and **4** as computed at the CCSD(T)/TZ2P level of theory, $r(N_2) = 1.103 \text{ \AA}$.

analysis on N and B are large (-0.79 on N and $+0.97$ on B) while the Wiberg bond index between B and N is only 1.46. These data make the resonance forms (Figure 3b) a more reasonable description of the electronic structure of **1** than does the BN triple bond, despite the isoelectronic relationship with *ortho*-benzyne. In a sense, the boron and nitrogen centers in **1** may be regarded as an internal frustrated Lewis pair.^[13] The empty n_B^* orbital is responsible for the pronounced Lewis acidity of **1** and allows binding of such a poor Lewis base as N_2 . According to CCSD(T)/TZ2P + ZPVE computations, the binding energy is $6.0 \text{ kcal mol}^{-1}$. The B–N₂ distance is 1.602 \AA , and the N–N distance is hardly elongated (Figure 3c). In contrast, the endocyclic B–N distance is increased from 1.318 \AA in **1** to 1.390 \AA in **3**. Note that the B–N distance in *tert*-butyl(*tert*-butylimino)borane is $1.258(4) \text{ \AA}$ and ranges between 1.330 – 1.340 \AA in some of its N-heterocyclic carbene adducts.^[9a,14] With the ambiphilic CO₂ molecule both the electron-deficient boron and the electron-rich nitrogen centers are involved in binding with an overall binding energy of 29 kcal mol^{-1} , as calculated at the CCSD(T)/TZ2P + ZPVE(B3LYP/6-311+G**) level of theory.

In summary, we have established the first synthesis and characterization of 1,2-azaborine, the BN analogue of *ortho*-benzyne. 1,2-Azaborine can be generated by flash vacuum thermolysis and can exist under cryogenic matrix isolation conditions as demonstrated by direct spectroscopic techniques. 1,2-Azaborine has a very Lewis-acidic boron center that undergoes reversible binding of a dinitrogen molecule, and also spontaneously binds CO₂. The research described herein opens the wide and uncharted field of BN aryne chemistry and is expected to allow access to novel boron-nitrogen-doped molecular architectures of importance in medicinal and materials chemistry.

Keywords: ab initio calculations · arynes · boron · matrix isolation · nitrogen heterocycles

How to cite: *Angew. Chem. Int. Ed.* **2015**, *54*, 7819–7822
Angew. Chem. **2015**, *127*, 7930–7933

- [1] R. Stoermer, B. Kahlert, *Ber. Dtsch. Chem. Ges.* **1902**, *35*, 1633–1640.
- [2] a) P. M. Tadross, B. M. Stoltz, *Chem. Rev.* **2012**, *112*, 3550–3577; b) C. M. Gampe, E. M. Carreira, *Angew. Chem. Int. Ed.* **2012**, *51*, 3766–3778; *Angew. Chem.* **2012**, *124*, 3829–3842; c) A. Bhunia, S. R. Yetra, A. T. Biju, *Chem. Soc. Rev.* **2012**, *41*, 3140–3152; d) C. Wentrup, *Aust. J. Chem.* **2010**, *63*, 979–986; e) T. Kitamura, *Aust. J. Chem.* **2010**, *63*, 987–1001; f) M. Winkler, W. Sander, *Aust. J. Chem.* **2010**, *63*, 1013–1047; g) H. H. Wenk, M. Winkler, W. Sander, *Angew. Chem. Int. Ed.* **2003**, *42*, 502–528; *Angew. Chem.* **2003**, *115*, 518–546; h) H. Pellissier, M. Santelli, *Tetrahedron* **2003**, *59*, 701–730.
- [3] P. J. Fazen, L. A. Burke, *Inorg. Chem.* **2006**, *45*, 2494–2500.
- [4] a) M. J. D. Bosdet, W. E. Piers, *Can. J. Chem.* **2008**, *86*, 8–29; b) P. G. Campbell, A. J. Marwitz, S. Y. Liu, *Angew. Chem. Int. Ed.* **2012**, *51*, 6074–6092; *Angew. Chem.* **2012**, *124*, 6178–6197; c) E. R. Abbey, A. N. Lamm, A. W. Baggett, L. N. Zakharov, S.-Y. Liu, *J. Am. Chem. Soc.* **2013**, *135*, 12908–12913; d) A. W. Baggett, M. Vasiliu, B. Li, D. A. Dixon, S.-Y. Liu, *J. Am. Chem. Soc.* **2015**, *137*, 5536–5541; e) H. Braunschweig, C. Hörl, L. Mailänder, K. Radacki, J. Wahler, *Chem. Eur. J.* **2014**, *20*, 9858–9861; f) H. Braunschweig, K. Geetharani, J. O. C. Jimenez-Halla, M. Schaefer, *Angew. Chem. Int. Ed.* **2014**, *53*, 3500–3504; *Angew. Chem.* **2014**, *126*, 3568–3572; g) H. Braunschweig, M. A. Celik, F. Hupp, I. Krummenacher, L. Mailänder, *Angew. Chem. Int. Ed.* **2015**, *54*, 6347–6351; *Angew. Chem.* **2015**, *127*, 6445–6449; h) S. A. Brough, A. N. Lamm, S.-Y. Liu, H. F. Bettinger, *Angew. Chem. Int. Ed.* **2012**, *51*, 10880–10883; *Angew. Chem.* **2012**, *124*, 11038–11041; i) H. F. Bettinger, O. Hauer, *Beilstein J. Org. Chem.* **2013**, *9*, 761–766.
- [5] M. Müller, C. Maichle-Mössmer, H. F. Bettinger, *Angew. Chem. Int. Ed.* **2014**, *53*, 9380–9383; *Angew. Chem.* **2014**, *126*, 9534–9537.
- [6] a) O. L. Chapman, K. Mattes, C. L. McIntosh, J. Pacansky, G. V. Calder, G. Orr, *J. Am. Chem. Soc.* **1973**, *95*, 6134–6135; b) O. L. Chapman, C. L. McIntosh, J. Pacansky, G. V. Calder, G. Orr, *J. Am. Chem. Soc.* **1973**, *95*, 4061–4062; c) J. G. Radziszewski, B. A. Hess, Jr., R. Zahradník, *J. Am. Chem. Soc.* **1992**, *114*, 52–57; d) R. Koch, R. J. Blanch, C. Wentrup, *J. Org. Chem.* **2014**, *79*, 6978–6986.
- [7] a) C. A. Jaska, D. J. H. Emslie, M. J. D. Bosdet, W. E. Piers, T. S. Sorensen, M. Parvez, *J. Am. Chem. Soc.* **2006**, *128*, 10885–10896; b) T. Hatakeyama, S. Hashimoto, S. Seki, M. Nakamura, *J. Am. Chem. Soc.* **2011**, *133*, 18614–18617; c) T. Hatakeyama, S. Hashimoto, T. Oba, M. Nakamura, *J. Am. Chem. Soc.* **2012**, *134*, 19600–19603.
- [8] a) C. Baldock, G.-J. de Boer, J. B. Rafferty, A. R. Stuitje, D. W. Rice, *Biochem. Pharmacol.* **1998**, *55*, 1541–1549; b) S. J. Baker, J. W. Tomsho, S. J. Benkovic, *Chem. Soc. Rev.* **2011**, *40*, 4279–4285; c) A. W. Baggett, Z. Cournia, M. S. Han, G. Patargas, A. C. Glass, S.-Y. Liu, B. J. Nolen, *ChemMedChem* **2012**, *7*, 1286–1294; d) D. H. Knack, J. L. Marshall, G. P. Harlow, A. Dudzik, M. Szaleńiec, S.-Y. Liu, J. Heider, *Angew. Chem. Int. Ed.* **2013**, *52*, 2599–2601; *Angew. Chem.* **2013**, *125*, 2660–2662; e) F. Montalbano, P. M. S. D. Cal, M. A. B. R. Carvalho, L. M. Gonçalves, S. D. Lucas, R. C. Guedes, L. F. Veiros, R. Moreira, P. M. P. Gois, *Org. Biomol. Chem.* **2013**, *11*, 4465–4472.
- [9] a) P. Paetzold, C. von Pllotho, G. Schmid, R. Boese, B. Schrader, D. Bougeard, U. Pfeiffer, R. Gleiter, W. Schüfer, *Chem. Ber.* **1984**, *117*, 1089–1102; b) P. Paetzold in *Advances in Inorganic Chemistry*, Vol. 31 (Eds.: H. J. Emeléus, A. G. Sharpe), Academic Press, New York, **1987**, pp. 123–170; c) P. Paetzold, *Phosphorus Sulfur Silicon Relat. Elem.* **1994**, *93*, 39–50.
- [10] A. J. V. Marwitz, M. H. Matus, L. N. Zakharov, D. A. Dixon, S.-Y. Liu, *Angew. Chem. Int. Ed.* **2009**, *48*, 973–977; *Angew. Chem.* **2009**, *121*, 991–995.

- [11] G. Maier, H. P. Reisenauer, J. Henkelmann, C. Kliche, *Angew. Chem. Int. Ed. Engl.* **1988**, *27*, 295–296; *Angew. Chem.* **1988**, *100*, 303–303.
- [12] a) D. V. Lanzisera, L. Andrews, *J. Phys. Chem. A* **1997**, *101*, 1482–1487; b) H. F. Bettinger, *Organometallics* **2007**, *26*, 6263–6267.
- [13] a) G. Kehr, S. Schwendemann, G. Erker, *Top. Curr. Chem.* **2013**, *332*, 45–84; b) D. W. Stephan, *Acc. Chem. Res.* **2015**, *48*, 306–316.
- [14] H. Braunschweig, W. C. Ewing, K. Geetharani, M. Schäfer, *Angew. Chem. Int. Ed.* **2015**, *54*, 1662–1665; *Angew. Chem.* **2015**, *127*, 1682–1685.

Received: March 31, 2015

Published online: June 11, 2015



Supporting Information

1,2-Azaborine: The Boron-Nitrogen Derivative of *ortho*-Benzyne**

*Klara Edel, Sarah A. Brough, Ashley N. Lamm, Shih-Yuan Liu, and Holger F. Bettinger**

[anie_201502967_sm_miscellaneous_information.pdf](#)

Methods

Matrix experiments. Precursor **2** was synthesized according to Liu et al.^[1] Matrix experiments were performed by standard techniques^[2] using a SHI CKW-21A displex closed-cycle helium cryostat. Pyrolyses were carried out with an Al₂O₃ tube with two inner canals with inner diameters of 1 mm each. The tube was resistively heated by tungsten wire coiled around it (10-15 mm). Temperatures were measured with Ni-Cr/Ni thermocouples (Thermocoax). Compound **2** was sublimed from a glass flask at room temperature, and all gaseous materials leaving the pyrolysis tube were condensed onto a cold CsI window with a large excess of argon 6.0 (Westfalen AG), dinitrogen 6.0 (Westfalen AG), ¹⁵N₂ 2.2 (Westfalen AG), carbon dioxide 5.0 (Westfalen AG), ¹³CO₂ 2.0 (Cambridge Isotope Laboratories, Inc.), C(¹⁸O)₂ 1.5 (Cambridge Isotope Laboratories, Inc) or mixtures of these gases, which were dosed to 2.0 sccm by a mass flow controller (MKS mass flow PR400B). The deposition temperature was 52 K in the experiments with carbon dioxide and 6 K in the experiments with argon and dinitrogen. Irradiation was achieved with a low-pressure mercury lamp (UVP, 253.7 nm) and an Osram HBO-500-W/2 high pressure mercury lamp in an Oriel housing with quartz optics, dichroic mirrors (260 – 320 and 350 – 450 nm) and two Schott cutoff filter (305 and 395 nm). FTIR spectra were measured between 4000 and 400 cm⁻¹ on a Bruker Vertex 70 spectrometer using a resolution of 0.5 cm⁻¹.

Electronic Structure Computations. The geometries of **1**, **3**, and **4** were optimized and harmonic vibrational frequencies were computed with Becke's^[3] hybrid functional in conjunction with the correlation functional of Lee, Yang, and Parr^[4] as implemented^[5] in Gaussian 09^[6] and the 6-311+G** basis set (B3LYP/6-311+G**). In order to describe the weak dative interaction between N₂ and **1** in the dinitrogen adduct **3**, Grimme's D3 dispersion correction was employed for adduct **3** (B3LYP-D3/6-311+G**).^[7] Natural bond orbital^[8]

analysis was carried out on **1** using the B3LYP/6-311+G** geometry and electron density with help of the NBO3 program included in Gaussian 09.

The geometries of **1** and **3** were reoptimized using analytical gradients^[9] and coupled cluster theory with singles, doubles, and a perturbative estimate of triples excitations, CCSD(T).^[10] Dunning triple- ζ basis set (TZ2P) augmented with two sets of polarization functions was employed.^[11] Harmonic vibrational frequencies for **1** and **3** were computed analytically at the CCSD(T) level of theory.^[12] Due to technical constraints, the harmonic vibrational frequencies could not be obtained for **4** at the CCSD(T)/TZ2P level, and those computed at B3LYP/6-311+G** were used instead. All CCSD(T) computations employed the frozen core approximation and were performed with CFOUR.^[13]

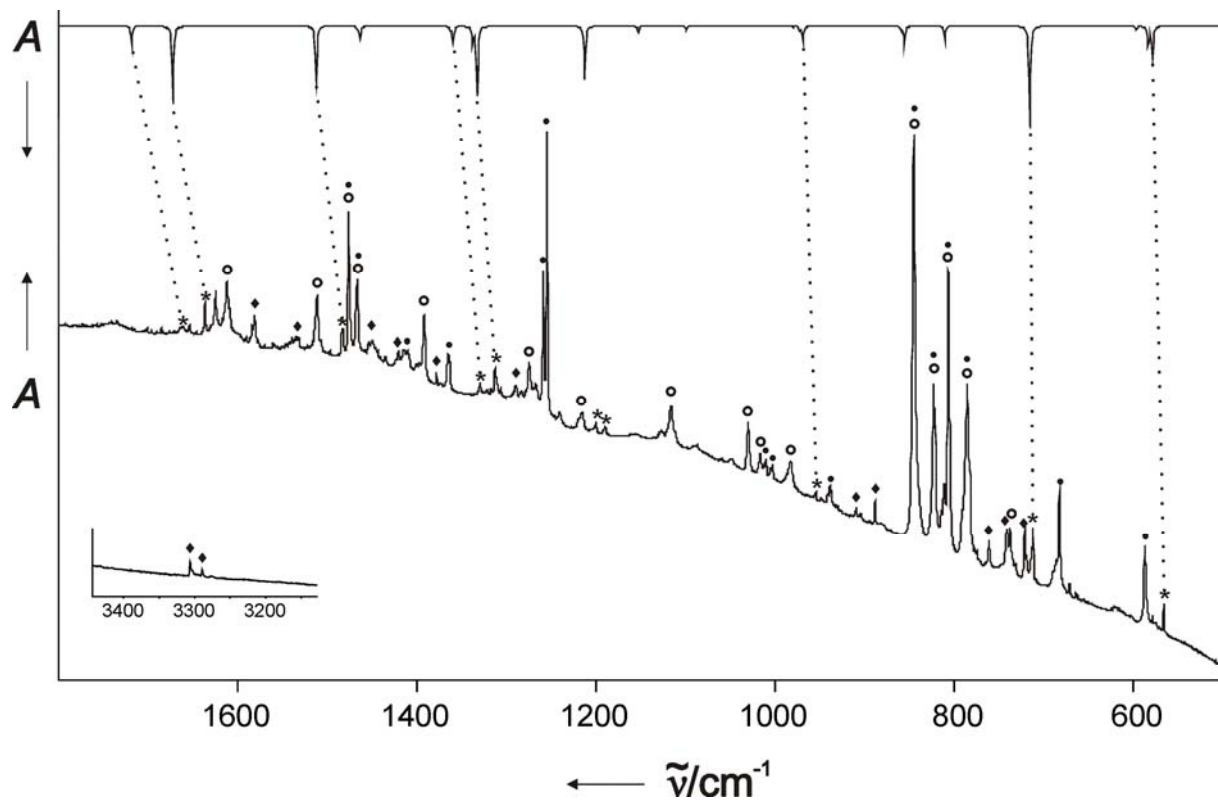


Figure S1. IR spectrum obtained after FVP (800–850 °C) of **2** and deposition with a large excess of neat argon at 6 K (bottom trace). The spectrum shows: **1** (*), the unconverted precursor **2** (O), silyl chloride (●), and other new signals (◆) that are not attributed to **1**. The signals for **1** are compared with the computed spectrum for **1** at the CCSD(T)/TZ2P level of theory (top trace).

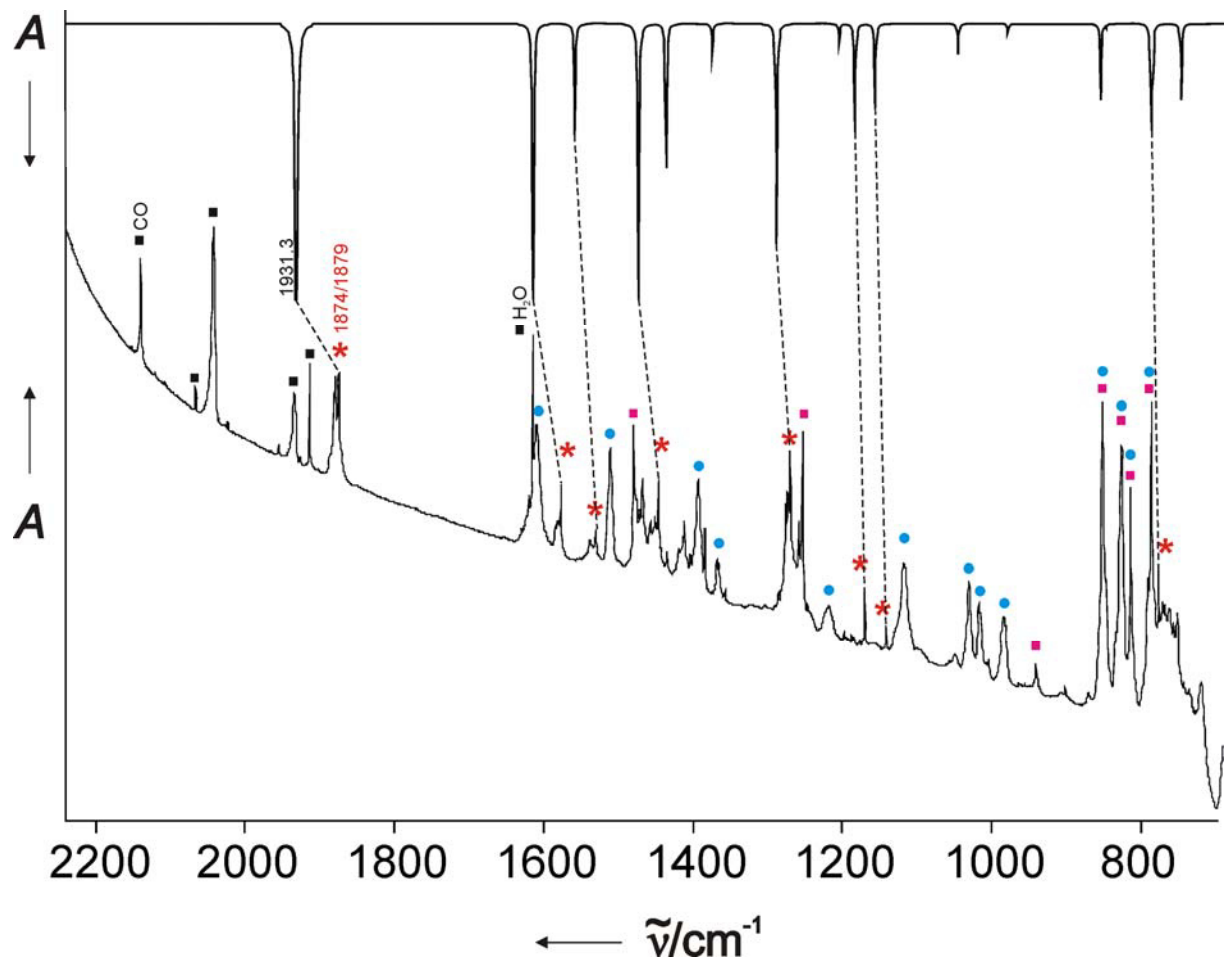


Figure S2. IR spectrum obtained after FVP ($800\text{ }^{\circ}\text{C}$) of **2** and deposition with a large excess of CO₂ at 52 K (bottom trace). Computed spectrum (B3LYP/6-311+G**) for **4** (top trace). **4** (＊), unconverted precursor **2** (●), silyl chloride (■), CO₂ and other impurities (■) are marked.

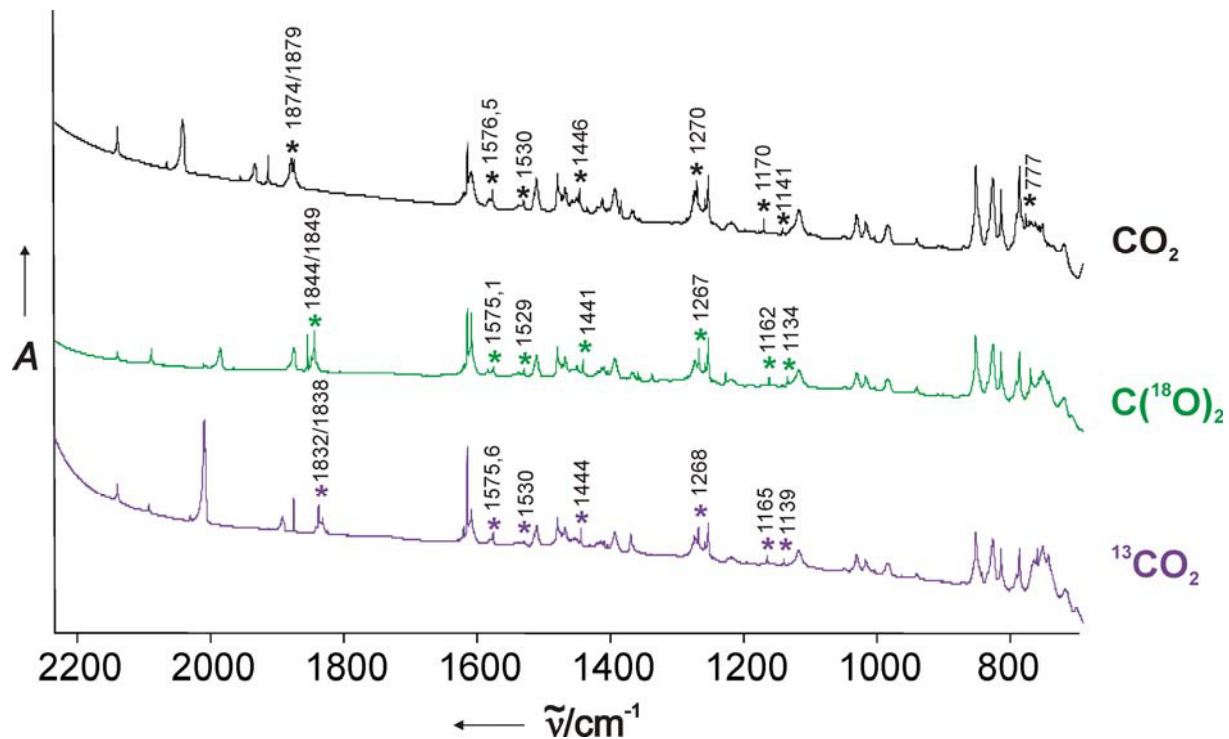


Figure S3. IR absorption spectra after FVP (800 °C) of **2** and deposition at 52 K with different isotopomers of carbon dioxide. Signals attributed to **4** are marked with stars in the colour of the respective carbon dioxide isotopomer which are listed on the right hand side.

Table S1. Experimental and computed vibrational frequencies of **3.** Experimental values in a matrix with 30 percent of dinitrogen and 70 percent of argon after FVP at 800-850 °C, and deposition at 6 K compared with harmonic values and intensities (in km mol⁻¹) computed at the CCSD(T)/TZ2P level of theory.

[¹⁴ N ₂]-3	[¹⁴ N ₂ - ¹¹ B]-3		[¹⁴ N ₂ - ¹⁰ B]-3	[¹⁵ N ₂]-3	[¹⁵ N ₂ - ¹¹ B]-3		[¹⁵ N ₂ - ¹⁰ B]-3
v _{exp} [cm ⁻¹]	ω _{theor} [cm ⁻¹]	Intensity	ω _{theor} [cm ⁻¹]	v _{exp} [cm ⁻¹]	ω _{theor} [cm ⁻¹]	ω _{theor} [cm ⁻¹]	
	115.0	1.55		116.1		113.7	114.7
	124.3	0.26		124.9		122.2	122.8
	320.1	14.53		320.4		312.5	312.7
	339.4	1.82		340.0		333.8	334.1
	388.0	3.31		388.5		387.8	387.8
	451.1	3.32		452.3		440.1	441.2
	481.3	6.99		490.7		477.3	486.5
	563.5	3.53		564.3		562.7	563.4
	623.1	1.16		634.5		623.1	634.2
670	668.5	13.25		677.3	670	669.0	677.3
739	739.2	57.35		742.5	738	741.3	742.3
	843.6	0.39		846.2		846.2	846.2
	932.0	1.25		942.7		932.4	942.7
933	944.3	9.97		955.6	932	944.8	955.5
	963.3	0.17		966.0		965.9	966.0
	978.1	0.00		981.1		981.0	981.1
	1003.6	2.66		1005.1		1005.0	1005.1
	1104.4	1.95		1107.6		1106.7	1107.5
1141	1159.0	9.11		1164.0	1141	1162.4	1163.9
1251	1252.9	19.67		1255.1	1250	1254.1	1255.0
	1302.1	6.38		1328.1		1304.6	1328.0
1371	1395.2	24.59		1399.1	1371	1397.5	1399.1
	1459.2	0.22		1469.3		1462.3	1469.2
1523	1552.9	14.57		1555.4	1522	1554.3	1555.4
1535	1565.9	33.67		1582.1	1538	1566.9	1582.0
2266	2283.8	161.46		2284.1	2191	2206.8	2206.9
	3137.2	30.35		3148.5		3148.5	3148.5
	3166.3	9.49		3177.7		3177.7	3177.7
	3193.2	11.38		3204.7		3204.6	3204.7
	3204.7	14.43		3216.2		3216.2	3216.2

Table S2. Experimental and computed vibrational frequencies of **1.** Experimental values obtained in a matrix with 30 percent of dinitrogen and 70 percent argon after irradiation ($\lambda > 395$ nm) of adduct **3** compared with harmonic values and intensities (in km mol^{-1}) computed at the CCSD(T)/TZ2P level of theory.

1		[¹¹B]-1		[¹⁰B]-1	
ν_{exp} [cm^{-1}]	rel. Int.	ω_{theor} [cm^{-1}]	Intensity	ω_{theor} [cm^{-1}]	
		387.4	0.54	390.1	ring tor
		407.9	1.48	414.4	ring tor
		458.5	16.46	461.6	ring def
565	0.30	578.6	26.52	582.8	ring tor
578	0.07	583.2	13.58	596.1	ring def
717	1.00	715.4	67.06	715.5	CH wagging
		810.7	10.09	810.9	CH wagging
847	^a	855.9	16.07	859.5	ring def
		940.4	0.33	940.5	CH wagging
		955.8	0.04	955.9	CH wagging
956	0.11	969.0	14.27	972.5	ring str
		980.8	1.23	985.3	ring str
		1098.0	3.06	1099.2	ring str and CH def
		1153.0	5.21	1153.7	ring str and CH def
1193/1203	0.32	1212.4	35.53	1212.4	ring str
1312/1310	0.64	1332.6	57.25	1337.1	ring str and CH def
1330	0.20	1359.3	14.78	1362.7	ring str and CH def
		1463.6	11.51	1466.4	ring str
1483	0.59	1512.6	36.13	1512.7	ring str
1637/1634 [¹¹ B]	0.59	1673.0	64.63	1718.3	BN str
1664 [¹⁰ B]	0.37				
		3168.6	3.77	3168.6	CH str
		3173.0	16.00	3173.0	CH str
		3219.6	6.44	3219.6	CH str
		3273.3	0.55	3273.4	CH str

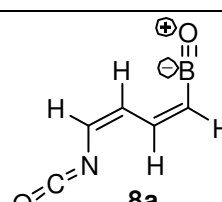
^a Not integrated due to strong overlap with other signals.

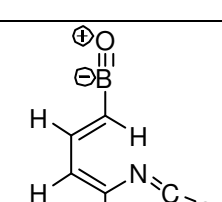
Table S3. Experimental and computed frequencies of 4. Experimental values were obtained after trapping in a matrix of the respective carbon dioxide isotopomer compared with harmonic vibrational frequencies and intensities (in km mol⁻¹) computed at the B3LYP/6-311+G** level of theory; only frequencies with intensities larger than 5 km mol⁻¹ are given.

[CO ₂]-4				[¹³ CO ₂]-4				[C(¹⁸ O) ₂]-4			
v _{exp} [cm ⁻¹]	rel. Int.	ω _{theor} [cm ⁻¹]	Int.	v _{exp} [cm ⁻¹]	rel. Int.	ω _{theor} [cm ⁻¹]	Int.	v _{exp} [cm ⁻¹]	rel. Int.	ω _{theor} [cm ⁻¹]	Int.
		470.9	7.78			469.8	7.97			469.6	7.55
		638.0	6.34			635.8	6.45			623.2	6.11
		670.3	11.24			665.3	8.59			669.5	11.05
		746.5	51.28			745.7	37.43			746.3	48.33
		784.6	23.68			770.8	79.23			760.3	30.29
777	^a	786.8	63.96			774.8	30.14			779.9	66.30
		788.7	19.42			781.7	14.90			782.3	9.58
		854.6	51.20			851.9	53.00			841.9	52.78
		978.6	6.14			978.6	6.15			978.3	5.95
		1045.7	20.59			1045.0	21.55			1042.2	16.02
1141	0.03	1156.0	57.05	1139	0.05	1153.4	73.80	1134	^a	1146.2	92.07
1170	0.05	1183.7	73.30	1165	0.07	1178.9	60.74	1162	0.10	1177.4	45.05
		1204.3	12.76			1203.9	9.07			1202.0	3.36
1270	^a	1288.5	149.26	1268	^a	1287.4	145.15	1267	^a	1287.0	142.48
		1375.0	19.64			1374.9	19.65			1372.6	19.45
		1436.8	98.27			1435.8	96.42			1435.9	90.90
1446	^a	1473.7	218.14	1444	^a	1473.3	215.00	1441	^a	1473.2	221.00
1530	0.16	1558.8	75.30	1530	0.25	1558.2	72.09	1529	0.35	1558.2	78.18
1576.5	0.31	1614.5	237.10	1575.6	0.35	1614.3	240.91	1575.1	0.49	1614.3	240.80
1879/ 1874	1.00	1931.3	718.80	1838/ 1832	1.00	1882.9	658.55	1849/ 1844	1.00	1894.7	696.49
		3142.3	13.83			3142.3	13.85			3142.3	13.84
		3194.4	5.28			3194.4	5.28			3194.4	5.29
		3215.9	5.95			3215.9	5.97			3215.9	5.96

^a Not integrated due to strong overlap with other signals.

Table S4. Computed vibrational frequencies of **8.** The most intense harmonic vibrational frequencies of **8** (intensities in km mol^{-1}) for different isotopomers computed at the B3LYP/6-311+G** level of theory. Among the many conceivable isomers, the s-trans isomer **8a** and cis,trans isomer **8b** were chosen.

[CO ₂]- 8a		[¹³ CO ₂]- 8a	[C(¹⁸ O) ₂]- 8a	Assignment	 8a
$\omega_{\text{theor}} [\text{cm}^{-1}]$	Intensity	$\omega_{\text{theor}} [\text{cm}^{-1}]$	$\omega_{\text{theor}} [\text{cm}^{-1}]$		
1672.7	359	1672.7	1672.3	$\nu (\text{CC})$	
2009.4	511	2009.3	1975.2	$\nu (^{11}\text{BO})$	
2075.3	560	2075.2	2042.4	$\nu (^{10}\text{BO})$	
2356.9	2241	2292.5	2339.5	$\nu (\text{NCO})$	

[CO ₂]- 8b		[¹³ CO ₂]- 8b	[C(¹⁸ O) ₂]- 8b	Assignment	 8b
$\omega_{\text{theor}} [\text{cm}^{-1}]$	Intensity	$\omega_{\text{theor}} [\text{cm}^{-1}]$	$\omega_{\text{theor}} [\text{cm}^{-1}]$		
1623	206	1622.9	1622.4	$\nu (\text{CC})$	
2010.5	564	2010.4	1976.7	$\nu (^{11}\text{BO})$	
2076.5	611	2076.4	2043.9	$\nu (^{10}\text{BO})$	
2353.0	1926	2288.7	2335.2	$\nu (\text{NCO})$	

Results of Computational Chemistry Investigation

Table S5. Computed absolute energies (in a.u.) and zero point vibrational energies (ZPVE, in kcal mol⁻¹) of compounds **1**, **3**, **4**, N₂, and CO₂ at various levels of theory.

Level of theory	1	3	4	N ₂	CO ₂
CCSD(T)/TZ2P	-233.87803	-343.23564	-422.20576	-109.34430	-188.27638
ZPVE	46.2	51.8	not avail.	3.3	7.1
B3LYP/6-311+G**	-234.46405	-344.038889	-423.15565	-109.55969	-188.64691
ZPVE	46.4	52.3	56.6	3.5	7.3
B3LYP-D3/6-311+G**	-234.46812	-344.04521	-423.163058	-109.55969	-188.64709
ZPVE	46.4	52.3	56.5	3.5	7.3

Cartesian Coordinates of Optimized Structures

I. Compound **1**

```

10
B3LYP/6-311+G**
C    1.282241   -0.896623     0.000000
C   -1.235174    0.588459     0.000000

```

```

C      0.000000   1.238926   0.000000
C      1.210162   0.509764   0.000000
H      2.223664   -1.421630   0.000000
H      -2.162147   1.157572   0.000000
H      0.030965   2.321715   0.000000
H      2.143305   1.068388   0.000000
B      -0.111069   -1.280082   0.000000
N      -1.317689   -0.766970   0.000000

```

```

10
B3LYP-D3/6-311+G**
6 1.282821 -0.896692 0.000000
6 -1.235669 0.588497 0.000000
6 0.000000 1.239464 0.000000
6 1.210825 0.510364 0.000000
1 2.224661 -1.421378 0.000000
1 -2.162613 1.157550 0.000000
1 0.030619 2.322258 0.000000
1 2.143943 1.068891 0.000000
5 -0.111314 -1.280883 0.000000
7 -1.318272 -0.767530 0.000000

```

```

10
CCSD(T)/TZ2P
C      -1.406065   -0.692167   0.000000
B      -0.050097   -1.222103   0.000000
N      1.216129   -0.855059   0.000000
C      1.269338   0.513825   0.000000
C      0.110349   1.294165   0.000000
C      -1.179305   0.700717   0.000000
H      -2.397529   -1.110925   0.000000
H      2.248349   0.981664   0.000000
H      0.197694   2.371998   0.000000
H      -2.042728   1.358555   0.000000

```

II. Compound 3

```

12
B3LYP/6-311+G**
6 1.201049 -1.548907 0.000000
6 -0.058002 -2.163695 0.000000
6 -1.237626 -1.398389 0.000000
7 -1.262378 -0.069113 0.000000
6 1.318033 -0.158719 0.000000
1 2.088530 -2.176144 0.000000
1 -0.131403 -3.245753 0.000000
1 -2.195782 -1.919831 0.000000
1 2.303498 0.294779 0.000000
5 0.000000 0.524852 0.000000
7 -0.035272 2.056366 0.000000
7 -0.046002 3.161455 0.000000

```

```

12
B3LYP-D3/6-311+G**
5 -0.523834 0.002545 0.000085
7 0.056622 -1.265527 -0.000086
6 1.385982 -1.253211 -0.000265
6 0.171258 1.315061 0.000053
6 1.560488 1.185251 -0.000004
6 2.162969 -0.080159 -0.000121
1 1.899151 -2.215777 -0.000242
1 -0.275298 2.303734 0.000094
1 2.196201 2.066636 0.000029
1 3.244305 -0.164292 -0.000124
7 -2.056490 -0.013388 0.000129
7 -3.161471 -0.007467 0.000220

```

```

12
CCSD(T)/TZ2P
C      -0.269363   1.349758   0.000000
B      0.418846   0.038271   0.000000
N      2.020587   0.023381   0.000000
C      -1.661777   1.192035   0.000000

```

C	-2.248224	-0.087596	0.000000
C	-1.455802	-1.247647	0.000000
N	-0.110382	-1.246569	0.000000
H	0.157513	2.345364	0.000000
H	-1.952174	-2.215451	0.000000
H	-3.326217	-0.186980	0.000000
H	-2.312021	2.060715	0.000000
N	3.124536	0.014935	0.000000

III. Compound 4

13
B3LYP/6-311+G**
C 1.685835 -0.066734 -0.000048
N 0.301149 -0.436451 -0.000352
B 0.012185 0.963605 -0.000157
C -1.419722 1.384615 -0.000022
C -2.288372 0.308550 0.000191
C -1.906926 -1.078961 0.000191
C -0.591683 -1.460132 -0.000389
H -1.822899 2.389368 0.000114
H -3.358094 0.503553 0.000609
H -2.678696 -1.837041 0.000606
H -0.241690 -2.484386 -0.000366
O 1.424484 1.301203 -0.000079
O 2.707720 -0.658501 0.000422

13
B3LYP-D3/6-311+G**
6 1.685899 -0.066291 -0.000115
7 0.301609 -0.435870 -0.000117
5 0.011675 0.964393 -0.000087
6 -1.421200 1.384787 0.000208
6 -2.288828 0.307386 0.000236
6 -1.905758 -1.080428 0.000103
6 -0.589929 -1.460325 0.000143
1 -1.825177 2.389277 0.000243
1 -3.358859 0.500882 0.000255
1 -2.676242 -1.839836 0.000017
1 -0.237960 -2.483801 0.000068
8 1.423237 1.302123 -0.000182
8 2.707699 -0.658144 -0.000166

13
CCSD(T)/TZ2P
C -1.487119 1.375787 0.000000
C -2.358839 0.298926 0.000000
C -1.980629 -1.099710 0.000000
C -0.666416 -1.487999 0.000000
N 0.232309 -0.458904 0.000000
B -0.046207 0.940717 0.000000
O 1.362154 1.287418 0.000000
C 1.624014 -0.092228 0.000000
O 2.647999 -0.685059 0.000000
H -1.891582 2.378649 0.000000
H -3.426669 0.495143 0.000000
H -2.754588 -1.853304 0.000000
H -0.320005 -2.511407 0.000000

IV. N₂

2
B3LYP/6-311+G**
7 0.000000 0.000000 0.547796
7 0.000000 0.000000 -0.547796

2
B3LYP-D3/6-311+G**
7 0.000000 0.000000 0.547796
7 0.000000 0.000000 -0.547796

2
 CCSD(T) /TZ2P
 N 0.000000 0.000000 0.551478
 N 0.000000 0.000000 -0.551478

V. CO₂

3
 B3LYP/6-311+G**
 6 0.000000 0.000000 0.000000
 8 0.000000 0.000000 1.160796
 8 0.000000 0.000000 -1.160796

3
 B3LYP-D3/6-311+G**
 6 0.000000 0.000000 0.000000
 8 0.000000 0.000000 1.160796
 8 0.000000 0.000000 -1.160796

4
 CCSD(T) /TZ2P
 C 0.000000 0.000000 0.000000
 O 0.000000 0.000000 -1.166568
 O 0.000000 0.000000 1.166568

VI. Compounds 8

13
 8a B3LYP/6-311+G**
 6 2.169770 1.118632 0.000333
 6 0.862261 0.770633 0.000250
 6 0.362057 -0.584342 0.000666
 6 -0.942597 -0.918325 0.000597
 1 0.111698 1.556252 -0.000175
 1 2.422166 2.174754 0.000122
 7 -1.961664 0.021175 0.000190
 6 -3.168773 0.048673 -0.000380
 8 -4.325335 0.202924 -0.000647
 1 -1.246870 -1.959712 0.000898
 1 1.077137 -1.400842 0.001020
 5 3.309305 0.126009 0.000494
 8 4.215920 -0.672968 -0.001160

13
 8b B3LYP/6-311+G**
 6 -1.451970 -0.187726 0.000019
 6 -1.211041 1.143765 -0.000011
 6 0.070643 1.828317 0.000000
 6 1.317243 1.317286 0.000005
 7 1.606243 -0.036256 0.000002
 5 -2.854479 -0.746572 0.000004
 8 -3.975271 -1.199096 -0.000008
 6 2.580388 -0.751901 -0.000003
 8 3.436512 -1.543374 -0.000007
 1 -0.622037 -0.885162 0.000058
 1 2.172197 1.985795 0.000012
 1 0.022721 2.911610 0.000002
 1 -2.065693 1.815728 -0.000044

References

- [1] A. J. V. Marwitz, M. H. Matus, L. N. Zakharov, D. A. Dixon, S.-Y. Liu, *Angew. Chem., Int. Ed. Engl.* **2009**, *48*, 973-977.
- [2] I. R. Dunkin, *Matrix-Isolation Techniques*, Oxford University Press, Oxford, **1998**.
- [3] A. D. Becke, *J. Chem. Phys.* **1993**, *98*, 5648.
- [4] C. Lee, W. Yang, R. G. Parr, *Phys. Rev. B* **1988**, *37*, 785-789.
- [5] P. J. Stephens, F. J. Devlin, C. F. Chabalowski, M. J. Frisch, *J. Phys. Chem.* **1994**, *98*, 11623-11627.
- [6] M. J. Frisch et al., Gaussian 09, Revision D.01, Gaussian Inc., Wallingford CT, **2009**.
- [7] S. Grimme, J. Antony, S. Ehrlich, H. Krieg, *J. Chem. Phys.* **2010**, *132*, 154104.
- [8] a) A. E. Reed, L. A. Curtiss, F. Weinhold, *Chem. Rev.* **1988**, *88*, 899-926; b) E. D. Glendening, C. R. Landis, F. Weinhold, *WIREs Comput. Mol. Sci.* **2012**, *2*, 1-42; c) F. Weinhold, *J. Comput. Chem.* **2012**, *33*, 2363-2379.
- [9] G. E. Scuseria, *J. Chem. Phys.* **1991**, *94*, 442-447.
- [10] K. Raghavachari, G. W. Trucks, J. A. Pople, M. Head-Gordon, *Chem. Phys. Lett.* **1989**, *157*, 479-483.
- [11] T. H. Dunning, *J. Chem. Phys.* **1971**, *55*, 716-723.
- [12] J. Gauss, J. F. Stanton, *Chem. Phys. Lett.* **1997**, *276*, 70-77.
- [13] Stanton, J. F. et al. *CFOUR*, Coupled-Cluster techniques for Computational Chemistry, Version 1.0, for the current version, see <http://www.cfour.de>.

Publikation 2

Isomerization and Fragmentation Pathways of 1,2-Azaborine

Klara Edel,^[a] Reinhold F. Fink,^[b] and Holger F. Bettinger^{*[a]}

The generation of 1,2-azaborine (**4**), the BN-analogue of *ortho*-benzyne, was recently achieved by elimination of *tert*-butyldimethylchlorosilane under the conditions of flash vacuum pyrolysis. The present investigation identifies by computational means pathways for the thermal isomerization and fragmentation of 1,2-azaborine. The computations were performed using single reference (hybrid/density functional, second order Møller-Plesset perturbation, and coupled cluster theories) as well as multiconfiguration methods (complete active space SCF based second order perturbation theory, multireference configuration interaction, and multiconfiguration coupled elec-

tron pair approximation) with basis sets up to polarized triple- ζ quality. The 1,2-azaborine is, despite the distortion of its molecular structure, the most stable C₄H₄BN isomer investigated. The formation of BN-endiyne isomers is highly unfavorable as the identified pathways involve barriers close to 80 kcal mol⁻¹. The concerted fragmentation to ethyne and 2-aza-3-borabutadiyne even has a barrier close to 120 kcal mol⁻¹. The fragmentation of BN-enediynes has energetic requirements similar to enediynes. © 2015 Wiley Periodicals, Inc.

DOI: 10.1002/jcc.24189

Introduction

Ortho-benzyne (**1**) is a well-known and extremely useful reactive intermediate in organic chemistry.^[1] In the 1980s, Brown and coworkers reported evidence for the equilibration between **1** and cyclopentadienylenecarbene (**2**) (Scheme 1) that was based on the observation of ¹³C scrambling in the product biphenylene after flash vacuum pyrolysis (FVP) of ¹³C-labeled precursors.^[2] The rearrangement was challenged by Wentrup et al. who proposed an alternative equilibration with an involvement of cyclopentadienyleneketene that results from the fragmentation of the precursors and a subsequent Wolff-type ring contraction.^[3] The mechanism is still unclear and presumably there is a contribution of both types of mechanism.^[4]

The rearrangement between the three different benzyne isomers (Scheme 2) was investigated by experimental and computational chemistry.^[5] The direct isomerization of *ortho* to *meta* and of *meta* to *para* isomers by [1,2]-H shifts is unlikely because of high activation barriers.^[5,6] *Meta*- and *para*-benzyne are known to undergo a ring opening reaction to 3-hexene-1,5-diyne (**3**) (Scheme 2).^[5–7] Another known reaction of **1** is the direct fragmentation to acetylene and diacetylene at high temperatures as was shown by Zhang et al. in 2007.^[8] However, the proposed concerted mechanism for the decomposition has an activation barrier of 90 kcal mol⁻¹^[6a,8,9] and is higher in energy than the pathway that includes the isomerization of **1** to *meta*-benzyne.^[10]

1,2-Azaborine (**4**) is a BN-derivative of **1** with an isoelectronic substitution of the CC-triple bond by a BN unit. We have recently reported the generation of **4** by FVP from precursor **5** and isolation in cryogenic matrices (Scheme 3).^[11] The spectrum after the thermal fragmentation of **5** and deposition with a large excess of argon shows, besides *tert*-butyldi-

methylchlorosilane, the unconverted precursor, and **4**, at least one set of additional signals. This set includes signals at 3306 and 3289 cm⁻¹ indicative of the CH stretching vibration of an alkyne. The question arises if **4** can undergo one of the aforementioned processes described for **1**. We present here a computational study of possible ring opening pathways to two isomeric BN substituted enediynes as well as a concerted fragmentation. In addition, we provide a comparison between **4** and its structural isomers nitrenoborole (**6**) and pyrrolylborylene (**7**) (Scheme 4).

Computational Methods

The study used the following basis sets: 6-31G*, 6-311+G**, and cc-pVTZ.^[12] The geometries were optimized and harmonic vibrational frequencies were computed using second order Møller-Plesset perturbation theory (MP2) and the B3LYP^[13] hybrid density functional as implemented^[14] in Gaussian 09.^[15] For a number of cases, intrinsic reaction coordinates were computed.^[16]

The energies were refined using the B3LYP/6-311+G** geometries for subsequent single point energy computations at the coupled cluster theory level with single, double, and a

[a] K. Edel, H. F. Bettinger

Institut Für Organische Chemie, Universität Tübingen, Auf Der Morgenstelle 18, Tübingen 72076, Germany
E-mail: holger.bettinger@uni-tuebingen.de

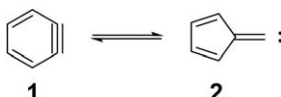
[b] R. F. Fink

Institut Für Physikalische Und Theoretische Chemie, Universität Tübingen, Auf Der Morgenstelle 18, Tübingen 72076, Germany

Contract grant sponsor: Deutsche Forschungsgemeinschaft

This article is dedicated to the memory of Paul von Ragué Schleyer, an outstanding chemist and an inspiring teacher. H.F.B. considers himself fortunate to have been able to work with and learn from Paul.

© 2015 Wiley Periodicals, Inc.



Scheme 1. Equilibration between *ortho*-benzene (**1**) and cyclopentadienylidene carbene (**2**).

perturbative estimate of triple excitations, CCSD(T),^[17] in conjunction with the cc-pVTZ basis set. A UHF-UCCSD(T) formalism was used for the triplet state 3A_2 -**6**. Unless noted otherwise, the CCSD(T) data is discussed in the text.

The investigation of the low-lying electronic states of nitrenoborole **6** was done with a multireference approach as open-shell and a potentially multireference singlet states are considered. The computations at the complete active space second-order perturbation theory level (CASPT2) described by Werner^[18] used an active space that consisted of seven orbitals [π_1 to π_5 of the borole ring, N(p_n), and N(p_o)] that was occupied by six electrons. Geometries were optimized at the CASPT2/6-31G* level using analytic gradients.^[19] Harmonic vibrational frequencies were subsequently computed by finite differences of analytic gradients. Energies were refined using internally contracted multireference configuration interaction (MRCI) including single and double excitations.^[20] The multireference Davidson correction was used to account for the lack of size-extensivity of the truncated CI wave functions (MRCI+Q).^[21] The energetic order of the electronic states of **6** was also obtained with the multiconfiguration coupled-electron-pair approach (MCCEPA)^[22] and the averaged-coupled-pair functional (ACPF)^[23] using single-configuration (restricted open-shell Hartree-Fock) reference wavefunctions.

Isomer **11** was investigated using a complete active space wavefunction composed of eight active orbitals (π_1 to π_6 and the two σ orbitals at nitrogen and the dehydro carbon atom) and eight electrons, similarly to previous computations for *meta*-benzyne.^[7a,24]

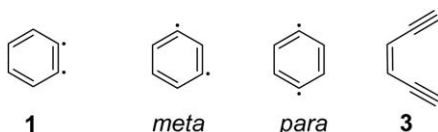
All post-Hartree-Fock methods used the frozen core approximation. The single reference computations were run with Gaussian 09^[15] while the multireference work was performed with the Molpro program.^[25]

The geometries of all stationary points are given as Cartesian coordinates in the Supporting Information, for graphical presentations of the B3LYP/6-311+G** molecular structures, see Supporting Information Figures S1, S3-S6.

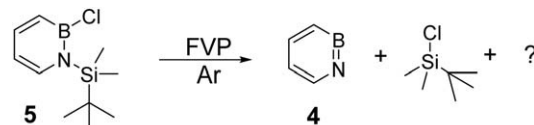
Results and Discussion

Ring contraction of 1,2-azaborine (**4**)

The ring contraction of **4** to BN substituted cyclopentadienylidene carbene can lead to two possible structural isomers, **6** and **7** (Scheme 4).



Scheme 2. Structures of *ortho*- (1), *meta*-, *para*-benzyne and (Z)-3-hexene-1,5-diyne (3).



Scheme 3. Formation of 1,2-azaborine (**4**) by FVP of precursor **5** as reported previously by Edel et al.^[11]

As a boryl nitrene, the electronic structure of **6** requires some consideration, in particular as the borole ring is a hetero antiaromatic moiety. Certain borylnitrenes were investigated earlier experimentally and computationally by our group.^[26] The closed-shell configuration of the 1A_1 state of **6** is:

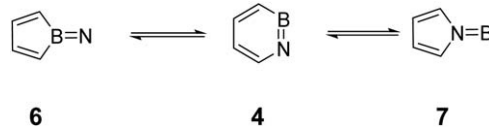
$$\dots (11 \ a_1)^2 (6 \ b_2)^2 (2 \ b_1)^2 (1 \ a_2)^2 (7 \ b_2)^0 (3 \ b_1)^0 \dots$$

The highest occupied molecular orbital (HOMO, $1a_2$) is the π_2 orbital of the borole ring while the HOMO-1 ($2b_1$) is a N(p_o) orbital that is orthogonal to the ring plane. The lowest unoccupied orbital (LUMO, $7b_2$) is the N(p_o) orbital that lies within the molecular plane, while LUMO+1 ($3b_1$) is the π_3 orbital of the borole ring. Taking into account that the LUMO is low in energy, there are a number of additional electronic states conceivable. These are $^{1,3}B_1$ due to HOMO \rightarrow LUMO and $^{1,3}A_2$ due to HOMO-1 \rightarrow LUMO excitations, each with either high spin or low spin coupling of the two electrons.

To elucidate the ordering of electronic states of **6**, we have performed geometry optimizations using second-order perturbation theory based on complete active space (CAS) multiconfiguration SCF wavefunctions (CASPT2) distributing six electrons over seven orbitals in the active space. As active orbitals, the six π ($1b_1$, $2b_1$, $1a_2$, $3b_1$, $2a_2$, $4b_1$) and the empty N(p_o) ($7b_2$) orbitals were considered for all electronic states. The energies were refined by internally contracted multireference configuration interaction computations that are based on the same size of the active space.

As expected based on previous work on borylnitrenes^[26b,27] and for example on phenylnitrene,^[28] the most stable state is \tilde{X}^3A_2 . The \tilde{A}^3B_1 state is 11.7 kcal mol⁻¹ higher in energy at the MRCI+Q level (see Table 1). Interestingly, the 1B_1 state is *lower* in energy than its triplet counterpart. It is also lower in energy than the 1A_1 state at CASPT2, but this ordering is reversed at the MRCI+Q level. Note that the tendency of CASPT2 to overestimate the stability of certain open shell states is well documented.^[29] While B3LYP places the 1A_1 state below 3A_2 , CCSD(T) arrives at the same state ordering as MRCI+Q. Note that CCSD(T) and MRCI+Q agree to within 2 kcal mol⁻¹ for these two states. This is good in view of the increased T₁ diagnostic^[30] of 0.034 for 1A_1 -**6**.

All electronic states of borylnitrene **6** considered here are of significant multireference character based on the composition



Scheme 4. Different isomers of 1,2-azaborine (4).

Table 1. Relative energies (in kcal mol⁻¹) of the low lying electronic states of **6** as computed at various levels of theory.

Level	¹ A ₁	¹ A ₂	¹ B ₁	³ A ₂	³ B ₁
CASPT2 ^[a]	0	+20.4	-6.3	-11.1	-5.4
MRCI+Q//CASPT2 ^[b]	0	+26.2	+6.3	-4.2	+7.5
B3LYP ^[c]	0	not avail.	not. avail.	+2.9	not avail.
CCSD(T)//B3LYP ^[b]	0	not. avail.	not. avail.	-1.8	not. avail.
ACPF//CASPT2	0	29.0	11.4	-1.7	12.5
MCCEPA//CASPT2	0	25.0	12.8	-5.4	11.4

[a] 6-31G* basis set. [b] cc-pVTZ basis for single point energy computation. [c] 6-311+G** basis set.

of the MRCI wavefunction (Table 2). The coefficient of the reference configuration in the ¹A₁ state is 0.860 while those of the H² → (L+1)² and (H-1)² → L² configurations are -0.150 and -0.110, respectively. The ¹A₂ and ¹B₁ states are of two determinant nature and hence cannot reasonably be considered by single-reference CCSD(T) and may also be problematic for DFT and hence were not computed by those methods. For the ¹A₂ state, the weight of the reference configuration [(1b₁)² (1a₂)² (2b₁)¹ (7b₂)¹] is 0.876, but the configuration [(1b₁)² (3b₁)² (2b₁)¹ (7b₂)¹] has a large contribution of -0.150. An even more pronounced multireference situation is obtained for the ¹B₁ state. Its reference configuration [(1b₁)² (2b₁)² (1a₂)¹ (7b₂)¹] has a rather low coefficient of 0.797 and large contributions from [(1b₁)² (3b₁)² (1a₂)¹ (7b₂)¹] (-0.24) and [(1b₁)² (2b₁)¹ (3b₁)¹ (1a₂)¹ (7b₂)¹] (0.246 and 0.145). A similar situation is found for the triplet states. The coefficient of the reference configuration of the ³A₂ state [(1b₁)² (1a₂)² (2b₁)¹ (7b₂)¹] is much larger (0.877) than that of the ³B₁ state [(1b₁)² (2b₁)² (1a₂)¹ (7b₂)¹] (0.795). The wavefunction of the latter state has significant contributions from excited configurations [(1b₁)² (3b₁)² (1a₂)¹ (7b₂)¹] (-0.263) and [(1b₁)² (2b₁)¹ (3b₁)¹ (1a₂)¹ (7b₂)¹] (0.246 and 0.157). The significant multireference character of the ^{1,3}B₁ states is deemed responsible for their incorrect relative energies at the CASPT2 level of theory.

Both MCCEPA and ACPF corroborate the conclusions of the MRCI+Q and CCSD(T) data, as they find the ³A₂ state as the energetically lowest one. According to the MCCEPA results, this state is at -5.4 kcal mol⁻¹ with respect to the ¹A₁ state, which is very similar to the MRCI+Q result, while

the ACPF result (-1.7 kcal mol⁻¹) is essentially identical to the CCSD(T) relative energy. In agreement with the MRCI+Q finding, both approaches predict the ¹B₁ and ³B₁ states clearly above the ³A₂ and ¹A₁ states. The singlet-triplet energy splitting of the B₁ states is within about one kcal mol⁻¹ as indicated by CASPT2 and MRCI+Q, while the ¹A₂ state is predicted by all approaches to be energetically higher by about 30 kcal mol⁻¹ than the corresponding triplet state. Overall, the perturbation due to the polar BN unit that induces antiaromaticity has significant impact on the electronic structure of **6**.

Chemically, the singlet states are particularly interesting as they should be involved due to spin conservation in thermal rearrangements of **4** or in thermally induced dinitrogen extrusion from azidoboroles. Our group recently investigated the latter reaction for the dibenzo derivative, 9-azido-9-borafluorene.^[31] We note that the geometries of the ¹A₁ and ¹B₁ states are so significantly different that at the geometry of the ¹A₁ state the ¹B₁ state is 5.7 kcal mol⁻¹ higher in energy (see Supporting Information, Figure S2, for the geometries of ¹A₁-**6** state the ¹B₁-**6**). Likewise, at the geometry of the ¹B₁ state, the ¹A₁ state is 18.2 kcal mol⁻¹ higher. Hence, we computed the Hessian by finite differences at CASPT2 and obtained one imaginary vibrational frequency for both ¹A₁-**6** (*i*289 cm⁻¹) and ¹B₁-**6** (*i*144 cm⁻¹). At the CASSCF(6,7) level, which does not take into account dynamic correlation, the ¹A₁-**6** state corresponds to a minimum. As both CASPT2 and B3LYP arrive at a first order saddle point for ¹A₁-**6**, we conclude that dynamic correlation has a significant impact on the nature of stationary points. In summary, the CASPT2 computations corroborate the previous B3LYP computations that indicated a concerted N₂ loss and ring enlargement of 9-azido-9-borafluorene, in agreement with experimental observations in azidoborane chemistry.^[32]

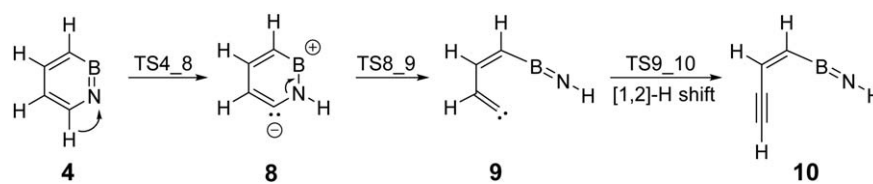
The aminoborylene isomer **7** has an aromatic pyrrole ring and is energetically (32 kcal mol⁻¹ above **4**) much more favorable than **6**. The transition state between **4** and **7** (**TS4_7**) lies about 65 kcal mol⁻¹ (see below) above **4**. The barrier computed here for the **7** → **4** rearrangement of 34 kcal mol⁻¹ is similar to the values (27.4 kcal mol⁻¹) reported previously for the parent system, that is, aminoborylene (H₂NB) to iminoborane (HNB).^[33] The comparison with **2** shows that the formation of **2** is more likely because **2** is only 30 kcal mol⁻¹ above **1** in energy and corresponds to a very shallow minimum on the potential energy surface (PES).^[6b,34]

Hydrogen Shifts and Ring Opening to BN-Enediynes

For the ring opening of **4**, we considered two pathways. Pathway 1 (Scheme 5) starts with a proton shift to the neighboring N atom to give **8**. The relative energy of **8** is about 46 kcal mol⁻¹ and the reaction barrier about 77 kcal mol⁻¹ (Fig. 1). The second step is the C-N bond cleavage that leads to vinylidene **9**. This occupies a very shallow minimum on the PES (relative energy of about 63 kcal mol⁻¹).^[6b] The subsequent [1,2]-H shift yields the BN substituted enediyne **10**. In agreement with numerous previous experimental and computational

Table 2. Composition of the wavefunctions of electronic states of borylnitrene **6** based on CAS(6,7)-MRCI/cc-pVTZ//CAS(6,7)-CASPT2/6-31G* computations.

State	Configuration	CI coefficient (singlet states)	CI coefficient (triplet states)
¹ A ₁	(1b ₁) ² (1a ₂) ² (2b ₁) ²	0.860	not computed
	(1b ₁) ² (2b ₁) ² (3b ₁) ²	-0.150	
	(1b ₁) ² (1a ₂) ² (7b ₂) ²	-0.110	
^{1,3} A ₂	(1b ₁) ² (1a ₂) ² (2b ₁) ¹ (7b ₂) ¹	0.876	0.877
	(1b ₁) ² (3b ₁) ² (2b ₁) ¹ (7b ₂) ¹	-0.150	-0.152
^{1,3} B ₁	[(1b ₁) ² (2b ₁) ² (1a ₂) ¹ (7b ₂) ¹]	0.797	0.795
	[(1b ₁) ² (3b ₁) ² (1a ₂) ¹ (7b ₂) ¹]	-0.284	-0.263
	[(1b ₁) ² (2b ₁) ¹ (3b ₁) ¹ (1a ₂) ¹ (7b ₂) ¹]	0.246	0.246
	[(1b ₁) ² (2b ₁) ¹ (3b ₁) ¹ (1a ₂) ¹ (7b ₂) ¹]	0.145	0.157
	Only CI coefficients larger than 0.100 are given.		



Scheme 5. Pathway 1 shows the ring opening of 1,2-azaborine (**4**) to BN-enediyne **10**.

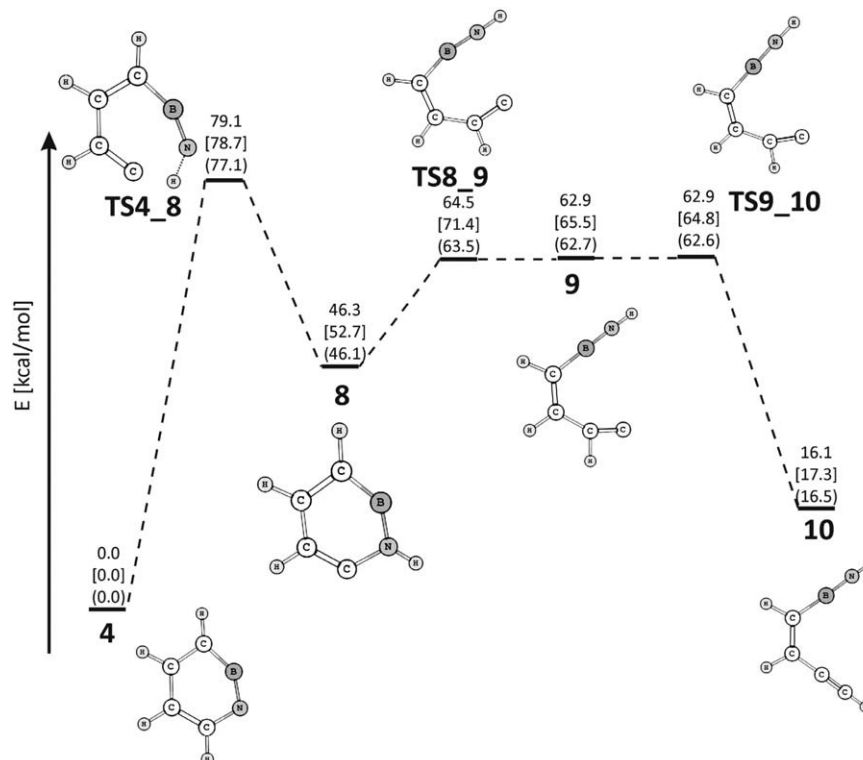
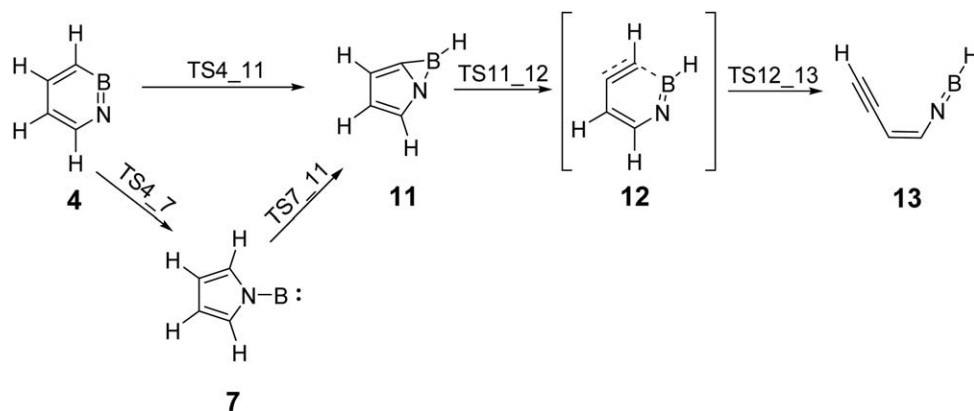


Figure 1. Potential energy diagram for pathway 1 computed at B3LYP/6-311+G**, [MP2/cc-pVTZ], and (CCSD(T)/cc-pVTZ//B3LYP/6-311+G**).

investigations for parent vinylidene, the barrier for the hydrogen shift is very low.^[35]

In pathway 2 (Scheme 6), **4** rearranges first to **7** and then the borylene unit inserts intramolecularly into the *ortho*-CH bond to form bicyclic **11**. Intramolecular CH insertion was pre-

viously reported for phenylborylene.^[36] The direct pathway from **4** to **11** by [1,2]-H shift is only slightly higher in energy (about 1 kcal mol⁻¹). In the all-carbon system, the rearrangement from **1** to *meta*-benzyne the pathway with an involvement of **2** is much more favourable than [1,2]-H shift.^[6b] The



Scheme 6. Pathway 2 shows the ring opening of 1,2-azaborine (**4**) to BN-enediyne **13**.

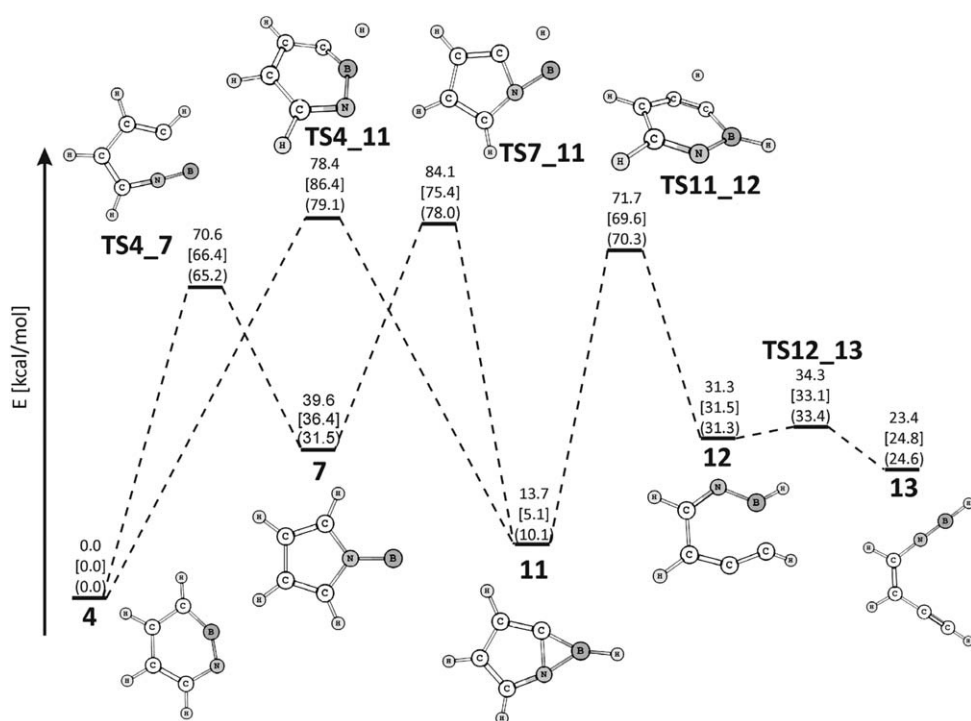


Figure 2. Potential energy diagram for pathway 2 computed at B3LYP/6-311+G**, [MP2/cc-pVTZ], and (CCSD(T)/cc-pVTZ//B3LYP/6-311+G**).

ring opening of **11** is concomitant with a [1,2]-H shift and leads to intermediate **12** that occupies a shallow minimum on PES with an activation barrier of 3 kcal mol⁻¹ to form BN-enediye **13** (Fig. 2).

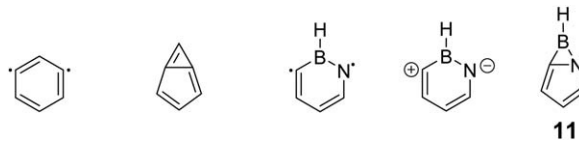
A brief discussion of the structural features of **11** is appropriate, as it is isolectronic to *meta*-benzyne (Scheme 7). The structure of *meta*-benzyne was discussed controversially. Depending on the level of theory, computations predict either a monocyclic biradical or a bicyclic anti-Bredt structure (Scheme 7) that is isosteric to **11**.^[24,37] The IR spectra measured for *meta*-benzyne, however, show agreement with the computed IR spectra of the monocyclic structure.^[7a] The computed structure of **11** is bicyclic at the spin restricted and spin-unrestricted B3LYP, at MP2, and at CASSCF(8,8) levels, while that of *meta*-benzyne is “open” at CASSCF(8,8).^[24] The electronegativity difference between carbon and nitrogen favors a zwitterionic over a diradical form for the “open” structure. The large Coulomb attraction between the 1,3 positions results in the “closed” structure **11** after full geometry optimization.

Fragmentation of 1,2-Azaborine. We also considered the concerted fragmentation of **4** to give acetylene and a BN substituted diacetylene **14** (Scheme 8).^[8,10] The reaction is energetically uphill by 112.5 kcal mol⁻¹. This is about twice as

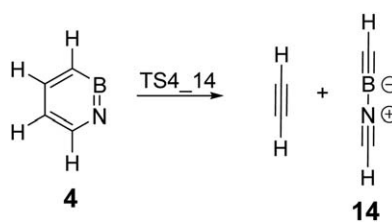
much as in the all-carbon system, indicating that the fragmentation is much more unfavorable for 1,2-azaborine than for *ortho*-benzyne. The concerted mechanism proceeds through transition state **TS4_14** and involves an energy barrier of 120 kcal mol⁻¹. This is also much larger than the 90 kcal mol⁻¹ computed for the all-carbon system.^[8,10] The Gibbs energies at selected temperatures between 500 K and 1100 K are given in the Supporting Information (Tables S6 and S7). As can be seen, this fragmentation pathway has a Gibbs energy of activation beyond 100 kcal mol⁻¹ at temperatures relevant in the previous FVP study.^[11]

Note that Ghigo et al. identified an additional pathway from **1** to C₂H₂ and C₄H₂ that involves diradical intermediates.^[10] As formation of **14** is very high in energy and much higher than in the all-carbon system, these pathways were not considered for **4**.

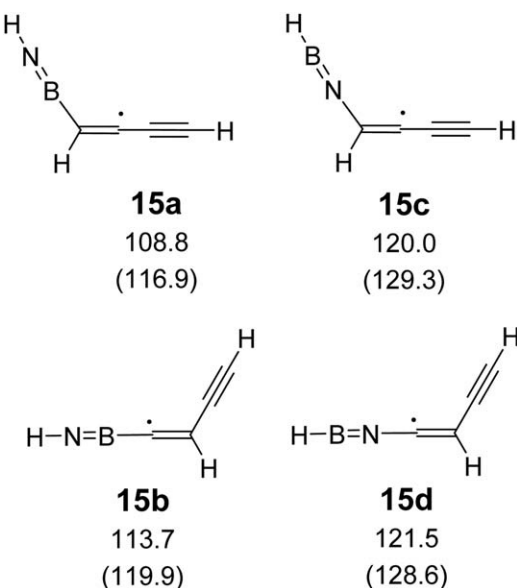
An alternative fragmentation of **1** is to C₆H₂ and hydrogen atoms which starts from the *cis*- and *trans*-enediye isomers (hexa-3-ene-1,5-diyne) and proceeds stepwise through enediynyl radicals.^[10] The relevant BN-enediynyl radicals (Scheme 9) **15a,b** are 117–120 kcal mol⁻¹ and **15c,d** are almost 130 kcal mol⁻¹ above **4** in energy (Supporting Information Tables S8 and S9).



Scheme 7. Structures of *meta*-benzyne.



Scheme 8. Fragmentation of 1,2-azaborine (**4**) to acetylene and a BN substituted diacetylene (**14**).



Scheme 9. BN-enediynyl radical isomers **15a-d**. Relative energies (in kcal mol^{-1}) are including zero point vibrational energy corrections, computed at UB3LYP/6-311+G** and (UCCSD(T)/cc-pVTZ//UB3LYP/6-311+G**).

In the all-carbon case, the barrier heights for C–H cleavage in enediynes are 0.1 kcal mol^{-1} higher than the heat of the reactions that are around 119 kcal mol^{-1} .^[10] Similar behavior can be expected for the fragmentation of BN-enediynes as the same type of bond, that is, $C_{\text{sp}^2}\text{-H}$, is cleaved. Hence, fragmentation of BN-enediynes to yield linear 1-aza-2-bora-hexatriyne and hydrogen atoms is expected to be as feasible as high temperatures as predicted for the all-carbon case.^[10]

Conclusions

The computational investigation of 1,2-azaborine (**4**) rearrangements and fragmentation mechanisms arrives at the following conclusions:

- Ring contraction of **4** to nitrenoborole **6** or pyrrolylborylene (**7**) is energetically unfavorable, and more so than that of *ortho*-benzyne to cyclopentadienylidenecarbene.
- Nitrenoborole **6** prefers a triplet ground state (${}^3\text{A}_2$), the lowest energy singlet state (${}^1\text{A}_1$) is 4–5 kcal mol^{-1} higher in energy at the most reliable (MRCI+Q, MCCEPA) levels of theory. Most importantly, ${}^1\text{A}_1\text{-}6$ corresponds to a first order stationary point and hence it is not expected to behave as a distinct transient intermediate.
- Rearrangement pathways to BN-enediynes were identified. The product with terminal NH bond (**10**) is thermodynamically more stable than the BH isomer (**13**). The barriers for the two pathways are remarkably high, up to 77–78 kcal mol^{-1} .
- Fragmentation of **4** to acetylene and 2-aza-3-borabutadiyne (**14**) is much more endothermic than the related reaction of *ortho*-benzyne. The concerted mechanism also involves a significantly higher barrier for the BN than the all-carbon system.

5. Fragmentation of the rearrangement product BN-enediynes to hydrogen atoms and 1-aza-2-bora-hexatriyne has similar energy requirements as the related fragmentation of hexa-3-ene-1,5-diyne.

Acknowledgments

This work was supported by the Deutsche Forschungsgemeinschaft. The authors gratefully thank the bwGRID project [<http://www.bwgrid.de>, member of the German D-Grid initiative, funded by Bundesministerium für Bildung und Forschung and Ministerium für Wissenschaft, Forschung und Kunst, Baden-Württemberg)] for the computational resources.

Keywords: BN heterocycles • arynes • nitrenes • ab initio • rearrangements

How to cite this article: K. Edel, R. F. Fink, H. F. Bettinger. *J. Comput. Chem.* **2016**, *37*, 110–116. DOI: 10.1002/jcc.24189

Additional Supporting Information may be found in the online version of this article.

- [1] (a) C. M. Gampe, E. M. Carreira, *Angew. Chem. Int. Ed.* **2012**, *51*, 3766; (b) P. M. Tadross, B. M. Stoltz, *Chem. Rev.* **2012**, *112*, 3550; (c) H. Yoshida, K. Takaki, *Synlett* **2012**, *23*, 1725; (d) A. Bhunia, S. R. Yetra, A. T. Biju, *Chem. Soc. Rev.* **2012**, *41*, 3140; (e) C. Wentrup, *Aust. J. Chem.* **2010**, *63*, 979; (f) T. Kitamura, *Aust. J. Chem.* **2010**, *63*, 987; (g) H. H. Wenk, M. Winkler, W. Sander, *Angew. Chem. Int. Ed.* **2003**, *42*, 502; (h) H. Pellissier, M. Santelli, *Tetrahedron* **2003**, *59*, 701.
- [2] M. Barry, R. F. C. Brown, F. W. Eastwood, D. A. Gunawardana, C. Vogel, *Aust. J. Chem.* **1984**, *37*, 1643.
- [3] C. Wentrup, R. Blanch, H. Briehl, G. Gross, *J. Am. Chem. Soc.* **1988**, *110*, 1874.
- [4] R. F. C. Brown, F. W. Eastwood, *Synlett* **1993**, *1993*, 9.
- [5] M. Winkler, W. Sander, *Aust. J. Chem.* **2010**, *63*, 1013.
- [6] (a) L. V. Moskaleva, L. K. Madden, M. C. Lin, *Phys. Chem. Chem. Phys.* **1999**, *1*, 3967; (b) M. Winkler, B. Cakir, W. Sander, *J. Am. Chem. Soc.* **2004**, *126*, 6135.
- [7] (a) W. Sander, M. Exner, M. Winkler, A. Balster, A. Hjerpe, E. Kraka, D. Cremer, *J. Am. Chem. Soc.* **2002**, *124*, 13072; (b) R. R. Jones, R. G. Bergman, *J. Am. Chem. Soc.* **1972**, *94*, 660; (c) R. G. Bergman, *Acc. Chem. Res.* **1973**, *6*, 25.
- [8] X. Zhang, A. T. MacCarrone, M. R. Nimlos, S. Kato, V. M. Bierbaum, G. B. Ellison, B. Ruscic, A. C. Simmonett, W. D. Allen, H. F. Schaefer, *J. Chem. Phys.* **2007**, *126*, 044312.
- [9] W. Deng, K. L. Han, J. P. Zhan, G. Z. He, *Chem. Phys. Lett.* **1998**, *288*, 33.
- [10] G. Ghigo, A. Maranzana, G. Tonachini, *Phys. Chem. Chem. Phys.* **2014**, *16*, 23944.
- [11] K. Edel, S. A. Brough, A. N. Lamm, S. Y. Liu, H. F. Bettinger, *Angew. Chem. Int. Ed.* **2015**, *54*, 7819.
- [12] (a) P. C. Hariharan, J. A. Pople, *Theor. Chim. Acta* **1973**, *28*, 213; (b) R. Krishnan, J. S. Binkley, R. Seeger, J. A. Pople, *J. Chem. Phys.* **1980**, *72*, 650; (c) T. H. Dunning, *J. Chem. Phys.* **1989**, *90*, 1007.
- [13] (a) A. D. Becke, *J. Chem. Phys.* **1993**, *98*, 5648; (b) C. Lee, W. Yang, R. G. Parr, *Phys. Rev. B* **1988**, *37*, 785.
- [14] P. J. Stephens, F. J. Devlin, C. F. Chabalowski, M. J. Frisch, *J. Phys. Chem.* **1994**, *98*, 11623.
- [15] M. J. Frisch, G. W. Trucks, H. B. Schlegel, G. E. Scuseria, M. A. Robb, J. R. Cheeseman, G. Scalmani, V. Barone, B. Mennucci, G. A. Petersson, H. Nakatsuji, M. Caricato, X. Li, H. P. Hratchian, A. F. Izmaylov, J. Bloino, G. Zheng, J. L. Sonnenberg, M. Hada, M. Ehara, K. Toyota, R. Fukuda, J. Hasegawa, M. Ishida, T. Nakajima, Y. Honda, O. Kitao, H. Nakai, T. Vreven, J. A. Montgomery, Jr., J. E. Peralta, F. Ogliaro, M. Bearpark, J. J. Heyd, E. Brothers, K. N. Kudin, V. N. Staroverov, R. Kobayashi, J.

- Normand, K. Raghavachari, A. Rendell, J. C. Burant, S. S. Iyengar, J. Tomasi, M. Cossi, N. Rega, M. J. Millam, M. Klene, J. E. Knox, J. B. Cross, V. Bakken, C. Adamo, J. Jaramillo, R. Gomperts, R. E. Stratmann, O. Yazyev, A. J. Austin, R. Cammi, C. Pomelli, J. W. Ochterski, R. L. Martin, K. Morokuma, V. G. Zakrzewski, G. A. Voth, P. Salvador, J. J. Dannenberg, S. Dapprich, A. D. Daniels, Ö. Farkas, J. B. Foresman, J. V. Ortiz, J. Cioslowski, D. J. Fox, Gaussian 09, Revision D.01, Wallingford CT, **2009**.
- [16] (a) H. P. Hratchian, H. B. Schlegel, *J. Chem. Phys.* **2004**, *120*, 9918; (b) H. P. Hratchian, H. B. Schlegel, *J. Chem. Theory Comput.* **2005**, *1*, 61.
- [17] K. Raghavachari, G. W. Trucks, J. A. Pople, M. Head-Gordon, *Chem. Phys. Lett.* **1989**, *157*, 479.
- [18] H. J. Werner, *Mol. Phys.* **1996**, *89*, 645.
- [19] P. Celani, H. J. Werner, *J. Chem. Phys.* **2003**, *119*, 5044.
- [20] (a) P. J. Knowles, H.-J. Werner, *Chem. Phys. Lett.* **1988**, *145*, 514; (b) H.-J. Werner, P. J. Knowles, *J. Chem. Phys.* **1988**, *89*, 5803.
- [21] (a) S. R. Langhoff, E. R. Davidson, *Int. J. Quant. Chem.* **1974**, *8*, 61; (b) W. Duch, G. H. F. Diercksen, *J. Chem. Phys.* **1994**, *101*, 3018.
- [22] R. Fink, V. Staemmler, *Theoret. Chim. Acta* **1993**, *87*, 129.
- [23] R. J. Gdanitz, R. Ahlrichs, *Chem. Phys. Lett.* **1988**, *143*, 413.
- [24] M. Winkler, W. Sander, *J. Phys. Chem. A* **2001**, *105*, 10422.
- [25] (a) H.-J. Werner, P. J. Knowles, G. Knizia, F. R. Manby, M. Schütz, *WIREs Comput Mol Sci* **2012**, *2*, 242; (b) H.-J. Werner, P. J. Knowles, G. Knizia, F. R. Manby, M. Schütz, P. Celani, T. Korona, R. Lindh, A. Mitrushenkov, G. Rauhut, K. R. Shamasundar, T. B. Adler, R. D. Amos, A. Bernhardsson, A. Berning, D. L. Cooper, M. J. O. Deegan, A. J. Dobbyn, F. Eckert, E. Goll, C. Hampel, A. Hesselmann, G. Hetzer, T. Hrenar, G. Jansen, C. Köpl, Y. Liu, A. W. Lloyd, R. A. Mata, A. J. May, S. J. McNicholas, W. Meyer, M. E. Mura, A. Nicklass, D. P. O'Neill, P. Palmieri, D. Peng, K. Pflüger, R. Pitzer, M. Reiher, T. Shiozaki, H. Stoll, A. J. Stone, R. Tarroni, T. Thorsteinsson, and M. Wang, MOLPRO, version 2012.1, a package of ab initio programs, see <http://www.molpro.net>.
- [26] (a) H. F. Bettinger, *Inorg. Chem.* **2007**, *46*, 5188; (b) H. F. Bettinger, H. Bornemann, *J. Am. Chem. Soc.* **2006**, *128*, 11128; (c) H. F. Bettinger, H. Bornemann, *Z. Anorg. Allg. Chem.* **2011**, *637*, 2169; (d) H. F. Bettinger, M. Filthaus, *Org. Biomol. Chem.* **2010**, *8*, 5477; (e) H. F. Bettinger, M. Filthaus, H. Bornemann, I. M. Oppel, *Angew. Chem. Int. Ed.* **2008**, *47*, 4744; (f) H. F. Bettinger, M. Filthaus, P. Neuhaus, *Chem. Commun.* **2009**, 2186; (g) M. Filthaus, L. Schwertmann, P. Neuhaus, R. W. Seidel, I. M. Oppel, H. F. Bettinger, *Organometallics* **2012**, *31*, 3894.
- [27] M. T. Nguyen, *J. Chem. Soc. Chem. Commun.* **1987**, 342.
- [28] (a) M. Winkler, *J. Phys. Chem. A* **2008**, *112*, 8649; (b) H. F. Bettinger, W. Sander, *J. Am. Chem. Soc.* **2003**, *125*, 9726.
- [29] (a) B. A. Smith, C. J. Cramer, *J. Am. Chem. Soc.* **1996**, *118*, 5490; (b) K. Andersson, B. O. Roos, *Int. J. Quant. Chem.* **1993**, *45*, 591; (c) K. Andersson, *Theor. Chim. Acta* **1995**, *91*, 31; (d) W. L. Karney, W. T. Borden, in *Advances in Carbene Chemistry*, Vol. 3; U. H. Brinker, Eds.; Elsevier: Amsterdam, **2001**; pp. 205.
- [30] T. J. Lee, P. R. Taylor, *Int. J. Quant. Chem.: Quant. Chem. Symp.* **1989**, *36*, 199.
- [31] (a) M. Müller, C. Maichle-Mössmer, H. F. Bettinger, *Angew. Chem. Int. Ed.* **2014**, *53*, 9380; (b) H. F. Bettinger, M. Müller, *J. Phys. Org. Chem.* **2015**, *28*, 97.
- [32] P. Paetzold, *Adv. Inorg. Chem.* **1987**, *31*, 123.
- [33] (a) V. M. Rosas-Garcia, T. D. Crawford, *J. Chem. Phys.* **2003**, *119*, 10647; (b) J.-G. Zhang, Q. S. Li, S.-W. Zhang, *J. Mol. Model.* **2006**, *12*, 190.
- [34] (a) N. A. Burton, G. E. Quelch, M. M. Gallo, H. F. Schaefer, III, *J. Am. Chem. Soc.* **1991**, *113*, 764; (b) E. W.-G. Diau, J. Casanova, J. D. Roberts, A. H. Zewail, *Proc. Natl. Acad. Sci. U.S.A.* **2000**, *97*, 1376; (c) M. Winkler, *J. Phys. Chem. A* **2005**, *109*, 1240.
- [35] (a) Y. Osamura, H. F. Schaefer, S. K. Gray, W. H. Miller, *J. Am. Chem. Soc.* **1981**, *103*, 1904; (b) M. M. Gallo, T. P. Hamilton, H. F. Schaefer, *J. Am. Chem. Soc.* **1990**, *112*, 8714; (c) N.-Y. Chang, M.-Y. Shen, C.-H. Yu, *J. Chem. Phys.* **1997**, *106*, 3237; (d) J. F. Stanton, J. Gauss, *J. Chem. Phys.* **1999**, *110*, 1831; (e) S. Zou, J. M. Bowman, *Chem. Phys. Lett.* **2003**, *368*, 421; (f) S. Joseph, A. J. C. Varandas, *J. Phys. Chem. A* **2010**, *114*, 13277; (g) K. M. Ervin, J. Ho, W. C. Lineberger, *J. Chem. Phys.* **1989**, *91*, 5974; (h) J. Levin, H. Feldman, A. Baer, D. Ben-Hamu, O. Heber, D. Zajfman, Z. Vager, *Phys. Rev. Lett.* **1998**, *81*, 3347.
- [36] H. F. Bettinger, *J. Am. Chem. Soc.* **2006**, *128*, 2534.
- [37] (a) B. A. Hess, Jr., *Eur. J. Org. Chem.* **2001**, 2185; (b) E. Kraka, J. Anglada, A. Hjerpe, M. Filatov, D. Cremer, *Chem. Phys. Lett.* **2001**, *348*, 115.

Received: 11 May 2015

Revised: 28 July 2015

Accepted: 30 July 2015

Published online on 29 September 2015

Supporting Information

Isomerization and fragmentation pathways of 1,2-azaborine

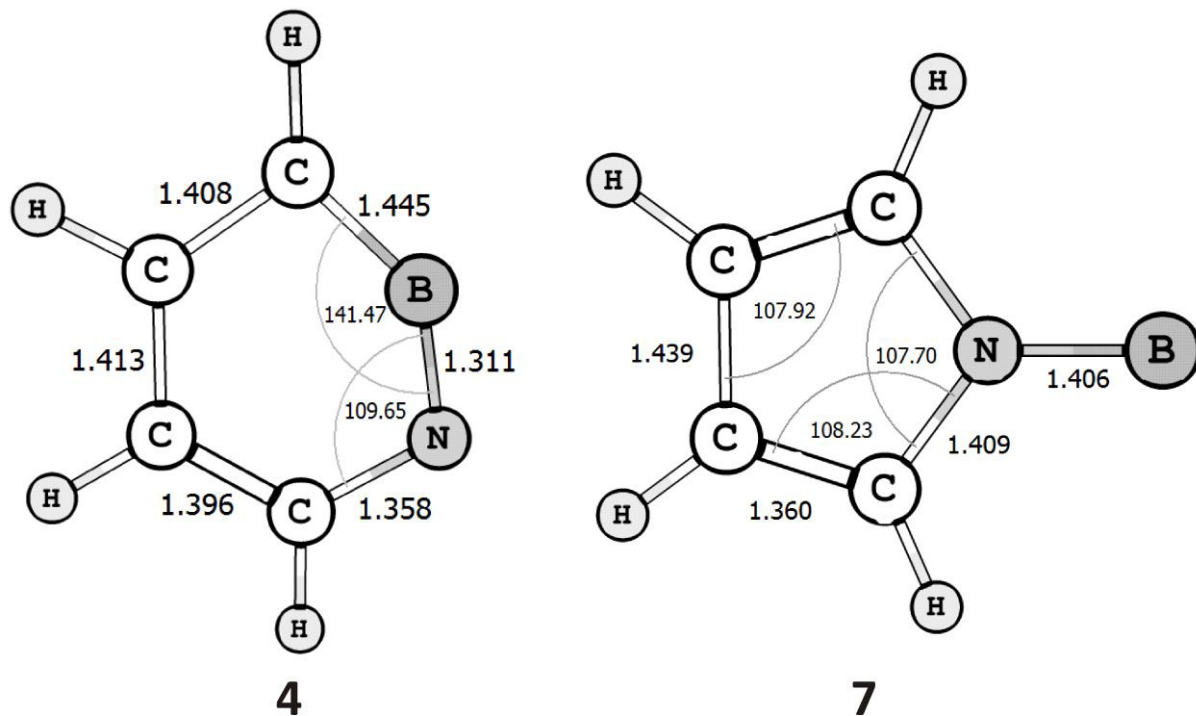
Klara Edel^a, Reinhold F. Fink^b and Holger F. Bettinger^{a,*}

^a Institut für Organische Chemie, Universität Tübingen, Auf der Morgenstelle 18, 72076
Tübingen, Germany.

E-mail: holger.bettinger@uni-tuebingen.de

^b Institut für Physikalische und Theoretische Chemie, Universität Tübingen, Auf der
Morgenstelle 18, 72076 Tübingen, Germany

Isomerization and fragmentation pathways of 1,2-azaborine



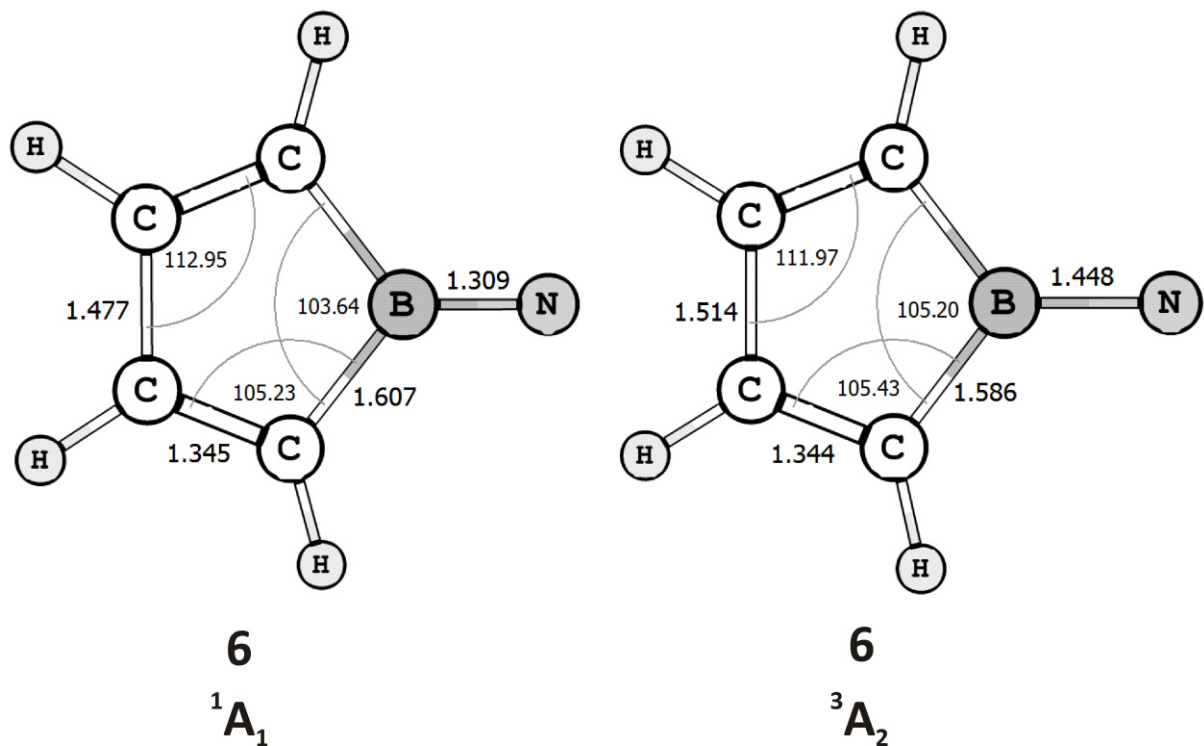


Figure S1. Structures of 1,2-azaborine (**4**) and its isomers **6** and **7** at the B3LYP/6-311+G** level of theory.

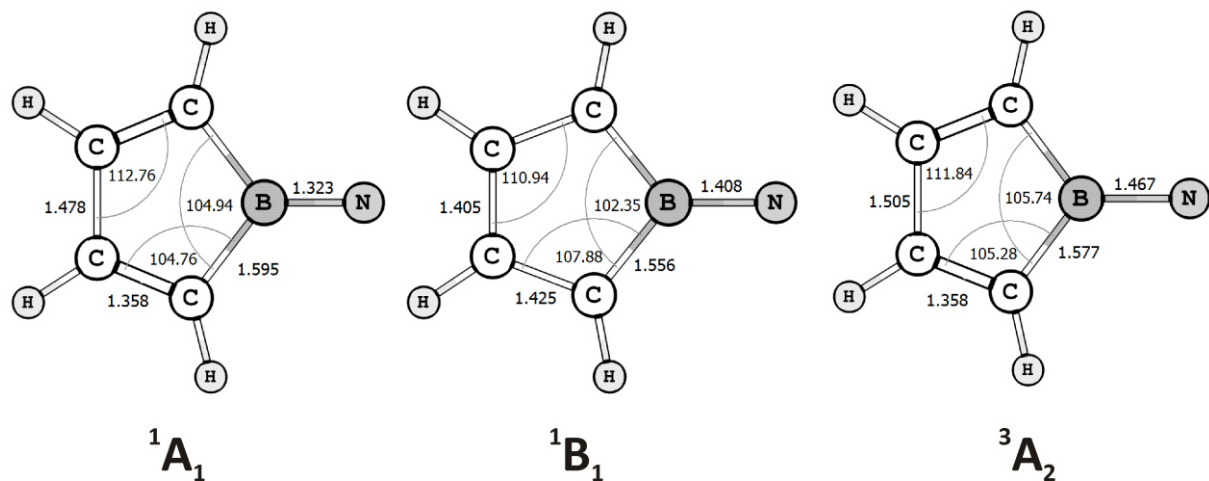


Figure S2. Geometries of electronic states of isomer **6** at the CASPT2/6-31G* level of theory.

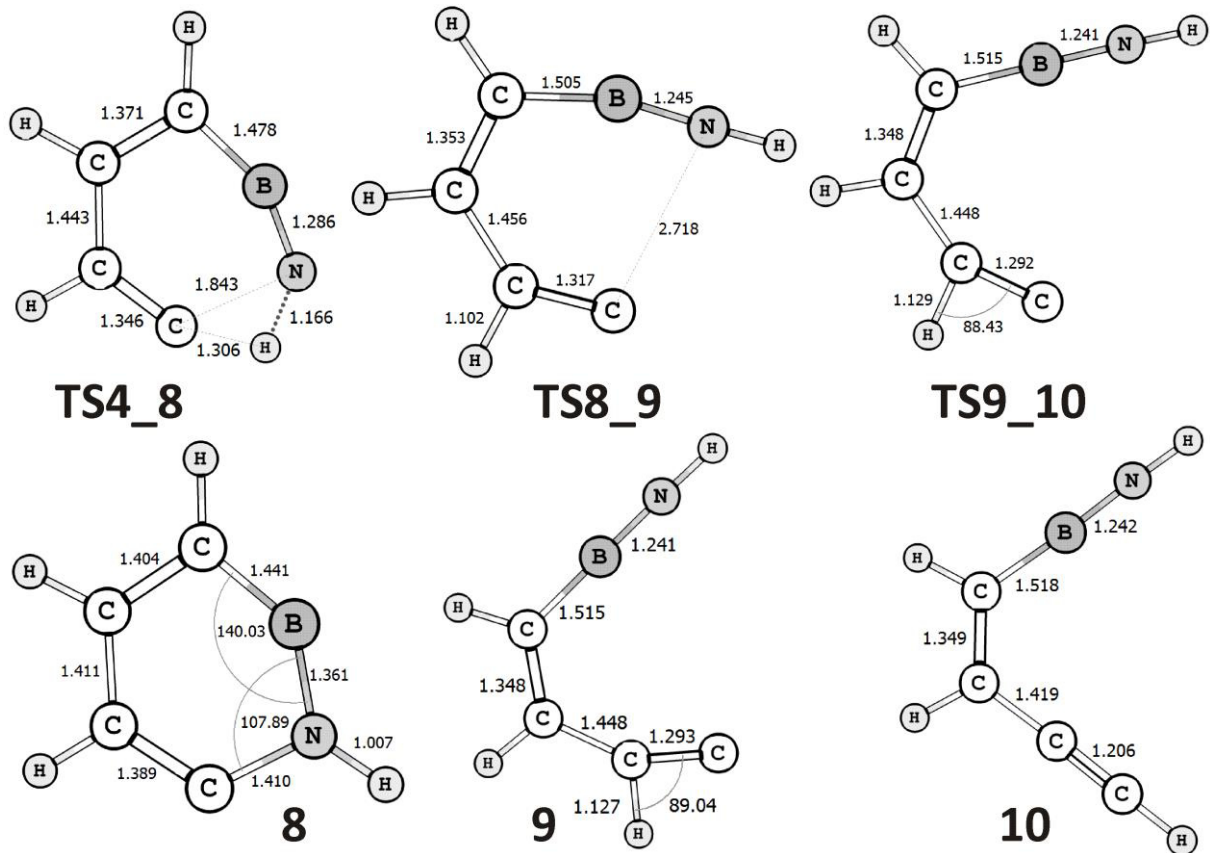
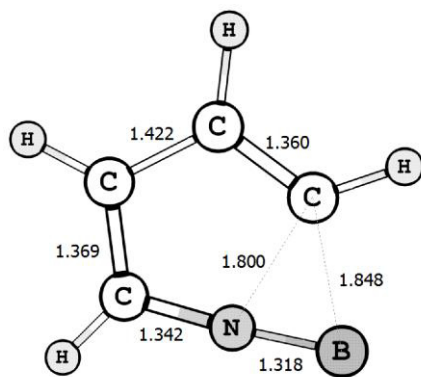
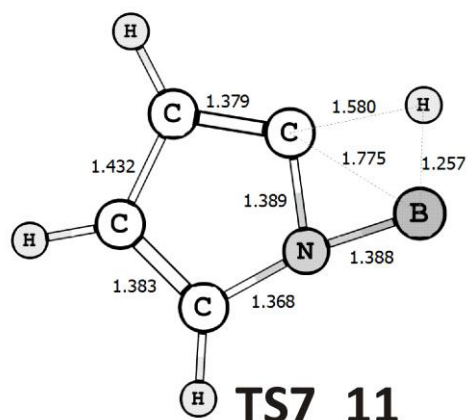


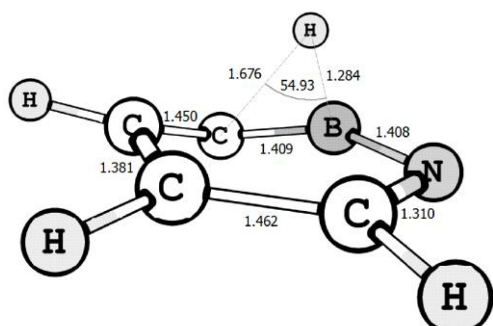
Figure S3. Structures of Pathway 1 at the B3LYP/6-311+G** level of theory.



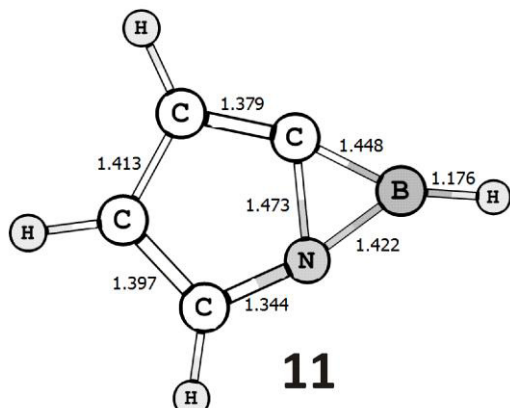
TS4_7



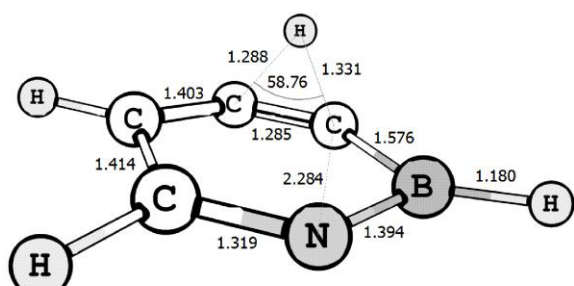
TS7_11



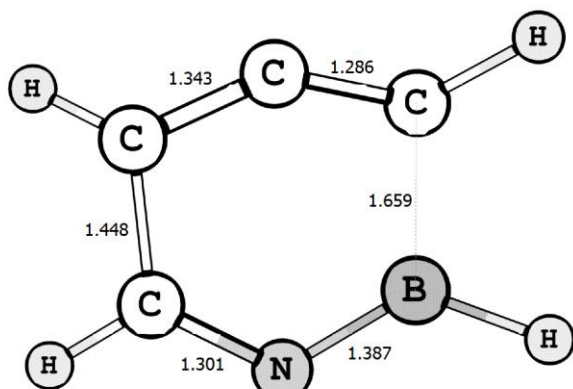
TS4_11



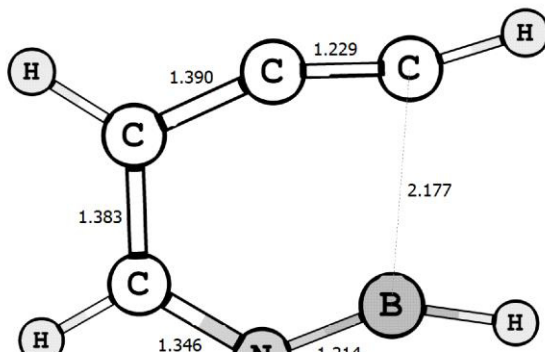
11



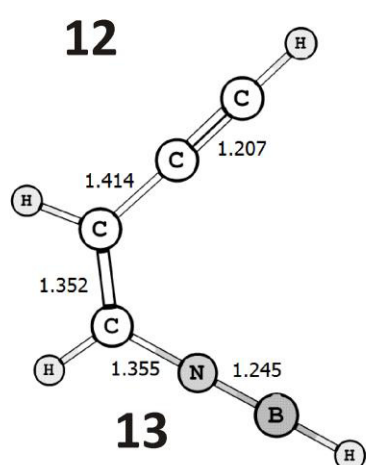
TS11_12



12



TS12_13



13

Figure S4. Structures of Pathway 2 at the B3LYP/6-311+G** level of theory.

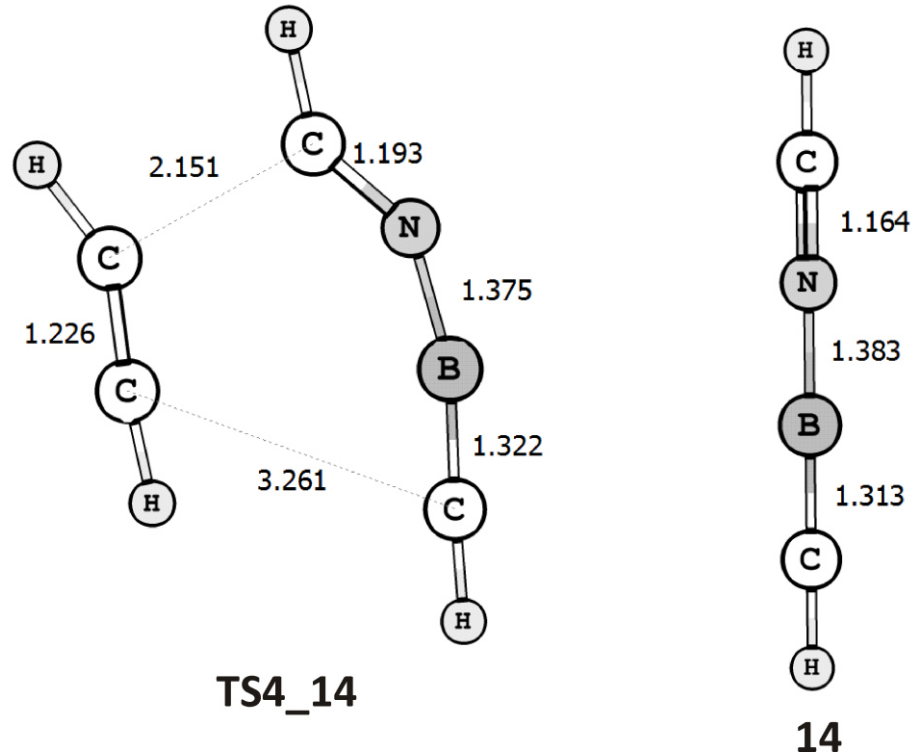


Figure S5. Structures of **TS4_14** and **14** computed at the B3LYP/6-311+G** level of theory.

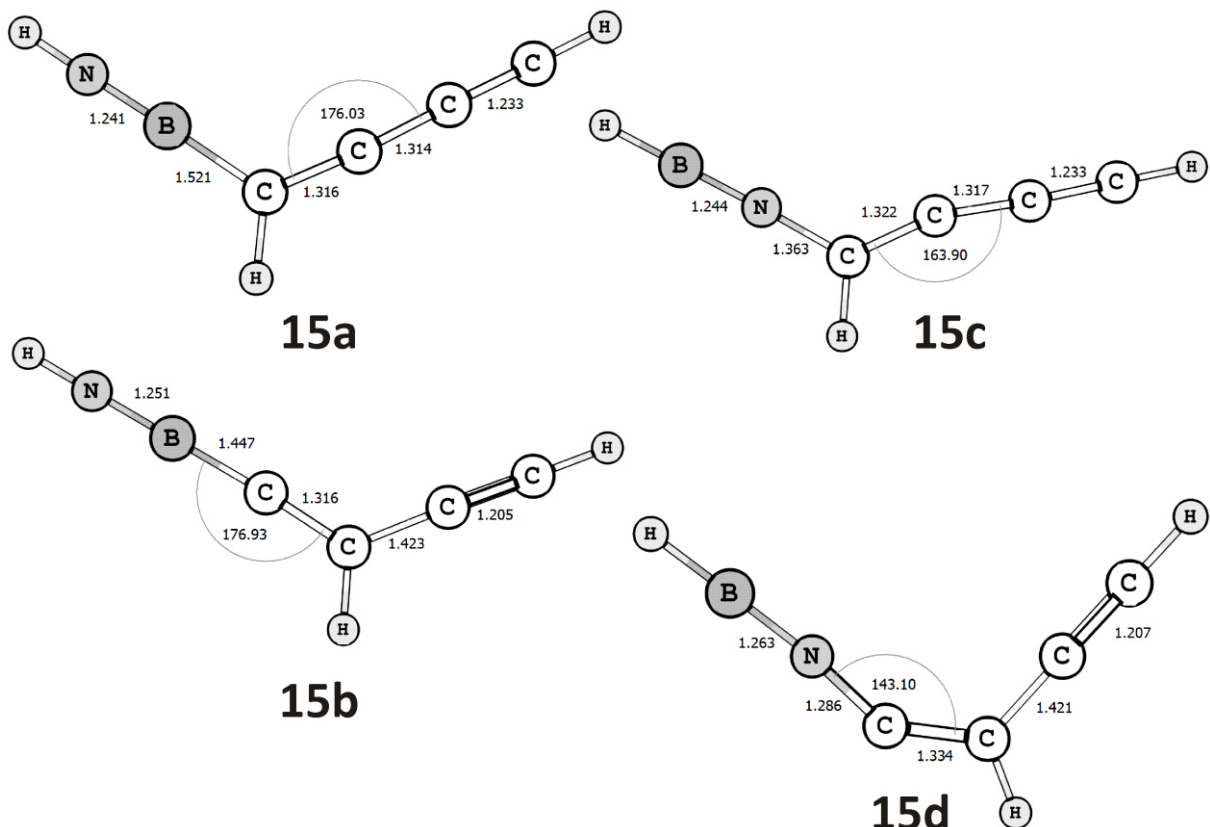


Figure S6. Structures of **15a-d** computed at the UB3LYP/6-311+G** level of theory.

Table S1. Computed absolute energies (in a.u.) and relative energies including zero point vibrational energy corrections (ΔE_{ZPVE} in kcal mol⁻¹) for all compounds at the B3LYP/6-31G* level of theory.

	E [a.u.]	ΔE_{ZPVE} [kcal/mol]	[cm ⁻¹]
4	-234.40070	0	
6 (1A₁)	-234.28567	69.4	
6 (3A₂)	-234.28302	71.0	
7	-234.33386	41.3	
TS4_8	-234.25923	83.4	1320.4i
8	-234.31964	50.1	
TS8_9	not avail.	not avail.	not avail.
9	not avail.	not avail.	
TS9_10	-234.27819	70.4	511.9i
10	-234.35638	24.8	
TS4_11	-234.26896	78.5	872.6i
TS4_7	-234.28313	71.5	733.3i
TS7_11	-234.26071	84.3	1290.7i
11	-234.38152	10.8	
TS11_12	-234.27651	72.4	1239.5i
12	-234.34647	30.9	
TS12_13	-234.33723	35.9	237.4i
13	-234.35273	26.7	
TS4_14	-234.18095	130.8	352.6i
14	-156.86762		
acetylene	-77.32565		
14 + acetylene	-234.19327	121.2	

Table S2. Computed absolute energies (in a.u.) and relative energies including zero point vibrational energy corrections (ΔE_{ZPVE} in kcal mol⁻¹) for all compounds at the B3LYP/6-311+G** level of theory.

	E [a.u.]	ΔE_{ZPVE} [kcal/mol]	[cm ⁻¹]
4	-234.46405	0	
6 (1A₁)	-234.35046	68.5	
6 (3A₂)	-234.34580	71.4	
7	-234.39994	39.6	
TS4_8	-234.32954	79.1	1342.9i
8	-234.38915	46.3	
TS8_9	-234.35498	64.5	82.1i
9	-234.35598	62.9	
TS9_10	-234.35598	62.9	18.0i
10	-234.43387	16.1	
TS4_11	-234.33249	78.4	878.9i
TS4_7	-234.34796	70.6	726.0i
TS7_11	-234.32435	84.1	1287.9i
11	-234.44027	13.7	
TS11_12	-234.34078	71.7	1209.2i
12	-234.40885	31.3	
TS12_13	-234.40350	34.3	260.3i
13	-234.42144	23.4	

TS4_14	-234.25891	121.8	395.1i
14	-156.92132		
acetylene	-77.35665		
14 + acetylene	-234.27797	109.2	

Table S3. Computed absolute energies (in a.u.) and relative energies including zero point vibrational energy corrections (ΔE_{ZPVE} in kcal mol⁻¹) for all compounds at the MP2/6-311+G** level of theory.

	E [a.u.]	ΔE_{ZPVE} [kcal/mol]	[cm ⁻¹]
4	-233.74736	0	
6 (1A₁)	-233.60736	85.2	
6 (3A₂)	-233.61750	80.5	
7	-233.68708	36.9	
TS4_8	-233.61212	79.7	1357.4i
8	-233.66152	53.0	
TS8_9	-233.62794	70.4	100.8i
9	-233.63524	65.0	
TS9_10	-233.63511	64.3	566.9i
10	-233.71529	17.0	
TS4_11	-233.60499	85.5	754.1i
TS4_7	-233.63506	68.0	822.5i
TS7_11	-233.61808	77.4	1074.6i
11	-233.73392	7.3	
TS11_12	-233.62680	70.5	871.8i
12	-233.69032	32.4	
TS12_13	-233.68765	33.6	237.9i
13	-233.70163	25.0	
TS4_14	-233.54543	120.3	387.6i
14	-156.44738		
acetylene	-77.11323		
14 + acetylene	-233.56061	107.5	

Table S4. Computed absolute energies (in a.u.) and relative energies including zero point vibrational energy corrections (ΔE_{ZPVE} in kcal mol⁻¹) for all compounds at the MP2/cc-pVTZ level of theory.

	E [a.u.]	ΔE_{ZPVE} [kcal/mol]	[cm ⁻¹]
4	-233.88521	0	
6 (1A₁)	-233.74174	87.3	
6 (3A₂)	-233.74999	83.6	
7	-233.82614	36.4	
TS4_8	-233.75163	78.7	1374.6i
8	-233.79995	52.7	
TS8_9	-233.76409	71.4	127.0i
9	-233.77212	65.5	
TS9_10	-233.77177	64.8	715.0i
10	-233.85241	17.3	
TS4_11	-233.74087	86.4	1100.7i
TS4_7	-233.77586	66.4	819.8i
TS7_11	-233.75936	75.4	1119.7i
11	-233.87526	5.1	

TS11_12	-233.76619	69.6	848.9i
12	-233.82914	31.5	
TS12_13	-233.82612	33.1	235.6i
13	-233.83974	24.8	
TS4_14	-233.68331	120.2	322.9i
14	-156.53633		
acetylene	-77.15920		
14 + acetylene	-233.69553	108.8	

Table S5. Computed absolute energies (in a.u.) and relative energies including zero point vibrational energy corrections (ΔE_{ZPVE} in kcal mol⁻¹) for all compounds at the CCSD(T)/cc-pVTZ//B3LYP/6-311+G** level of theory.

	E [a.u.]	ΔE_{ZPVE} [kcal/mol]	T ₁ Diagnostic
4	-233.95462	0	0.01819
6 (1A₁)	-233.84352	66.9	0.03442
6 (3A₂)	-233.84060	68.7	0.01903
7	-233.90342	31.5	0.01251
TS4_8	-233.82320	77.1	0.01975
8	-233.87998	46.1	0.03810
TS8_9	-233.84714	63.5	0.01714
9	-233.84697	62.7	0.01652
TS9_10	-233.84698	62.6	0.01650
10	-233.92373	16.5	0.01487
TS4_11	-233.82192	79.1	0.02466
TS4_7	-233.84702	65.2	0.01897
TS7_11	-233.82458	78.0	0.01510
11	-233.93656	10.1	0.01174
TS11_12	-233.83373	70.3	0.02830
12	-233.89940	31.3	0.02743
TS12_13	-233.89548	33.4	0.01990
13	-233.91011	24.6	0.01538
TS4_14	-233.74662	123.6	0.02567
14	-156.57575		0.02564
acetylene	-77.18745		0.01297
14 + acetylene	-233.76320	112.5	

Table S6. Computed Gibbs free energies (in kcal mol⁻¹) for **TS4_14** and the fragmentation products (**14 + acetylene**) for selected temperatures at the B3LYP/6-311+G** level of theory.

p [atm]	T [K]	TS4_14	14 + acetylene
1.0	500	117.2	89.9
	600	115.6	85.2
	700	114.0	80.4
	800	112.3	75.6
	900	110.7	70.7
	1000	109.0	65.9
	1100	107.3	61.0
0.00001	500	117.2	78.5
	600	115.6	71.4
	700	114.0	64.4

	800	112.3	57.2
	900	110.7	50.1
	1000	109.0	43.0
	1100	107.3	35.9

Table S7. Computed Gibbs free energies (in kcal mol⁻¹) for **TS4_14** and the fragmentation products (**14** + acetylene) for selected temperatures at the CCSD(T)/cc-pVTZ//B3LYP/6-311+G** level of theory.

p [atm]	T [K]	TS4_14	14 + acetylene
1.0	500	119.0	93.3
	600	117.4	88.5
	700	115.8	83.7
	800	114.1	78.9
	900	112.4	74.1
	1000	110.8	69.2
	1100	109.1	64.4
0.00001	500	119.0	81.8
	600	117.4	74.8
	700	115.8	67.7
	800	114.1	60.6
	900	112.4	53.5
	1000	110.8	46.3
	1100	109.1	39.2

Table S8. Computed absolute energies (in a.u.) and relative energies including zero point vibrational energy corrections (ΔE_{ZPVE} in kcal mol⁻¹) for different isomers of **15** at the UB3LYP/6-311+G** level of theory.

	E [a.u.]	ΔE_{ZPVE} [kcal/mol]
15a	-233.77008	108.2
15b	-233.76235	113.7
15c	-233.75083	120.0
15d	-233.74965	121.5
H atom	-0.50216	

Table S9. Computed absolute energies (in a.u.) and relative energies including zero point vibrational energy corrections (ΔE_{ZPVE} in kcal mol⁻¹) for different isomers of **15** at the UCCSD(T)/cc-pVTZ//UB3LYP/6-311+G** level of theory.

	E [a.u.]	ΔE_{ZPVE} [kcal/mol]
15a	-233.24915	116.9
15b	-233.24532	119.9
15c	-233.22893	129.3
15d	-233.23126	128.6
H atom	-0.49981	

Geometries of electronic states of isomer 6.

3A_2

10

CASPT2/6-31G* ENERGY=-233.52229820

C	1.2575871136	0.00000000000	-0.1306716210
C	-1.2575871136	0.00000000000	-0.1306716210
H	2.3159462984	0.00000000000	0.1018050827
H	-2.3159462984	0.00000000000	0.1018050827
C	0.7524491864	0.00000000000	-1.3908158692
C	-0.7524491864	0.00000000000	-1.3908158692
H	1.3271078134	0.00000000000	-2.3137870892
H	-1.3271078134	0.00000000000	-2.3137870892
B	0.00000000000	0.00000000000	0.8213967389
N	0.00000000000	0.00000000000	2.2888442546

3B_1

10

CASPT2/6-31G* ENERGY=-233.51330784

C	1.2124209609	0.00000000000	-0.0994778547
C	-1.2124209609	0.00000000000	-0.0994778547
H	2.2803726715	0.00000000000	0.1019618271
H	-2.2803726715	0.00000000000	0.1019618271
C	0.7029595625	0.00000000000	-1.4281867559
C	-0.7029595625	0.00000000000	-1.4281867559
H	1.3052634435	0.00000000000	-2.3327292546
H	-1.3052634435	0.00000000000	-2.3327292546
B	0.00000000000	0.00000000000	0.8822441233
N	0.00000000000	0.00000000000	2.2779219531

1A_1

10

CASPT2/6-31G* ENERGY=-233.50463554

C	1.264769	0.000000	-0.130496
C	-1.264769	0.000000	-0.130496
H	2.314337	0.000000	0.130174
H	-2.314337	0.000000	0.130174
C	0.739132	0.000000	-1.383107
C	-0.739132	0.000000	-1.383107
H	1.327575	0.000000	-2.297598
H	-1.327575	0.000000	-2.297598
B	0.000000	0.000000	0.840973
N	0.000000	0.000000	2.164384

1A_2

10

CASPT2/6-31G* ENERGY=-233.47204909

C	1.2586847643	0.00000000000	-0.1293211837
C	-1.2586847643	0.00000000000	-0.1293211837
H	2.3157048834	0.00000000000	0.1080265125
H	-2.3157048834	0.00000000000	0.1080265125
C	0.7511474102	0.00000000000	-1.3898048663
C	-0.7511474102	0.00000000000	-1.3898048663
H	1.3275619520	0.00000000000	-2.3117217464

H	-1.3275619520	0.0000000000	-2.3117217464
B	0.0000000000	0.0000000000	0.8287794404
N	0.0000000000	0.0000000000	2.2601651274

¹B₁

10

CASPT2/6-31G* ENERGY=-233.51471151

C	1.211907	0.000000	-0.099152
C	-1.211907	0.000000	-0.099152
H	2.279497	0.000000	0.103936
H	-2.279497	0.000000	0.103936
C	0.702728	0.000000	-1.429829
C	-0.702728	0.000000	-1.429829
H	1.306350	0.000000	-2.333292
H	-1.306350	0.000000	-2.333292
B	0.000000	0.000000	0.876035
N	0.000000	0.000000	2.283941

Geometry of 11 computed at the CASSCF(8,8)/6-31G* level.

10

CASSCF(8,8)/6-31G* ENERGY=-232.96869431

C	1.0802929111	-0.3502164950	0.0000000000
B	-0.3508641553	-0.5562327241	0.0000000000
N	0.0472922342	0.7871142338	0.0000000000
C	0.7464343879	1.9326816223	0.0000000000
C	2.1070570395	1.6659579504	0.0000000000
C	2.3066724026	0.2632064961	0.0000000000
H	0.2481859829	2.8803132666	0.0000000000
H	2.8788477616	2.4117561556	0.0000000000
H	3.2534525382	-0.2380082145	0.0000000000
H	-1.3368011028	-1.1979422910	0.0000000000

Cartesian coordinates computed at B3LYP/6-31G*.

10

1,2-Azaborine, 4

B	0.0000000000	0.0000000000	0.0000000000
N	0.0000000000	0.0000000000	1.315571000
C	0.888047000	0.0000000000	-1.143160000
C	1.285715000	0.0000000000	1.755789000
C	2.158035000	0.0000000000	-0.531455000
C	2.364874000	0.0000000000	0.867841000
H	0.770108000	0.0000000000	-2.217238000
H	1.454653000	0.0000000000	2.833343000
H	3.037179000	0.0000000000	-1.176125000
H	3.377840000	0.0000000000	1.258294000

10

6 (¹A₁)

B	0.0000000000	0.0000000000	0.929827000
N	0.0000000000	0.0000000000	2.244746000

C	0.000000000	1.265768000	-0.061247000
C	0.000000000	-1.265768000	-0.061247000
C	0.000000000	0.738970000	-1.301630000
C	0.000000000	-0.738970000	-1.301630000
H	0.000000000	2.312342000	0.212912000
H	0.000000000	-2.312342000	0.212912000
H	0.000000000	1.328416000	-2.216826000
H	0.000000000	-1.328416000	-2.216826000

10

6 (3A₂)

B	0.000000000	0.000000000	0.000000000
N	0.000000000	0.000000000	1.453225000
C	1.262374000	0.000000000	-0.961671000
C	-1.262374000	0.000000000	-0.961671000
C	0.756973000	0.000000000	-2.209006000
C	-0.756973000	0.000000000	-2.209006000
H	2.320866000	0.000000000	-0.726936000
H	-2.320866000	0.000000000	-0.726936000
H	1.326764000	0.000000000	-3.136362000
H	-1.326764000	0.000000000	-3.136362000

10

7

N	0.000000000	0.000000000	0.000000000
B	0.000000000	0.000000000	1.415323000
C	1.136202000	0.000000000	-0.831683000
C	-1.136202000	0.000000000	-0.831683000
C	0.719750000	0.000000000	-2.129089000
C	-0.719750000	0.000000000	-2.129089000
H	2.125515000	0.000000000	-0.399090000
H	-2.125515000	0.000000000	-0.399090000
H	1.363583000	0.000000000	-2.998568000
H	-1.363583000	0.000000000	-2.998568000

10

8

B	-0.318476000	-1.217342000	0.000001000
N	-1.465496000	-0.476920000	-0.000002000
C	1.116584000	-1.026406000	0.000001000
C	-1.101579000	0.883781000	0.000003000
C	1.337748000	0.360233000	-0.000004000
C	0.240511000	1.250224000	-0.000001000
H	1.932238000	-1.737179000	0.000010000
H	-2.447195000	-0.713345000	-0.000001000
H	2.361048000	0.749578000	0.000003000
H	0.445169000	2.319099000	0.000005000

10

10

B	-1.515614000	0.006708000	-0.000026000
---	--------------	-------------	--------------

N	-2.350414000	-0.915265000	-0.000008000
C	-0.550590000	1.183126000	0.000054000
C	2.193549000	-1.146918000	0.000217000
C	0.798276000	1.084181000	-0.000031000
C	1.530599000	-0.133492000	-0.000193000
H	-0.967359000	2.189476000	0.000172000
H	-2.987260000	-1.678907000	0.000024000
H	1.398571000	1.994291000	0.000043000
H	2.756017000	-2.052925000	-0.000331000

10

TS4_8

B	-0.433103000	-1.148441000	-0.000135000
N	-1.624733000	-0.656703000	0.000079000
C	1.047657000	-1.088560000	0.000027000
C	-0.988096000	1.086614000	0.000163000
C	1.384636000	0.241612000	-0.000018000
C	0.351732000	1.252989000	-0.000112000
H	1.792082000	-1.874187000	0.000011000
H	-2.107151000	0.392854000	-0.000446000
H	2.426965000	0.562347000	0.000398000
H	0.651170000	2.302184000	-0.000203000

10

TS9_10

B	1.507609000	0.070180000	0.000005000
N	2.377159000	-0.817398000	-0.000015000
C	0.475174000	1.186977000	0.000028000
C	-2.036550000	-1.413657000	0.000068000
C	-0.865906000	1.018201000	-0.000014000
C	-1.525188000	-0.250835000	-0.000051000
H	0.830218000	2.216038000	0.000089000
H	3.043970000	-1.555627000	-0.000036000
H	-1.523944000	1.884511000	-0.000010000
H	-2.813581000	-0.418151000	-0.000155000

10

11

C	-1.006727000	0.120958000	0.000000000
C	1.216264000	-0.389943000	0.000000000
C	1.065933000	1.001113000	0.000000000
C	-0.313258000	1.314278000	0.000000000
H	2.122874000	-0.981298000	0.000000000
H	1.882401000	1.714930000	0.000000000
H	-0.746896000	2.305651000	0.000000000
B	-1.385512000	-1.276606000	0.000000000
N	0.000000000	-0.959846000	0.000000000
H	-2.104094000	-2.215767000	0.000000000

10

12

C	-1.505033000	-0.511167000	-0.084963000
C	1.301478000	0.356317000	0.041582000
C	0.942744000	-1.051224000	0.046988000
C	-0.396553000	-1.171444000	0.020867000
H	2.370631000	0.572381000	-0.033526000
H	1.672745000	-1.810428000	-0.197721000
H	-2.518532000	-0.676327000	0.248840000
B	-0.941152000	1.036166000	-0.034263000
N	0.423454000	1.315345000	-0.026503000
H	-1.839080000	1.791243000	0.192394000

10

13			
C	-0.750082000	-1.025899000	-0.000154000
C	2.229069000	0.978299000	-0.000258000
C	0.603148000	-1.086650000	0.000077000
C	1.463745000	0.038696000	0.000400000
H	-1.317633000	-1.955739000	-0.000369000
H	1.063069000	-2.071974000	-0.000014000
H	2.890346000	1.814396000	-0.000006000
N	-1.481449000	0.114907000	-0.000069000
B	-2.150736000	1.166694000	0.000079000
H	-2.787235000	2.148820000	0.000083000

10

TS4_11			
C	1.197826000	-0.966811000	-0.287554000
C	1.335338000	0.430968000	0.094523000
B	-0.151199000	-1.254665000	0.022366000
C	-1.142452000	0.645048000	-0.026687000
C	0.202751000	1.217826000	-0.002795000
N	-1.417602000	-0.639082000	0.001946000
H	-1.980878000	1.348958000	-0.022833000
H	0.281141000	2.303809000	-0.036843000
H	2.308114000	0.896816000	0.269025000
H	0.510051000	-1.764868000	1.000270000

10

TS4_7			
C	-0.653579000	1.032783000	-0.000036000
C	0.525814000	-1.175006000	-0.000120000
C	1.415543000	-0.130328000	0.000100000
C	0.709690000	1.104706000	0.000089000
H	0.729906000	-2.238990000	0.000006000
H	2.491397000	-0.247024000	0.000301000
H	1.204495000	2.070979000	-0.000019000
B	-1.975877000	-0.248222000	0.000420000
N	-0.748620000	-0.749381000	-0.000238000
H	-1.290878000	1.908883000	-0.000914000

10

TS7_11

C	-0.573068000	0.844015000	0.000172000
C	0.507556000	-1.159021000	-0.000164000
C	1.451958000	-0.147250000	0.000420000
C	0.778341000	1.117900000	-0.000106000
H	0.609975000	-2.234276000	0.001175000
H	2.525819000	-0.299285000	-0.000641000
H	1.237444000	2.096570000	0.000157000
B	-2.049943000	-0.160063000	0.000683000
N	-0.713145000	-0.542120000	-0.000728000
H	-2.120239000	1.098287000	-0.000945000

10

TS11_12

C	0.636995000	1.190522000	-0.108395000
C	-0.598853000	-1.099447000	0.007934000
C	-1.441127000	0.037276000	0.041326000
C	-0.654345000	1.191265000	-0.111637000
H	-1.090242000	-2.074596000	-0.027354000
H	-2.520757000	-0.024671000	0.087220000
H	-0.044237000	1.915551000	0.765223000
B	1.627431000	-0.024580000	0.028781000
N	0.722148000	-1.084269000	-0.013386000
H	2.807022000	-0.021200000	0.149336000

10

TS12_13

C	1.827531000	-0.186297000	0.000002000
C	-1.386754000	-0.179581000	0.000000000
C	-0.523976000	-1.256826000	0.000000000
C	0.830009000	-0.907331000	-0.000002000
H	-2.462254000	-0.352609000	0.000002000
H	-0.869960000	-2.282214000	0.000007000
H	2.822500000	0.200303000	-0.000003000
B	0.297328000	1.517611000	0.000000000
N	-0.938772000	1.094555000	-0.000001000
H	1.113620000	2.364791000	0.000006000

4

Acetylene

C	0.000000000	0.000000000	0.602484000
H	0.000000000	0.000000000	1.669128000
C	0.000000000	0.000000000	-0.602485000
H	0.000000000	0.000000000	-1.669121000

6

14

N	0.000000000	0.000000000	0.676930000
C	0.000000000	0.000000000	1.847691000
H	0.000000000	0.000000000	2.914669000

B	0.000000000	0.000000000	-0.704584000
C	0.000000000	0.000000000	-2.020899000
H	0.000000000	0.000000000	-3.091012000

10

TS4_14

N	0.000000000	-1.248889000	0.000000000
C	1.179276000	-1.047671000	0.000000000
C	1.589071000	1.096027000	0.000000000
H	2.124204000	-1.571056000	0.000000000
H	2.660697000	1.057435000	0.000000000
B	-1.283864000	-0.755977000	0.000000000
C	-2.406824000	-0.051395000	0.000000000
C	0.544169000	1.746377000	0.000000000
H	-3.328832000	0.491885000	0.000000000
H	-0.470902000	2.083823000	0.000000000

Cartesian coordinates computed at B3LYP/6-311+G.**

10

1,2-Azaborine, 4

B	-0.111258000	-1.281011000	0.000000000
N	-1.317128000	-0.766547000	0.000000000
C	1.282007000	-0.896638000	0.000000000
C	-1.235247000	0.588733000	0.000000000
C	1.210042000	0.509727000	0.000000000
C	0.000000000	1.238990000	0.000000000
H	2.223434000	-1.421705000	0.000000000
H	-2.162252000	1.157708000	0.000000000
H	2.143246000	1.068209000	0.000000000
H	0.030946000	2.321800000	0.000000000

10

6 (¹A₁)

B	0.000000000	0.000000000	0.931222000
N	0.000000000	0.000000000	2.240605000
C	0.000000000	1.263001000	-0.061946000
C	0.000000000	-1.263001000	-0.061946000
C	0.000000000	0.738352000	-1.300740000
C	0.000000000	-0.738352000	-1.300740000
H	0.000000000	2.305783000	0.216100000
H	0.000000000	-2.305783000	0.216100000
H	0.000000000	1.332137000	-2.210159000
H	0.000000000	-1.332137000	-2.210159000

10

6 (³A₂)

B	0.000000000	0.000000000	0.891111000
N	0.000000000	0.000000000	2.339525000
C	0.000000000	1.259527000	-0.071925000

C	0.000000000	-1.259527000	-0.071925000
C	0.000000000	0.756836000	-1.318012000
C	0.000000000	-0.756836000	-1.318012000
H	0.000000000	2.315153000	0.163598000
H	0.000000000	-2.315153000	0.163598000
H	0.000000000	1.330140000	-2.240089000
H	0.000000000	-1.330140000	-2.240089000

10

7

N	0.000000000	0.000000000	0.881005000
B	0.000000000	0.000000000	2.287229000
C	0.000000000	1.137797000	0.049806000
C	0.000000000	-1.137797000	0.049806000
C	0.000000000	0.719381000	-1.244441000
C	0.000000000	-0.719381000	-1.244441000
H	0.000000000	2.126283000	0.477765000
H	0.000000000	-2.126283000	0.477765000
H	0.000000000	1.361833000	-2.111548000
H	0.000000000	-1.361833000	-2.111548000

10

8

B	-0.307399000	-1.213721000	-0.000002000
N	-1.457744000	-0.486578000	0.000008000
C	1.121097000	-1.021205000	-0.000006000
C	-1.106936000	0.879385000	-0.000010000
C	1.331075000	0.366766000	0.000014000
C	0.231337000	1.251156000	0.000000000
H	1.937211000	-1.727144000	-0.000021000
H	-2.434100000	-0.732080000	0.000008000
H	2.350028000	0.758933000	0.000002000
H	0.428633000	2.318330000	-0.000016000

10

9

B	1.313444000	0.532326000	0.000000000
N	2.384745000	-0.093801000	0.000000000
C	0.000000000	1.287902000	0.000000000
C	-0.989869000	-1.932088000	0.000000000
C	-1.216984000	0.707621000	0.000000000
C	-1.446002000	-0.722280000	0.000000000
H	0.027452000	2.373876000	0.000000000
H	3.229971000	-0.616475000	0.000000000
H	-2.106711000	1.328214000	0.000000000
H	-2.494021000	-1.137564000	0.000000000

10

10

B	-1.515978000	0.006114000	0.000081000
N	-2.355419000	-0.908615000	0.000002000

C	-0.547691000	1.174827000	-0.000076000
C	2.194537000	-1.142201000	-0.000131000
C	0.798390000	1.079388000	0.000000000
C	1.534480000	-0.133342000	0.000244000
H	-0.969961000	2.176421000	-0.000229000
H	-2.998081000	-1.665992000	-0.000106000
H	1.395860000	1.988270000	-0.000112000
H	2.761709000	-2.040996000	-0.000190000

10

TS4_8

B	-0.426540000	-1.154433000	0.000004000
N	-1.613177000	-0.659341000	-0.000003000
C	1.049242000	-1.081241000	0.000001000
C	-0.991347000	1.075817000	-0.000001000
C	1.379997000	0.248944000	-0.000002000
C	0.343095000	1.252955000	0.000001000
H	1.795207000	-1.861959000	-0.000001000
H	-2.106866000	0.396580000	0.000005000
H	2.419057000	0.571057000	-0.000006000
H	0.631616000	2.303029000	0.000004000

10

TS8_9

B	-1.133639000	-0.649391000	0.000001000
N	-1.994374000	0.250501000	0.000000000
C	0.160270000	-1.417065000	0.000000000
C	0.286205000	1.728766000	0.000000000
C	1.276663000	-0.652057000	0.000000000
C	1.222272000	0.802737000	0.000000000
H	0.245876000	-2.496375000	-0.000001000
H	-2.711081000	0.940154000	0.000000000
H	2.262215000	-1.108142000	-0.000001000
H	2.159345000	1.383527000	0.000001000

10

TS9_10

B	1.314777000	0.533949000	0.000000000
N	2.388120000	-0.088630000	0.000000000
C	0.000000000	1.287363000	0.000000000
C	-0.998200000	-1.936475000	0.000000000
C	-1.216551000	0.706207000	0.000000000
C	-1.444069000	-0.723493000	0.000000000
H	0.026341000	2.373381000	0.000000000
H	3.234907000	-0.608761000	0.000000000
H	-2.106768000	1.326079000	0.000000000
H	-2.492289000	-1.141643000	0.000000000

10

11

C	-1.004789000	0.118869000	0.000000000
---	--------------	-------------	-------------

C	1.216711000	-0.387663000	0.000000000
C	1.064857000	1.001148000	0.000000000
C	-0.313971000	1.312097000	0.000000000
H	2.122098000	-0.976058000	0.000000000
H	1.877868000	1.714692000	0.000000000
H	-0.748820000	2.299825000	0.000000000
B	-1.385188000	-1.278297000	0.000000000
N	0.000000000	-0.957593000	0.000000000
H	-2.102056000	-2.210533000	0.000000000

10

12			
C	-1.501240000	-0.521149000	-0.074894000
C	1.301015000	0.357419000	0.037601000
C	0.944501000	-1.046291000	0.042109000
C	-0.393128000	-1.166503000	0.017944000
H	2.367179000	0.575636000	-0.033756000
H	1.676590000	-1.807640000	-0.177434000
H	-2.523443000	-0.676150000	0.223671000
B	-0.941369000	1.040244000	-0.031770000
N	0.418773000	1.312356000	-0.022272000
H	-1.851786000	1.779584000	0.165712000

10

13			
C	2.221627000	0.977727000	0.000206000
C	-0.747487000	-1.025459000	0.000060000
C	0.603001000	-1.083348000	0.000383000
C	1.462934000	0.039278000	-0.000424000
H	-1.311467000	-1.954658000	0.000641000
H	1.065143000	-2.064808000	0.001423000
H	2.885222000	1.807291000	-0.000340000
B	-2.146821000	1.164932000	0.000658000
N	-1.481155000	0.113419000	-0.001151000
H	-2.777156000	2.144399000	0.001697000

10

TS4_11			
C	1.163496000	-0.977048000	-0.293667000
C	1.347212000	0.407021000	0.097421000
B	-0.178715000	-1.263807000	0.025382000
C	-1.126526000	0.667255000	-0.025962000
C	0.229565000	1.211771000	-0.000536000
N	-1.424541000	-0.608381000	0.001853000
H	-1.948628000	1.386406000	-0.024152000
H	0.330391000	2.293427000	-0.039463000
H	2.328324000	0.847009000	0.269019000
H	0.472799000	-1.803130000	0.991180000

10

TS4_7

C	-0.644087000	1.045035000	0.000010000
C	0.518733000	-1.176593000	0.000007000
C	1.410455000	-0.137534000	-0.000009000
C	0.714630000	1.102166000	-0.000006000
H	0.722366000	-2.238264000	-0.000010000
H	2.483033000	-0.259898000	-0.000027000
H	1.214889000	2.062854000	-0.000005000
B	-1.969837000	-0.243052000	-0.000042000
N	-0.754174000	-0.751152000	0.000028000
H	-1.290267000	1.910191000	0.000050000

10

TS7_11

C	-0.577581000	0.837260000	-0.000108000
C	0.513898000	-1.157317000	0.000022000
C	1.450925000	-0.140555000	0.000056000
C	0.771649000	1.120518000	0.000005000
H	0.622595000	-2.229309000	0.000013000
H	2.523153000	-0.285259000	0.000168000
H	1.222914000	2.099844000	0.000055000
B	-2.043670000	-0.163014000	0.000195000
N	-0.709505000	-0.545746000	-0.000173000
H	-2.137127000	1.090581000	0.000153000

10

TS11_12

C	0.648378000	1.190082000	-0.111059000
C	-0.609050000	-1.094213000	0.008026000
C	-1.439599000	0.049807000	0.038253000
C	-0.636942000	1.191357000	-0.107842000
H	-1.111336000	-2.061678000	-0.020286000
H	-2.516897000	0.000290000	0.084052000
H	-0.034545000	1.920292000	0.766948000
B	1.623826000	-0.039926000	0.029953000
N	0.709866000	-1.091037000	-0.013504000
H	2.797864000	-0.044215000	0.149781000

10

TS12_13

C	1.775780000	-0.269165000	0.000000000
C	-1.390605000	-0.081786000	0.000000000
C	-0.607617000	-1.222358000	0.000000000
C	0.756691000	-0.956342000	-0.000001000
H	-2.473340000	-0.179592000	0.000001000
H	-1.023965000	-2.218261000	0.000000000
H	2.786803000	0.064384000	0.000001000
B	0.431755000	1.443278000	0.000000000
N	-0.848581000	1.149754000	0.000000000
H	1.286296000	2.246703000	0.000000000

Acetylene

C	0.0000000000	0.0000000000	0.599686000
H	0.0000000000	0.0000000000	1.662817000
C	0.0000000000	0.0000000000	-0.599686000
H	0.0000000000	0.0000000000	-1.662817000

6

14

N	0.0000000000	0.0000000000	0.678446000
C	0.0000000000	0.0000000000	1.842226000
H	0.0000000000	0.0000000000	2.906145000
B	0.0000000000	0.0000000000	-0.704392000
C	0.0000000000	0.0000000000	-2.017024000
H	0.0000000000	0.0000000000	-3.084523000

10

TS4_14

N	0.0000000000	-1.286614000	0.0000000000
C	1.172296000	-1.066202000	0.0000000000
C	1.531923000	1.054092000	0.0000000000
H	2.132429000	-1.555845000	0.0000000000
H	2.601523000	1.023657000	0.0000000000
B	-1.263711000	-0.745267000	0.0000000000
C	-2.321026000	0.048717000	0.0000000000
C	0.490589000	1.701188000	0.0000000000
H	-3.200902000	0.653673000	0.0000000000
H	-0.457189000	2.184373000	0.0000000000

Cartesian coordinates of stationary points computed at MP2/6-311+G.**

10

1,2-Azaborine, 4

B	-0.109150000	-1.269527000	0.0000000000
N	-1.334164000	-0.777584000	0.0000000000
C	1.293664000	-0.898584000	0.0000000000
C	-1.238728000	0.588355000	0.0000000000
C	1.217317000	0.513828000	0.0000000000
C	0.0000000000	1.238330000	0.0000000000
H	2.239219000	-1.420572000	0.0000000000
H	-2.166560000	1.159884000	0.0000000000
H	2.151159000	1.076096000	0.0000000000
H	0.027558000	2.323746000	0.0000000000

10

6 (¹A₁)

B	0.0000000000	0.0000000000	0.919627000
N	0.0000000000	0.0000000000	2.231032000
C	0.0000000000	1.270186000	-0.050232000
C	0.0000000000	-1.270186000	-0.050232000
C	0.0000000000	0.741460000	-1.300468000

C	0.000000000	-0.741460000	-1.300468000
H	0.000000000	2.319952000	0.209488000
H	0.000000000	-2.319952000	0.209488000
H	0.000000000	1.334197000	-2.212969000
H	0.000000000	-1.334197000	-2.212969000

10

6 (3A₂)

B	0.000000000	0.000000000	0.887354000
N	0.000000000	0.000000000	2.359595000
C	0.000000000	1.264832000	-0.078060000
C	0.000000000	-1.264832000	-0.078060000
C	0.000000000	0.752681000	-1.318011000
C	0.000000000	-0.752681000	-1.318011000
H	0.000000000	2.325367000	0.143739000
H	0.000000000	-2.325367000	0.143739000
H	0.000000000	1.324183000	-2.244283000
H	0.000000000	-1.324183000	-2.244283000

10

7

N	0.000000000	0.000000000	0.877934000
B	0.000000000	0.000000000	2.297124000
C	0.000000000	1.138520000	0.054687000
C	0.000000000	-1.138520000	0.054687000
C	0.000000000	0.718041000	-1.252132000
C	0.000000000	-0.718041000	-1.252132000
H	0.000000000	2.128467000	0.487481000
H	0.000000000	-2.128467000	0.487481000
H	0.000000000	1.365662000	-2.118388000
H	0.000000000	-1.365662000	-2.118388000

10

8

B	-0.302629000	-1.171712000	-0.000001000
N	-1.475590000	-0.506448000	0.000005000
C	1.140317000	-1.019076000	-0.000004000
C	-1.118797000	0.878553000	-0.000007000
C	1.347831000	0.367413000	0.000008000
C	0.225375000	1.240587000	0.000001000
H	1.948674000	-1.736410000	-0.000014000
H	-2.454690000	-0.744187000	0.000007000
H	2.366074000	0.768077000	0.000002000
H	0.413865000	2.311359000	-0.000008000

10

9

B	1.468307000	0.093420000	0.000013000
N	2.319622000	-0.819930000	0.016795000
C	0.447830000	1.233565000	-0.017174000
C	-1.920599000	-1.470553000	-0.062532000

C	-0.894560000	1.045052000	0.005898000
C	-1.484480000	-0.267860000	-0.009608000
H	0.797911000	2.262838000	-0.049458000
H	2.966797000	-1.577499000	0.033056000
H	-1.577277000	1.890999000	0.000435000
H	-2.655462000	-0.545146000	0.398832000

10

10

B	-1.489879000	0.022207000	-0.000001000
N	-2.294468000	-0.935204000	-0.000005000
C	-0.543487000	1.223379000	0.000021000
C	2.120067000	-1.191174000	0.000034000
C	0.809990000	1.111242000	-0.000010000
C	1.498960000	-0.137817000	-0.000053000
H	-0.959307000	2.228846000	0.000052000
H	-2.912849000	-1.715871000	-0.000005000
H	1.427269000	2.008345000	0.000011000
H	2.642379000	-2.119699000	0.000033000

10

TS4_8

B	-0.398743000	-1.127855000	0.000002000
N	-1.606260000	-0.657594000	-0.000001000
C	1.077631000	-1.068233000	0.000000000
C	-1.025245000	1.022668000	0.000000000
C	1.390629000	0.279179000	-0.000001000
C	0.324882000	1.244775000	0.000001000
H	1.829492000	-1.845567000	-0.000001000
H	-2.196781000	0.291978000	0.000003000
H	2.427237000	0.618817000	-0.000002000
H	0.570215000	2.306867000	0.000001000

10

TS8_9

B	1.152552000	-0.625730000	-0.000004000
N	2.022926000	0.275646000	0.000003000
C	-0.138882000	-1.425911000	-0.000001000
C	-0.366046000	1.766014000	0.000000000
C	-1.281847000	-0.687075000	0.000001000
C	-1.226480000	0.766736000	0.000000000
H	-0.203831000	-2.508868000	0.000001000
H	2.759876000	0.947787000	0.000001000
H	-2.260513000	-1.161037000	0.000004000
H	-2.139240000	1.402660000	-0.000002000

10

TS9_10

B	-1.469921000	0.082317000	-0.000997000
N	-2.325090000	-0.827143000	-0.020193000
C	-0.455608000	1.229152000	0.016931000

C	1.954935000	-1.440742000	0.085878000
C	0.888532000	1.049902000	-0.007330000
C	1.482062000	-0.258908000	0.021525000
H	-0.813816000	2.255657000	0.057718000
H	-2.969170000	-1.587402000	-0.037389000
H	1.566595000	1.899905000	0.002863000
H	2.622100000	-0.666165000	-0.578877000

10

11

C	-1.013920000	0.126255000	0.0000000000
C	1.220225000	-0.395125000	0.0000000000
C	1.072072000	1.001615000	0.0000000000
C	-0.306228000	1.320258000	0.0000000000
H	2.124397000	-0.990445000	0.0000000000
H	1.891538000	1.712315000	0.0000000000
H	-0.736535000	2.312982000	0.0000000000
B	-1.398099000	-1.278167000	0.0000000000
N	0.0000000000	-0.964707000	0.0000000000
H	-2.121801000	-2.209090000	0.0000000000

10

12

C	-1.612221000	-0.420493000	-0.067450000
C	1.361881000	0.208994000	0.014005000
C	0.840040000	-1.110149000	0.023917000
C	-0.524799000	-1.077556000	0.033846000
H	2.446436000	0.324847000	-0.029374000
H	1.451424000	-1.994411000	-0.087858000
H	-2.668040000	-0.357498000	0.109480000
B	-0.788960000	1.117243000	-0.005761000
N	0.574706000	1.280983000	-0.018488000
H	-1.697369000	1.869195000	0.140071000

10

13

C	2.170549000	1.005321000	-0.000199000
C	-0.755076000	-1.053537000	-0.000051000
C	0.599700000	-1.122188000	0.000500000
C	1.437886000	0.026180000	0.000099000
H	-1.342798000	-1.969169000	0.000308000
H	1.064523000	-2.103876000	0.001652000
H	2.803984000	1.861646000	-0.000454000
B	-2.081710000	1.205436000	0.000908000
N	-1.451601000	0.119650000	-0.001481000
H	-2.674299000	2.212008000	0.002229000

10

TS4_11

C	1.250115000	-0.956911000	-0.309712000
C	1.328567000	0.451786000	0.090495000

B	-0.108540000	-1.243800000	0.076764000
C	-1.167312000	0.626234000	-0.031143000
C	0.170677000	1.218647000	0.022497000
N	-1.406476000	-0.670598000	-0.041478000
H	-2.021317000	1.308776000	-0.049246000
H	0.238088000	2.306536000	-0.000407000
H	2.287907000	0.961012000	0.198673000
H	0.391069000	-1.701680000	1.124671000

10

TS4_7

C	-0.693012000	1.011735000	-0.002804000
C	0.557875000	-1.171228000	-0.005749000
C	1.418760000	-0.089269000	0.007792000
C	0.683570000	1.118767000	0.003015000
H	0.787845000	-2.229412000	0.003106000
H	2.497403000	-0.180042000	0.022360000
H	1.140361000	2.102999000	-0.000513000
B	-1.960301000	-0.275221000	0.030425000
N	-0.726221000	-0.773726000	-0.020064000
H	-1.343713000	1.878613000	-0.050155000

10

TS7_11

C	-0.576153000	0.847948000	-0.000233000
C	0.499084000	-1.166090000	0.000050000
C	1.455678000	-0.147156000	-0.000004000
C	0.793061000	1.115504000	0.000111000
H	0.596580000	-2.242163000	0.000022000
H	2.528919000	-0.306168000	0.000269000
H	1.250155000	2.095215000	0.000029000
B	-2.058383000	-0.149185000	0.000253000
N	-0.712015000	-0.543876000	-0.000199000
H	-2.129657000	1.104934000	0.000266000

10

TS11_12

C	0.655485000	1.170734000	-0.117964000
C	-0.611550000	-1.091290000	0.006907000
C	-1.451521000	0.047793000	0.040467000
C	-0.655208000	1.201274000	-0.112220000
H	-1.106974000	-2.063851000	-0.023175000
H	-2.530928000	-0.012536000	0.104129000
H	-0.035414000	1.812207000	0.813474000
B	1.645505000	-0.026732000	0.037788000
N	0.714507000	-1.075714000	-0.021587000
H	2.820998000	-0.043227000	0.164595000

10

TS12_13

C	1.773278000	-0.301207000	0.000000000
---	-------------	--------------	-------------

C	-1.397964000	-0.056445000	0.0000000000
C	-0.640365000	-1.215235000	0.0000000000
C	0.740638000	-0.995528000	0.0000000000
H	-2.484359000	-0.126907000	0.0000000000
H	-1.091665000	-2.198643000	0.0000000000
H	2.788873000	0.030389000	0.0000000000
B	0.461875000	1.459575000	0.0000000000
N	-0.818482000	1.168916000	0.0000000000
H	1.353633000	2.225363000	0.0000000000

4

Acetylene

C	0.0000000000	0.0000000000	0.608076000
H	0.0000000000	0.0000000000	1.672813000
C	0.0000000000	0.0000000000	-0.608076000
H	0.0000000000	0.0000000000	-1.672813000

6

14

N	0.0000000000	0.0000000000	0.672710000
C	0.0000000000	0.0000000000	1.864375000
H	0.0000000000	0.0000000000	2.929985000
B	0.0000000000	0.0000000000	-0.698275000
C	0.0000000000	0.0000000000	-2.037324000
H	0.0000000000	0.0000000000	-3.109889000

10

TS4_14

N	0.0000000000	-1.372005000	0.0000000000
C	1.183125000	-1.102662000	0.0000000000
C	1.378535000	1.005437000	0.0000000000
H	2.153658000	-1.579276000	0.0000000000
H	2.449940000	0.983204000	0.0000000000
B	-1.245238000	-0.794479000	0.0000000000
C	-2.036235000	0.286242000	0.0000000000
C	0.300960000	1.619818000	0.0000000000
H	-2.795304000	1.046453000	0.0000000000
H	-0.540417000	2.273040000	0.0000000000

Cartesian coordinates of stationary points computed at MP2/cc-pVTZ.

10

1,2-Azaborine, 4

B	-0.107464000	-1.267868000	0.0000000000
N	-1.331006000	-0.772745000	0.0000000000
C	1.291156000	-0.895600000	0.0000000000
C	-1.234619000	0.588133000	0.0000000000
C	1.211281000	0.510939000	0.0000000000
C	0.0000000000	1.232764000	0.0000000000
H	2.234090000	-1.411603000	0.0000000000
H	-2.156416000	1.159524000	0.0000000000

H	2.140286000	1.070554000	0.000000000
H	0.029493000	2.312664000	0.000000000

10

6 ($^1\text{A}_1$)

B	0.0000000000	0.0000000000	0.915611000
N	0.0000000000	0.0000000000	2.227336000
C	0.0000000000	1.266591000	-0.052093000
C	0.0000000000	-1.266591000	-0.052093000
C	0.0000000000	0.738732000	-1.295435000
C	0.0000000000	-0.738732000	-1.295435000
H	0.0000000000	2.311855000	0.204033000
H	0.0000000000	-2.311855000	0.204033000
H	0.0000000000	1.328395000	-2.203569000
H	0.0000000000	-1.328395000	-2.203569000

10

6 ($^3\text{A}_2$)

B	0.0000000000	0.0000000000	0.883665000
N	0.0000000000	0.0000000000	2.353211000
C	0.0000000000	1.260994000	-0.078048000
C	0.0000000000	-1.260994000	-0.078048000
C	0.0000000000	0.750564000	-1.313844000
C	0.0000000000	-0.750564000	-1.313844000
H	0.0000000000	2.316809000	0.141045000
H	0.0000000000	-2.316809000	0.141045000
H	0.0000000000	1.319910000	-2.235089000
H	0.0000000000	-1.319910000	-2.235089000

10

7

N	0.0000000000	0.0000000000	0.874101000
B	0.0000000000	0.0000000000	2.289395000
C	0.0000000000	1.134005000	0.054057000
C	0.0000000000	-1.134005000	0.054057000
C	0.0000000000	0.714864000	-1.247198000
C	0.0000000000	-0.714864000	-1.247198000
H	0.0000000000	2.119226000	0.485177000
H	0.0000000000	-2.119226000	0.485177000
H	0.0000000000	1.359625000	-2.109169000
H	0.0000000000	-1.359625000	-2.109169000

10

8

B	-0.307792000	-1.169033000	-0.000001000
N	-1.476431000	-0.498664000	0.000016000
C	1.132732000	-1.017735000	-0.000016000
C	-1.108122000	0.878459000	-0.000028000
C	1.345405000	0.361330000	0.000026000
C	0.231355000	1.234323000	0.000003000
H	1.936375000	-1.732897000	-0.000042000

H	-2.453615000	-0.723969000	0.000027000
H	2.360622000	0.755139000	0.000014000
H	0.422373000	2.299279000	-0.000018000

10

9

B	1.345221000	0.588367000	0.000000000
N	2.452381000	0.015918000	0.000000000
C	0.000000000	1.309094000	0.000000000
C	-1.291899000	-2.029593000	0.000000000
C	-1.189940000	0.673643000	0.000000000
C	-1.298600000	-0.754922000	0.000000000
H	-0.024325000	2.390987000	0.000000000
H	3.314927000	-0.474154000	0.000000000
H	-2.116017000	1.232514000	0.000000000
H	-2.384721000	-1.391936000	0.000000000

10

10

B	-1.481634000	0.022977000	-0.000065000
N	-2.288337000	-0.929266000	0.000011000
C	-0.537047000	1.221159000	0.000012000
C	2.105549000	-1.191696000	-0.000025000
C	0.809083000	1.107283000	0.000021000
C	1.494758000	-0.137784000	-0.000042000
H	-0.949906000	2.222093000	0.000058000
H	-2.903641000	-1.706664000	0.000100000
H	1.423760000	1.999853000	0.000071000
H	2.622265000	-2.119075000	0.000218000

10

TS4_8

B	-0.382305000	-1.134486000	0.000000000
N	-1.589735000	-0.663186000	0.000000000
C	1.088223000	-1.053728000	0.000000000
C	-1.034640000	1.004530000	0.000000000
C	1.378718000	0.293464000	0.000000000
C	0.308165000	1.241501000	0.000000000
H	1.850278000	-1.813605000	0.000000000
H	-2.201135000	0.269807000	0.000001000
H	2.406255000	0.643410000	0.000000000
H	0.541480000	2.300512000	0.000000000

10

TS8_9

B	1.149495000	-0.613391000	0.000000000
N	2.024594000	0.279512000	0.000000000
C	-0.133697000	-1.421981000	0.000000000
C	-0.391255000	1.767202000	-0.000001000
C	-1.275234000	-0.693677000	0.000000000
C	-1.218381000	0.752326000	0.000000000

H	-0.191220000	-2.500156000	0.000001000
H	2.751433000	0.955848000	0.000000000
H	-2.247146000	-1.168947000	0.000000000
H	-2.121298000	1.400409000	0.000000000

10

TS19_10

B	1.475635000	0.084363000	-0.001537000
N	2.323936000	-0.828584000	-0.009461000
C	0.459532000	1.223699000	0.006418000
C	-1.955454000	-1.431450000	0.037663000
C	-0.876886000	1.038739000	-0.002446000
C	-1.476142000	-0.258977000	0.009961000
H	0.810208000	2.247355000	0.028246000
H	2.966526000	-1.584388000	-0.016984000
H	-1.553781000	1.882984000	0.005790000
H	-2.774989000	-0.599740000	-0.252717000

10

11

C	-1.011851000	0.130491000	0.000000000
C	1.214252000	-0.395906000	0.000000000
C	1.069644000	0.995167000	0.000000000
C	-0.301377000	1.315609000	0.000000000
H	2.114562000	-0.987464000	0.000000000
H	1.886387000	1.701108000	0.000000000
H	-0.725658000	2.305159000	0.000000000
B	-1.396031000	-1.267346000	0.000000000
N	0.000000000	-0.965445000	0.000000000
H	-2.119148000	-2.196122000	0.000000000

10

12

C	-1.617632000	-0.421375000	-0.000470000
C	1.361997000	0.196589000	0.000100000
C	0.832744000	-1.108033000	0.000191000
C	-0.529217000	-1.064153000	0.000094000
H	2.443005000	0.303986000	-0.000073000
H	1.434036000	-1.999632000	-0.000416000
H	-2.680920000	-0.344450000	0.001335000
B	-0.775522000	1.126199000	-0.000094000
N	0.583943000	1.273592000	-0.000113000
H	-1.693464000	1.875788000	0.000932000

10

13

C	2.160438000	1.001330000	-0.000518000
C	-0.752274000	-1.050228000	-0.000280000
C	0.595878000	-1.118433000	0.001326000
C	1.431759000	0.025018000	0.000245000

H	-1.334419000	-1.963217000	0.000548000
H	1.056244000	-2.096336000	0.003848000
H	2.792674000	1.853786000	-0.001184000
B	-2.066945000	1.206271000	0.002124000
N	-1.448919000	0.116233000	-0.003380000
H	-2.652147000	2.214658000	0.005185000

10

TS4_11

C	0.972232000	-1.021164000	-0.315797000
C	1.432699000	0.211848000	0.146647000
B	-0.371617000	-1.248612000	-0.012647000
C	-0.996459000	0.800492000	-0.016131000
C	0.402058000	1.154513000	-0.031633000
N	-1.523807000	-0.420075000	0.045718000
H	-1.693416000	1.636585000	0.020171000
H	0.644461000	2.203122000	-0.168783000
H	2.449541000	0.496555000	0.391628000
H	0.260973000	-2.026812000	0.801671000

10

TS4_7

C	-0.691678000	1.006127000	0.000003000
C	0.558152000	-1.164603000	-0.000002000
C	1.413827000	-0.085567000	0.000003000
C	0.678765000	1.114244000	0.000000000
H	0.792828000	-2.216766000	-0.000012000
H	2.487572000	-0.173674000	0.000001000
H	1.130082000	2.095367000	-0.000009000
B	-1.954288000	-0.274252000	0.000001000
N	-0.721573000	-0.774680000	0.000001000
H	-1.342427000	1.867886000	-0.000018000

10

TS7_11

C	-0.578688000	0.842901000	-0.000044000
C	0.502149000	-1.159446000	-0.000022000
C	1.450418000	-0.140597000	0.000071000
C	0.784019000	1.111978000	-0.000033000
H	0.607473000	-2.229832000	0.000023000
H	2.519396000	-0.293511000	0.000100000
H	1.235142000	2.088970000	0.000042000
B	-2.048469000	-0.149361000	0.000115000
N	-0.708090000	-0.550352000	-0.000091000
H	-2.110419000	1.104627000	0.000067000

10

TS11_12

C	0.649382000	1.157680000	-0.116270000
C	-0.608935000	-1.085417000	0.006078000
C	-1.446991000	0.047478000	0.036140000

C	-0.655124000	1.197173000	-0.109803000
H	-1.100026000	-2.054517000	-0.020078000
H	-2.520958000	-0.014557000	0.100563000
H	-0.031921000	1.774367000	0.826862000
B	1.645255000	-0.020776000	0.032619000
N	0.711105000	-1.065592000	-0.017266000
H	2.818901000	-0.043745000	0.153546000

10

TS12_13

C	1.237360000	-1.304841000	0.000000000
C	-1.152858000	0.785804000	0.000000000
C	-1.233717000	-0.589663000	0.000000000
C	0.000000000	-1.236325000	0.000000000
H	-2.063962000	1.372200000	0.000000000
H	-2.178518000	-1.106234000	0.000000000
H	2.244388000	-1.649059000	0.000000000
B	1.242541000	0.905576000	0.000000000
N	0.038329000	1.420126000	0.000000000
H	2.412376000	0.984478000	0.000000000

4

Acetylene

C	0.000000000	0.000000000	0.605656000
H	0.000000000	0.000000000	1.666971000
C	0.000000000	0.000000000	-0.605656000
H	0.000000000	0.000000000	-1.666971000

6

14

N	0.000000000	0.000000000	0.672098000
C	0.000000000	0.000000000	1.858729000
H	0.000000000	0.000000000	2.921012000
B	0.000000000	0.000000000	-0.696128000
C	0.000000000	0.000000000	-2.032749000
H	0.000000000	0.000000000	-3.100936000

10

TS4_14

N	0.000000000	-1.366842000	0.000000000
C	1.183050000	-1.135066000	0.000000000
C	1.369740000	1.023780000	0.000000000
H	2.146404000	-1.613914000	0.000000000
H	2.434870000	0.974851000	0.000000000
B	-1.243116000	-0.789605000	0.000000000
C	-2.014066000	0.301580000	0.000000000
C	0.285778000	1.613339000	0.000000000
H	-2.762370000	1.066203000	0.000000000
H	-0.550338000	2.266982000	0.000000000

Cartesian coordinates computed at UB3LYP/6-311+G.**

9

15a

C	0.585301000	0.942180000	0.000011000
C	-0.645970000	0.478940000	0.000001000
C	-1.840443000	-0.067677000	-0.000007000
C	-2.971918000	-0.558240000	-0.000017000
B	1.809302000	0.039491000	0.000000000
N	2.823273000	-0.676233000	-0.000002000
H	0.744581000	2.024485000	-0.000013000
H	3.624454000	-1.263436000	0.000007000
H	-3.940274000	-0.996097000	0.000098000

9

15b

C	0.498457000	0.372727000	0.001380000
C	-0.739419000	0.819933000	-0.000443000
C	-1.902275000	-0.000726000	-0.000210000
C	-2.907774000	-0.664791000	-0.000129000
B	1.884138000	-0.045408000	0.000416000
N	3.080583000	-0.410035000	-0.000339000
H	4.029649000	-0.704900000	-0.001200000
H	-3.787818000	-1.260798000	-0.000033000
H	-0.920532000	1.900121000	-0.002061000

9

15c

C	0.669030000	0.691040000	-0.000027000
C	-0.530064000	0.133490000	-0.000002000
C	-1.831872000	-0.068997000	-0.000002000
C	-3.037683000	-0.325243000	-0.000024000
N	1.852013000	0.015041000	0.000009000
B	2.952899000	-0.564488000	0.000057000
H	0.751827000	1.781088000	-0.000109000
H	3.982071000	-1.110035000	0.000091000
H	-4.078946000	-0.535646000	-0.000001000

9

15d

C	0.677389000	0.864151000	-0.000074000
C	-0.644613000	1.039860000	-0.000141000
C	-1.575100000	-0.033868000	-0.000050000
C	-2.372343000	-0.939865000	0.000035000
N	1.595278000	-0.036962000	0.000060000
B	2.585495000	-0.820858000	0.000175000
H	3.506154000	-1.532832000	0.000281000
H	-3.073999000	-1.737475000	0.000086000
H	-1.038569000	2.051660000	-0.000281000

Publikation 3

Photoreactions of Phenylborylene with Dinitrogen and Carbon Monoxide

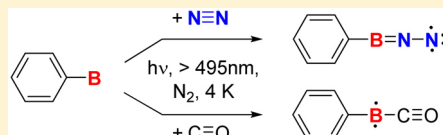
Klara Edel,[†] Matthias Krieg,[†] Dirk Grote,[‡] and Holger F. Bettinger*,[†] 

[†]Institut für Organische Chemie, Universität Tübingen, Auf der Morgenstelle 18, 72076 Tübingen, Germany

[‡]Lehrstuhl für Organische Chemie II, Ruhr-Universität Bochum, Universitätsstr. 150, 44780 Bochum, Germany

Supporting Information

ABSTRACT: Formal removal of two bonding partners from boranes, BR_3 , yields borylenes, RB , which have been inferred as reactive intermediates in a number of reactions. Phenylborylene ($\text{R} = \text{C}_6\text{H}_5$; **1**) is accessible from phenyldiazidoborane by photochemical extrusion of dinitrogen under matrix isolation conditions. Concomitantly, the nitrene PhNBN is formed via phenyl rearrangement. Here we used a combination of UV-vis, IR, and ESR spectroscopy under cryogenic matrix isolation conditions to investigate the properties and reactivity of phenylborylene. We detected an absorption band of phenylborylene at 375 nm ($S_0 \rightarrow S_2$) and tentatively assigned the $S_0 \rightarrow S_1$ transition to a very weak band at 518 nm. We also show for the first time that an electrophilic borylene such as **1** can react with N_2 reversibly and with CO irreversibly under photochemical conditions. The corresponding photoproducts PhBNN and PhBCO have triplet electronic ground states. Their small E values are in agreement with the linear arrangements $\text{Ph}-\text{B}-\text{N}-\text{N}$ and $\text{Ph}-\text{B}-\text{C}-\text{O}$ obtained by density functional theory computations. The D values decrease in the series $\text{PhNBN} > \text{PhBNN} > \text{PhBCO}$ and approach the value for phenylcarbene (PhCH). Indeed, the boron center in PhBCO is isoelectronic with the carbene center in PhCH . The compounds are the first examples of boron analogues of diazoalkanes (R_2CNN) and ketenes (R_2CCO), and their formation may serve as a demonstration of the high reactivity of phenylborylene.



INTRODUCTION

The boron analogues of carbenes, borylenes, which are also known as borenes or boranediyls, are an underrepresented class of reactive intermediates in the chemical literature. This is not due to a lack of interest in these fundamental species of boron chemistry but rather to the difficulties in obtaining them. For example, early claims¹ of methylborylene (CH_3B) generation by reductive elimination of dibromomethylborane (CH_3BBr_2) were later on refuted.^{2,3} Likewise, the reported photochemical generation of (1-naphthyl)borylene from tris(1-naphthyl)-borane⁴ was shown to be incorrect.⁵

A number of trapping experiments were interpreted as evidence for the involvement of borylenes. Timms, for example, obtained 1,4-diboracyclohexadiene derivatives from trapping of BF and BCl with ethyne (Scheme 1a).^{6–9} The borylenes were obtained by comproportionation of the corresponding trihalides over solid boron at very high temperatures. Pachaly and West¹⁰ ascribed the products obtained from photolysis of trisilylboranes in organic glasses in the presence of bis(trimethylsilyl)acetylene at 77 K to result from trapping of silylborylenes (Scheme 1b). Curiously, the authors could not obtain spectral evidence for the formation of silylborylenes in the organic glass by optical spectroscopy.¹⁰ Grigsby and Power¹¹ reduced sterically encumbered arylboron dihalides and interpreted the isolated products as resulting from insertion of a transient borylene into a C–C σ bond (Scheme 1c). Tokitoh and co-workers¹² photolyzed sterically encumbered bis(methylseleno)arylboranes in the presence of 1,2-diketones. The isolated 1,3,2-dioxaboroles were ascribed to result from the

reaction of the transient arylborylene with the 1,2-diketone (Scheme 1d).¹²

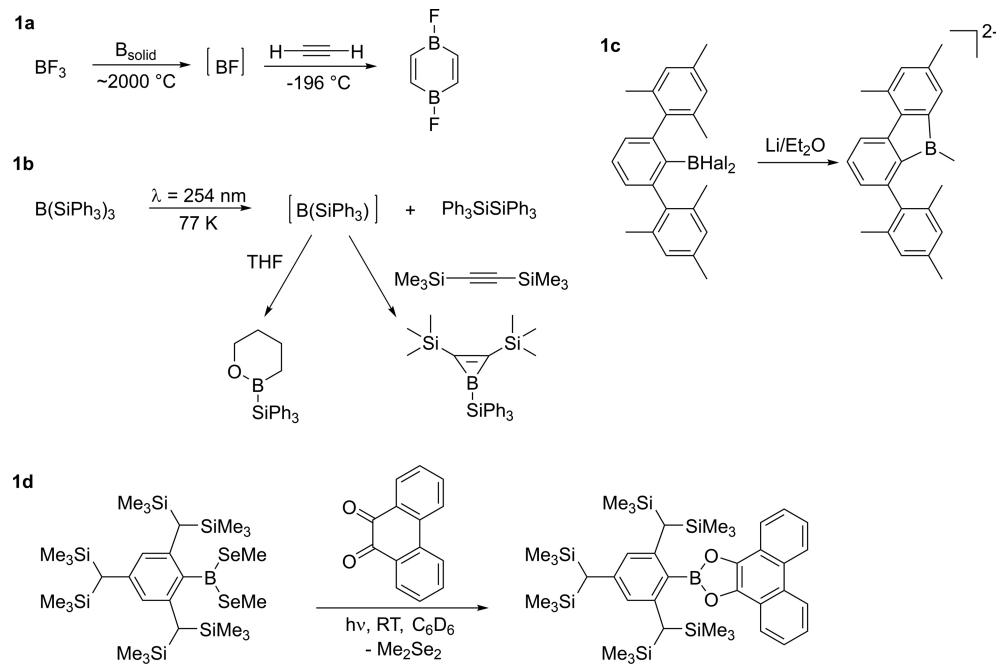
The reductive elimination of the adducts of dichloroboranes and N-heterocyclic carbenes (NHCs) was investigated more recently.^{13,14} The reduction of a $\text{mes}_2\text{BB}(\text{Cl})_2\text{NHC}$ with potassium graphite yielded the product that was ascribed to result from intramolecular CH insertion of a $\text{R}_2\text{BB}-\text{NHC}$ species (Scheme 2a).¹³ The reduction of $\text{NHC}-\text{BHCl}_2$ with sodium naphthalide produced a cycloadduct that was inferred to result from cycloaddition of $\text{NHC}-\text{BH}$ to naphthaline (Scheme 2b).¹⁴ This interpretation was challenged, however, and a boryl radical mechanism was suggested instead.¹⁵ An interesting recent observation is the CO extrusion from $\text{ArB}(\text{CO})(\text{CAAC})$ (CAAC = cyclic (alkyl)(amino)carbene) to give the $\text{ArB}(\text{CAAC})$ adduct, which was trapped intramolecularly or by an added neutral donor L (Scheme 2c).¹⁶

The reactant in Scheme 2c is an example of compounds of the type RBL_2 , with L being a neutral formal two-electron donor, which are currently receiving some attention as summarized in a recent review.¹⁷ When, e.g., a CAAC or CO is used as a neutral donor, stable compounds RBL_2 ^{18,19} or RBL ^{20,21} result. These were considered as having boron in the formal oxidation state +1 and hence were perceived as stabilized borylenes. The boron center has lost its electrophilic nature and acts as a Brønsted or Lewis base toward a proton or a Lewis acid.^{18,22}

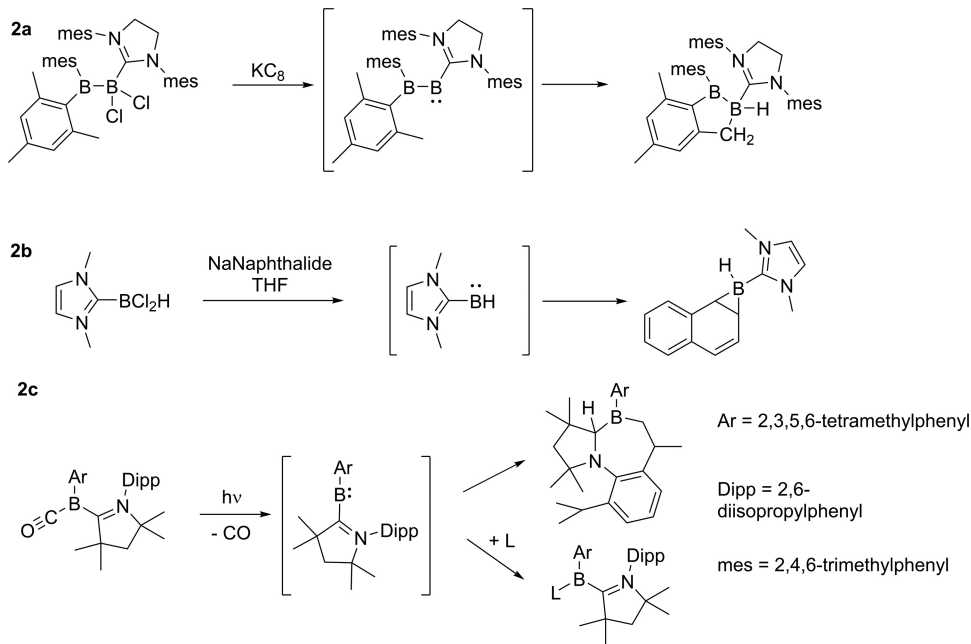
Received: August 10, 2017

Published: October 10, 2017

Scheme 1. Trapping Experiments of Borylenes



Scheme 2. Trapping Experiments of Borylene–NHC or Borylene–CAAC Adducts



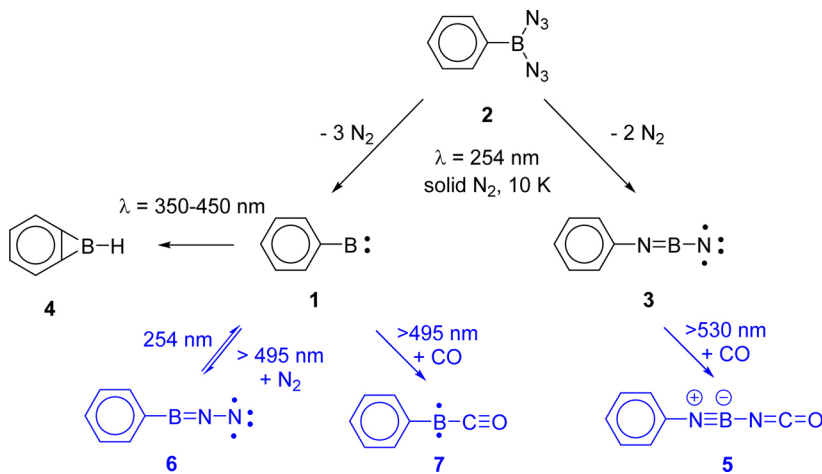
Direct spectroscopic observation of organoborylenes, RB, is extremely scarce. Andrews et al.²³ observed by IR spectroscopy that cocondensation of laser-ablated boron atoms and acetylene in an argon matrix gives ethynylborylene next to a number of additional products. We have reported that phenylborylene (**1**) can be obtained by UV photolysis of phenyldiazidoborane (**2**) in a nitrogen matrix along with nitrene **3** (Scheme 3).²⁴ The subvalent organoboron compound **1** was found to be photolabile, as longer-wavelength irradiation resulted in the formation of benzoborirene (**4**).²⁴ A computational analysis of various PhBN_x isomers identified **3** as the thermodynamically least stable isomer of PhBN_2 stoichiometry and the trans-

formation **2** \rightarrow **1** + 3 N_2 as considerably exothermic (-21 kcal mol^{-1}).²⁵

The available experimental evidence from trapping studies suggests that borylenes RB are highly reactive transient species. Computational analysis of the reactions with prototypical carbon multiple bonds has revealed that borylenes behave as electrophilic species because of their vacant p orbitals.^{26,27} The transition states for cycloaddition resemble those of carbenes, and changes in barrier heights, distances, and angles can similarly be associated with varying borylene philicities.^{26,27}

In our preliminary report,²⁴ we focused on IR characterization of the products formed from **2** upon irradiation. We now report and discuss the observations from UV-vis and

Scheme 3. Photochemical Decomposition of Phenyliazidoborane (2) Isolated in Solid Nitrogen at 10 K Results in Phenylborylene (1), B-Nitreno-N-phenyliminoborane (3), and Benzoborirene (4); The Reactions and Reaction Products B-Isocyanato-N-phenyliminoborane (5), N-Nitreno-B-phenyliminoborane or Phenyliazoborane (6), and Phenylboraketene (7) (Drawn in Blue) Are the Subject of the Present Work



electron spin resonance (ESR) spectroscopy along with additional IR measurements in a nitrogen matrix as well as in a CO-doped nitrogen matrix. The experimental investigations are further complemented by detailed computational investigations. We report for the first time spectroscopic evidence for the photoreaction of phenylborylene with the N_2 and CO molecules (Scheme 3, blue part). The products PhBL (L = N_2 , CO) are shown to have triplet ground states.

RESULTS AND DISCUSSION

UV/Vis Spectroscopy. Diazide 2 has its absorption of maximum intensity at 250 nm in solid nitrogen (Figure S1). Irrespective of the conformation of diazide 2, a strong absorption ($S_0 \rightarrow S_2$) is computed in the 4.5–4.6 eV (270–280 nm) range (Table S5). A much weaker (by a factor of 100) absorption ($S_0 \rightarrow S_1$) is obtained at longer wavelengths (272–292 nm). It is thus assumed that the strong band is due to the $S_0 \rightarrow S_2$ transition.

Irradiation was performed with the output of a low-pressure mercury lamp ($\lambda = 254 \text{ nm}$). Under these conditions, a decrease of the diazide band (250 nm) was accompanied by a growth of signals due to 3 (709, 623, 557, 504, 413, 325, and 317 nm) and 1 (375 nm) (Figure 1). The assignments are based on the behavior of the bands in subsequent irradiations at various wavelengths in the absence and presence of small amounts of CO (up to 5%), complementary IR and ESR spectroscopy, and computations as detailed below.

The bands assigned to 3 decreased upon irradiation into the long-wavelength transitions ($\lambda > 530 \text{ nm}$) in the presence of CO (Figure 2). Although no characteristic new bands were observed in the UV-vis spectra, the formation of the isocyanate PhNB(NCO) (5) was confirmed by IR spectroscopy (see below). The only band growing under these irradiation conditions is at around 250 nm. The isocyanate has its strongest and longest-wavelength absorption at 265 nm ($f = 0.472$), and hence, experiment and theory are in agreement with respect to the changes in the optical spectra under these irradiation conditions ($\lambda > 530 \text{ nm}$) in the presence of CO. In the absence of CO, only slight bleaching of the bands associated with 3 was observed upon $\lambda > 530 \text{ nm}$ irradiation (Figure 1). There is some similarity to the photochemical

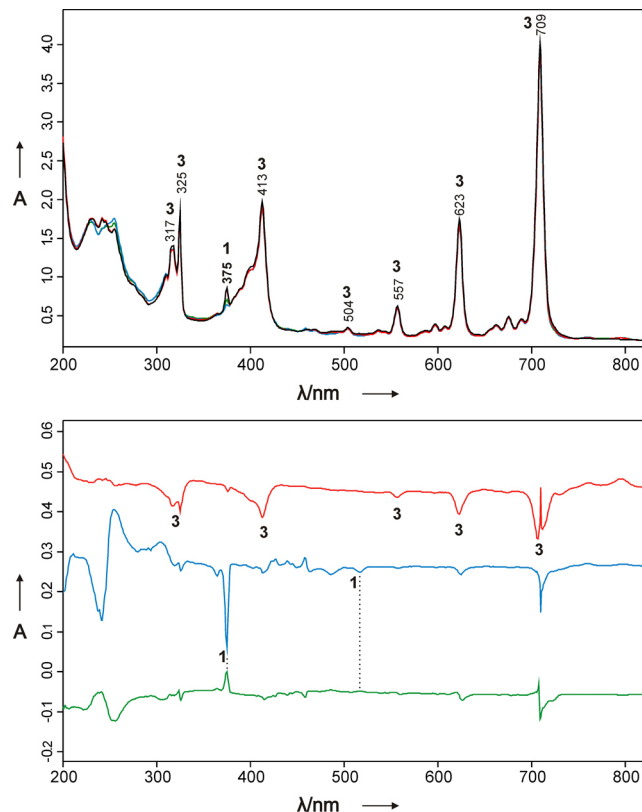


Figure 1. UV/vis spectra of the photodecomposition of diazide 2. The UV/vis spectrum of diazide 2 is not shown. Top panel: black trace, after irradiation of a nitrogen matrix containing diazide 2 for 35 min at $\lambda = 254 \text{ nm}$; red trace, after irradiation of the black trace for 2 h at $530 \text{ nm} < \lambda < 630 \text{ nm}$; blue trace, after irradiation of the red trace at $495 \text{ nm} < \lambda < 630 \text{ nm}$ for 1 h; green trace, after irradiation of the blue trace at $\lambda = 254 \text{ nm}$ for 25 min. Bottom panel: difference spectra (bands pointing downward decrease and bands pointing upward increase during irradiation): red trace, after irradiation at $530 \text{ nm} < \lambda < 630 \text{ nm}$ for 2 h; blue trace, after irradiation at $495 \text{ nm} < \lambda < 630 \text{ nm}$ for 1 h; green trace, after irradiation at $\lambda = 254 \text{ nm}$ for 25 min.

behavior of the triplet borylnitrene CatBN (Cat = catecholato), which upon long-wavelength irradiation was found to react

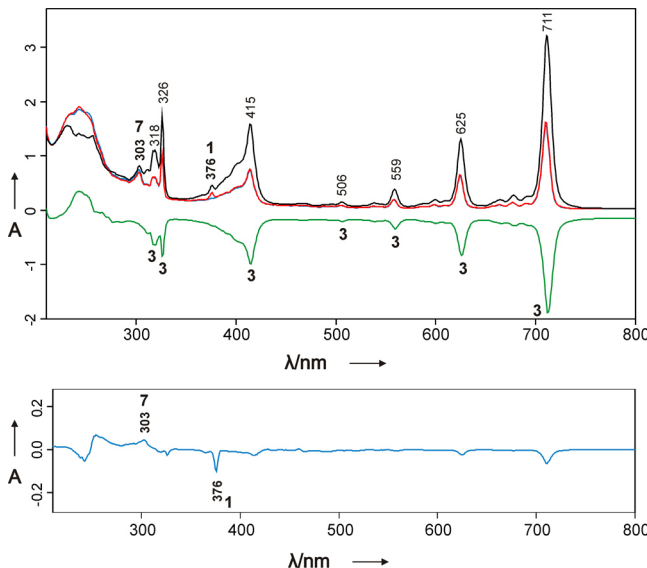


Figure 2. UV-vis spectra of the photodecomposition of diazide **2** in a CO (5%) doped N₂ matrix. UV-vis spectrum of diazide **2** is not shown. Top panel: black trace, after irradiation of diazide **2** for 33 min at $\lambda = 254$ nm; red trace, after irradiation of the black trace for 2 h at $530 \text{ nm} < \lambda < 630 \text{ nm}$; blue trace, after irradiation of the red trace at $495 \text{ nm} < \lambda < 630 \text{ nm}$ for 1 h; green trace, difference spectrum obtained from the red and black traces showing decreasing signals of **3**. Bottom panel: difference spectrum obtained from the blue and red traces in the top panel, showing the decreasing signal of **1** and increasing signal of **7**. In the difference spectra, bands pointing downward decrease and bands pointing upward increase during irradiation.

readily with N₂ to form its azide CatBN₃ and with CO to form its isocyanate CatB(NCO).²⁸

The absorption spectrum of **3** computed at the TD-B3LYP level places the S₀ \rightarrow S₂ transition at 2.0 eV (634 nm) with considerable oscillator strength. The experimental transition energy (1.7 eV, 709 nm) is in reasonable agreement with the computations. The S₀ \rightarrow S₁ transition of **3** (1.6 eV) is not dipole-allowed because S₁ is 1³A₁ according to these computations. The spacings between the signals in the visible are 1947, 1902, and 1888 cm⁻¹, indicating that the three bands of lower intensity (623, 557, and 504 nm) are due to a vibronic progression that is associated with the BN stretching vibration of **3**. Low-energy excited states (up to 600 nm) and a pronounced vibrational progression were also observed in the absorption spectrum of the triplet borylnitrene CatBN in argon.²⁸

The band at 375 nm was the only signal that did not change intensity upon $\lambda > 530$ nm irradiation in the presence of CO (Figure 2). However, the signal was quickly bleached in the absence of CO upon shorter-wavelength irradiation ($\lambda = 350$ –450 nm), while the other bands associated with **3** were hardly affected. We have previously shown by IR spectroscopy that 350–450 nm irradiation results in the photoreaction of **1** to form **4**.²⁴ Hence, the feature at 375 nm is assigned to **1**. A computational investigation of the low-lying excited states of various borylenes was reported recently.²⁹ For borylenes such as **1**, two low-energy excited states, 1¹B₁ (S₁) and 1¹B₂ (S₂), exist as a result of excitation from the HOMO (13a₁) to the LUMO (3b₁) or LUMO+1 (8b₂). The stronger absorption is due to the S₀ \rightarrow S₂ transition that is computed for **1** at 392 nm (TD-B3LYP, $f = 0.041$).²⁹ The S₀ \rightarrow S₁ transition is weaker by

a factor of 4 and is expected to appear at much longer wavelengths (529 nm).²⁹ The long-wavelength absorption of **1** was difficult to detect in our experiments, and it is tentatively assigned to a very weak band at 518 nm that shows the same behavior as the band at 375 nm in irradiation experiments. The presence of the weak band of **1** can be demonstrated by irradiation with light of wavelength $\lambda > 495$ nm after first irradiating with $\lambda > 530$ nm. Under these irradiation conditions, the 375 nm band decreases quickly while the bands of **3** are hardly affected (Figure 1). This photoreaction is partially reversible, and irradiation with 254 nm light resulted in growth of the signals of **1** (Figure 1). Complementary IR and ESR experiments (see below) demonstrated that these conditions resulted in the photoreaction of **1** with N₂ to give PhB(NN) (**6**). Bands grew in the 250–260 nm region, around 305 nm, and at 459 nm (2.7 eV). Computations for **6** arrived at a weak band at 3.1 eV (396 nm, $f = 0.047$) and a stronger one at 4.0 eV (311 nm, $f = 0.120$), in reasonable agreement with the experimental observations.

Shorter-wavelength irradiation ($\lambda > 495$ nm) in the presence of CO, i.e., into the very weak transition of **1**, also resulted in the disappearance of the bands of **1** (Figure 2). Under these conditions, a single band at 303 nm grew. IR and ESR spectroscopy (discussed below) demonstrated that the product of the photoreaction of **1** with CO is PhB(CO) (**7**). Computations were in agreement with assignment of the 303 nm band to **7**, as the strongest absorption was computed to be at 306 nm ($f = 0.320$). Further discussion of the electronic structures of **6** and **7** is presented below.

IR Spectroscopy. The previous IR spectroscopic investigation found that irradiation at $\lambda = 350$ –450 nm turned **1** into **4**.²⁴ In the 1417–1387 cm⁻¹ range a number of weak bands that could not be assigned at that time also increased under these irradiation conditions.²⁴ As we deduced from the UV-vis experiments and the computations²⁹ that there are two low-lying excited states of **1** (see above), we irradiated the mixture of **1** and **3** with long-wavelength light. Upon >530 nm irradiation, **1** was photostable while IR bands associated with **3** were hardly changed (Figure 3). Upon >495 nm irradiation, the bands of **1** quickly decreased in intensity and new signals grew. These bands do not belong to **4** but are assigned to **6** on the basis of computations and isotopic labeling studies using ¹⁵N₂. The IR signals for ¹⁵N-labeled **6** are observed at 1373–1367 cm⁻¹. The measured isotopic shift of approximately 25–28 cm⁻¹ is in agreement with the computed one (24.9 cm⁻¹). The band of the ν(BNN) stretching vibration is tentatively assigned to the feature observed at 1691 cm⁻¹ (1752.8 cm⁻¹ calculated at the B3LYP/6-311+G** level). However, the band for the isotopically labeled compound PhB(¹⁵N¹⁵N) could not be assigned because of overlap with other signals. As observed by UV-vis spectroscopy, the photoreaction PhB + N₂ is reversible upon 254 nm irradiation, as the signals due to **6** decreased while those of **1** increased in intensity (Figure 3).

In a CO-doped N₂ matrix, nitrene **3** reacts with CO upon >530 nm irradiation to form PhNB(NCO), as shown by the growth of the typical isocyanate bands at 2315–2332 cm⁻¹ and the stretching vibration of the iminoborane unit (Figure 4). The latter band shows the typical 1:4 intensity ratio of the ¹⁰B and ¹¹B isotopologues at 2131 and 2081 cm⁻¹. The assignment is supported by the finding that the isocyanate band shifts upon isotopic substitution (60–61 cm⁻¹ for ¹³CO and 16–17 cm⁻¹ for C¹⁸O) while the iminoborane stretching vibration is essentially insensitive. The observed isotopic shifts are in

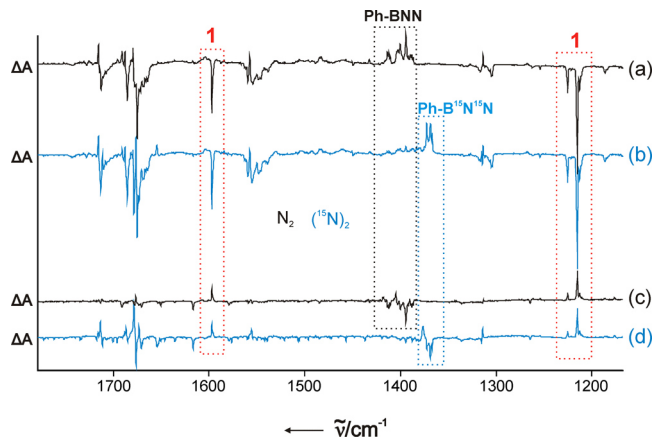


Figure 3. IR difference spectra showing the photoreversible reaction between **1** and **6**. Signals of **1** are framed in a red box. Black traces show spectra of a dinitrogen matrix and blue traces those of a $^{15}\text{N}_2$ matrix. Before irradiation at $495 \text{ nm} < \lambda < 630 \text{ nm}$, matrixes containing diazide **2** were irradiated at $\lambda = 254$ and $530\text{--}630 \text{ nm}$. (a, b) Difference spectra after irradiation at $495 \text{ nm} < \lambda < 630 \text{ nm}$ for 80 min; (c, d) difference spectra after irradiation at $\lambda = 254 \text{ nm}$ for 30 min. In the difference spectra, bands pointing downward decrease and bands pointing upward increase during irradiation.

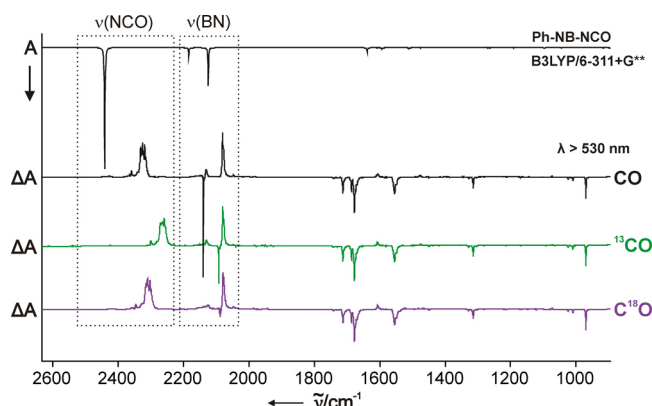


Figure 4. IR difference spectra showing the photoreaction between **CO** and **5** to form **1** through irradiation at $530 \text{ nm} < \lambda < 630 \text{ nm}$ for 2 h in a dinitrogen matrix doped with 5% isotopically labeled carbon monoxide. Before irradiation at $530 \text{ nm} < \lambda < 630 \text{ nm}$, matrixes containing diazide **2** were irradiated at $\lambda = 254 \text{ nm}$ for 30 min. The top trace shows a spectrum of **5** computed at the B3LYP/6-311+G** level of theory. In the difference spectra, bands pointing downward decrease and bands pointing upward increase during irradiation.

agreement with those computed for **5** (63.4 cm^{-1} for ^{13}CO and 13.6 cm^{-1} for C^{18}O , see Table S1). Interestingly, computations arrived at a linear structure for this isocyanate (see Figure S2). This is most likely due to the adjacent electron-deficient dicoordinate boron center, similar to the situation in electron-deficient linear ketenimines.³⁰ While isocyanates of iminoboranes were not considered previously, dimethylisocyanatoborane, $(\text{CH}_3)_2\text{BNCO}$, was found to feature a bent isocyanato group with a very low barrier for isomerization,³¹ in agreement with our computations (see Figure S2).

After much of nitrene **3** was converted to **5**, switching the wavelength of irradiation to $>495 \text{ nm}$ resulted in a quick decrease of the bands of **1** and the growth of a set of new signals (Figure 5). The photoproduct is assigned to boraketene **7** on the basis of isotopic shifts (^{13}CO and C^{18}O) and comparison with computed harmonic vibrational frequencies.

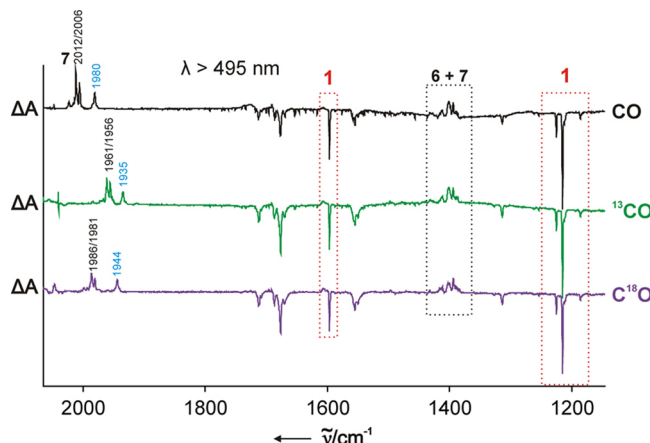


Figure 5. IR difference spectra showing the photoreaction between **1** and **CO** to form **7** through irradiation at $495 \text{ nm} < \lambda < 630 \text{ nm}$ for 1 h in a dinitrogen matrix doped with 5% isotopically labeled carbon monoxide. Before irradiation at $495 \text{ nm} < \lambda < 630 \text{ nm}$, matrixes containing diazide **2** were irradiated at $\lambda = 254 \text{ nm}$ for 30 min and at $530\text{--}630 \text{ nm}$ for 2 h. Decreasing signals of **1** are framed in a red box. In the difference spectra, bands pointing downward decrease and bands pointing upward increase during irradiation.

The same set of signals was already observed in the previous irradiation of the same **CO**-doped matrix at $\lambda = 254 \text{ nm}$. The signals at $2012/2006 \text{ cm}^{-1}$ belong to the $\nu(\text{BCO})$ stretching vibration and show isotopic shifts of 51 and 26 cm^{-1} upon the use of ^{13}CO and C^{18}O , respectively, in good agreement with the computed values of 52.8 and 26.1 cm^{-1} for $\text{PhB}(\text{CO})$ and $\text{PhB}(\text{C}^{18}\text{O})$, respectively, obtained at the B3LYP/6-311+G** level of theory. Signals around 1400 cm^{-1} overlap with signals of **6** which is formed under the same irradiation conditions because of the presence of an excess of dinitrogen in the matrix. Besides the signals of **7**, a new band at 1980 cm^{-1} was observed upon irradiation at $>495 \text{ nm}$. This signal behaves differently than the signals of **7** upon irradiation at $\lambda = 254 \text{ nm}$. Because of the shift of the band in the presence of ^{13}CO , its assignment to PhBO ($\tilde{\nu} = 1977\text{--}1971 \text{ cm}^{-1}$ in Ar)³² is excluded. While the newly formed species cannot be assigned, we note that a possible candidate could be the bis-CO derivative $\text{PhB}(\text{CO})_2$ (Table S4).¹⁹

In summary, the behaviors of the bands assigned to **1** and **3** under various irradiation conditions are identical under both IR and UV-vis spectroscopic detection in support of the assignments to **1** and **3**.

ESR Spectroscopy. The earlier assignment of triplet **3** as the major product of photodecomposition of diazide **2** was based on IR spectroscopy and supported by an ESR spectroscopy investigation.²⁴ A triplet signal observed in argon with zero-field splitting (zfs) parameters $|D/hc| = 1.240 \text{ cm}^{-1}$ and $|E/hc| = 0.0021 \text{ cm}^{-1}$ was observed after extended irradiation ($\lambda = 254 \text{ nm}$) and assigned to **3**.²⁴ In the present work, additional measurements were performed in solid nitrogen at 4 K. This results in slightly changed zfs parameters for **3** ($|D/hc| = 1.247 \text{ cm}^{-1}$ and $|E/hc| = 0.002 \text{ cm}^{-1}$).

An additional but much weaker signal with smaller zfs parameters (in argon,²⁴ $|D/hc| = 0.870 \text{ cm}^{-1}$ and $|E/hc| = 0.0007 \text{ cm}^{-1}$; in nitrogen, $|D/hc| = 0.882 \text{ cm}^{-1}$ and $|E/hc| < 0.001 \text{ cm}^{-1}$) was also observed after irradiation of **2** at $\lambda = 254 \text{ nm}$. The carrier of this signal could not be firmly assigned in our previous investigation.²⁴ Monitoring the subsequent longer-wavelength irradiation ($\lambda = 350\text{--}450 \text{ nm}$) by ESR spectroscopy

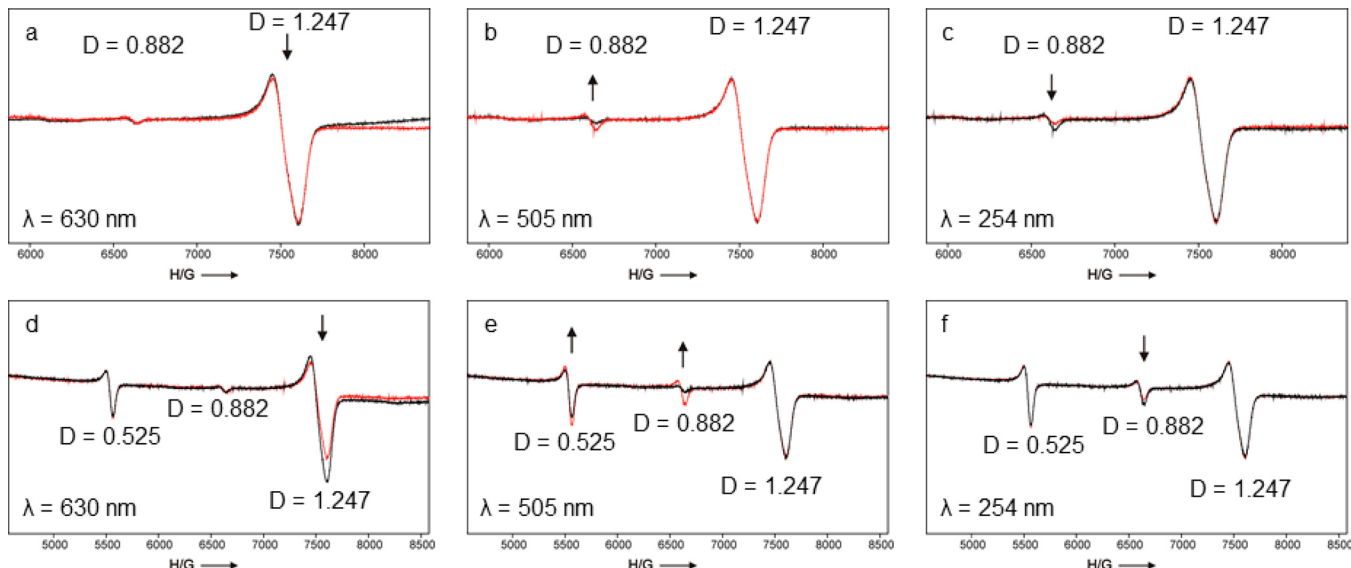


Figure 6. ESR spectra (4 K) obtained after 254 nm irradiation of **2** in (a–c) N_2 and (d–f) CO -doped N_2 (5%). Black, spectra before irradiation given in the panel; red, spectra after irradiation given in the panel. Arrows pointing up or down indicate an increase or decrease in the corresponding absorption under the irradiation conditions given.

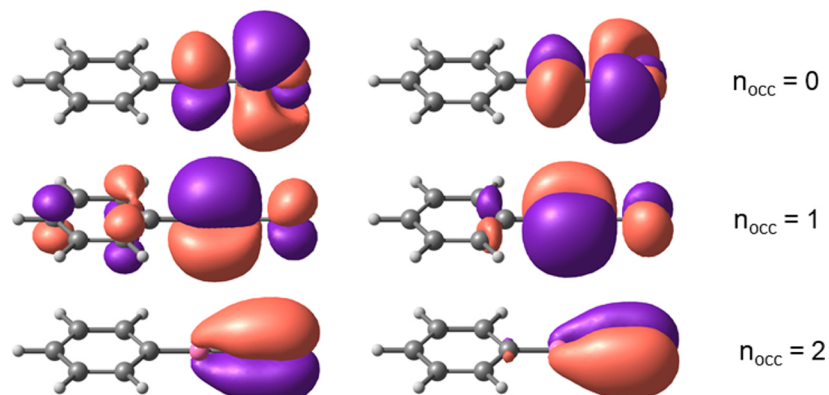


Figure 7. Natural orbitals and occupation numbers of the B–C–O unit of PhBCO (${}^3\text{A}_2$) computed at the UB3LYP/6-311+G** level of theory.

in the present work showed that the weak signal intensifies while the strong one associated with **3** stays almost constant (Figure S3). Under these irradiation conditions, **1** undergoes the photoreaction to form benzoborirene,²⁴ an ESR-silent singlet species, and reacts with N_2 to afford **6**, as shown above by IR spectroscopy. Switching the wavelength of irradiation to $\lambda = 308$ nm (XeCl excimer laser) reduces the intensity of the signal with the smaller D value, while the signal due to **3** again stays constant.

As the IR and UV/vis experiments showed wavelength-selective photochemistry of **3** (>530 nm) and **1** (>495 nm) in the absence or presence of CO, additional experiments were performed. In the absence of CO, irradiation at 630 nm using a light-emitting diode (LED) results in weakening of the ESR signal of **3** (Figure 6a), probably as a result of the reaction with N_2 to give PhNBN_3 . Switching the irradiation wavelength to 505 nm (LED) causes an increase in the weaker signal (Figure 6b), while this signal decreases again upon short-wavelength irradiation (254 nm) (Figure 6c). As under long-wavelength irradiation conditions **1** reacts with molecular nitrogen to afford **6** and as this can be cleaved to **1** + N_2 upon short-wavelength irradiation according to IR and UV/vis measurements, the weak

ESR signal is assigned to the xy_2 transition of the triplet ground state of **6**, in agreement with the previous suggestion.²⁴

In the presence of CO, the strongest ESR signal is still due to **3** after photodecomposition of the diazide by 254 nm irradiation (Figure 6d). This strongest signal decreases in intensity upon irradiation with 630 nm light (Figure 6d). This observation is in agreement with the IR and UV/vis measurements and is due to the formation of isocyanate **5**. Besides the weak signal of **6**, another triplet signal ($|D/hc| = 0.525 \text{ cm}^{-1}$ and $|E/hc| < 0.0005 \text{ cm}^{-1}$) of higher intensity can be observed already after 254 nm irradiation (Figure 6d). The signal of medium intensity and that of **6** increase upon 505 nm irradiation (Figure 6e). Upon short-wavelength irradiation, only the signal of **6** decreases (Figure 6f). As the IR and UV/vis measurements confirmed the formation of **6** and **7** under these irradiation conditions, the new signal is assigned to the latter compound. The small E value ($<0.0005 \text{ cm}^{-1}$) is indicative of a structure that is almost cylindrical, in agreement with the computed linear arrangement of the Ph–B–C–O unit.

The preference of a triplet electronic ground state (${}^3\text{A}_2$) for **3** and **6** was discussed previously on the basis of results obtained with multireference second-order perturbation theory (MRMP2).²⁵ Briefly, simple molecular orbital (MO) analysis

revealed that each of the two compounds features two orthogonal π systems with three π orbitals at the NBN or BNN termini that are almost degenerate. As each of the termini has six π electrons, a high-spin state results, and this was confirmed by the MRMP2 computations.²⁵ For isoelectronic **7** a similar electronic structure was expected and confirmed by computations (see the MOs in Figure 7).

The ground state of linear **7** is the 3A_2 state, while the 1A_2 and 1A_1 states are higher in energy by 10.1 and 12.0 kcal mol⁻¹ at the CASPT2-CAS(12,12)/cc-pVTZ//B3LYP/6-311+G** level of theory (Table 1). The triplet ground state of **7** is in line with the ESR spectroscopy experiments discussed above.

Table 1. Vertical Excitation Energies (in kcal mol⁻¹) Computed at the CASPT2-CAS(12,12)/cc-pVTZ//B3LYP/6-311+G Level of Theory**

compound	3A_2	1A_2	1A_1
PhNBN	0	16.1	18.5
PhBNN	0	15.5	18.2
PhBCO	0	10.1	12.0

The spin density at the terminal nitrogen center is larger in **3** than in **6** according to computations (Figure 8). This is in agreement with the larger $|D/hc|$ value of **3** (1.247 cm^{-1}), which is in the range that is typical for nitrenes with weak delocalization. For example, the closely related boryl nitrenes CatBN and PinBN (Pin = pinacolato) have $|D/hc|$ values of 1.49 and 1.57 cm^{-1} , respectively,^{28,33,34} while the $|D/hc|$ value for phenylnitrene is 0.99 cm^{-1} .³⁵ The spin density at the boron center is quite large in **6**, and in agreement with the stronger delocalization, the $|D/hc|$ value is smaller (0.882 cm^{-1}). In comparison with **6**, the spin density at the boron center is still larger in **7**. The boron atom in **7** is isoelectronic to the carbon center in a carbene (RCR), and indeed, the $|D/hc|$ value of 0.525 cm^{-1} is similar to that of phenylcarbene ($|D/hc| = 0.518\text{ cm}^{-1}$ in Fluorolube at 77 K).³⁶

CONCLUSIONS

The present investigation of the photodecomposition of phenyldiazidoborane (**2**) upon 254 nm irradiation showed

that phenylborylene (**1**) forms along with nitrene PhNBN (**3**), which is the major persistent photoproduct. PhNBN could be characterized by ESR, IR, and UV/vis spectroscopy. This nitrene absorbs in the visible region beyond 700 nm with rather sharp absorption bands and a pronounced vibrational progression. PhNBN reacts photochemically with CO upon $>530\text{ nm}$ irradiation to give the linear isocyanate PhNB(NCO) (**5**).

Compound **1** is a minor product of the photodecomposition of **2**. We could determine the energies of the two lowest-energy excited states, which are in the visible (tentatively 518 nm) and UV (375 nm) regions. This marks the first observation of the absorption energies of a borylene larger than a diatomic one and is expected to be very important for future transient absorption spectroscopy experiments with phenylborylene, in particular as the experimental observations confirm earlier computations.²⁹

Our study provides the first example of the direct observation of a reaction of a borylene (RB). Phenylborylene reacts under photochemical conditions with visible light ($>495\text{ nm}$) with N_2 and CO to give PhBNN (**6**) and PhBCO (**7**), respectively. The photoproducts are ground-state triplet species with a linear arrangement at the boron center according to ESR and computational investigations. The $|D/hc|$ value of 0.5 cm^{-1} for **7** is similar to that of phenylcarbene (PhCH), showing that the isoelectronic relationship of the dicoordinate boron and carbon centers is also reflected in the electronic properties.

EXPERIMENTAL DETAILS

Synthesis and Handling of $\text{PhB}(\text{N}_3)_2$. CAUTION! Phenyl-diazidoborane is explosive. While no explosions were experienced in our laboratory, utmost care must be taken when handling the compound. We used a face shield, Kevlar gauntlets and gloves, and a leather apron. The compound was only prepared in small amounts (max. 10 mg) from commercially available dichlorophenylborane and chlorotrimethylsilane in dichloromethane following the procedure described by Mennekes and Paetzold.³⁷

Matrix Isolation Experiments. Matrix experiments were performed by standard techniques³⁸ using a SHI CKW-21A dispex closed-cycle helium cryostat (IR and ESR) and a CTI Cryogenics 8200 compressor (Brooks Automation) (UV). Phenyldiazidoborane was sublimed from a glass flask at $0\text{ }^\circ\text{C}$ and condensed onto a cold CsI (IR) or sapphire (UV) window or on a copper rod (ESR) with a large

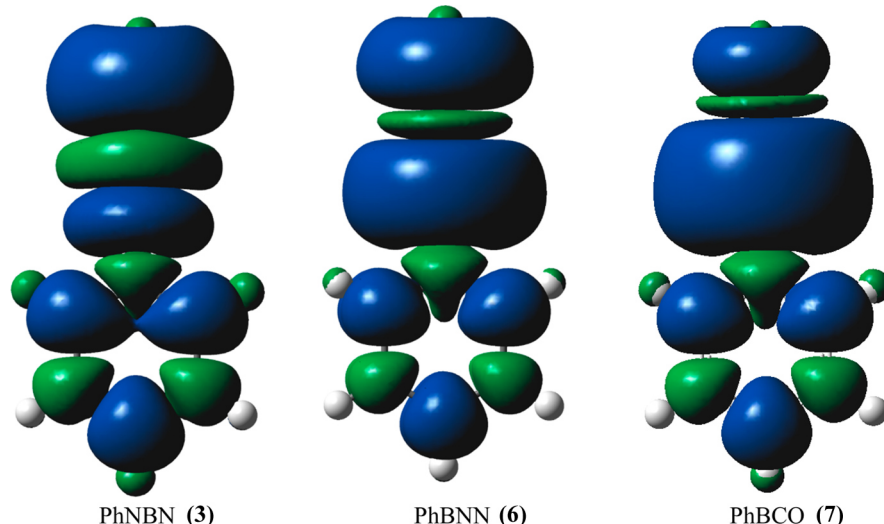


Figure 8. Computed (UB3LYP/6-311+G**) spin densities.

excess of dinitrogen 6.0 (Westfalen AG), $^{15}\text{N}_2$ 2.2 (Westfalen AG), or dinitrogen doped with 5% carbon monoxide 3.7 (Westfalen AG), C^{18}O 2.0 (95% ^{18}O) (Sigma-Aldrich), or ^{13}CO 2.3 (99.1% ^{13}C) (Westfalen AG). The gases or gas mixtures were dosed to 2.0 sccm (IR), 1.5 sccm (UV), or 3.5 sccm (ESR) by a mass flow controller (MKS mass flow PR400B). The deposition temperature was 28 K. FTIR spectra were measured between 4000 and 400 cm^{-1} on a Bruker Vertex 70 spectrometer using a resolution of 0.5 cm^{-1} . UV-vis spectra were measured on a PerkinElmer Lambda 1050 spectrophotometer. X-band ESR spectra were recorded on a Bruker Elexsys E500 ESR spectrometer with an ER077R magnet (75 mm pole cap distance), an ER047 XG-T microwave bridge, and an oxygen-free high-conductivity copper rod (75 mm length, 3 mm diameter) cooled by a closed-cycle cryostat. Computer simulations of the ESR spectra were performed using the XSophe computer simulation software suite (version 1.0.4),³⁹ developed by the Centre for Magnetic Resonance and Department of Mathematics, University of Queensland (Brisbane, Australia) and Bruker Analytik GmbH (Rheinstetten, Germany).

Irradiations were achieved with a low-pressure mercury lamp (UVP, 253.7 nm) and an Osram HBO-500-W/2 high-pressure mercury lamp in an Oriel housing with quartz optics and dichroic mirrors (350–450 and 420–630 nm). Appropriate cutoff filters (Schott) were used. For the ESR experiments, LEDs with maximum outputs at 505 and 630 nm and a XeCl excimer laser ($\lambda = 308 \text{ nm}$) were used.

Computations. Geometries were optimized using the B3LYP hybrid density functional^{40,41} as implemented⁴² in Gaussian 09⁴³ using the 6-311+G** basis set. Harmonic vibrational frequencies were computed at the B3LYP/6-311+G** level analytically. The B3LYP/6-311+G** geometries were employed for the computation of excitation energies and oscillator strengths using time-dependent DFT (TD-B3LYP/6-311+G**).⁴⁴

Vertical excitation energies were computed for PhNBN, PhB(N_2), and PhB(CO) at the B3LYP/6-311+G** geometry of the X^3A_2 state using internally contracted complete-active-space second-order perturbation theory (CASPT2) as described by Werner^{45,46} in conjunction with Dunning's correlation-consistent triple- ζ basis set (cc-pVTZ).⁴⁷ The active space chosen was identical to that used in earlier adiabatic MRMP2 computations, which were run, however, with the much smaller 6-31G* basis set.²⁵ In particular, the active space consisted of 12 orbitals (π_1 to π_6 of the phenyl ring as well as three p_{π} and three p_{σ} orbitals at the X–Y–Z terminus) and was occupied by 12 electrons. The correlated computations applied the frozen core approximation and were run using the Molpro program.^{48,49}

ASSOCIATED CONTENT

Supporting Information

The Supporting Information is available free of charge on the ACS Publications website at DOI: [10.1021/jacs.7b08497](https://doi.org/10.1021/jacs.7b08497).

Additional UV-vis and ESR spectra, computed geometry of PhNBNCO (5), IR spectroscopic data, computed excitation energies, Cartesian coordinates, and complete refs 43 and 49 (PDF)

AUTHOR INFORMATION

Corresponding Author

*holger.bettinger@uni-tuebingen.de

ORCID

Holger F. Bettinger: [0000-0001-5223-662X](https://orcid.org/0000-0001-5223-662X)

Notes

The authors declare no competing financial interest.

ACKNOWLEDGMENTS

This work was supported by the German Research Foundation (DFG). We thank Andreas Schnepf and Lars Wesemann for support and fruitful discussions. The computations were

performed on the BwForCluster JUSTUS. The authors acknowledge support by the state of Baden-Württemberg through bwHPC and the DFG through Grant INST 40/467-1 FUGG.

REFERENCES

- (1) van der Kerk, S. M.; Boersma, J.; van der Kerk, G. J. M. *Tetrahedron Lett.* **1976**, 17, 4765–4766.
- (2) Schlögl, R.; Wrackmeyer, B. *Polyhedron* **1985**, 4, 885–892.
- (3) Eisch, J. J.; Becker, H. P. *J. Organomet. Chem.* **1979**, 171, 141–153.
- (4) Ramsey, B. G.; Anjo, D. M. *J. Am. Chem. Soc.* **1977**, 99, 3182–3183.
- (5) Calhoun, G. C.; Schuster, G. B. *J. Org. Chem.* **1984**, 49, 1925–1928.
- (6) Timms, P. L. *J. Am. Chem. Soc.* **1967**, 89, 1629–1632.
- (7) Timms, P. L. *J. Am. Chem. Soc.* **1968**, 90, 4585–4589.
- (8) Timms, P. L. *Acc. Chem. Res.* **1973**, 6, 118–123.
- (9) Krasowska, M.; Bettinger, H. F. *Chem. - Eur. J.* **2016**, 22, 10661–10670.
- (10) Pachaly, B.; West, R. *Angew. Chem., Int. Ed. Engl.* **1984**, 23, 454–455.
- (11) Grigsby, W. J.; Power, P. P. *J. Am. Chem. Soc.* **1996**, 118, 7981–7988.
- (12) Ito, M.; Tokitoh, N.; Kawashima, T.; Okazaki, R. *Tetrahedron Lett.* **1999**, 40, 5557–5560.
- (13) Bissinger, P.; Braunschweig, H.; Damme, A.; Dewhurst, R. D.; Kupfer, T.; Radacki, K.; Wagner, K. *J. Am. Chem. Soc.* **2011**, 133, 19044–19047.
- (14) Bissinger, P.; Braunschweig, H.; Kraft, K.; Kupfer, T. *Angew. Chem., Int. Ed.* **2011**, 50, 4704–4707.
- (15) Curran, D. P.; Boussonniere, A.; Geib, S. J.; Lacote, E. *Angew. Chem., Int. Ed.* **2012**, 51, 1602–1605.
- (16) Braunschweig, H.; Krummenacher, I.; Légaré, M.-A.; Matler, A.; Radacki, K.; Ye, Q. *J. Am. Chem. Soc.* **2017**, 139, 1802–1805.
- (17) Soleilhavoup, M.; Bertrand, G. *Angew. Chem., Int. Ed.* **2017**, 56, 10282–10292.
- (18) Kinjo, R.; Donnadieu, B.; Celik, M. A.; Frenking, G.; Bertrand, G. *Science* **2011**, 333, 610–613.
- (19) Braunschweig, H.; Dewhurst, R. D.; Hupp, F.; Nutz, M.; Radacki, K.; Tate, C. W.; Vargas, A.; Ye, Q. *Nature* **2015**, 522, 327–330.
- (20) Dahchek, F.; Martin, D.; Stephan, D. W.; Bertrand, G. *Angew. Chem., Int. Ed.* **2014**, 53, 13159–13163.
- (21) Ledet, A. D.; Hudnall, T. W. *Dalton Trans.* **2016**, 45, 9820–9826.
- (22) Braunschweig, H.; Dewhurst, R. D.; Pentecost, L.; Radacki, K.; Vargas, A.; Ye, Q. *Angew. Chem., Int. Ed.* **2016**, 55, 436–440.
- (23) Andrews, L.; Hassanzadeh, P.; Martin, J. M. L.; Taylor, P. R. *J. Phys. Chem.* **1993**, 97, 5839–5847.
- (24) Bettinger, H. F. *J. Am. Chem. Soc.* **2006**, 128, 2534–2535.
- (25) Bettinger, H. F. *J. Organomet. Chem.* **2006**, 691, 4480–4485.
- (26) Krasowska, M.; Bettinger, H. F. *J. Am. Chem. Soc.* **2012**, 134, 17094–17103.
- (27) Krasowska, M.; Bettinger, H. F. *Chem. - Eur. J.* **2014**, 20, 12858–12863.
- (28) Bettinger, H. F.; Bornemann, H. *J. Am. Chem. Soc.* **2006**, 128, 11128–11134.
- (29) Krasowska, M.; Edelmann, M.; Bettinger, H. F. *J. Phys. Chem. A* **2016**, 120, 6332–6341.
- (30) Finnerty, J.; Mitschke, U.; Wentrup, C. *J. Org. Chem.* **2002**, 67, 1084–1092.
- (31) Hausser-Wallis, R.; Oberhammer, H.; Einholz, W.; Paetzold, P. *O. Inorg. Chem.* **1990**, 29, 3286–3289.
- (32) Bettinger, H. F. *Organometallics* **2007**, 26, 6263–6267.
- (33) Filthaus, M.; Schwertmann, L.; Neuhaus, P.; Seidel, R. W.; Oppel, I. M.; Bettinger, H. F. *Organometallics* **2012**, 31, 3894–3903.

- (34) Bettinger, H. F.; Filthaus, M.; Bornemann, H.; Oppel, I. M. *Angew. Chem., Int. Ed.* **2008**, *47*, 4744–4747.
- (35) Wasserman, E.; Smolinsky, G.; Yager, W. A. *J. Am. Chem. Soc.* **1964**, *86*, 3166–3167.
- (36) Trozzolo, A. M.; Murray, R. W.; Wasserman, E. *J. Am. Chem. Soc.* **1962**, *84*, 4990–4991.
- (37) Mennekes, T.; Paetzold, P. Z. *Anorg. Allg. Chem.* **1995**, *621*, 1175–1177.
- (38) Dunkin, I. R. *Matrix-Isolation Techniques*; Oxford University Press: Oxford, U.K., 1998.
- (39) Griffin, M.; Muys, A.; Noble, C.; Wang, D.; Eldershaw, C.; Gates, K. E.; Burrage, K.; Hanson, G. R. *Mol. Phys. Rep.* **1999**, *26*, 60–84.
- (40) Becke, A. D. *J. Chem. Phys.* **1993**, *98*, 5648–5652.
- (41) Lee, C.; Yang, W.; Parr, R. G. *Phys. Rev. B: Condens. Matter Mater. Phys.* **1988**, *37*, 785–789.
- (42) Stephens, P. J.; Devlin, F. J.; Chabalowski, C. F.; Frisch, M. J. *J. Phys. Chem.* **1994**, *98*, 11623–11627.
- (43) Frisch, M. J.; et al. *Gaussian 09*, revision D.01; Gaussian, Inc.: Wallingford, CT, 2009.
- (44) Stratmann, R. E.; Scuseria, G. E.; Frisch, M. J. *J. Chem. Phys.* **1998**, *109*, 8218–8224.
- (45) Werner, H.-J. *Mol. Phys.* **1996**, *89*, 645–661.
- (46) Celani, P.; Werner, H.-J. *J. Chem. Phys.* **2000**, *112*, 5546–5557.
- (47) Dunning, T. H. *J. Chem. Phys.* **1989**, *90*, 1007–1023.
- (48) Werner, H.-J.; Knowles, P. J.; Knizia, G.; Manby, F. R.; Schütz, M. *WIREs Comput. Mol. Sci.* **2012**, *2*, 242–253.
- (49) Werner, H.-J.; et al. *MOLPRO, a Package of ab Initio Programs*, version 2015.1; see <http://www.molpro.net>.

■ NOTE ADDED AFTER ASAP PUBLICATION

This paper was published on October 10, 2017. Schemes 1 and 2 have been corrected and the paper was re-posted on October 13, 2017.

Supporting Information

Photoreactions of Phenylborylene with Dinitrogen and Carbon Monoxide

Klara Edel,^a Matthias Krieg,^a Dirk Grote,^b Holger F. Bettinger^{a,*}

^a Institut für Organische Chemie, Auf der Morgenstelle 18, 72076 Tübingen, Germany

^b Lehrstuhl für Organische Chemie II, Ruhr-Universität Bochum, Universitätsstr. 150, 44780
Bochum, Germany

holger.bettinger@uni-tuebingen.de

Table of Contents

1. UV/vis spectrum of diazdiophenylborane (2)	S2
2. Computed Geometry of PhNB(NCO) (5)	S2
3. ESR spectra obtained from 350-450 nm irradiation	S3
4. IR spectroscopic data and comparison with computational results	S4
5. Computed excited state energies	S6
6. Cartesian Coordinates	S8
7. Full references 43 and 49	S10

1. UV/vis spectrum of diazdiophenylborane (2)

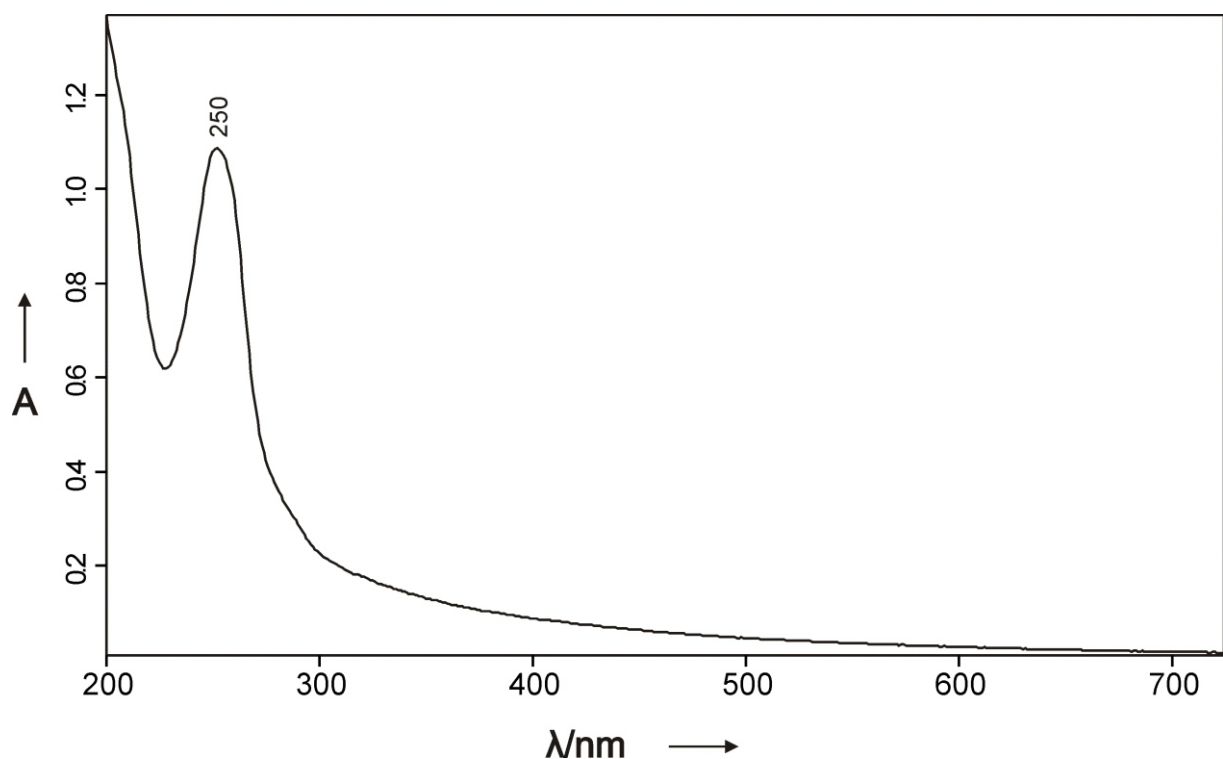
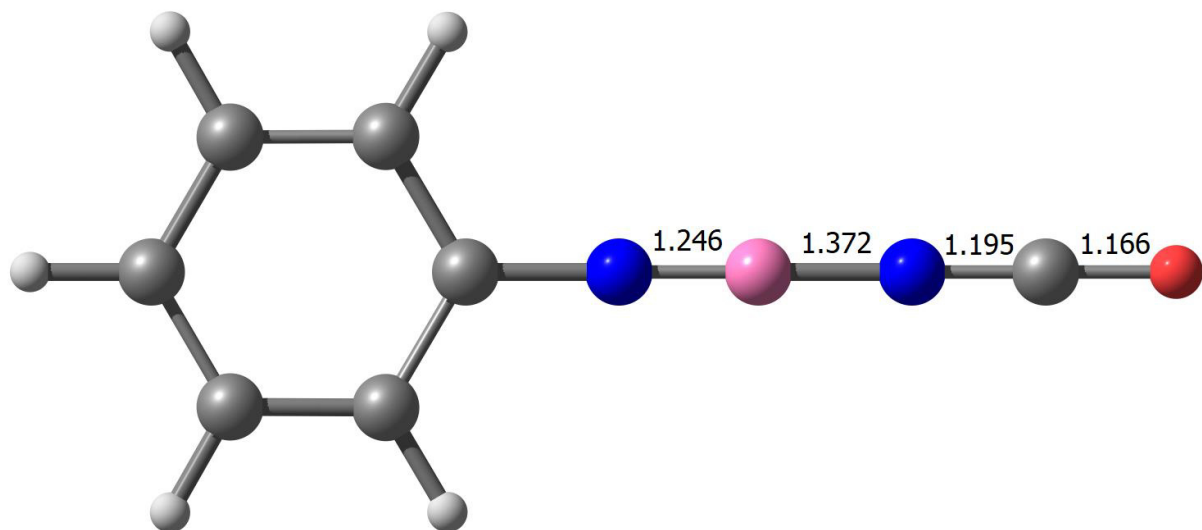


Figure S1. UV/vis spectrum of diazide **2** in a dinitrogen matrix at 28 K.

2. Computed Geometry of PhNB(NCO)



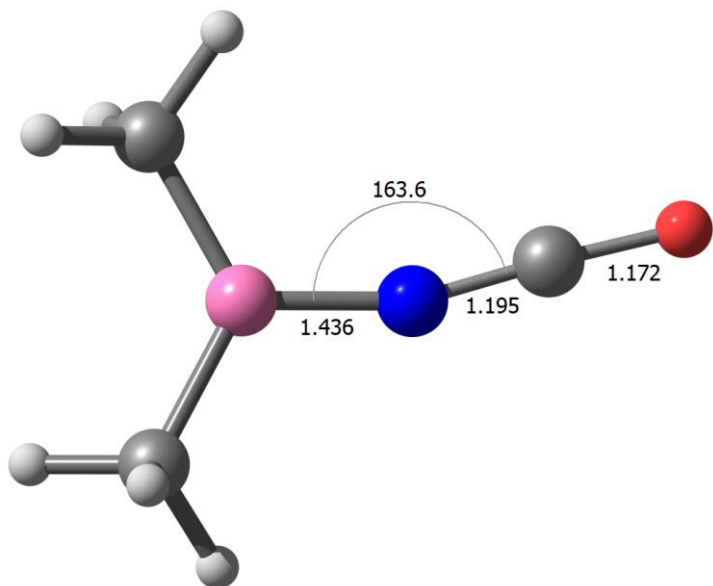


Figure S2. Structure of PhNB(NCO) in C_{2v} symmetry computed at the B3LYP/6-311+G** level of theory. The structure of (isocyanato)dimethylborane (in C_1) is given for comparison. Important bond lengths are given in Å.

3. ESR spectra obtained from 350-450 nm irradiation

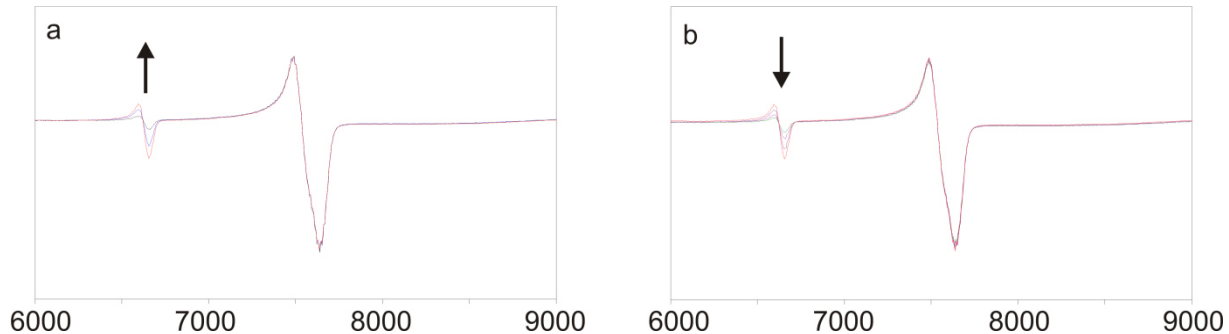


Figure S3. ESR spectra (N_2 , 15 K) obtained after irradiation of **2**. a) Increase of the small D signal due $350 \text{ nm} < \lambda < 450 \text{ nm}$ irradiation; black: $\lambda = 254 \text{ nm}/30\text{min}$; blue: $350 \text{ nm} < \lambda < 450 \text{ nm}$, 10 min; red: $350 \text{ nm} < \lambda < 450 \text{ nm}$, additional 20 min. b) Decrease of the small D signal due to 308-nm-irradiation: red: identical to red trace in a.

4. IR Spectroscopic Data and Comparison with Computational Results

Table S1. Experimental and computed (B3LYP/6-311+G**) vibrational frequencies of PhNBNCO (**5**), computed intensities (in km mol⁻¹), and the corresponding isotopic shifts.

Ph-NB-NCO			Ph-NB-N ¹³ CO		Ph-NB-NC ¹⁸ O		
v _{exp} [cm ⁻¹]	ω _{theor} [cm ⁻¹]	Intensity	v _{exp} [cm ⁻¹]	ω _{theor} [cm ⁻¹]	v _{exp} [cm ⁻¹]	ω _{theor} [cm ⁻¹]	Assignment
2315-2332	2441.9	2968.5	2255-2272	2378.5	2299-2316	2428.3	v(NCO)
2081.2	2125.2	1055.2	2080.6	2123.8	2079.7	2123.9	v(BN)
2131	2184.6		2131	2182.6	2126	2183.1	v(¹⁰ BN)
594/596	594.7	25.2	577/579	577.5	588/590	589.3	δ(NCO)
~ 605	589.1	26.1	~ 589	572.1	~ 600	583.7	δ(NCO)
			Δv _{exp} [cm ⁻¹]	Δω _{theor} [cm ⁻¹]	Δv _{exp} [cm ⁻¹]	Δω _{theor} [cm ⁻¹]	
			60	63.4	16	13.6	v(NCO)
			0.6	1.4	1.5	1.3	v(BN)
			0	2.0	5	1.5	v(¹⁰ BN)
			17	17.2	6	5.4	δ(NCO)
			~ 16	17.0	~ 5	5.4	δ(NCO)

Table S2. Experimental and computed (B3LYP/6-311+G**) vibrational frequencies of PhB(CO) (**7**), computed intensities (in km mol⁻¹), and the corresponding isotopic shifts.

PhB(CO)			PhB(¹³ CO)		PhB(C ¹⁸ O)		
v _{exp} [cm ⁻¹]	ω _{theor} [cm ⁻¹]	Intensity	v _{exp} [cm ⁻¹]	ω _{theor} [cm ⁻¹]	v _{exp} [cm ⁻¹]	ω _{theor} [cm ⁻¹]	Assignment
2012/2006	2058.8	781.8	1961/1956	2006.0	1986/1981	2032.7	v(BCO)
1402	1432.9	168.2	1402	1432.5	1393 ^a	1421.2	δ(in-plane)/v(BCO)
			Δv _{exp} [cm ⁻¹]	Δω _{theor} [cm ⁻¹]	Δv _{exp} [cm ⁻¹]	Δω _{theor} [cm ⁻¹]	
			51/50	52.8	26/25	26.1	v(BCO)
			0	0.4	9	11.7	δ(in-plane)/v(BCO)

^a Tentative assignment due to overlap with signals of PhB(NN).

Table S3. Experimental and computed (B3LYP/6-311+G**) vibrational frequencies of PhB(NN) (**6**), computed intensities (in km mol⁻¹), and the corresponding isotopic shifts.

Ph-BNN			Ph-B ¹⁵ (N) ₂				
v _{exp} [cm ⁻¹]	ω _{theor} [cm ⁻¹]	Intensity	v _{exp} [cm ⁻¹]	ω _{theor} [cm ⁻¹]	Δv _{exp} [cm ⁻¹]	Δω _{theor} [cm ⁻¹]	Assignment
1691	1752.8	108.5		1724.0		28.8	v(BNN)
1417-1387	1433.0	286.1	1373-1367	1408.1	~ 25-28	24.9	δ(in-plane)/v(BNN)

Table S4. Computed (B3LYP/6-311+G**) vibrational frequencies of PhB(CO)₂, computed intensities (in km mol⁻¹), and the corresponding isotopic shifts.

PhB(CO) ₂		PhB(¹³ CO) ₂		PhB(¹⁸ O) ₂		
ω_{theor} [cm ⁻¹]	Intensity	ω_{theor} [cm ⁻¹]	$\Delta\omega_{\text{theor}}$ [cm ⁻¹]	ω_{theor} [cm ⁻¹]	$\Delta\omega_{\text{theor}}$ [cm ⁻¹]	Assignment
2175.2	489.3	2120.4	54.8	2133.5	41.7	$\nu_{\text{sym}}(\text{CO})$
2069.0	1573.1	2017.7	51.3	2029.3	39.7	$\nu_{\text{asym}}(\text{CO})$

5. Computed excited state energies

Table S5. Excited states symmetries, energies (eV), absorption wavelengths (nm), and oscillator strengths computed for conformers of PhB(N₃)₂, isomers of PhBN₂ stoichiometry, PhB, and PhNBNCO at the TD-B3LYP/6-311+G**//B3LYP/6-311+G** level of theory. The most intensive absorptions are highlighted in green.

Compound	State	eV	nm	f	Compound	State	eV	nm	f
C6H5B(N3)2 conformer1	Singlet-B2	4.25	292	f=0.0058	C6H5BN2 3ring	Singlet-B1	2.72	456	f=0.0019
	Singlet-A1	4.47	277	f=0.4346		Singlet-A2	3.82	324	f=0.0000
	Singlet-A2	4.62	269	f=0.0000		Singlet-A1	4.70	264	f=0.0012
	Singlet-B1	4.87	254	f=0.0001		Singlet-B2	4.77	260	f=0.0014
	Singlet-B2	4.88	254	f=0.0587		Singlet-B2	4.96	250	f=0.0231
	Singlet-A2	4.94	251	f=0.0000		Singlet-B1	5.16	240	f=0.0002
	Singlet-A2	5.15	241	f=0.0000		Singlet-A1	5.56	223	f=0.2035
	Singlet-B2	5.63	220	f=0.0034		Singlet-B2	5.97	208	f=0.0007
	Singlet-B1	5.72	217	f=0.0003		Singlet-A2	6.23	199	f=0.0000
	Singlet-A2	5.83	213	f=0.0000		Singlet-A1	6.53	190	f=0.0463
conformer2	Singlet-A'	4.41	281	f=0.0171	PhNBN, ³ A ₂		1.61	772	f=0.0000
	Singlet-A'	4.61	269	f=0.3306			1.95	634	f=0.0921
	Singlet-A'	4.97	249	f=0.1418			2.57	482	f=0.0024
	Singlet-A"	4.98	249	f=0.0002			2.65	468	f=0.0031
	Singlet-A"	5.14	241	f=0.0000			2.71	457	f=0.0000
	Singlet-A"	5.21	238	f=0.0005			2.79	444	f=0.0025
	Singlet-A"	5.25	236	f=0.0000			3.08	403	f=0.0000
	Singlet-A"	5.49	226	f=0.0001			3.42	362	f=0.1444
	Singlet-A"	5.59	222	f=0.0003			4.05	306	f=0.2110
	Singlet-A'	5.67	219	f=0.0057			4.33	286	f=0.0303
conformer3	Singlet-B	4.56	272	f=0.0045	PhBNN, ³ A ₂		3.13	396	f=0.0469
	Singlet-A	4.61	269	f=0.1143			3.31	375	f=0.0000
	Singlet-B	4.80	258	f=0.0081			3.69	336	f=0.0001
	Singlet-B	5.06	245	f=0.2195			3.99	311	f=0.1202
	Singlet-A	5.21	238	f=0.0013			4.02	308	f=0.0087

Singlet-B	5.33	233	f=0.0017		4.29	289	f=0.0002		
Singlet-A	5.41	229	f=0.0058		4.41	281	f=0.0000		
Singlet-B	5.51	225	f=0.0004		4.42	281	f=0.0510		
Singlet-A	5.65	219	f=0.0056		4.46	278	f=0.0000		
Singlet-B	5.71	217	f=0.0068		4.52	274	f=0.0037		
C6H5B	Singlet-B1	2.34	529	f=0.0128	C6H5NBNCO	Singlet-A1	4.68	265	f=0.4720
Singlet-B2	3.16		392	f=0.0412		Singlet-A2	4.75	261	f=0.0000
Singlet-A2	3.87	320	f=0.0000		Singlet-B2	4.84	256	f=0.0021	
Singlet-B2	4.59	270	f=0.0227		Singlet-B1	5.07	245	f=0.0023	
Singlet-A1	5.02	247	f=0.0815		Singlet-A2	5.36	231	f=0.0000	
Singlet-B1	5.10	243	f=0.0720		Singlet-B1	5.68	218	f=0.0013	
Singlet-A2	5.18	239	f=0.0000		Singlet-B2	5.75	215	f=0.1421	
Singlet-B1	5.21	238	f=0.0035		Singlet-B1	5.93	209	f=0.0003	
Singlet-A1	5.27	235	f=0.1912		Singlet-A1	5.94	209	f=0.0281	
Singlet-B2	5.59	222	f=0.0240		Singlet-A2	6.04	205	f=0.0000	

6. Cartesian Coordinates

The Cartesian coordinates computed at the B3LYP/6-311+G** level of the isomers of PhBN₆,¹ PhBN₂,¹ and PhB² isomer were published in Supporting Information sections of previous publications.

Cartesian coordinates were obtained at the B3LPY/6-311+G** level of theory and are given in Å.

12
PhNB (NCO) -479.523703733

6	0.000000000	0.000000000	-3.785371000
6	0.000000000	1.204267000	-3.081738000
6	0.000000000	1.210048000	-1.690871000
6	0.000000000	0.000000000	-0.977623000
6	0.000000000	-1.210048000	-1.690871000
6	0.000000000	-1.204267000	-3.081738000
7	0.000000000	0.000000000	0.392774000
5	0.000000000	0.000000000	1.639044000
7	0.000000000	0.000000000	3.011172000
1	0.000000000	2.146520000	-3.618473000
1	0.000000000	2.143168000	-1.140165000
1	0.000000000	-2.143168000	-1.140165000
1	0.000000000	-2.146520000	-3.618473000
1	0.000000000	0.000000000	-4.869103000
6	0.000000000	0.000000000	4.206078000
8	0.000000000	0.000000000	5.372043000

12
(CH₃)₂BNCO

5	0.933796000	-0.001232000	0.002291000
7	-0.482618000	-0.236579000	0.009688000
6	-1.669056000	-0.092883000	0.001014000
8	-2.837751000	-0.009115000	-0.004929000
6	1.894110000	-1.242734000	0.006706000
1	2.866786000	-1.027882000	0.457904000
1	1.461469000	-2.128599000	0.477775000
1	2.096725000	-1.513222000	-1.040652000
6	1.464920000	1.478202000	-0.010177000
1	0.749724000	2.209268000	-0.394258000
1	1.687702000	1.763931000	1.028711000
1	2.409102000	1.576129000	-0.554585000

16
C₆H₅B (CO)₂

C	-0.336302	0.091887	-2.607730
C	-1.530464	-0.180776	-1.942545
C	-1.560976	-0.237240	-0.550740
C	-0.404317	-0.002231	0.211159
C	0.787324	0.281185	-0.476770
C	0.823987	0.317678	-1.869094
B	-0.442326	-0.054827	1.786444
C	0.611146	-0.630265	2.622315
O	1.457113	-1.086579	3.254471
H	-2.438856	-0.359517	-2.507562
H	-2.495424	-0.476828	-0.053616
H	1.696351	0.485597	0.079658
H	1.758256	0.532226	-2.376519

H	-0.310166	0.128054	-3.690958
C	-1.535768	0.465302	2.607093
O	-2.411939	0.879820	3.226772

7. Full references 43 and 49

Reference 43:

Frisch, M. J.; Trucks, G. W.; Schlegel, H. B.; Scuseria, G. E.; Robb, M. A.; Cheeseman, J. R.; Scalmani, G.; Barone, V.; Mennucci, B.; Petersson, G. A.; Nakatsuji, H.; Caricato, M.; Li, X.; Hratchian, H. P.; Izmaylov, A. F.; Bloino, J.; Zheng, G.; Sonnenberg, J. L.; Hada, M.; Ehara, M.; Toyota, K.; Fukuda, R.; Hasegawa, J.; Ishida, M.; Nakajima, T.; Honda, Y.; Kitao, O.; Nakai, H.; Vreven, T.; Montgomery, J. A.; Peralta, J. E.; Ogliaro, F.; Bearpark, M.; Heyd, J. J.; Brothers, E.; Kudin, K. N.; Staroverov, V. N.; Kobayashi, R.; Normand, J.; Raghavachari, K.; Rendell, A.; Burant, J. C.; Iyengar, S. S.; Tomasi, J.; Cossi, M.; Rega, N.; Millam, J. M.; Klene, M.; Knox, J. E.; Cross, J. B.; Bakken, V.; Adamo, C.; Jaramillo, J.; Gomperts, R.; Stratmann, R. E.; Yazyev, O.; Austin, A. J.; Cammi, R.; Pomelli, C.; Ochterski, J. W.; Martin, R. L.; Morokuma, K.; Zakrzewski, V. G.; Voth, G. A.; Salvador, P.; Dannenberg, J. J.; Dapprich, S.; Daniels, A. D.; Farkas, Ö.; Foresman, J. B.; Ortiz, J. V.; Cioslowski, J.; Fox, D. J., Gaussian 09, Revision D.01, Wallingford CT, 2009.

Reference 49:

Werner, H.-J.; Knowles, P. J.; Knizia, G.; Manby, F. R.; Schütz, M.; Celani, P.; Györffy, W.; Kats, D.; Korona, T.; Lindh, R.; Mitrushenkov, A.; Rauhut, G.; Shamasundar, K. R.; Adler, T. B.; Amos, R. D.; Bernhardsson, A.; Berning, A.; Cooper, D. L.; Deegan, M. J. O.; Dobbyn, A. J.; Eckert, F.; Goll, E.; Hampel, C.; Hesselmann, A.; Hetzer, G.; Hrenar, T.; Jansen, G.; Köpll, C.; Liu, Y.; Lloyd, A. W.; Mata, R. A.; May, A. J.; McNicholas, S. J.; Meyer, W.; Mura, M. E.; Nicklass, A.; O'Neill, D. P.; Palmieri, P.; Peng, D.; Pflüger, K.; Pitzer, R.; Reiher, M.; Shiozaki, T.; Stoll, H.; Stone, A. J.; Tarroni, R.; Thorsteinsson, T.; Wang, M., MOLPRO, version 2015.1, a package of ab initio programs.

References

1. Bettinger, H. F. *J. Organomet. Chem.* **2006**, *691*, 4480-4485.
2. Bettinger, H. F. *J. Am. Chem. Soc.* **2006**, *128*, 2534-2535.

Publikation 4

Photoisomerization

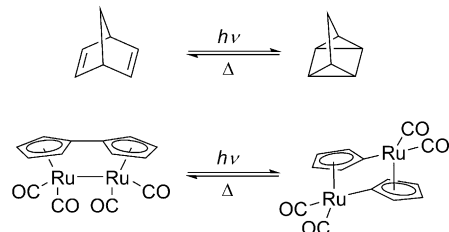
International Edition: DOI: 10.1002/anie.201712683
 German Edition: DOI: 10.1002/ange.201712683

The Dewar Isomer of 1,2-Dihydro-1,2-azaborinines: Isolation, Fragmentation, and Energy Storage

Klara Edel, Xinyu Yang, Jacob S. A. Ishibashi, Ashley N. Lamm, Cäcilia Machle-Mössmer, Zachary X. Giustra, Shih-Yuan Liu,* and Holger F. Bettinger*

Abstract: The photochemistry of 1,2-dihydro-1,2-azaborinine derivatives was studied under matrix isolation conditions and in solution. Photoisomerization occurs exclusively to the Dewar valence isomers upon irradiation with UV light ($>280\text{ nm}$) with high quantum yield (46%). Further photolysis with UV light (254 nm) results in the formation of cyclobutadiene and an iminoborane derivative. The thermal electrocyclic ring-opening reaction of the Dewar valence isomer back to the 1,2-dihydro-1-tert-butylmethyldimethylsilyl-2-mesityl-1,2-azaborinine has an activation barrier of $(27.0 \pm 1.2)\text{ kcal mol}^{-1}$. In the presence of the Wilkinson catalyst, the ring opening occurs rapidly and exothermically ($\Delta H = (-48 \pm 1)\text{ kcal mol}^{-1}$) at room temperature.

Solar energy as a renewable energy technology is an important part of the solution of the increasing world energy demand and limited fossil energy sources. The development of technologies for storing solar energy is, however, challenging. A promising technology is molecular solar thermal systems (MOST),^[1] in which photons induce photoisomerization to a high-energy species that has a sufficiently high activation barrier for the reversible reaction and releases thermal energy only on demand (e.g., in the presence of a catalyst). Beside *E/Z* isomerization of CC or NN double bonds^[2] and photodimerization of anthracene,^[3] several valence isomer pairs, such as norbornadiene/quadracyclane,^[1g,4] the fulvalene diruthenium system,^[5] and hexamethylbenzene (HMB), which undergoes photoisomerization to hexamethyl Dewar benzene (HMDB) and hexamethylprismane,^[6] are considered as potential MOST systems (Scheme 1). Herein we present a new valence isomer pair as a candidate for the storage of solar energy that is based on the

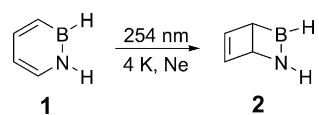


Scheme 1. Valence isomer pairs studied in the context of energy storage.

photoisomerization of 1,2-dihydro-1,2-azaborinine (**1**) to its Dewar valence isomer **2**.

The replacement of two adjacent carbon atoms in benzene by the isoelectronic BN unit leads to 1,2-dihydro-1,2-azaborinines, heterocyclic compounds that have in common with benzene a considerable degree of aromaticity.^[7] The polarity of the BN unit modifies the electronic properties,^[8] and this heterocycle is therefore of interest in biomedical research^[9] and materials science.^[10] First syntheses of substituted 1,2-dihydro-1,2-azaborinines were reported by Dewar and Marr^[11] and White^[12] in the 1960s. Further progress was made by the research groups of Ashe,^[13] Perepichka,^[10i] Yamaguchi,^[10a] Liu,^[7a,14] and Braunschweig.^[10d,15] Liu and co-workers developed the first synthesis of the parent compound 1,2-dihydro-1,2-azaborinine (**1**).^[7a] The photochemistry of 1,2-dihydro-1,2-azaborinine (**1**) under matrix isolation conditions was investigated by our group (Scheme 2).^[16] The irradiation of **1** isolated in a neon matrix with light of wavelength 254 nm led to full conversion exclusively to the Dewar isomer **2**.

We also explored the thermal ring-opening reaction of **2** by computational chemistry techniques.^[17] Beside the classical conrotatory and disrotatory transition states, two further *stepwise* ring-opening pathways were identified that were found to be lower in energy than the conrotatory ring opening. With an activation barrier of $22.2\text{ kcal mol}^{-1}$ [CCSD(T)/cc-pVQZ//CCSD(T)/TZ2P], the lifetime of **2** should be long enough to allow its detection in solution. It was also found computationally that the polarity of the BN unit would lead to very facile dimerization or oligomerization of **2**.^[17a]



Scheme 2. Photoisomerization of 1,2-dihydro-1,2-azaborinine (**1**) to the Dewar valence isomer (**2**).

[*] K. Edel, H. F. Bettinger

Institut für Organische Chemie, Universität Tübingen
 Auf der Morgenstelle 18, 72076 Tübingen (Germany)
 E-mail: Holger.Bettinger@uni-tuebingen.de

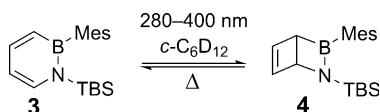
X. Yang, J. S. A. Ishibashi, Z. X. Giustra, S.-Y. Liu
 Department of Chemistry, Boston College
 Chestnut Hill, MA 02467-3860 (USA)
 E-mail: liusd@bc.edu

C. Machle-Mössmer
 Institut für Anorganische Chemie, Universität Tübingen
 Auf der Morgenstelle 18, 72076 Tübingen (Germany)

A. N. Lamm, S.-Y. Liu
 Department of Chemistry and Biochemistry, University of Oregon
 Eugene, OR 97403-1253 (USA)

Supporting information and the ORCID identification number(s) for the author(s) of this article can be found under:
<https://doi.org/10.1002/anie.201712683>.

Encouraged by the finding of a sizable barrier for thermal ring opening of **2**, we investigated the photochemistry of 1,2-dihydro-1,2-azaborinines in solution. We reasoned that oligomerization of the aminoborane moiety could be suppressed by kinetic stabilization by bulky substituents at B and N. Herein we report the photoconversion of 1,2-dihydro-1-*tert*-butyldimethylsilyl-2-mesityl-1,2-azaborinine^[10e] (**3**) into the corresponding Dewar valence isomer **4** in solution in cyclohexane at room temperature (Scheme 3). To our surprise, **4** turned out to be stable for weeks at room temperature under inert conditions and was converted back into **3** only slowly.



Scheme 3. Photoisomerization of 1,2-dihydro-1-*tert*-butyldimethylsilyl-2-mesityl-1,2-azaborinine (**3**) to the Dewar isomer (**4**).

We irradiated a solution of **3** in deuterated cyclohexane (*c*-C₆D₁₂) in a J. Young quartz tube with 280–400 nm light to follow the reaction progress by NMR spectroscopy. The NMR spectra showed decreasing signals of **3** and new increasing signals of **4** without the formation of any by-products. After extended irradiation, full conversion into **4** was observed. The quantum yield of the transformation was determined to be 0.46 ± 0.08 (see the Supporting Information for details). The NMR signals of **4** were unambiguously assigned through 2D NMR spectroscopy experiments and comparison with DFT computations of chemical shifts at the B3LYP/6-311 + G** level of theory (see Tables S2 and S4 in the Supporting Information). For example, the boron NMR spectrum showed a new signal at 52.9 ppm (*c*-C₆D₁₂) in accordance with the computed downfield shift of 13.0 ppm as compared to the signal of **3** at 40.3 ppm (*c*-C₆D₁₂). The bridgehead protons were observed at 3.00 and 4.75 ppm (Figure 1), as expected for non-aromatic methine protons, and showed the corresponding coupling in the COSY NMR spectrum (see Figure S9 in the Supporting Information). The two methyl groups of the TBS (*tert*-butyldimethylsilyl) substituent are diastereotopic owing to the adjacent bridgehead stereocenter.

The Dewar isomer **4** could be isolated after the photoreaction. The compound was obtained as a colorless oil in all attempted syntheses, and it was not possible to grow crystals suitable for single-crystal X-ray analysis despite a considerable number of attempts using various techniques, including the crystalline sponge method^[18] and the *in situ* crystallization technique (see Figure S23 for a computed structure).

We also investigated the thermal ring opening of Dewar isomer **4** back to the

starting material **3** by NMR spectroscopy. Owing to its high thermal stability, deuterated 1,1,2,2-tetrachloroethane ([D₂]TCE) was chosen as the solvent. The ¹H NMR spectrum only showed the growth of signals due to **3**, without any formation of by-products. The half-life at 100 °C was around 25 min. The kinetics of ring opening were studied by NMR spectroscopy in [D₂]TCE over a rather narrow temperature range (358–373 K). Arrhenius treatment of the first-order reaction data gave an activation energy (*E*_a) of (27.0 ± 1.2) kcal mol⁻¹ and a preexponential factor of log *A* = (12.5 ± 0.7) s⁻¹.

The experimentally determined activation energy is much higher than the barrier computed previously for the ring opening of **2**.^[17a] As these data were obtained with coupled cluster theory, the “gold standard” of quantum chemistry, it was worthwhile investigating the origin of the difference. As **4** is much too large for computational treatment at the coupled cluster level, we reinvestigated the ring opening of **2** using density functional theory (DFT) at the B3LYP/6-311 + G** level. Gratifyingly, the DFT results are in very good agreement with those of the computationally significantly more involved CCSD(T) method (see Table S10) reported earlier.^[17a] Hence, we investigated the ring opening of **4** at the B3LYP/6-311 + G** level. In the presence of the bulky substituents, the thermal ring-opening reaction is no longer stepwise, but rather concerted with a strongly distorted transition state (see Figure S24), as evidenced by computation of the intrinsic reaction coordinate. The lowest energy barrier of 26.1 kcal mol⁻¹ obtained is in very good agreement with experiment and shows that the bulky substituents not only stabilize the Dewar isomer with respect to oligomerization, but also retard ring opening. This is probably due to the increased steric repulsion of the adjacent bulky groups in the

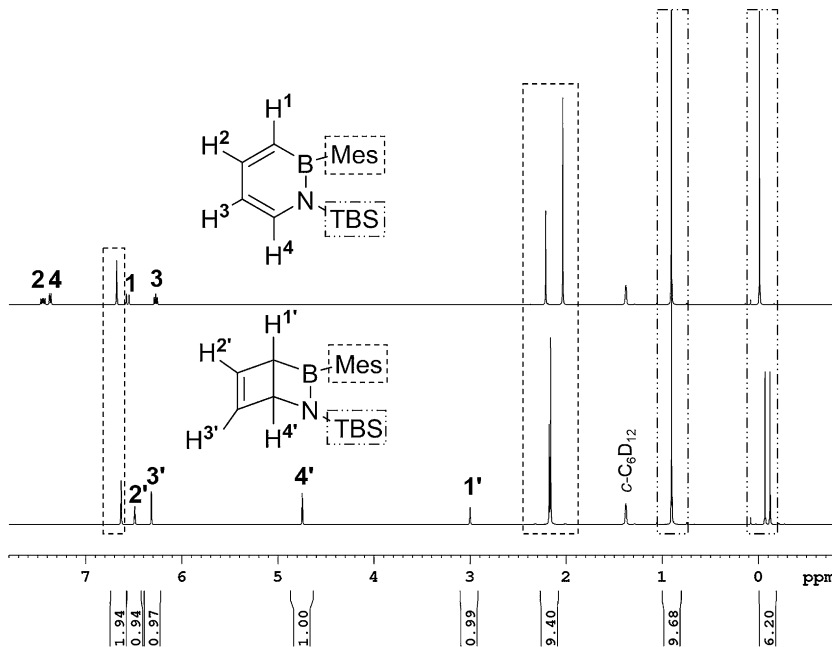


Figure 1. ¹H NMR spectra in *c*-C₆D₁₂ of 1,2-dihydro-1-*tert*-butyldimethylsilyl-2-mesityl-1,2-azaborinine (**3**, top trace) and of its Dewar valence isomer (**4**) after irradiation with 280–400 nm light (bottom trace).

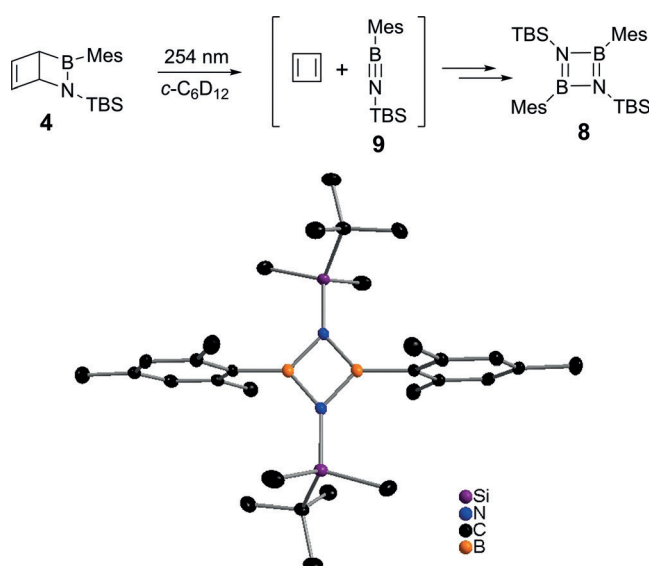
planar geometrical arrangement in **3**, as the computed heat of reaction is lowered by more than 10 kcal mol⁻¹ for the isomerization of **4**→**3** versus **2**→**1** (see Table S10).

We also investigated the photochemistry of the related chloro derivative 1,2-dihydro-1-*tert*-butyldimethylsilyl-2-chloro-1,2-azaborinine (**5**) and found that it also underwent photoisomerization in solution. The corresponding Dewar isomer **6** was also obtained as an oil; however, it was quite readily hydrolyzed by trace amounts of water. As **5** is a thermal precursor to a BN aryne studied by matrix isolation techniques,^[19] we also investigated its photochemistry in an argon matrix. Photolysis of **5** with 280–400 nm irradiation quickly led to the formation of the Dewar valence isomer, based on the comparison of experimental and computed IR spectra, as the only photo product. UV spectra showed the disappearance of **5** owing to photolysis at 280–400 nm and the formation of a new band at 215 nm (see Figure S21) that can be assigned to **6** as based on the behavior deduced by IR spectroscopy. A weak absorption ($S_0 \rightarrow S_1$) was computed for **6** at 216 nm ($f=0.013$) at the TD-B3LYP/6-311+G** level of theory.

Irradiation of **5** with 254 nm light also quickly resulted in photoisomerization to **6**, but upon extended photolysis at 254 nm, the Dewar isomer slowly underwent cycloreversion to the corresponding iminoborane **7** and cyclobutadiene. The latter underwent further cycloreversion to two acetylene molecules upon prolonged irradiation (Scheme 4).^[20] The IR signals of **7** could be assigned by comparison with a computed spectrum [B3LYP/6-311+G**] and showed the natural ratio of ¹⁰B and ¹¹B isotopes (see Figure S22).

We previously observed that the parent Dewar isomer **2** also underwent a slow photodecomposition reaction, and hence reinvestigated this reaction in light of the results described above. Indeed, prolonged irradiation of the parent systems (both the B–H/N–H and B–D/N–D isotopologues were investigated) resulted in the formation of cyclobutadiene and acetylene. However, the corresponding parent iminoboranes HBNH and DBND could not be observed unambiguously, as the degree of photoisomerization and photodecomposition was lower for the parent system.

Motivated by the matrix isolation study, we explored the photochemistry of **4** in solution. The NMR spectra after irradiation with 254 nm light showed the disappearance of **4** and formation of new compounds, including 1,3,2,4-diazabidoboretidine **8** (Scheme 5), which is stable under conventional conditions and can be purified by column chromatography. A single crystal suitable for X-ray crystallography was obtained by slow evaporation of *n*-pentane (Scheme 5).^[21] The ¹¹B NMR spectrum showed a signal at 17.4 ppm after irradiation that was in the typical range for *N*-silyl-substituted



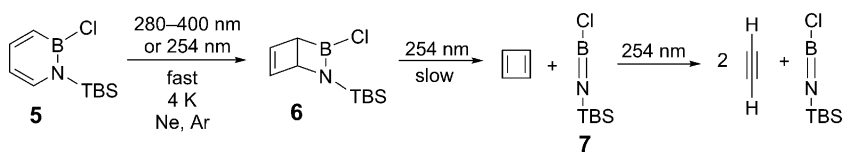
Scheme 5. Cycloreversion of the Dewar valence isomer of 1,2-dihydro-1-*tert*-butyldimethylsilyl-2-mesilyl-1,2-azaborinine (**4**) leads to the formation of **8**.

iminoboranes (16–22 ppm).^[21b,22] The computed chemical shift of 17.2 ppm supports the assignment of the intermediate as iminoborane **9**. Other photo products could not be identified.

These results show that 1,2-dihydro-1,2-azaborinines can undergo a stepwise photoinduced cycloreversion to the acetylene and iminoborane building blocks. The fragmentation discovered in this study is formally the reversion of azaborinine synthesis from iminoborane and acetylenes reported by Braunschweig et al.^[23]

Finally, we screened a variety of catalysts to promote the ring-opening reaction at room temperature. In an initial survey of metal catalysts we found that the Wilkinson catalyst was uniquely effective, furnishing cleanly the 1,2-dihydro-1,2-azaborinine **3** from **4** in less than 1 h at room temperature at 3 mol % catalyst loading (see Table S11). More detailed screening of rhodium-based catalysts revealed [Rh(C₂H₄)₂Cl]₂ as an equally effective catalyst (see Table S11). On the other hand, cyclooctadiene- or norbornadiene-containing neutral and cationic Rh^I complexes as well as the Rh^{III} complex [Rh(Cp*)Cl₂]₂ were not suitable ring-opening catalysts (see Table S11). To determine the energy stored in the photo-generated strained Dewar compound **4**, we measured the heat of the ring-opening reaction in a reaction calorimeter. Thus, integration of the heat-flow curve of the ring-opening reaction catalyzed by the Wilkinson catalyst (3 mol %) gave consistently $\Delta H = (-48 \pm 1)$ kcal mol⁻¹.^[24] This value compares favorably to those of other known MOST systems (e.g., $\Delta H = -21$ kcal mol⁻¹ for the norbornadiene/quadracyclane system;^[25] $\Delta H = -20$ kcal mol⁻¹ for the fulvalene diruthenium system),^[5d] and agrees with our DFT computations (see Table S10).

In summary, we have demonstrated the isolation of the Dewar valence isomer



Scheme 4. Photochemistry of 1,2-dihydro-1-*tert*-butyldimethylsilyl-2-chloro-1,2-azaborinine (**5**) under matrix isolation conditions.

of two 1,2-dihydro-1,2-azaborinines in solution on a preparative scale. Irradiation of a substituted 1,2-dihydro-1,2-azaborinine in solution in cyclohexane led to full conversion with high quantum yield ($(46 \pm 8)\%$) exclusively into the Dewar valence isomer, which was stable for weeks at room temperature under inert conditions. Further irradiation with shorter wavelength UV light led to cycloreversion of the Dewar valence isomer to the corresponding iminoborane and cyclobutadiene. The substituted Dewar isomer is kinetically stable towards thermal electrocyclic ring opening which has an activation energy of (27.0 ± 1.2) kcal mol $^{-1}$. The thermal ring-opening reaction can be catalyzed efficiently by the Wilkinson catalyst. The energy stored in the strained bicyclic Dewar valence isomer has been determined by calorimetric measurement to be (48 ± 1) kcal mol $^{-1}$. This study provides a proof of concept of the potential utility of 1,2-dihydro-1,2-azaborinine valence isomer pairs in molecular solar thermal system applications. Current efforts are directed toward tuning the absorption profile of our system to the visible range.

Acknowledgements

The research in Tübingen was supported by the Deutsche Forschungsgemeinschaft. The computations were performed on the BwForCluster JUSTUS. We acknowledge support by the state of Baden-Württemberg through bwHPC and the German Research Foundation (DFG) through grant no. INST 40/467-1 FUGG. We thank Dr. Klaus Merz for attempting in situ crystallization, and Prof. Dr. Günter Gauglitz and Prof. Dr. Suning Wang for helpful discussions concerning the determination of the quantum yield. This research was supported in part by the National Institutes of Health NIGMS (R01-GM094541). S.-Y.L. thanks the Humboldt Foundation for the Friedrich Wilhelm Bessel Research Award.

Conflict of interest

The authors declare no conflict of interest.

Keywords: boron–nitrogen heterocycles · electrocyclic reactions · photoisomerization · sustainable chemistry · valence isomerization

How to cite: *Angew. Chem. Int. Ed.* **2018**, *57*, 5296–5300
Angew. Chem. **2018**, *130*, 5394–5398

- [1] a) A. Lennartson, K. Moth-Poulsen in *Molecular Devices for Solar Energy Conversion and Storage* (Eds.: H. Tian, G. Boschloo, A. Hagfeldt), Springer, Singapore, **2018**, pp. 327–352; b) A. Lennartson, A. Roffey, K. Moth-Poulsen, *Tetrahedron Lett.* **2015**, *56*, 1457–1465; c) T. J. Kucharski, Y. Tian, S. Akbulatov, R. Boulatov, *Energy Environ. Sci.* **2011**, *4*, 4449–4472; d) K. Jorner, A. Dreos, R. Emanuelsson, O. El Bakouri, I. F. Galvan, K. Börjesson, F. Feixas, R. Lindh, B. Zietz, K. Moth-Poulsen, H. Ottosson, *J. Mater. Chem. A* **2017**, *5*, 12369–12378; e) A. Dreos, K. Börjesson, Z. Wang, A. Roffey, Z. Norwood, D.

Kushnir, K. Moth-Poulsen, *Energy Environ. Sci.* **2017**, *10*, 728–734; f) K. Börjesson, A. Lennartson, K. Moth-Poulsen, *ACS Sustainable Chem. Eng.* **2013**, *1*, 585–590; g) D. A. Dubonosov, A. V. Bren, V. A. Chernovianov, *Russ. Chem. Rev.* **2002**, *71*, 917–927.

- [2] a) V. Caia, G. Cum, R. Gallo, V. Mancini, E. Pitoni, *Tetrahedron Lett.* **1983**, *24*, 3903–3904; b) C. Bastianelli, V. Caia, G. Cum, R. Gallo, V. Mancini, *J. Chem. Soc. Perkin Trans. 2* **1991**, *679*–683; c) A. M. Kolpak, J. C. Grossman, *Nano Lett.* **2011**, *11*, 3156–3162; d) Y. Feng, H. Liu, W. Luo, E. Liu, N. Zhao, K. Yoshino, W. Feng, *Sci. Rep.* **2013**, *3*, 3260; e) T. J. Kucharski, N. Ferralis, A. M. Kolpak, J. O. Zheng, D. G. Nocera, J. C. Grossman, *Nat. Chem.* **2014**, *6*, 441–447.
- [3] G. Stein, *Isr. J. Chem.* **1975**, *14*, 213–225.
- [4] a) V. Gray, A. Lennartson, P. Ratanalert, K. Börjesson, K. Moth-Poulsen, *Chem. Commun.* **2014**, *50*, 5330–5332; b) Z.-I. Yoshida, *J. Photochem.* **1985**, *29*, 27–40.
- [5] a) K. Moth-Poulsen, D. Coso, K. Börjesson, N. Vinokurov, S. K. Meier, A. Majumdar, K. P. C. Vollhardt, R. A. Segelman, *Energy Environ. Sci.* **2012**, *5*, 8534–8537; b) K. Börjesson, A. Lennartson, K. Moth-Poulsen, *J. Fluorine Chem.* **2014**, *161*, 24–28; c) K. Börjesson, D. Dzebo, B. Albinsson, K. Moth-Poulsen, *J. Mater. Chem. A* **2013**, *1*, 8521–8524; d) Y. Kanai, V. Srinivasan, S. K. Meier, K. P. C. Vollhardt, J. C. Grossman, *Angew. Chem. Int. Ed.* **2010**, *49*, 8926–8929; *Angew. Chem.* **2010**, *122*, 9110–9113; e) M. R. Harpham, S. C. Nguyen, Z. Hou, J. C. Grossman, C. B. Harris, M. W. Mara, A. B. Stickrath, Y. Kanai, A. M. Kolpak, D. Lee, D.-J. Liu, J. P. Lomont, K. Moth-Poulsen, N. Vinokurov, L. X. Chen, K. P. C. Vollhardt, *Angew. Chem. Int. Ed.* **2012**, *51*, 7692–7696; *Angew. Chem.* **2012**, *124*, 7812–7816.
- [6] a) W. Schaefer, H. Hellmann, *Angew. Chem. Int. Ed. Engl.* **1967**, *6*, 518–525; *Angew. Chem.* **1967**, *79*, 566–573; b) J. F. M. Oth, *Recl. Trav. Chim. Pays-Bas* **1968**, *87*, 1185–1195; c) H. Hogeweegen, H. C. Volger, *Chem. Commun.* **1967**, 1133–1134; d) W. Adam, J. C. Chang, *Int. J. Chem. Kinet.* **1969**, *1*, 487–492.
- [7] a) A. J. V. Marwitz, M. H. Matus, L. N. Zakharov, D. A. Dixon, S.-Y. Liu, *Angew. Chem. Int. Ed.* **2009**, *48*, 973–977; *Angew. Chem.* **2009**, *121*, 991–995; b) E. R. Abbey, L. N. Zakharov, S.-Y. Liu, *J. Am. Chem. Soc.* **2008**, *130*, 7250–7252.
- [8] a) Z. Liu, T. B. Marder, *Angew. Chem. Int. Ed.* **2008**, *47*, 242–244; *Angew. Chem.* **2008**, *120*, 248–250; b) M. J. D. Bosdet, W. E. Piers, *Can. J. Chem.* **2009**, *87*, 8–29; c) P. G. Campbell, A. J. V. Marwitz, S.-Y. Liu, *Angew. Chem. Int. Ed.* **2012**, *51*, 6074–6092; *Angew. Chem.* **2012**, *124*, 6178–6197; d) X.-Y. Wang, J.-Y. Wang, J. Pei, *Chem. Eur. J.* **2015**, *21*, 3528–3539.
- [9] a) L. Liu, A. J. V. Marwitz, B. W. Matthews, S.-Y. Liu, *Angew. Chem. Int. Ed.* **2009**, *48*, 6817–6819; *Angew. Chem.* **2009**, *121*, 6949–6951; b) D. H. Knack, J. L. Marshall, G. P. Harlow, A. Dudzik, M. Szaleńiec, S.-Y. Liu, J. Heider, *Angew. Chem. Int. Ed.* **2013**, *52*, 2599–2601; *Angew. Chem.* **2013**, *125*, 2660–2662; c) H. Lee, M. Fischer, B. K. Shiochet, S.-Y. Liu, *J. Am. Chem. Soc.* **2016**, *138*, 12021–12024.
- [10] a) T. Taniguchi, S. Yamaguchi, *Organometallics* **2010**, *29*, 5732–5735; b) A. J. V. Marwitz, J. T. Jenkins, L. N. Zakharov, S.-Y. Liu, *Angew. Chem. Int. Ed.* **2010**, *49*, 7444–7447; *Angew. Chem.* **2010**, *122*, 7606–7609; c) A. J. V. Marwitz, A. N. Lamm, L. N. Zakharov, M. Vasiliu, D. A. Dixon, S.-Y. Liu, *Chem. Sci.* **2012**, *3*, 825–829; d) H. Braunschweig, C. Hörl, L. Mailänder, K. Radacki, J. Wahler, *Chem. Eur. J.* **2014**, *20*, 9858–9861; e) A. W. Baggett, M. Vasiliu, B. Li, D. A. Dixon, S.-Y. Liu, *J. Am. Chem. Soc.* **2015**, *137*, 5536–5541; f) M. Saif, J. R. Widom, S. Xu, E. R. Abbey, S.-Y. Liu, A. H. Marcus, *J. Phys. Chem. B* **2015**, *119*, 7985–7993; g) A. W. Baggett, F. Guo, B. Li, S.-Y. Liu, F. Jäkle, *Angew. Chem. Int. Ed.* **2015**, *54*, 11191–11195; *Angew. Chem.* **2015**, *127*, 11343–11347; h) C. J. Murphy, D. P. Miller, S. Simpson, A. Baggett, A. Pronschinske, M. L. Liriano, A. J. Therrien, A. Enders, S.-Y. Liu, E. Zurek, E. C. H. Sykes, *J. Phys.*

- Chem. C* **2016**, *120*, 6020–6030; i) M. Lepeltier, O. Lukoyanova, A. Jacobson, S. Jeeva, D. F. Perepichka, *Chem. Commun.* **2010**, *46*, 7007–7009.
- [11] M. J. S. Dewar, P. A. Marr, *J. Am. Chem. Soc.* **1962**, *84*, 3782–3782.
- [12] D. G. White, *J. Am. Chem. Soc.* **1963**, *85*, 3634–3636.
- [13] a) A. J. Ashe, X. Fang, *Org. Lett.* **2000**, *2*, 2089–2091; b) A. J. Ashe, X. Fang, X. Fang, J. W. Kampf, *Organometallics* **2001**, *20*, 5413–5418.
- [14] E. R. Abbey, A. N. Lamm, A. W. Baggett, L. N. Zakharov, S.-Y. Liu, *J. Am. Chem. Soc.* **2013**, *135*, 12908–12913.
- [15] a) H. Braunschweig, A. Gackstatter, T. Kupfer, T. Scheller, F. Hupp, A. Damme, N. Arnold, W. C. Ewing, *Chem. Sci.* **2015**, *6*, 3461–3465; b) H. Braunschweig, M. A. Celik, F. Hupp, I. Krummenacher, L. Mailänder, *Angew. Chem. Int. Ed.* **2015**, *54*, 6347–6351; *Angew. Chem.* **2015**, *127*, 6445–6449.
- [16] S. A. Brough, A. N. Lamm, S.-Y. Liu, H. F. Bettinger, *Angew. Chem. Int. Ed.* **2012**, *51*, 10880–10883; *Angew. Chem.* **2012**, *124*, 11038–11041.
- [17] a) H. F. Bettinger, O. Hauler, *Beilstein J. Org. Chem.* **2013**, *9*, 761–766; b) M.-D. Su, *Chem. Eur. J.* **2013**, *19*, 9663–9667; c) J. Kim, J. Moon, J. S. Lim, *ChemPhysChem* **2015**, *16*, 1670–1675.
- [18] a) Y. Inokuma, S. Yoshioka, J. Ariyoshi, T. Arai, Y. Hitora, K. Takada, S. Matsunaga, K. Rissanen, M. Fujita, *Nature* **2013**, *495*, 461–466; b) M. Hoshino, A. Khutia, H. Xing, Y. Inokuma, M. Fujita, *IUCrJ* **2016**, *3*, 139–151; c) G. W. Waldhart, N. P. Mankad, B. D. Santarsiero, *Org. Lett.* **2016**, *18*, 6112–6115.
- [19] K. Edel, S. A. Brough, A. N. Lamm, S.-Y. Liu, H. F. Bettinger, *Angew. Chem. Int. Ed.* **2015**, *54*, 7819–7822; *Angew. Chem.* **2015**, *127*, 7930–7933.
- [20] O. L. Chapman, C. L. McIntosh, J. Pacansky, *J. Am. Chem. Soc.* **1973**, *95*, 614–617.
- [21] a) Compound **8** crystallizes in the monoclinic space group $P2_1/c$ with two molecules in a unit cell. The alternate BN distances of 1.460 and 1.466 Å of the nearly planar rhombic ring with angles of 98.05(9)° at the boron atoms and 81.94(9)° at the nitrogen atoms are consistent with literature data; b) P. Paetzold, *Adv. Inorg. Chem.* **1987**, *31*, 123–170.
- [22] a) M. Haase, U. Klingebiel, *Angew. Chem. Int. Ed. Engl.* **1985**, *24*, 324–324; *Angew. Chem.* **1985**, *97*, 335–336; b) G. Elter, M. Neuhaus, A. Meller, D. Schmidt-Bäse, *J. Organomet. Chem.* **1990**, *381*, 299–313; c) H. Nöth, *Angew. Chem. Int. Ed. Engl.* **1988**, *27*, 1603–1623; *Angew. Chem.* **1988**, *100*, 1664–1684.
- [23] a) H. Braunschweig, A. Damme, J. O. C. Jimenez-Halla, B. Pfaffinger, K. Radacki, J. Wolf, *Angew. Chem. Int. Ed.* **2012**, *51*, 10034–10037; *Angew. Chem.* **2012**, *124*, 10177–10180; b) H. Braunschweig, K. Geetharani, J. O. C. Jimenez-Halla, M. Schäfer, *Angew. Chem. Int. Ed.* **2014**, *53*, 3500–3504; *Angew. Chem.* **2014**, *126*, 3568–3572.
- [24] N. N. Tyutyulkov, O. E. Polansky, J. Fabian, *Z. Naturforsch. A* **1975**, *30*, 1308–1310.
- [25] X.-W. An, Y.-D. Xie, *Thermochim. Acta* **1993**, *220*, 17–25.

Manuscript received: December 10, 2017

Accepted manuscript online: February 19, 2018

Version of record online: March 30, 2018



Supporting Information

The Dewar Isomer of 1,2-Dihydro-1,2-azaborinines: Isolation, Fragmentation, and Energy Storage

Klara Edel, Xinyu Yang, Jacob S. A. Ishibashi, Ashley N. Lamm, Cäcilia Maichle-Mössmer, Zachary X. Giustra, Shih-Yuan Liu, and Holger F. Bettinger**

[anie_201712683_sm_miscellaneous_information.pdf](#)

Table of Contents

1. Methods	S2-5
2. Synthesis	S6-7
3. NMR spectroscopic data and comparison with computational results	S8-9
4. NMR spectra	S10-16
5. Results of Matrix Isolation Study	S17-26
6. Results of Computational Chemistry Investigation	S27-29
7. Cartesian Coordinates of Optimized Structures	S30-37
8. Catalyzed Cycloreversion Reactions	S38-39
9. Summary of crystallographic data for compound 8	S40
10. References	S41

1. Methods

General. Precursors **1**, **3** and **5** were synthesized according to Liu et al.^[1] All experiments were performed under anhydrous conditions using argon as protective gas or in a glove box. Dry solvents were collected from a commercially available solvent purification system. All NMR spectra (except for those that were used in the kinetic study) were recorded on Bruker Avance III HD 400 spectrometer. The NMR spectra were measured at room temperature in deuterated cyclohexane (*c*-C₆D₁₂) (Deutero GmbH) and deuterated dichloromethane (CD₂Cl₂) (Sigma Aldrich). The solvents were dried over molecular sieve (4 Å) and degassed by three freeze-pump-thaw cycles prior to photoreactions. The spectra were referenced to residual solvent signals (¹H, ¹³C: SiMe₄)^[2] and externally (¹¹B: BF₃·OEt₂). Electron impact ionization mass spectrometry (EI-MS) was measured on an MSD 5977 (Agilent MSD), and high resolution mass spectrometry (EI-HRMS) was measured on a MAT95 (Finnigan MAT). UV-Vis spectra were measured on a Perkin Elmer Lambda 1050. Elemental analyses were performed on a HEKAtch Euro 3000 CHN analyzer. Irradiation was achieved with a low-pressure mercury lamp (UVP, 253.7 nm) and an Osram HBO-500-W/2 high pressure mercury lamp in an Oriel housing with quartz optics and a dichroic mirror (280 – 400 nm). Chromatography was done using silica gel (Machery-Nagel, 60 M, 0.04-0.063 mm).

Kinetic study. The kinetic constants were measured for T = 373, 370, 367, 364, 361 and 358 K using NMR spectroscopy (Bruker Avance III HDX 400). For each temperature three experiments were performed. A solution of **4** (15-20 mg) in 3.5-4 mL deuterated 1,1,2,2-tetrachloroethane (C₂D₂Cl₄) that was purchased from Deutero GmbH (dried over molecular sieve (4 Å) and degassed by three freeze-pump-thaw cycles) was placed in a J. Young quartz tube. The sample was allowed to reach the desired temperature. Every 3 min (373-361 K) or every 5 min (358 K) a ¹H NMR spectrum was recorded (16 scans; total t = 126 s) for at least 3 half-life periods. For determining the rate constants the integrals of the signals at 4.75 and 3.00 ppm were determined. The residual proton signal of the solvent was taken as a reference.

Table 1. Rate constants for the reaction **4** → **3** in C₂D₂Cl₄.

T [K]	k [s ⁻¹]
373	0.0004662
370	0.0003543
367	0.0002527
364	0.0001865
361	0.0001388
358	0.0001023

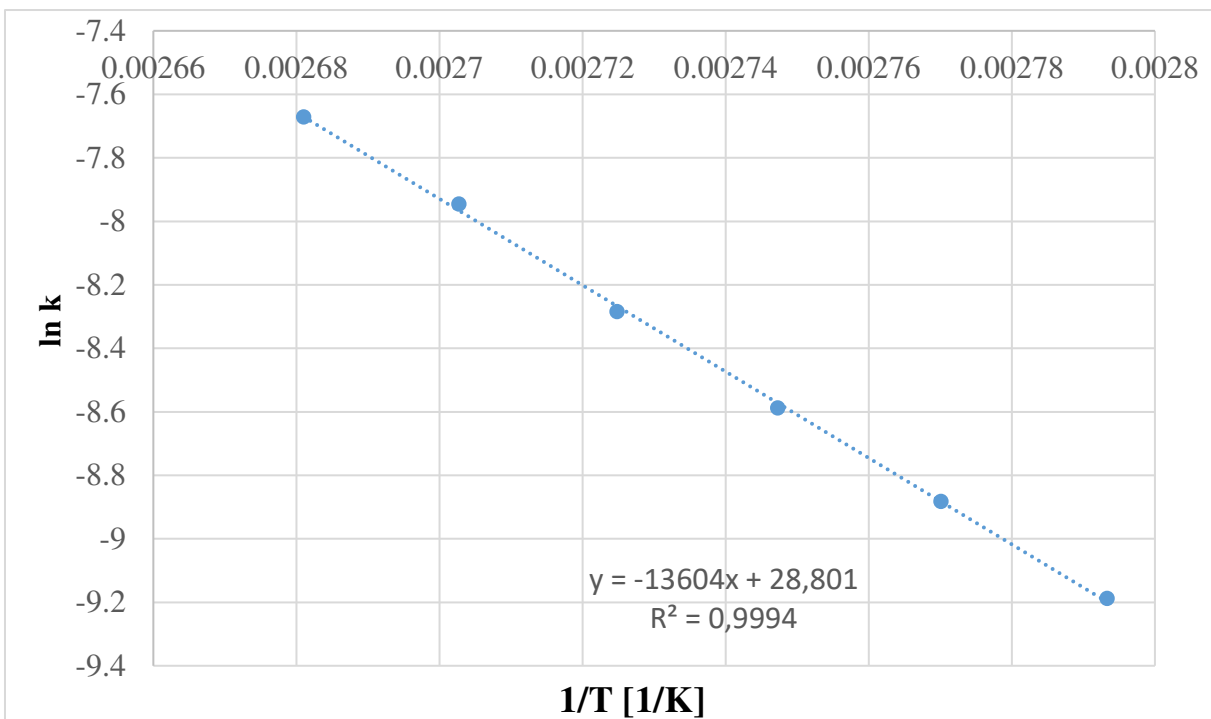


Figure S1. Arrhenius plot for the first order kinetic reaction **4** → **3**.

Quantum yield measurements. As light source for irradiation a VARIAN Cary Eclipse fluorescence spectrometer was used. Absorbance was measured using a PERKIN-ELMER Lambda 9 UV/VIS/NIR Spectrophotometer. As reference ferrioxalate actinometry^[3] was taken. A solution of **3** in dry *n*-hexane was irradiated with 284 nm, and every 30 s the absorbance was measured until a 5% conversion to **4** was achieved. The absorbance at 284 nm was plotted vs. time. An example is shown in Figure S2.

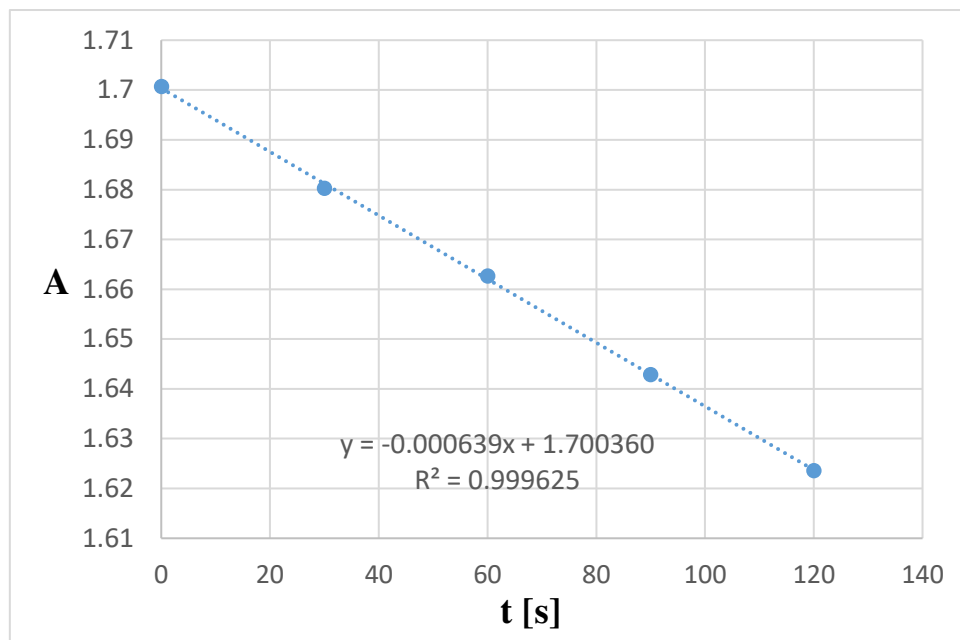


Figure S2. Example of a plot absorbance vs. time for the quantum yield determination of the photoreaction **3** → **4**.

Following equation^[4] was used to calculate the quantum yield of the photoisomerization **3** → **4**:

$$\Phi = \frac{m \cdot V}{q_{n,p} \cdot \epsilon(284 \text{ nm}) \cdot l}$$

Φ: quantum yield

m: slope of the fitting curve

V: volume of the irradiated sample

q_{n,p}: photon flux, amount basis

ε(284 nm): extinction coefficient of **3** at 284 nm

l: optical path length of the irradiation cell

Matrix experiments. Matrix experiments were performed by standard techniques^[5] using a SHI CKW-21A displex closed-cycle helium cryostat (IR) and a CTI Cryogenics 8200 compressor (Brooks Automation) (UV). Compound **1** and **5** were sublimed from a glass flask at -80 °C and at room temperature respectively, and were condensed onto a cold CsI (IR) or sapphire (UV) window with a large excess of argon 6.0 (Westfalen AG), or neon 5.0 (Westfalen AG), which were dosed to 2.0 sccm by a mass flow controller (MKS mass flow PR400B). The deposition temperature was 30 K in the experiments with argon and 4 K in the experiments with neon.

FTIR spectra were measured between 4000 and 400 cm⁻¹ on a Bruker V70 spectrometer using a resolution of 0.5 cm⁻¹. UV-Vis spectra were measured on a Perkin Elmer Lambda 1050.

Electronic Structure Computations. All geometries were optimized and harmonic vibrational frequencies, nuclear magnetic shielding tensors using the GIAO method^[6] and nuclear spin-spin coupling constants^[7] were computed with Becke's^[8] hybrid functional in conjunction with the correlation functional of Lee, Yang, and Parr^[9] as implemented^[10] in Gaussian 09^[11] and the 6-311+G**^[12] basis set (B3LYP/6-311+G**). Chemical shifts were determined with reference to the experimental chemical shifts of tetramethylsilane (¹H, 0.0 ppm and ¹³C, 0.0 ppm) and of **3** (¹¹B, 40.3 ppm) for mesityl **5** (¹¹B, 35.7 ppm) for chloro derivatives.

X-Ray Crystallography. Compound **8**: Crystals suitable for X-ray crystallography were grown by standard techniques from solutions using *n*-pentane at -20°C. Single crystals were selected, coated with Parabar 10312 (previously known as Paratone N, Hampton Research) and fixed on a microloop.

Data were collected on a Bruker APEX DUO instrument equipped with an I μ S microfocus sealed tube and QUAZAR optics for MoK α radiation ($\lambda = 0.71073 \text{ \AA}$). The data collection strategy was determined using COSMO^[13] employing ω - and ϕ scans. Raw data were processed using APEX^[14] and SAINT,^[15] corrections for absorption effects were applied using SADABS.^[16]

The structure was solved by direct methods and refined against all data by full-matrix least-squares methods on F² using SHELXTL^[17] and Shelxle.^[18]

2. Synthesis

Dewar isomer of 1,2-dihydro-1-tert-butyldimethylsilyl-2-mesityl-1,2-azaborinine 4. A solution of **3** (20 mg, 0.064 mmol) in 0.5 mL dry *c*-C₆D₁₂ was irradiated in J. Young quartz tube with 280-400 nm light for 4 hours at room temperature. The photoreaction was followed by ¹H and ¹¹B NMR. After the solvent was removed a colorless oil was obtained.

¹H NMR (400 MHz, *c*-C₆D₁₂): δ 6.63 (s, 2 H), 6.49 (t, ³J_{HH} = 2.3 Hz, 1H), 6.32 (d, ³J_{HH} = 2.3 Hz, 1H), 4.75 (t, ³J_{HH} = 2.2 Hz, 1 H), 3.00 (d, ³J_{HH} = 2.1 Hz, 1 H), 2.18 (s, 3 H), 2.16 (s, 6 H), 0.90 (s, 9 H), -0.07 (s, 3 H), -0.12 (s, 3 H). ¹³C{¹H} NMR (400 MHz, *c*-C₆D₁₂): δ 143.9, 139.6, 138.2, 137.1, 127.4, 64.1, 44 (br.), 26.8, 22.6, 21.4, 18.8, -5.3, -5.6. ¹¹B{¹H} NMR (400 MHz, *c*-C₆D₁₂): δ 52.9. EI-HRMS found: 311.22127, calc. for C₁₉H₃₀NSiB (M⁺): 311.224058. EA found: C, 72.99; N, 4.45; H, 9.78; calc. for C₁₉H₃₀NSiB C, 73.30; N, 4.50; H, 9.71.

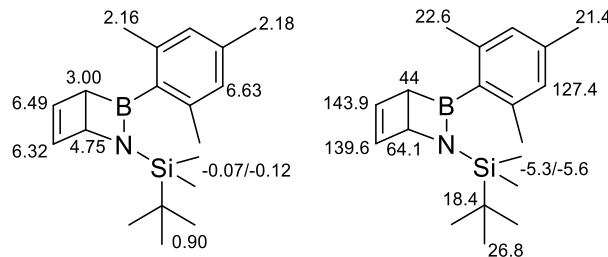


Figure S3. Assignments to **4** of ¹H (left) and ¹³C signals (right) based on HSQC.

Dewar isomer of 1,2-dihydro-1-tert-butyldimethylsilyl-2-chloro-1,2-azaborinine 6. A solution of **5** (25 mg, 0.11 mmol) in 0.5 mL dry *c*-C₆D₁₂ was irradiated in J. Young quartz tube with 280-400 nm light for 16 hours at room temperature. The photoreaction was followed by ¹H and ¹¹B NMR.

¹H NMR (400 MHz, *c*-C₆D₁₂): δ 6.43 (t, ³J_{HH} = 2.4 Hz, 1 H), 6.19 (d, ³J_{HH} = 2.3 Hz, 1 H), 4.47 (t, ³J_{HH} = 2.3 Hz, 1 H), 2.89 (s, 1 H), 0.93 (s, 9 H), 0.17 (s, 3 H), 0.13 (s, 3 H). ¹³C{¹H} NMR (400 MHz, *c*-C₆D₁₂): δ 143.0, 140.0, 60.5, 43 (br.), 26.8, 18.8, -5.2, -5.7. ¹¹B{¹H} NMR (400 MHz, *c*-C₆D₁₂): δ 42.4.

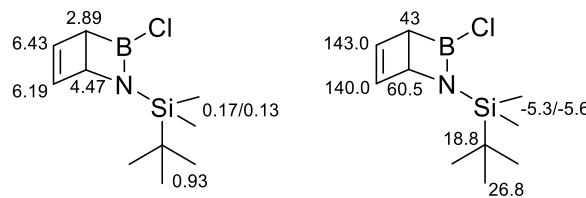


Figure S4. Assignments to **6** of ¹H (left) and ¹³C signals (right) based on HSQC.

1,3-Di-tert-butyldimethylsilyl-2,4-dimesityl-1,3-diaza-2,4-diboretidine **8**. A solution of **4** (100 mg, 0.32 mmol) in 7 mL dry *c*-C₆D₁₂ was irradiated in four NMR quartz tubes with 254 nm light for 17 hours at room temperature. The photoreaction was followed by ¹H and ¹¹B NMR. After removing the solvent the residues were combined and purified by column chromatography (silica, *n*-hexane, R_f = 0.47). Compound **8** was obtained as a colorless solid (30 mg, 0.058 mmol, 36 %).

¹H NMR (400 MHz, CD₂Cl₂): δ 6.81 (s, 2 H), 2.42 (s, 6 H), 2.28 (s, 3 H), 0.67 (s, 9 H), -0.30 (s, 6 H). ¹³C{¹H} NMR (400 MHz, *c*-C₆D₁₂): δ 138.2, 138.1, 127.3, 26.5, 23.0, 21.4, 18.3, -4.0. ¹¹B{¹H} NMR (400 MHz, *c*-C₆D₁₂): δ 46.8. EI-HRMS found: 517.37975, calc. for C₃₀H₅₁N₂Si₂B₂ (M-1⁺): 517.377690. EA found: C, 69.21; N, 5.18; H, 10.13; calc. for C₃₀H₅₂N₂Si₂B₂ C, 69.49; N, 5.40; H, 10.11. UV/Vis (hexane, nm): 277, 265, 260.

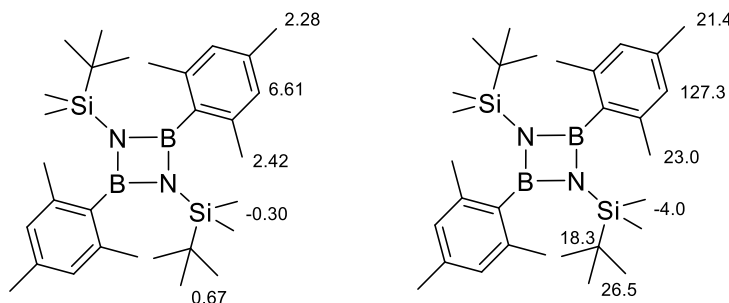
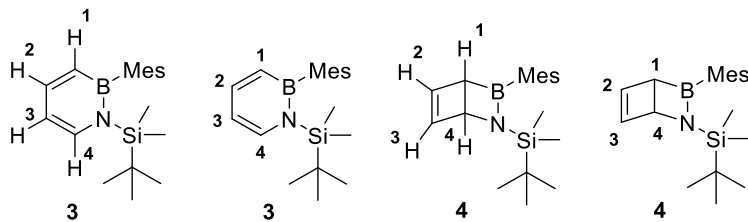


Figure S5. Assignments to **8** of ¹H (left) and ¹³C signals (right) based on HSQC.

NMR signals of N-tert-butyldimethylsilyl-B-mesityl-iminoborane **9**. The compound is a transient intermediate that could not be isolated. Due to low concentration a ¹³C NMR spectrum could not be recorded. In the ¹H spectrum (400 MHz, *c*-C₆D₁₂) of the mixture signals are detected at 6.76 (s), 0.97 (s), 0.10 (s) that decrease while signals at 2.42 (s), 2.26 (s) overlap with signals of the dimer **8**. Integration is precluded due to overlap with signals of precursor and products. ¹¹B{¹H} NMR (400 MHz, *c*-C₆D₁₂): δ 17.4.

3. NMR spectroscopic data and comparison with computational results

Table S2. Experimental (400 MHz, *c*-C₆D₁₂) and computed (B3LYP/6-311+G**) ¹H and ¹³C NMR shifts of **3** and **4**. The computed spectra were referenced to SiMe₄ (B3LYP/6-311+G**). The computed ¹¹B downfield shift of **4** compared to **3** is 13.0 ppm (B3LYP/6-311+G**).

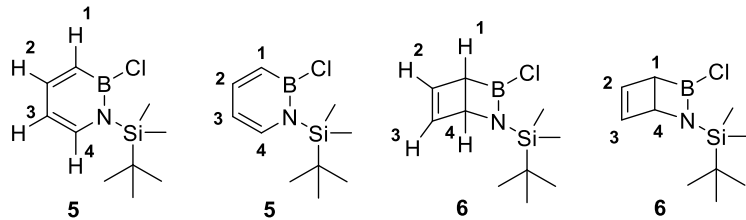


Assignment	3		4	
	δ_{exp} [ppm]	δ_{theor} [ppm]	δ_{exp} [ppm]	δ_{theor} [ppm]
B	40.3		52.9	53.3
H¹	6.56	6.85	3.00	3.16
H²	7.45	7.90	6.49	7.05
H³	6.27	6.59	6.32	6.84
H⁴	7.37	7.62	4.75	4.84
C¹	133 (br.)	138.36	44 (br.)	47.52
C²	143.0	149.97	143.9	154.13
C³	112.2	116.97	139.6	148.12
C⁴	138.2	147.24	64.1	67.45

Table S3. Computed total nuclear spin-spin coupling constants of **3** and **4** (B3LYP/6-311+G**).

	3	4
	J [Hz]	J [Hz]
H ¹ -H ⁴	0.73	2.54
H ² -H ⁴	0.95	1.64
H ³ -H ⁴	8.09	0.03
H ¹ -H ²	12.16	1.14
H ¹ -H ³	1.24	0.72
H ² -H ³	7.32	2.65

Table S4. Experimental (400 MHz, *c*-C₆D₁₂) and computed (B3LYP/6-311+G**) ¹H- and ¹³C-NMR shifts of **5** and **6**. The computed spectra were referenced to SiMe₄ (B3LYP/6-311+G**) for ¹H and ¹³C. The computed ¹¹B downfield shift of **6** compared to **5** is 7.3 ppm (B3LYP/6-311+G**).



Assignment	5		6	
	δ_{exp} [ppm]	δ_{theor} [ppm]	δ_{exp} [ppm]	δ_{theor} [ppm]
B	35.7		42.4	43.0
H¹	6.59	6.96	2.89	2.98
H²	7.39	7.73	6.43	6.93
H³	6.17	6.45	6.19	6.60
H⁴	7.14	7.46	4.47	4.52
C¹	130 (br.)	135.84	43 (br.)	47.31
C²	145.0	151.18	143.0	153.00
C³	111.9	117.07	140.0	148.21
C⁴	138.1	146.38	60.5	64.15

Table S5. Computed (B3LYP/6-311+G**) total nuclear spin-spin coupling constants of **5** and **6**.

	5	6
	J [Hz]	J [Hz]
H ¹ -H ⁴	0.63	2.73
H ² -H ⁴	1.12	1.71
H ³ -H ⁴	8.08	0.05
H ¹ -H ²	12.42	1.35
H ¹ -H ³	1.13	0.83
H ² -H ³	7.32	2.69

4. NMR Spectra

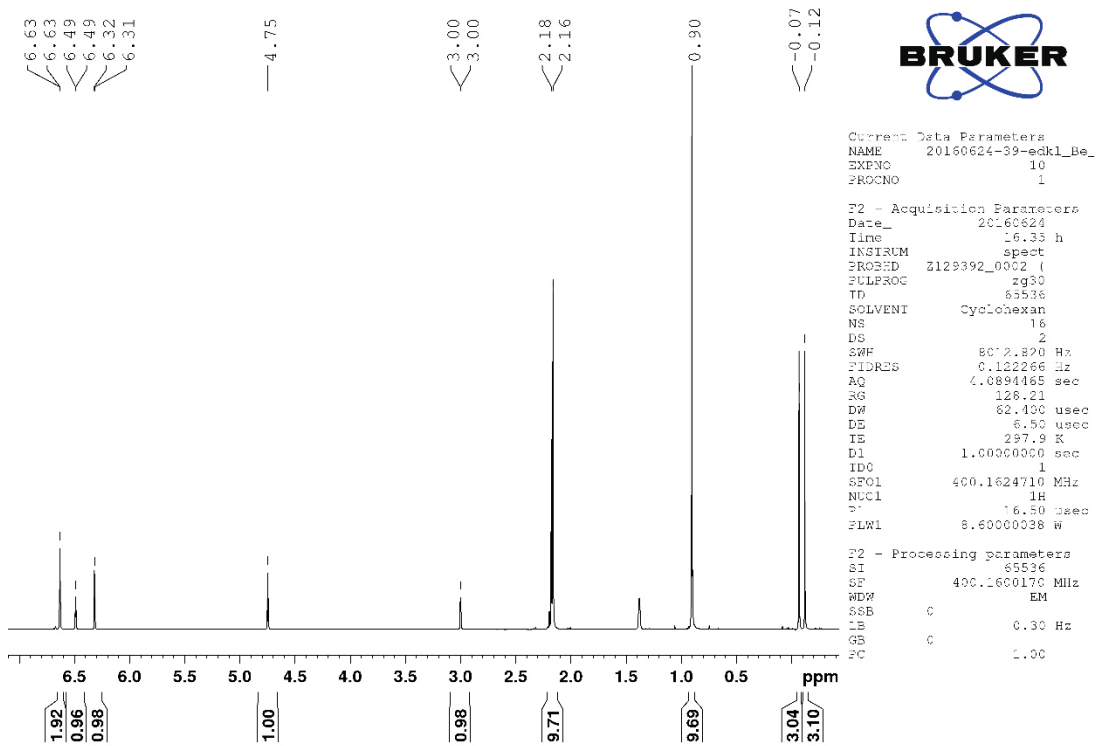


Figure S6. ^1H NMR (400 MHz, $c\text{-C}_6\text{D}_{12}$) spectrum of **4**.

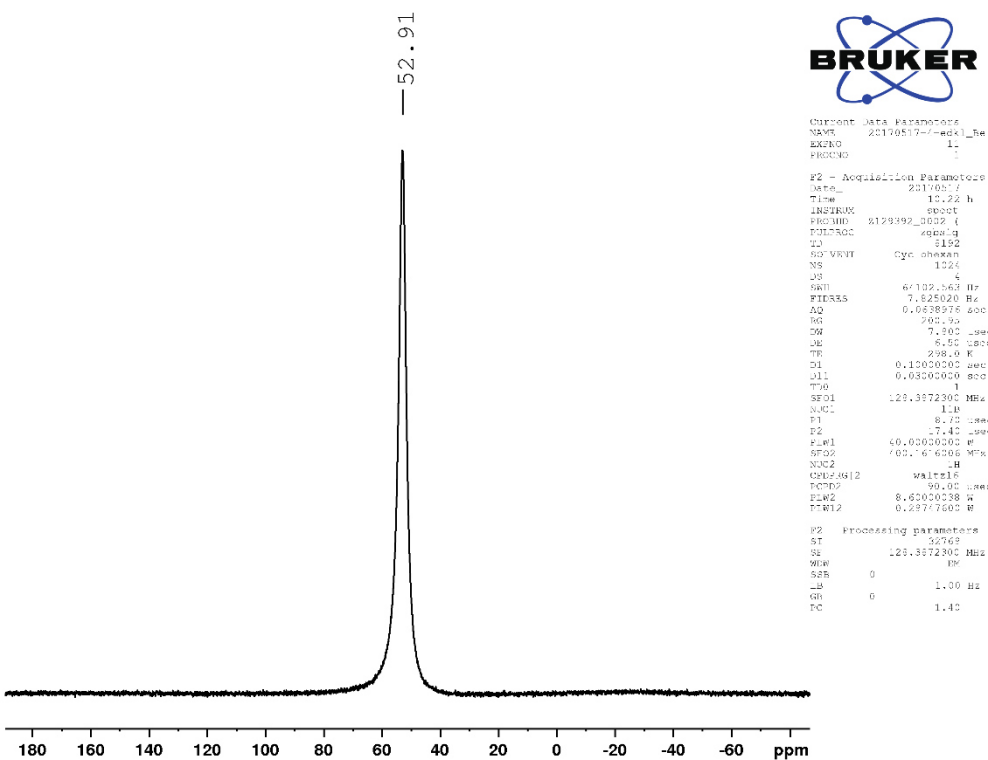


Figure S7. $^{11}\text{B}\{\text{H}\}$ NMR (400 MHz, *c*-C₆D₁₂) spectrum of **4**.

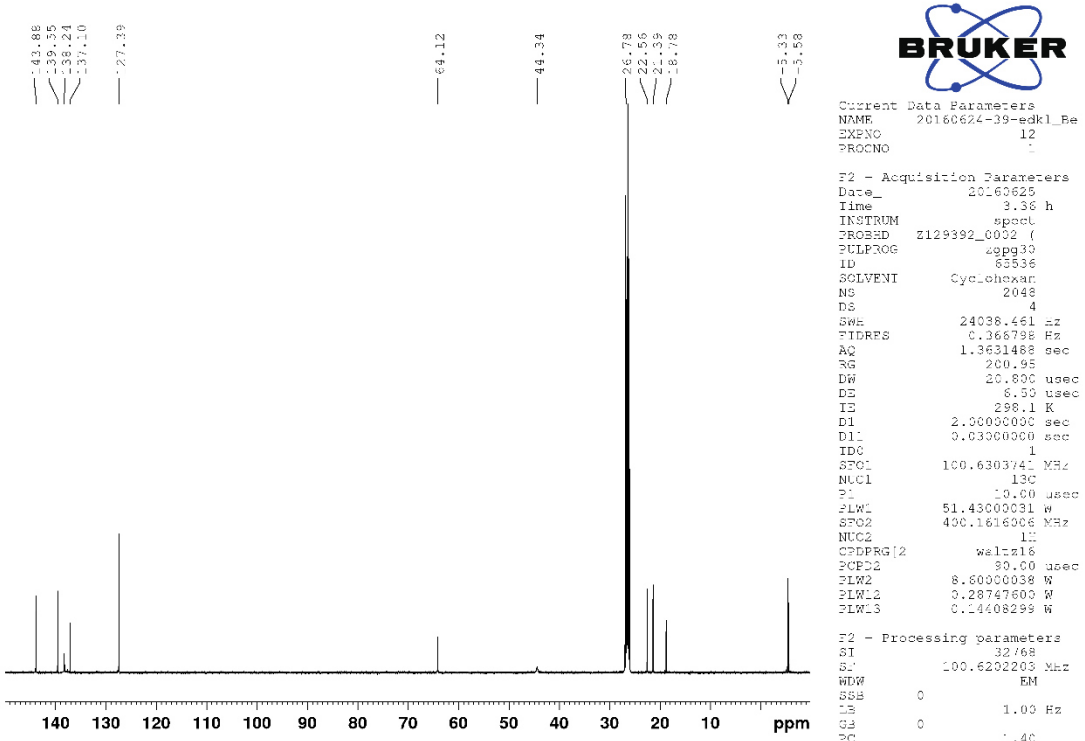


Figure S8. $^{13}\text{C}\{\text{H}\}$ NMR (400 MHz, *c*-C₆D₁₂) spectrum of **4**.

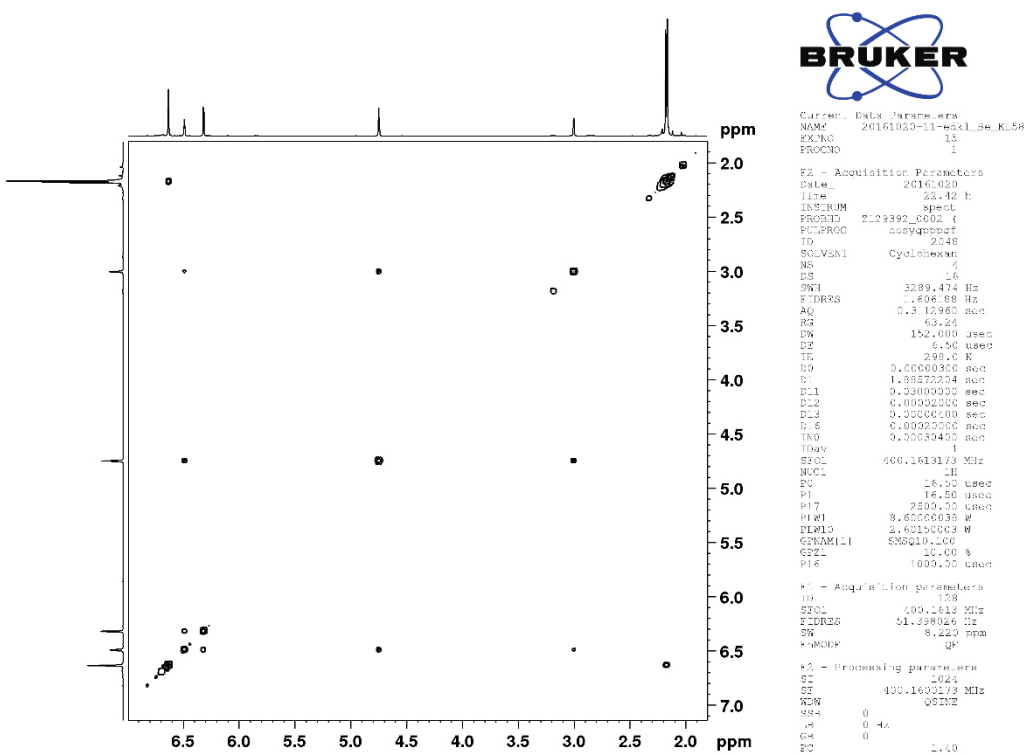


Figure S9. $^1\text{H},^1\text{H}$ -COSY NMR (400 MHz, *c*-C₆D₁₂) spectrum of **4**.

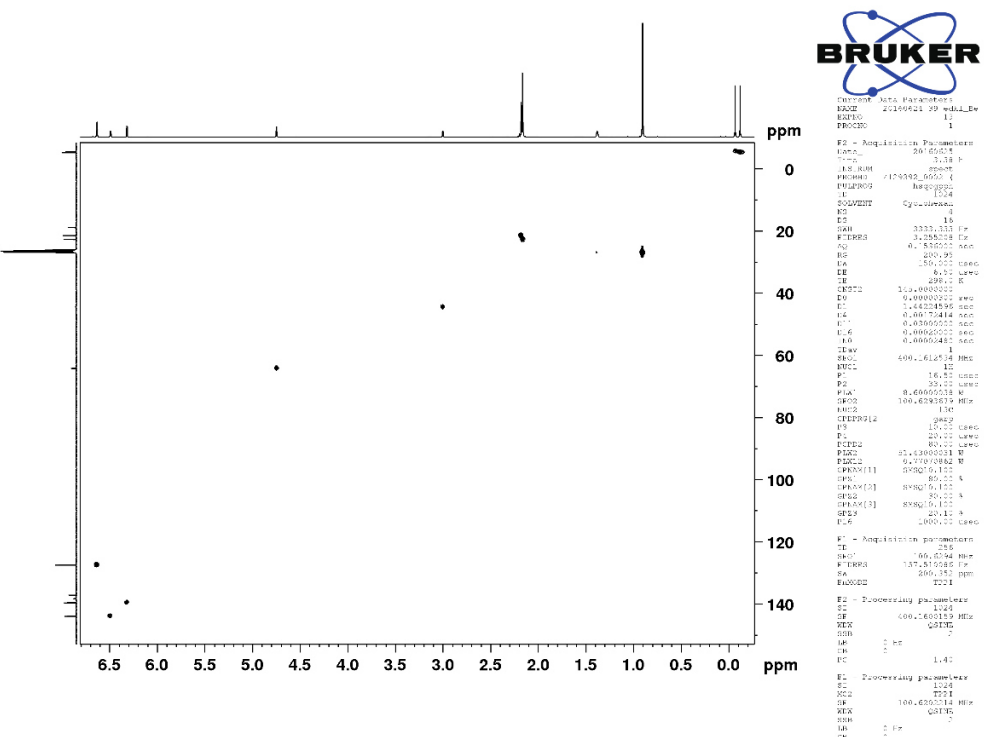


Figure S10. $^1\text{H},^{13}\text{C}$ -HSQC NMR (400 MHz, *c*-C₆D₁₂) spectrum of **4**.

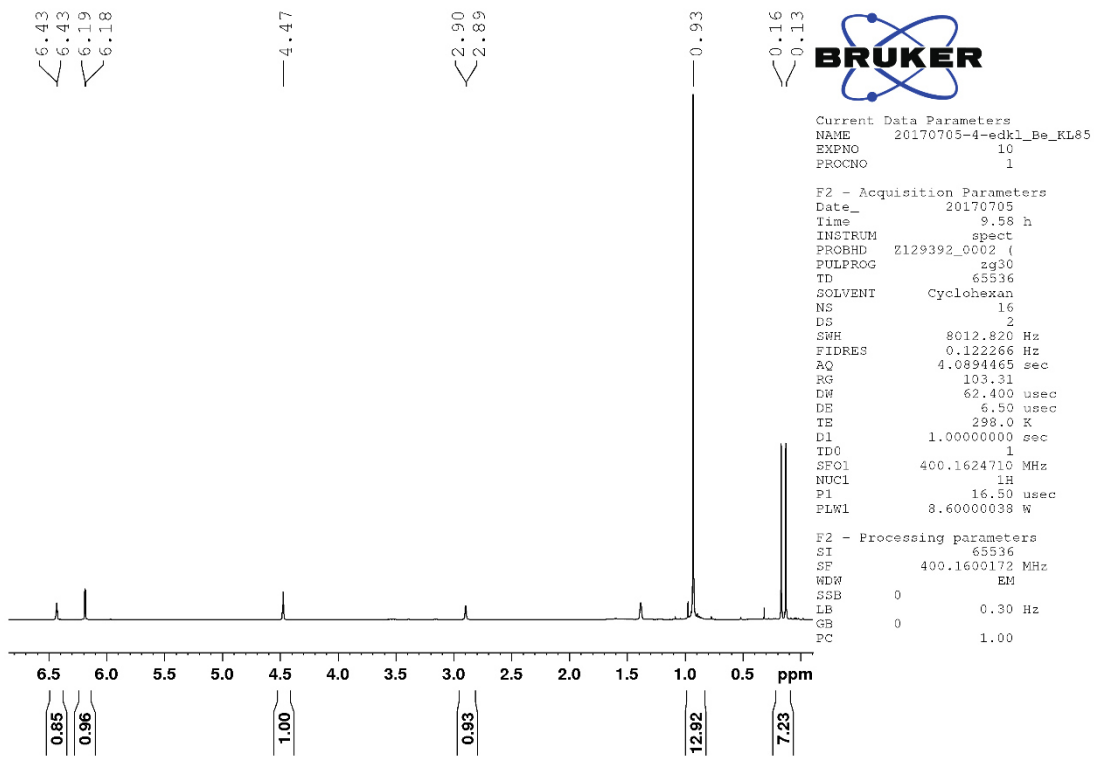


Figure S11. ^1H NMR (400 MHz, *c*-C₆D₁₂) spectrum of **6**.

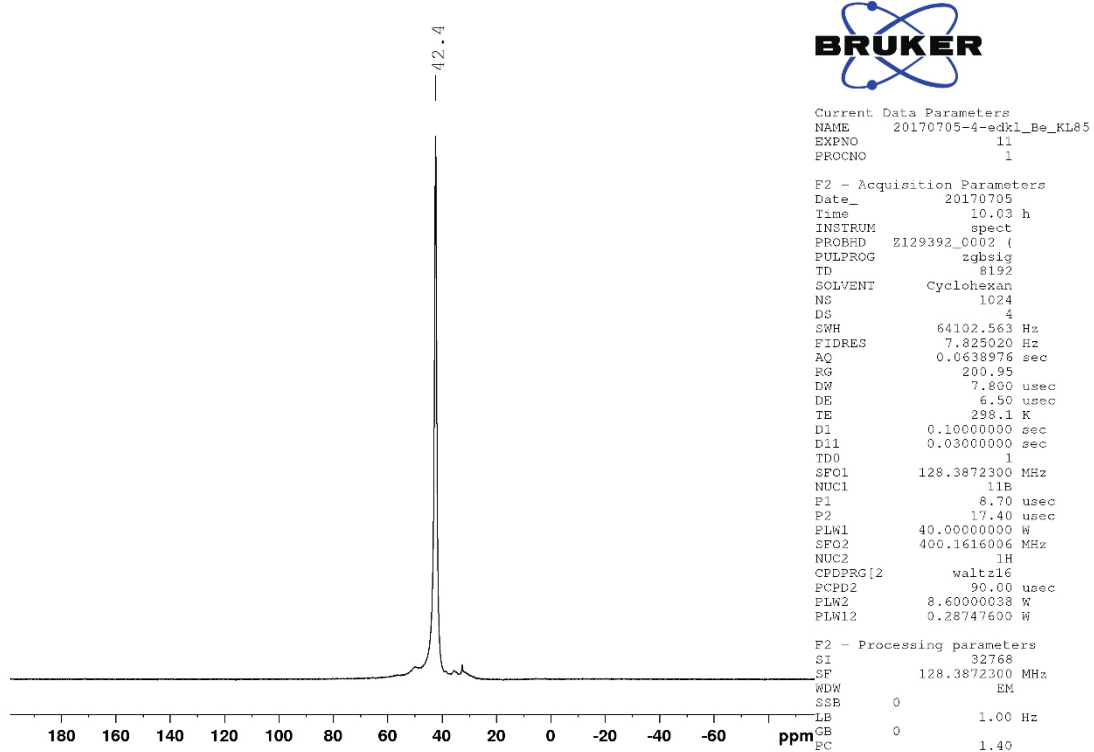


Figure S12. $^{11}\text{B}\{^1\text{H}\}$ NMR (400 MHz, *c*-C₆D₁₂) spectrum of **6**.

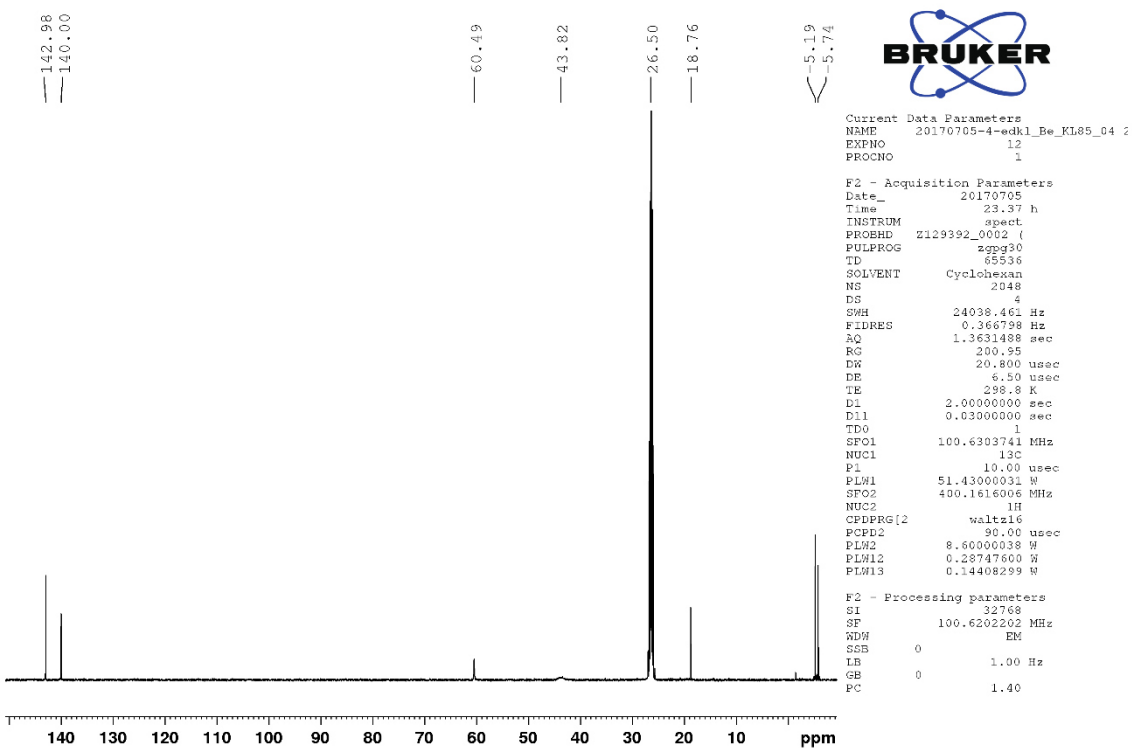


Figure S13. $^{13}\text{C}\{^1\text{H}\}$ NMR (400 MHz, *c*-C₆D₁₂) spectrum of **6**.

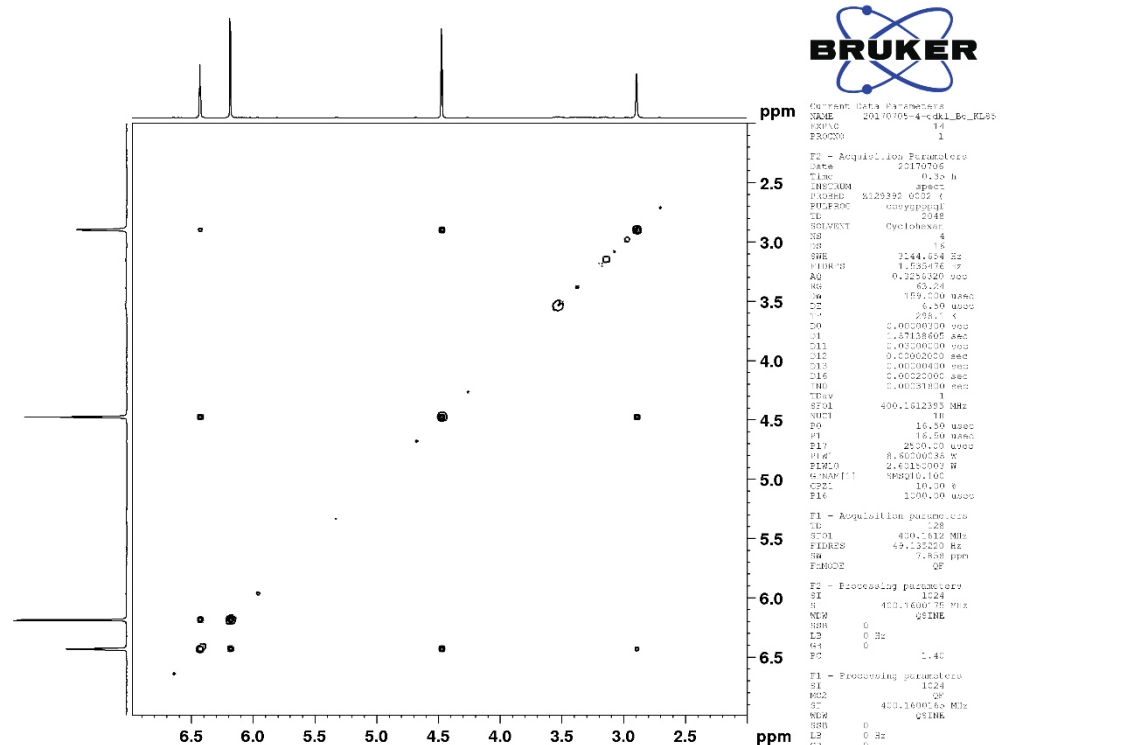


Figure S14. $^1\text{H},^1\text{H}$ -COSY NMR (400 MHz, *c*-C₆D₁₂) spectrum of **6**.

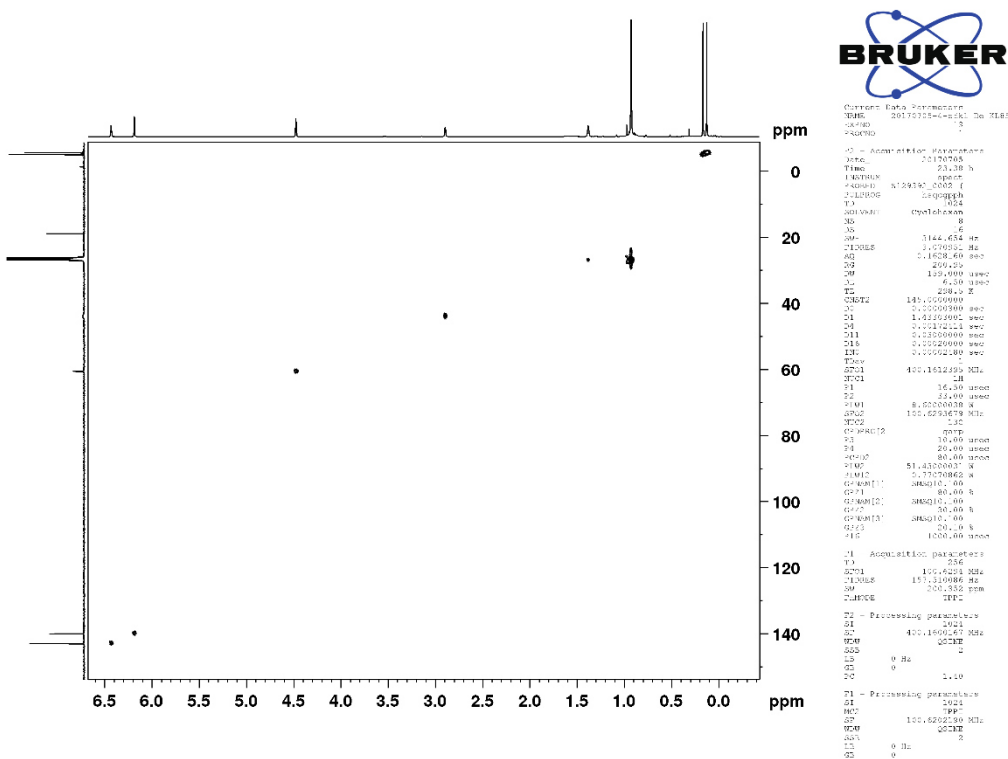


Figure S15. $^1\text{H}, ^{13}\text{C}$ -HSQC NMR (400 MHz, *c*-C₆D₁₂) spectrum of **6**.

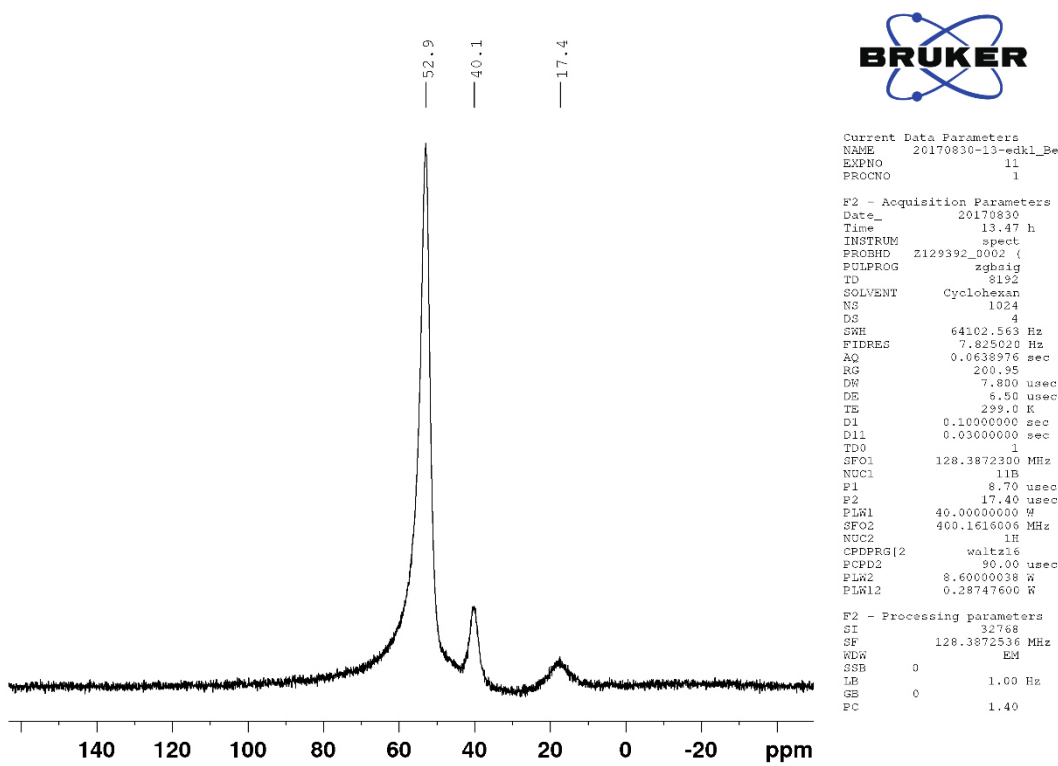


Figure S16. $^{11}\text{B}\{\text{H}\}$ NMR (400 MHz, *c*-C₆D₁₂) spectrum after photolysis of **4** with UV light (254 nm) indicating the formation of **9** by the signal at 17.4 ppm. The signal at 53 ppm belongs to **4** and the signal at 40 ppm belongs to **3**.

5. Results of Matrix Isolation Study

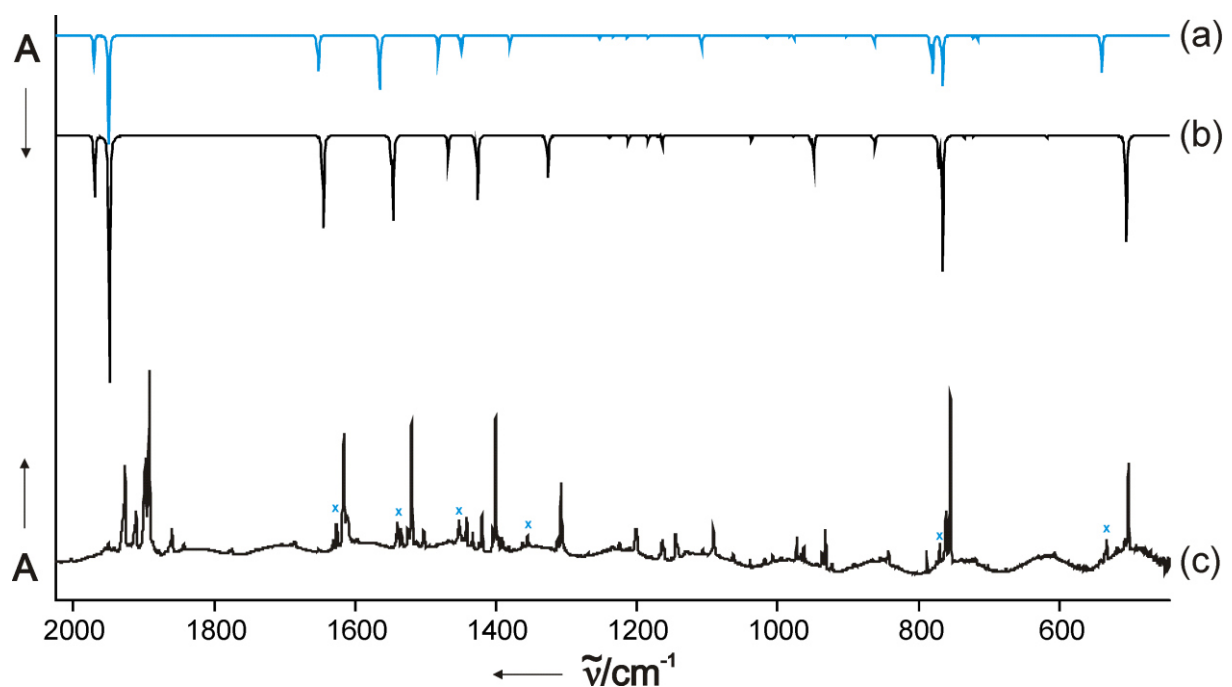


Figure S17. 1,2-Dideuterio-1,2-azaborinine. Computed (B3LYP/6-311+G**) IR spectra of 1-hydro-2-deuterio-1,2-azaborinine (trace a) and of 1,2-dideuterio-1,2-azaborinine (trace b) compared with the observed IR spectrum (Ne, 4 K, trace c) of 1,2-dideuterio-1,2-azaborinine. Signals that belong to 1-hydro-2-deuterio-1,2-azaborinine are marked (**x**).

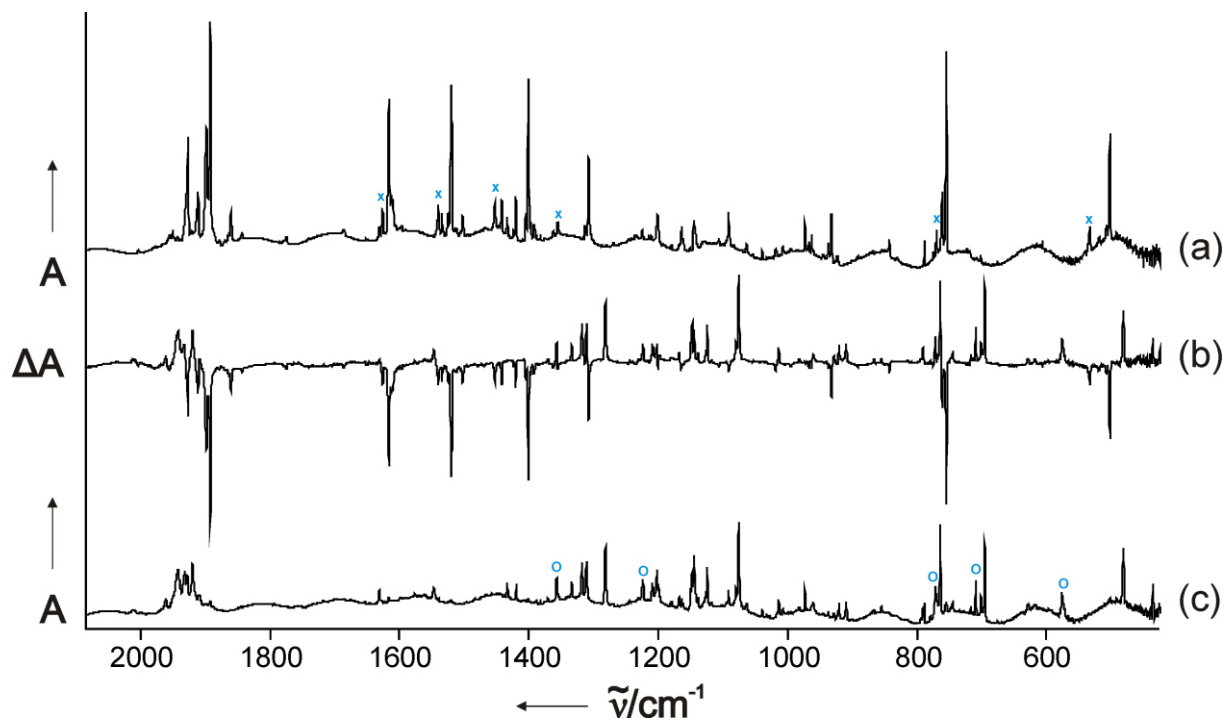


Figure S18. Observed IR spectra (Ne, 4 K) a) before and c) after irradiation (60 min, $\lambda = 254 \text{ nm}$) of 1,2-dideutero-1,2-azaborinine; b) difference spectrum: bands pointing downwards disappear and bands pointing upwards appear during irradiation. Signals that belong to 1-hydro-2-deutero-1,2-azaborinine (**x**) and its Dewar valence isomer (**o**) are marked.

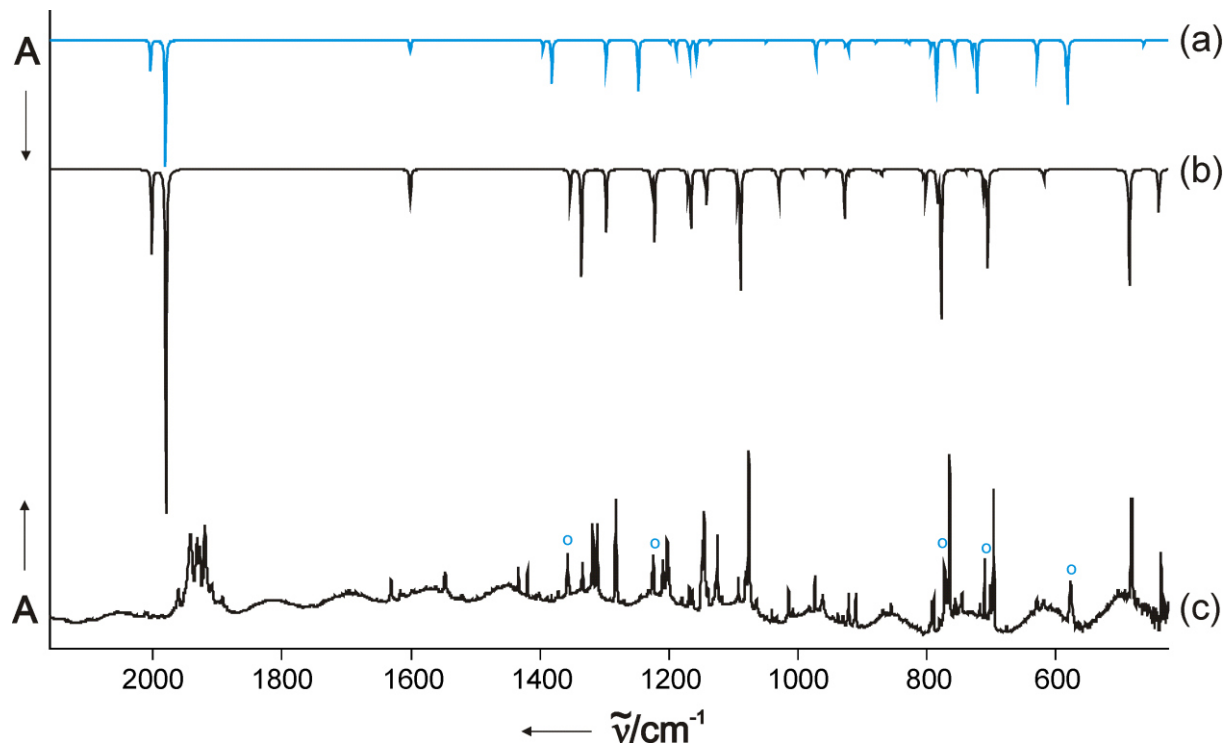


Figure S19. Dewar valence isomer of 1,2-Dideuterio-1,2-azaborinine. Computed (B3LYP/6-311+G**) IR spectra of the Dewar valence isomers of 1-hydro-2-deuterio-1,2-azaborinine (trace a) and of 1,2-dideuterio-1,2-azaborinine (trace b) compared with the observed IR spectrum after irradiation (60 min 254 nm, Ne, 4 K, trace c) of 1,2-dideuterio-1,2-azaborinine. Signals that belong to the Dewar valence isomer of 1-hydro-2-deuterio-1,2-azaborinine are marked (○).

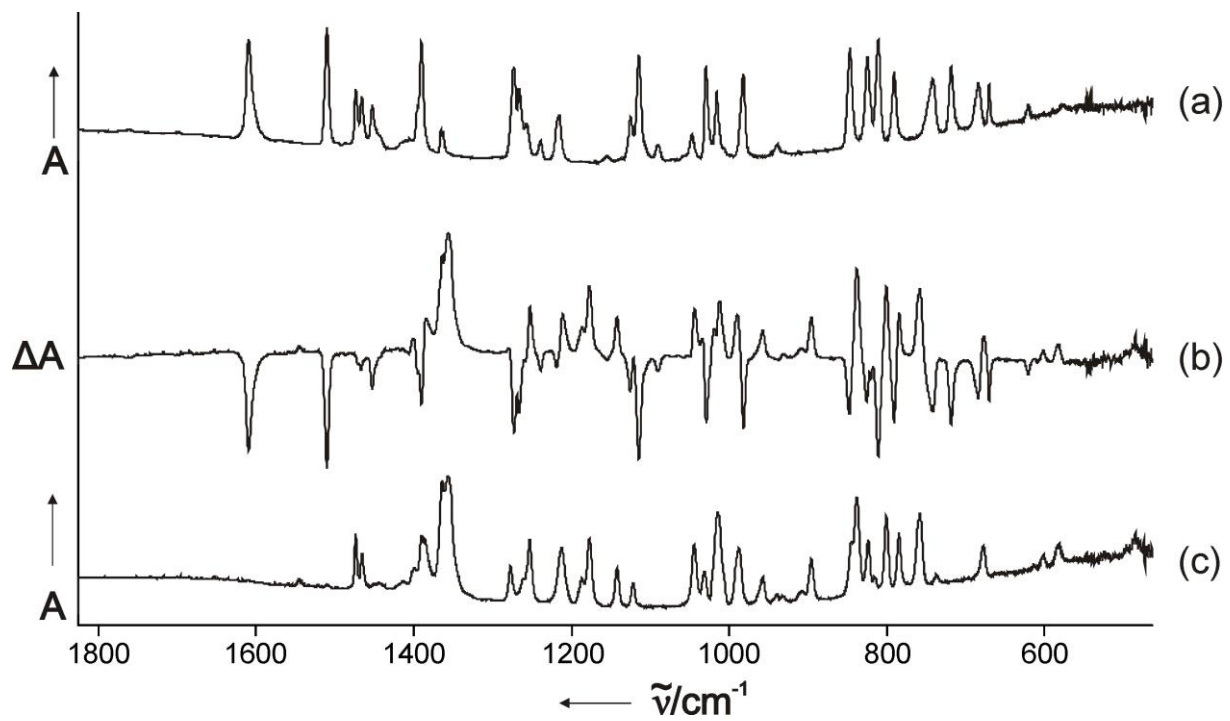


Figure S20. Observed IR spectra (Ar, 4 K) a) before and c) after irradiation (260 min, $\lambda = 280$ -400 nm) of **5**; b) difference spectrum: bands pointing downwards disappear and bands pointing upwards appear during irradiation. The bands at 1473.8 and 1466.2 cm^{-1} are probably due to an unknown contamination.

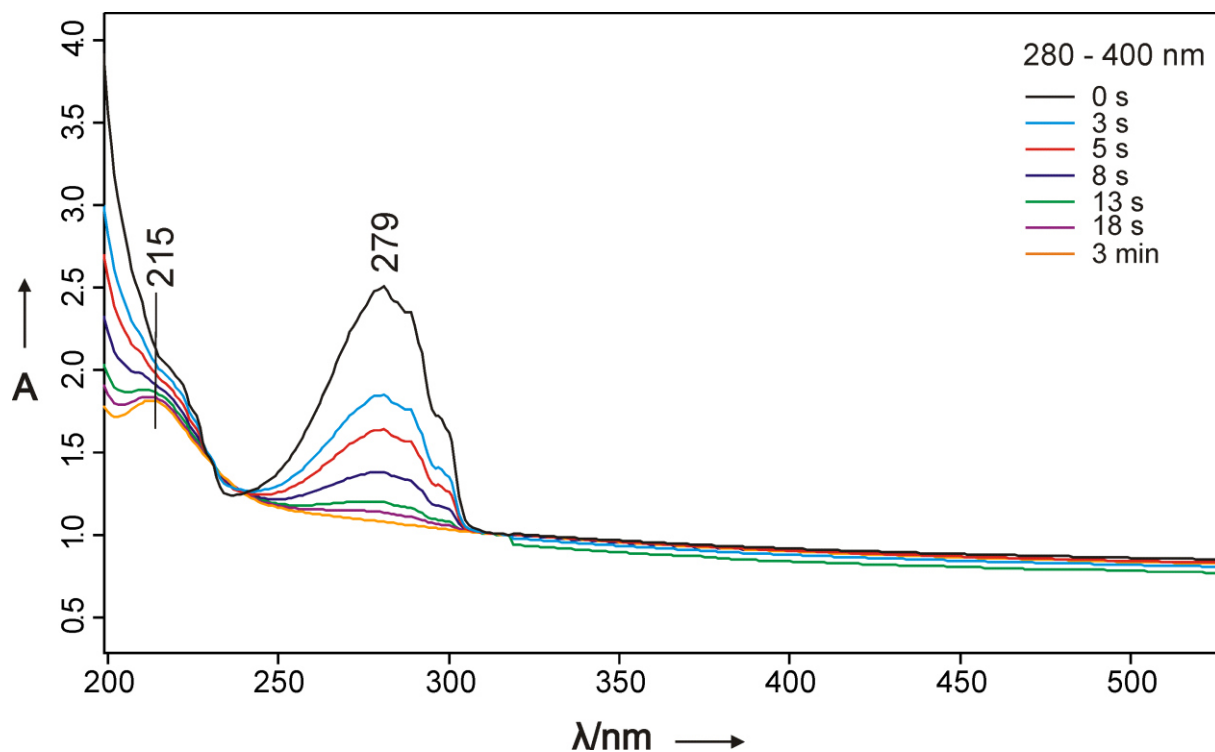


Figure S21. Observed UV/vis spectrum (Ar, 7 K) of **5** (black trace) and UV/vis spectra after irradiation with $\lambda = 280\text{-}400\text{ nm}$. After full conversion to **6** a band at 215 nm is observed.

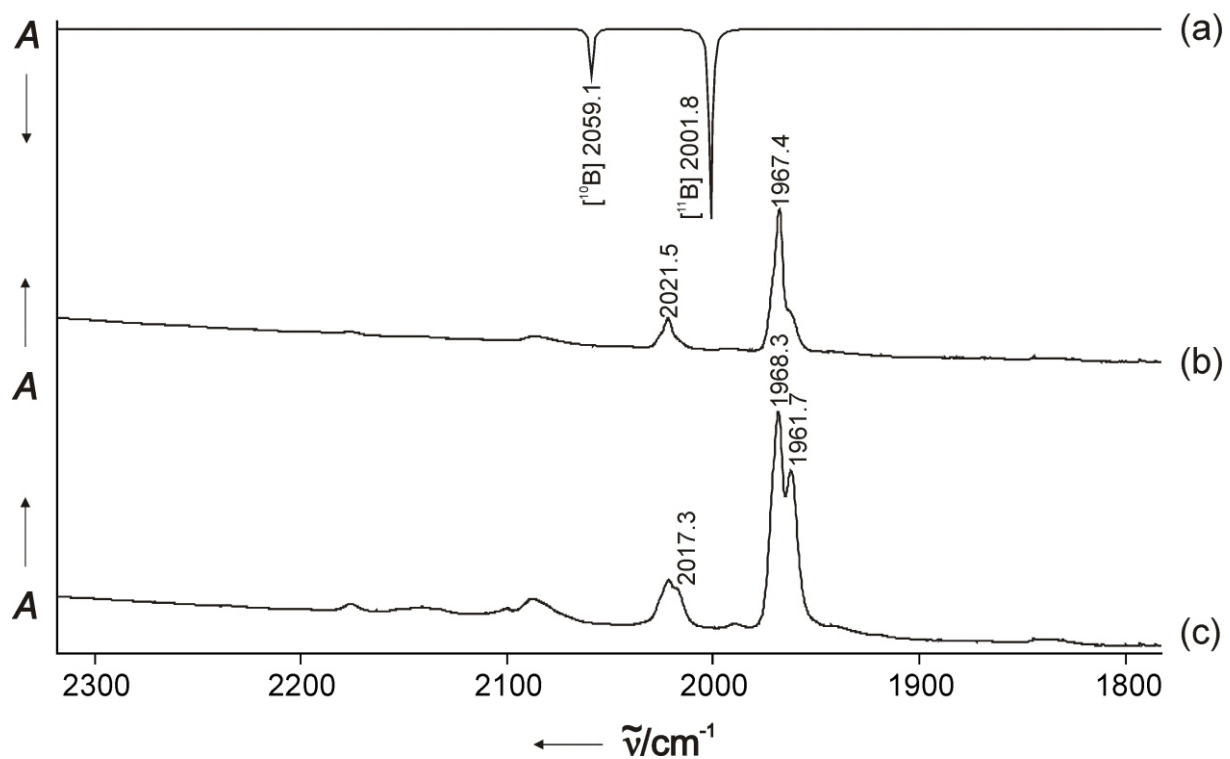


Figure S22. Computed (B3LYP/6-311+G**) IR spectrum (a) and observed (Ne, 4 K) and IR spectra of **7** after 3.5 hours (b) and 27 hours (c) of irradiation of **5** with 254 nm. The relative intensities of ^{11}B and ^{10}B are 4.5:1 in (b) and 4.4:1 in (c).

Table S6. Experimental and computed (B3LYP/6-311+G**) vibrational frequencies of 1,2-dihydro-1,2-azaborinine^[19] (**1a**) and of 1,2-dideutero-1,2-azaborinine (**1b**), computed intensities (in km mol⁻¹), and the corresponding isotopic shifts.

1a	1b		1a		1b			
ν_{exp} [cm ⁻¹]	ν_{exp} [cm ⁻¹]	$\Delta \nu_{\text{exp}}$ [cm ⁻¹]	ω_{theor} [cm ⁻¹]	Intensity	ω_{theor} [cm ⁻¹]	Intensity	$\Delta \omega_{\text{theor}}$ [cm ⁻¹]	Assignment
3046.3- 3008.2	3046.3- 2982.4		3201.5- 3131.2		3201.5- 3131.2			v(CH)
3463.1	2564.1	899	3604.8	35.9	2640.9	25.4	963.9	v(N-H,D)
2547.8- 2527.0	1926.8- 1892.4	621- 634	2620.9	181.8	1949.5	136.7	671.4	v(B-H,D)
1622.3	1616.1	6.2	1652.8	48.1	1645.5	48.9	7.3	v(CC)
1543.4			1572.0	84.5	1549.7	45.8		v(¹⁰ BN)
1540.1	1520.1	20.0	1569.0	84.0	1546.7	46.5	22.3	v(¹¹ BN)
1453.6, 1460.7			1486.8	32.2				δ (in-plane)
1430.3	1400.1	30.2	1459.5	21.3	1426.5	34.69	33.0	δ (in-plane)
	1307.7				1326.4	23.0		δ (in-plane) v(BN)
903.4			924.4	49.3				δ (out-of- plane) ¹⁰ B
897.4			914.6	47.8				δ (out-of- plane) ¹¹ B
816.7			830.5	21.2				δ (out-of- plane)
	754.8				766.1	74.7		δ (out-of- plane)
709.2			722.9	35.5				δ (out-of- plane)
574.2	502.2	72.0	584.4	67.5	505.6	52.6	78.8	δ (out-of- plane)

Table S7. Experimental and computed (B3LYP/6-311+G**) vibrational frequencies of Dewar valence isomer of 1,2-dihydro-1,2-azaborinine^[19] (**2a**) and of 1,2-dideutero-1,2-azaborinine (**2b**), computed intensities (in km mol⁻¹), and the corresponding isotopic shifts.

2a	2b		2a		2b			
ν_{exp} [cm ⁻¹]	ν_{exp} [cm ⁻¹]	$\Delta \nu_{\text{exp}}$ [cm ⁻¹]	ω_{theor} [cm ⁻¹]	Intensity	ω_{theor} [cm ⁻¹]	Intensity	$\Delta \omega_{\text{theor}}$ [cm ⁻¹]	Assignment
3117.8- 2958.5	3117.8- 2958.5		3199.3- 3086.0		3199.3- 3086.0			v(CH)
3482.2	2585.0	897.2	3618.2	16.6	2655.7	15.3	962.5	v(N-H,D)
2602.3- 2566.5	1913.2- 1948.0	618.5- 689.1	2653.4[¹¹ B] 2666.4[¹⁰ B]	177.8	1980.3[¹¹ B] 2002.8[¹⁰ B]	129.0 137.3	673.1 663.6	v(B-H,D)
		1546.7			1601.6	9.49		v(CC)
1392.8	1333.7	59.1	1417.4	61.2	1353.7	43.4	63.7	v(¹⁰ BN)
1374.5	1318.0; 1310.8	56.5; 63.7	1398.5	58.2	1335.3	40.5	63.2	v(¹¹ BN)
1283.6	1281.9	1.7	1298.0	23.0	1297.5	18.8	0.5	δ (in-plane)
1229.8	1075.6		1253.5	61.9	1088.4	45.0		v(CN) δ (ring) [¹¹ B]
1179.7	1202.3	-22.6	1201.5	16.6	1222.9	27.0	-21.4	δ (ring)
	1126.8		1179.3	18.0	1144.6	18.3	34.7	δ (ring) [¹⁰ B]
1161.0	1124.3	36.7	1175.2	20.7	1141.4	12.8	33.8	δ (ring) [¹¹ B]
1143.7	1144.7	-1	1164.2	13.4	1165.5	19.9	-1.3	δ (out-of-plane)
	1080.3				1093.3	44.9		v(CN) δ (ring) [¹⁰ B]
1039.3	1014.0	25.3	1055.2	1.2	1029.7	10.0	25.5	δ (out-of-plane)
	920.7; 909.6		924.3	13.6	927.7	16.4	-3.4	δ (ring)
	790.5				801.5	9.1		δ (out-of-plane)
753.0	769.4	-16.4	767.1	73.6	783.3	48.7	-16.2	δ (CH, ¹⁰ BH)
747.6	764.2	-16.6	762.3	82.8	777.1	55.7	-14.8	δ (CH, ¹¹ BH)
	701.1		730.9	21.8	711.5	40.8	19.4	δ (CH, ¹⁰ BH)
716.6	695.6	21.0	723.9	13.1	705.3	36.8	18.6	δ (CH, ¹¹ BH)
582.7	481.2	101.5	589.9	90.5	485.6	39.1	104.3	δ (NH,D)
468.3	435.7	32.6	472.2	4.5	439.4	12.9	32.8	δ (ND)

Table S8. Experimental vibrational frequencies of **5** in a neon and in an argon matrix.

Neon		Argon	
v _{exp} [cm ⁻¹]	rel. Intensity	v _{exp} [cm ⁻¹]	rel. Intensity
3090.7, 3081.2, 3054.8, 3046.8, 3042.3, 3004.7, 2971.0, 2948.7, 2939.6, 2907.4, 2888.9, 2871.0	2.91	3073.7, 3043.8, 3001.3, 2969.7, 2964.6, 2956.4, 2946.9, 2941.2, 2936.5, 2865.8	2.88
1614.1	1.00	1611.8	1.00
1512.7	0.67	1510.6	0.66
1476.7, 1469.4	0.62	1474.4, 1466.5, 1453.3	0.58
1398.9, 1393.5	0.64	1396.2, 1390.8	0.60
1369.2, 1365.8	0.09	1366.0, 1362.7	0.07
1280.1, 1275.4, 1269.6, 1260.0	1.16	1274.5, 1267.0, 1258.1	1.09
1240.4	0.07	1238.3	0.08
1216.9	0.36	1214.6	0.31
1130.1, 1127.0, 1118.1, 1114.8	1.20	1125.4, 1114.6	1.04
1090.1	0.08	1088.2	0.06
1049.4	0.09	1047.2	0.12
1031.2	0.53	1029.7	0.45
1017.9	0.27	1015.4	0.23
982.9	0.56	980.8	0.56
848.8	0.61	846.5	0.65
826.2, 812.5	1.53	825.7, 823.7, 810.0	1.48
791.5	0.39	790.8	0.37
741.0	0.38	740.9, 739.0	0.41
720.5	0.36	719.0	0.39
688.2, 684.9	0.24	689.5, 686.5, 681.6	0.26
671.5	0.06	670.2	0.07
621.6	0.03	620.7	0.03
573.6	0.03	575.7	0.03
438.7	0.15	435.3	0.20
419.9	0.05	419.5	0.05

Table S9. Experimental vibrational frequencies of the Dewar isomer of **6** in a neon and in an argon matrix.

Neon		Argon
$\nu_{\text{exp}} [\text{cm}^{-1}]$	rel. Intensity	$\nu_{\text{exp}} [\text{cm}^{-1}]$
3119.2	0.02	3113.1
3062.5, 3051.3	0.06	3046.8, 3044.7
2964.4, 2938.5, 2914.8, 2906.9, 2893.2, 2869.3	1.22	2962.2, 2953.4, 2939.3, 2905.9, 2888.3, 2869.1
1477.2, 1469.2	0.16	1473.8, 1466.2
1393.2, 1389.2	0.23	1383.0
1366.8, 1364.8, 1358.0	1.00	1363.3, 1352.9
1280.2, 1255.7	0.33	1278.5, 1261.2, 1253.1
1213.5	0.22	1216.0
1190.1, 1180.0	0.24	1192.1, 1182.7
1144.0	0.08	1145.0
1124.2	0.03	1122.9
1046.2	0.19	1046.3
1036.2	0.04	1038.6
1018.9, 1007.6	0.46	1022.2, 1017.7
990.1	0.17	991.1
958.8	0.06	958.1
897.3	0.08	899.6, 896.1
846.6, 841.1	0.41	846.6, 838.7
824.4	0.12	822.9
802.1	0.16	801.0
786.0	0.13	784.1
758.8	0.22	
679.0	0.07	675.4
		600.8
584.3	0.06	582.5
		496.0

6. Results of Computational Chemistry Investigation

Table S10. Absolute energies (in a.u.) and relative energies including zero point vibrational energy corrections and relative Gibbs free energies (in kcal/mol) computed at the B3LYP/6-31G* level of theory and comparison with CCSD(T)/cc-pVQZ//CCSD(T)/TZ2P (ZPVE were obtained at CCSD(T)/DZP).

	E_{\min} [a.u.]	ΔE_{ZPVE} [kcal/mol]	ΔG [kcal/mol]	$\Delta E_{\text{ZPVE}}^{\text{a}}$ [kcal/mol]
1	-235.74590	-64.4	-64.4	-59.3
TS min→1	-235.60918	18.2	18.1	19.1
min	-235.61432	15.5	15.3	17.8
TS 2→min	-235.60874	18.8	18.8	22.2
2	-235.64030	0	0	0
3	-1111.54627	-51.9	-50.9	
TS 4→3	-1111.41677	26.1	26.7	
4	-1111.46071	0	0	
5	-1222.13191	-54.3	-53.5	
TS 6→5	-1221.99400	28.8	29.3	
6	-1222.04272	0	0	

^a Data taken from Reference [20]

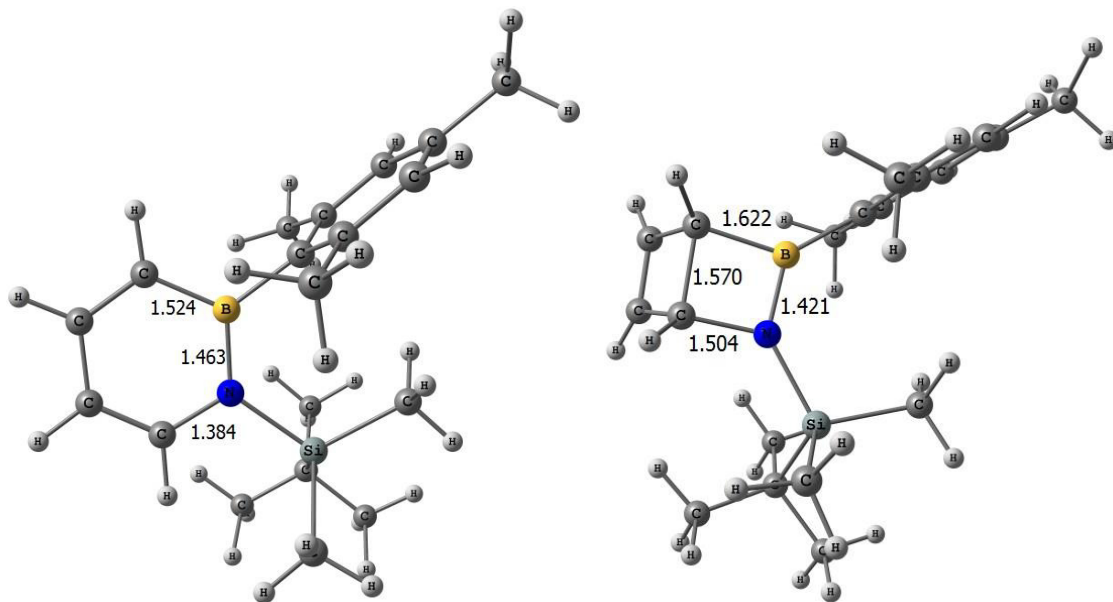


Figure S23. Geometry of **3** (left) and **4** (right) computed at the B3LYP/6-311+G** level of theory. Bond lengths are given in angstroms (\AA).

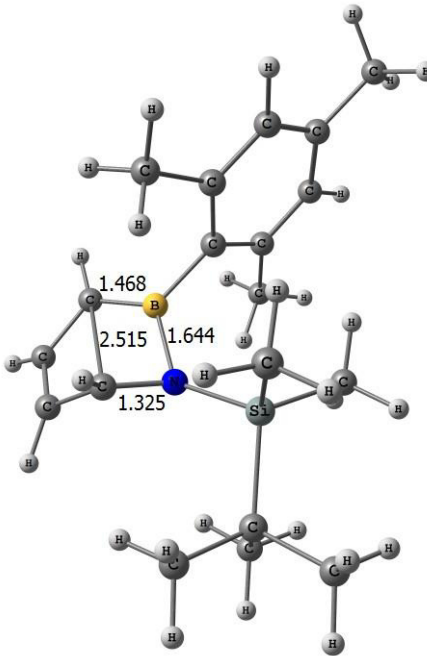


Figure S24. Geometry of **TS 4→3** computed at the B3LYP/6-311+G** level of theory. Bond lengths are given in angstroms (\AA).

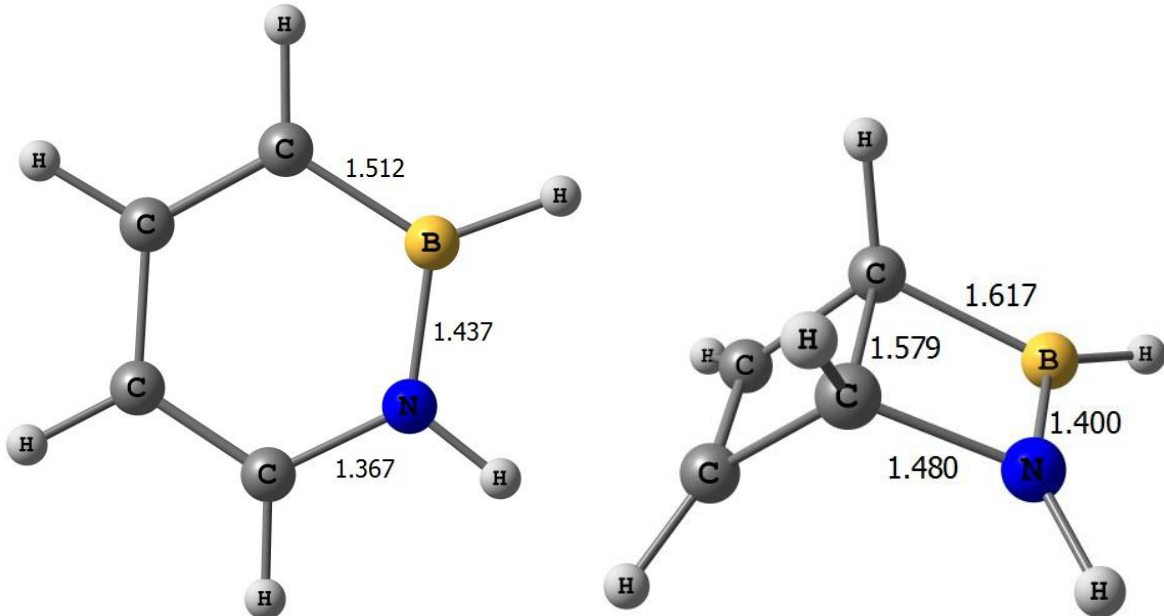


Figure S25. Geometry of **1** (left) and **2** (right) computed at the B3LYP/6-311+G** level of theory. Bond lengths are given in angstroms (\AA).

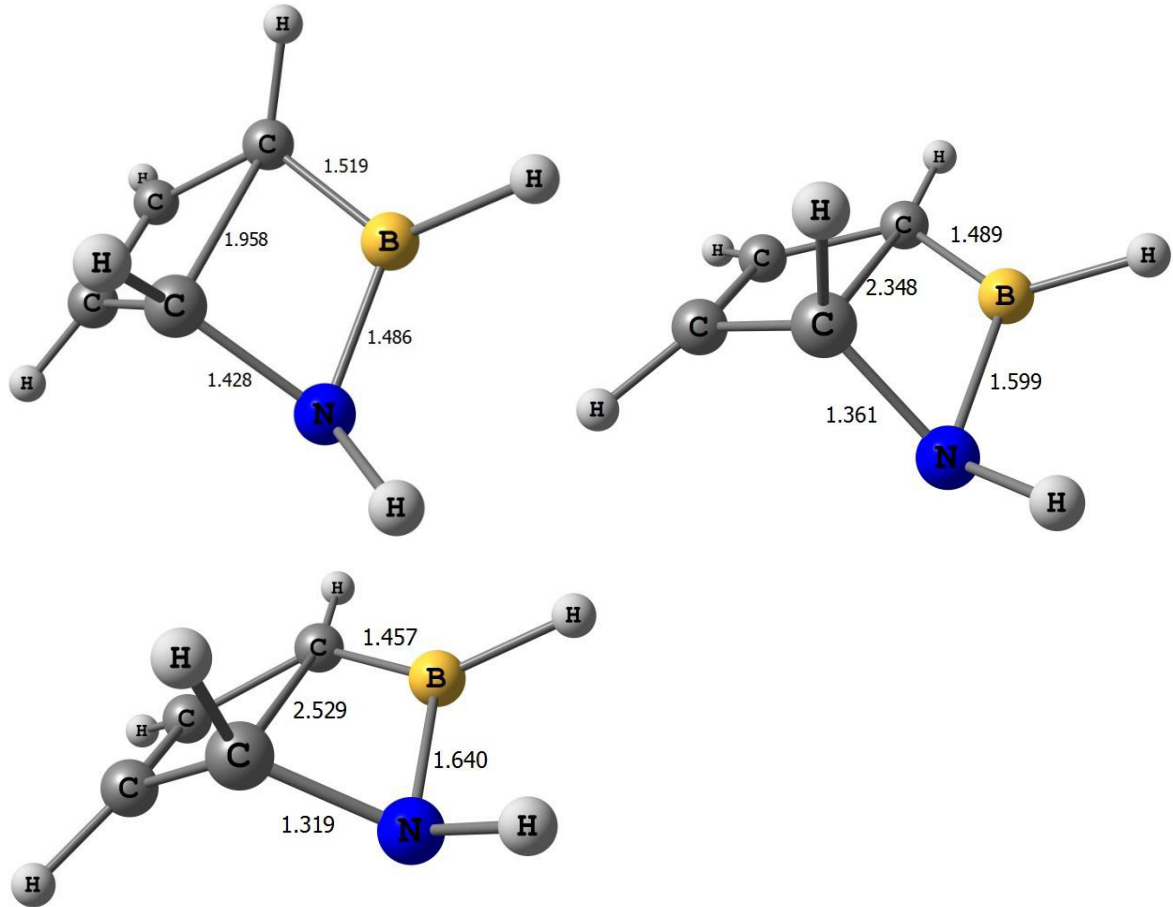


Figure S26. Geometry of TS 2 \rightarrow min (left top), min (right) and TS min \rightarrow 1 (left bottom) (see Table S10) computed at the B3LYP/6-311+G** level of theory. Bond lengths are given in angstroms (\AA).

7. Cartesian Coordinates of Optimized Structures

B3LYP/6-311+G**, in Ångstrom

Compound 1

12			
6	-0.050385000	-1.473777000	0.000000000
6	-1.208972000	-0.732899000	0.000000000
6	-1.189687000	0.689954000	0.000000000
6	0.000000000	1.361460000	0.000000000
7	1.185211000	0.680966000	0.000000000
5	1.278539000	-0.753307000	0.000000000
1	-0.135933000	-2.556229000	0.000000000
1	0.050781000	2.443956000	0.000000000
1	-2.113703000	1.253773000	0.000000000
1	-2.180796000	-1.221292000	0.000000000
1	2.019278000	1.251254000	0.000000000
1	2.365461000	-1.240119000	0.000000000

Compound 2

12			
6	-1.368989000	0.579606000	-0.281142000
6	-0.093743000	0.881754000	0.497288000
6	-1.225209000	-0.752825000	-0.260512000
1	-0.173056000	1.466623000	1.414299000
1	-1.764931000	-1.575576000	-0.713598000
5	1.292405000	0.796013000	-0.330326000
6	0.061803000	-0.688668000	0.553955000
1	0.119975000	-1.222720000	1.503362000
7	1.330107000	-0.597435000	-0.203333000
1	-2.100995000	1.238739000	-0.734348000
1	1.856652000	-1.366986000	-0.588767000
1	2.046406000	1.542702000	-0.863521000

Compound 3

52			
6	-2.106172000	1.908540000	0.206275000
6	0.333910000	2.848352000	-0.788093000
5	0.244228000	1.421294000	-0.261346000
7	-1.073117000	0.987159000	0.205027000
1	-3.056869000	1.574302000	0.603149000
1	1.267797000	3.247685000	-1.175066000
14	-1.593587000	-0.668425000	0.785559000
6	-0.145799000	-1.821420000	1.099933000
1	-0.549364000	-2.763968000	1.484305000
1	0.446473000	-2.040418000	0.211517000
1	0.533487000	-1.423691000	1.855017000
6	-2.785520000	-1.480103000	-0.500968000
6	-2.477593000	-0.402553000	2.435755000
1	-2.628728000	-1.365266000	2.932907000
1	-1.865739000	0.216321000	3.098703000
1	-3.455741000	0.075567000	2.346367000
6	-2.036270000	-1.755074000	-1.820496000
1	-1.680265000	-0.831172000	-2.283632000
1	-1.175864000	-2.414100000	-1.674657000
1	-2.705199000	-2.246536000	-2.538028000
6	-3.275103000	-2.825734000	0.085526000
1	-2.452974000	-3.517351000	0.288673000
1	-3.840070000	-2.689424000	1.012655000
1	-3.942771000	-3.319313000	-0.631207000
6	-4.026154000	-0.618436000	-0.817101000
1	-4.692540000	-1.168887000	-1.492945000
1	-4.606934000	-0.378029000	0.079058000
1	-3.762753000	0.317912000	-1.314477000
6	-0.763111000	3.666594000	-0.763271000
6	-1.997234000	3.191277000	-0.244364000
1	-0.714308000	4.691690000	-1.124146000

1	-2.866203000	3.836024000	-0.195798000
6	1.563752000	0.542724000	-0.175271000
6	2.318421000	0.537804000	1.023774000
6	2.095236000	-0.125219000	-1.295135000
6	3.523965000	-0.159022000	1.092981000
6	3.308174000	-0.819517000	-1.191419000
6	4.034027000	-0.859346000	-0.004651000
1	4.087873000	-0.146974000	2.022246000
1	3.698221000	-1.329852000	-2.068314000
6	1.845497000	1.304013000	2.241782000
1	1.653099000	2.354128000	2.002167000
1	0.911892000	0.899367000	2.646787000
1	2.591141000	1.271894000	3.039184000
6	5.335188000	-1.618616000	0.099884000
1	6.136601000	-0.983732000	0.489850000
1	5.241643000	-2.473607000	0.777859000
1	5.652197000	-1.999830000	-0.873254000
6	1.384363000	-0.124512000	-2.632625000
1	0.738231000	-1.001690000	-2.744343000
1	0.757575000	0.760533000	-2.760380000
1	2.103517000	-0.148725000	-3.455570000

Compound 4

52			
6	-1.465166000	2.026037000	0.798990000
6	-0.054467000	2.693479000	0.625990000
5	0.400420000	1.161810000	0.347887000
7	-0.918272000	0.656030000	0.503652000
1	-2.016884000	2.105696000	1.737050000
1	0.402260000	3.264640000	1.436150000
14	-1.735609000	-0.917500000	0.580206000
6	-0.456512000	-2.246309000	0.205192000
1	-0.889495000	-3.240115000	0.353093000
1	-0.085728000	-2.190667000	-0.821150000
1	0.408319000	-2.157408000	0.866811000
6	-3.198519000	-1.008440000	-0.669145000
6	-2.383335000	-1.139296000	2.341684000
1	-2.956634000	-2.065612000	2.444929000
1	-1.551035000	-1.187014000	3.050312000
1	-3.032243000	-0.314936000	2.650422000
6	-2.723898000	-0.592611000	-2.076754000
1	-2.342268000	0.431356000	-2.092011000
1	-1.931636000	-1.249075000	-2.450101000
1	-3.555604000	-0.650471000	-2.790629000
6	-3.726985000	-2.458942000	-0.729326000
1	-2.970267000	-3.157808000	-1.096841000
1	-4.068301000	-2.815745000	0.247645000
1	-4.583981000	-2.518201000	-1.412218000
6	-4.358122000	-0.087437000	-0.231881000
1	-5.177406000	-0.142315000	-0.960199000
1	-4.768321000	-0.380338000	0.738967000
1	-4.056340000	0.961098000	-0.164003000
6	-0.706569000	3.454266000	-0.515591000
6	-1.906227000	2.866095000	-0.393228000
1	-0.308546000	4.186694000	-1.209887000
1	-2.821995000	2.907251000	-0.970511000
6	1.779392000	0.459224000	0.091804000
6	2.266779000	0.274332000	-1.218871000
6	2.584822000	0.049358000	1.176070000
6	3.5127779000	-0.324230000	-1.421748000
6	3.824949000	-0.547553000	0.938318000
6	4.306946000	-0.749568000	-0.356087000
1	3.874416000	-0.455626000	-2.438067000
1	4.432821000	-0.855635000	1.784795000
6	2.124668000	0.260442000	2.602989000
1	2.863491000	-0.111893000	3.315631000
1	1.963480000	1.322032000	2.817863000
1	1.179147000	-0.252735000	2.805096000
6	5.636389000	-1.424330000	-0.595764000
1	6.090968000	-1.087913000	-1.530744000
1	6.339534000	-1.220732000	0.215697000
1	5.519793000	-2.511994000	-0.661570000
6	1.452944000	0.717085000	-2.416083000
1	0.548069000	0.112411000	-2.534108000
1	1.128842000	1.757590000	-2.320691000

1 2.030542000 0.631587000 -3.338972000

Compound 5

33			
6	-1.274684000	-1.696363000	0.176399000
6	-3.195540000	0.272819000	-0.407704000
5	-1.786798000	0.651398000	-0.026502000
7	-0.830400000	-0.388121000	0.278251000
1	-0.554177000	-2.471088000	0.400919000
1	-3.952717000	1.015717000	-0.635233000
14	0.933829000	-0.173949000	0.747866000
17	-1.319228000	2.398791000	0.027112000
6	1.177305000	1.315069000	1.869604000
1	2.116279000	1.184734000	2.417278000
1	1.220392000	2.261817000	1.332980000
1	0.372200000	1.388041000	2.605354000
6	2.005627000	-0.089379000	-0.843928000
6	1.404203000	-1.690024000	1.775650000
1	2.384088000	-1.512030000	2.228745000
1	0.693854000	-1.843734000	2.593493000
1	1.475696000	-2.622065000	1.211160000
6	1.624276000	1.119509000	-1.722224000
1	0.594008000	1.057834000	-2.080509000
1	1.732901000	2.068746000	-1.191420000
1	2.278148000	1.157352000	-2.602520000
6	3.486194000	0.048813000	-0.420590000
1	3.664986000	0.962963000	0.153387000
1	3.827640000	-0.800064000	0.179706000
1	4.125307000	0.094491000	-1.310759000
6	1.838456000	-1.379163000	-1.674910000
1	2.458371000	-1.324146000	-2.578261000
1	2.151131000	-2.271196000	-1.123658000
1	0.804512000	-1.525939000	-1.999885000
6	-3.518324000	-1.056230000	-0.470233000
6	-2.543898000	-2.049218000	-0.178192000
1	-4.520055000	-1.379202000	-0.742726000
1	-2.794189000	-3.101534000	-0.227564000

Compound 6

33			
6	-1.628560000	-1.324017000	0.725970000
6	-2.913361000	-0.539704000	0.259861000
5	-1.847043000	0.630941000	0.099061000
7	-0.734650000	-0.127161000	0.511085000
1	-1.567706000	-1.753532000	1.725863000
1	-3.773479000	-0.428393000	0.920619000
14	1.012870000	0.039130000	0.803757000
17	-1.946084000	2.340010000	-0.380886000
6	1.301192000	1.717310000	1.606333000
1	2.363532000	1.880732000	1.810397000
1	0.947773000	2.537189000	0.976949000
1	0.766019000	1.778181000	2.558444000
6	2.006186000	-0.120353000	-0.833715000
6	1.469288000	-1.338188000	2.009486000
1	2.526366000	-1.281475000	2.284414000
1	0.887969000	-1.249808000	2.932288000
1	1.289241000	-2.334768000	1.596652000
6	1.644013000	1.036118000	-1.788947000
1	0.579847000	1.043007000	-2.039899000
1	1.892561000	2.012821000	-1.364093000
1	2.202665000	0.936817000	-2.728237000
6	3.518835000	-0.061925000	-0.525671000
1	3.808885000	0.879947000	-0.049836000
1	3.838854000	-0.880935000	0.125658000
1	4.093929000	-0.143858000	-1.456434000
6	1.690319000	-1.459449000	-1.531448000
1	2.273519000	-1.547925000	-2.456674000
1	1.943625000	-2.321408000	-0.906043000
1	0.633711000	-1.534711000	-1.801606000
6	-2.969707000	-1.579823000	-0.851772000
6	-1.864038000	-2.235055000	-0.471060000
1	-3.656159000	-1.698509000	-1.682380000

1	-1.295140000	-3.055422000	-0.890746000
---	--------------	--------------	--------------

Compound 7

25			
6	0.877412000	1.814356000	1.538198000
14	0.564837000	0.769641000	-0.000074000
6	0.877300000	1.814271000	-1.538426000
7	-1.106624000	0.301995000	0.000004000
5	-2.321085000	0.002758000	0.000112000
17	-3.972937000	-0.410839000	0.000282000
6	1.641035000	-0.820941000	-0.000070000
6	1.334031000	-1.663228000	-1.255751000
6	3.137424000	-0.441847000	-0.000246000
6	1.334279000	-1.663048000	1.255794000
1	1.915302000	2.156768000	1.590759000
1	0.236684000	2.701084000	1.523687000
1	0.656364000	1.262024000	2.455210000
1	1.915137000	2.156844000	-1.590970000
1	0.656379000	1.261833000	-2.455405000
1	0.236429000	2.700898000	-1.524012000
1	3.414521000	0.139532000	-0.885038000
1	3.414694000	0.139689000	0.884390000
1	3.756714000	-1.347674000	-0.000224000
1	1.576617000	-1.126849000	2.178363000
1	0.280346000	-1.951448000	1.302707000
1	1.929943000	-2.584789000	1.248939000
1	1.929721000	-2.584953000	-1.248896000
1	0.280095000	-1.951658000	-1.302400000
1	1.576160000	-1.127151000	-2.178447000

Compound 8

88			
5	0.938321000	0.161832000	-0.009453000
7	-0.195531000	1.039284000	0.306022000
5	-0.967942000	-0.180563000	0.018679000
7	0.164509000	-1.058640000	-0.292504000
14	0.393266000	-2.729186000	-0.801655000
6	-1.301059000	-3.509435000	-1.087896000
1	-1.181886000	-4.521742000	-1.485104000
1	-1.895452000	-3.575784000	-0.173355000
1	-1.885305000	-2.939082000	-1.813208000
6	1.349283000	-3.772248000	0.511870000
6	1.345059000	-2.762266000	-2.433833000
1	1.521064000	-3.790681000	-2.764667000
1	0.775712000	-2.258395000	-3.220882000
1	2.315878000	-2.267033000	-2.354924000
6	0.735793000	-3.570856000	1.912201000
1	0.793728000	-2.529627000	2.238418000
1	-0.316266000	-3.871964000	1.944192000
1	1.270030000	-4.180825000	2.652299000
6	1.251432000	-5.270598000	0.145348000
1	0.221571000	-5.636853000	0.174704000
1	1.654489000	-5.480217000	-0.850704000
1	1.831152000	-5.868846000	0.859955000
6	2.841322000	-3.381594000	0.548628000
1	3.362409000	-3.955625000	1.326140000
1	3.340250000	-3.596258000	-0.400870000
1	2.991263000	-2.321725000	0.764229000
6	-2.515637000	-0.449085000	0.035233000
6	-3.171549000	-0.776788000	1.240478000
6	-3.277082000	-0.359332000	-1.148976000
6	-4.552863000	-0.984981000	1.246365000
6	-4.656789000	-0.572563000	-1.106575000
6	-5.315948000	-0.887670000	0.082265000
1	-5.045567000	-1.223007000	2.185426000
1	-5.232283000	-0.483068000	-2.024186000
6	-2.630284000	-0.062870000	-2.486043000
1	-3.294316000	0.525515000	-3.124069000
1	-1.694133000	0.489458000	-2.382983000
1	-2.401956000	-0.988961000	-3.025261000
6	-6.804964000	-1.136888000	0.104486000
1	-7.239060000	-0.872756000	1.071792000

1	-7.317924000	-0.558268000	-0.667513000
1	-7.028394000	-2.194182000	-0.076646000
6	-2.402578000	-0.949997000	2.532836000
1	-2.131848000	-1.999906000	2.687770000
1	-1.476613000	-0.371901000	2.541553000
1	-2.999078000	-0.637169000	3.393417000
6	2.484997000	0.438990000	-0.028260000
6	3.236962000	0.412691000	1.165512000
6	3.148566000	0.727933000	-1.240180000
6	4.611160000	0.660430000	1.128641000
6	4.524865000	0.966012000	-1.240550000
6	5.277389000	0.934186000	-0.065931000
1	5.175252000	0.639297000	2.057543000
1	5.020329000	1.188065000	-2.182135000
6	2.599923000	0.094767000	2.502439000
1	1.513102000	0.193371000	2.478216000
1	2.829288000	-0.929622000	2.814145000
1	2.977461000	0.759851000	3.284108000
6	2.394271000	0.840373000	-2.547957000
1	2.987539000	0.453114000	-3.380309000
1	1.451198000	0.291613000	-2.529422000
1	2.160341000	1.885850000	-2.774060000
6	6.769471000	1.163553000	-0.090848000
1	7.120372000	1.606470000	0.844377000
1	7.309066000	0.219884000	-0.228482000
1	7.057571000	1.826609000	-0.910142000
14	-0.459486000	2.701086000	0.830013000
6	-1.645742000	2.702881000	2.300685000
1	-2.586408000	2.195080000	2.074023000
1	-1.193419000	2.200546000	3.161068000
1	-1.884196000	3.725594000	2.609014000
6	1.190436000	3.424124000	1.391492000
1	1.633644000	2.819271000	2.186031000
1	1.922007000	3.487349000	0.582219000
1	1.043400000	4.431660000	1.791439000
6	-1.188428000	3.810961000	-0.572773000
6	-2.670314000	3.470394000	-0.831803000
6	-0.390449000	3.628824000	-1.878689000
1	0.668144000	3.875331000	-1.749468000
1	-0.449749000	2.603586000	-2.252585000
1	-0.785671000	4.289392000	-2.661367000
1	-2.818177000	2.422706000	-1.101851000
1	-3.059656000	4.082367000	-1.656043000
1	-3.291373000	3.673674000	0.045154000
6	-1.101447000	5.294652000	-0.148556000
1	-0.067682000	5.630256000	-0.029964000
1	-1.564912000	5.929941000	-0.914217000
1	-1.627372000	5.488583000	0.791751000

Compound 9

44			
5	0.379061000	0.140384000	-0.321139000
7	-0.869430000	0.212920000	-0.459401000
14	-2.579852000	0.327350000	-0.668141000
6	-3.033870000	2.144643000	-0.903849000
1	-4.111957000	2.282601000	-1.030352000
1	-2.711833000	2.751974000	-0.053802000
1	-2.541661000	2.539856000	-1.797613000
6	-3.447697000	-0.400240000	0.887905000
6	-3.063382000	-0.634500000	-2.219127000
1	-4.134807000	-0.558096000	-2.427475000
1	-2.527475000	-0.236896000	-3.086263000
1	-2.810048000	-1.694550000	-2.132699000
6	-3.052166000	0.412446000	2.138258000
1	-1.970446000	0.405067000	2.299355000
1	-3.374331000	1.455918000	2.067020000
1	-3.524106000	-0.013608000	3.033107000
6	-4.980496000	-0.342628000	0.715694000
1	-5.341378000	0.682052000	0.582454000
1	-5.321075000	-0.932592000	-0.140821000
1	-5.477418000	-0.747677000	1.606608000
6	-3.019359000	-1.867916000	1.090970000
1	-3.496429000	-2.282389000	1.988537000
1	-3.309645000	-2.501076000	0.246805000
1	-1.937135000	-1.956687000	1.219638000

6	1.887731000	0.053601000	-0.146990000
6	2.545445000	-1.194213000	-0.246148000
6	2.640368000	1.222367000	0.112650000
6	3.928980000	-1.249902000	-0.081694000
6	4.022020000	1.122069000	0.270379000
6	4.684754000	-0.104647000	0.180686000
1	4.430932000	-2.209482000	-0.162041000
1	4.596795000	2.022388000	0.466088000
6	1.768684000	-2.458677000	-0.529925000
1	1.225095000	-2.388298000	-1.476805000
1	2.432204000	-3.323536000	-0.585990000
1	1.026903000	-2.653809000	0.250481000
6	6.176297000	-0.193936000	0.389222000
1	6.411822000	-0.342695000	1.448917000
1	6.606877000	-1.032855000	-0.162175000
1	6.679726000	0.720976000	0.068374000
6	1.965237000	2.570176000	0.214331000
1	2.689310000	3.357852000	0.430316000
1	1.452696000	2.829577000	-0.716995000
1	1.210736000	2.578878000	1.006633000

TS min→1

12			
6	-0.836755000	1.158321000	0.120414000
5	0.610946000	1.224454000	-0.029277000
7	1.458061000	-0.117983000	-0.442412000
6	0.721161000	-0.814130000	0.401608000
6	-0.649185000	-1.191912000	-0.033265000
6	-1.471686000	-0.127040000	-0.108068000
1	1.122203000	-1.148349000	1.365263000
1	-1.442980000	2.028743000	0.346495000
1	-2.509933000	-0.218996000	-0.416016000
1	-0.828067000	-2.189193000	-0.419043000
1	1.391530000	2.083041000	0.227757000
1	2.424882000	-0.003079000	-0.145312000

min

12			
6	-0.782331000	1.147465000	0.042457000
5	0.703153000	1.085165000	-0.043918000
7	1.466884000	-0.245618000	-0.495423000
6	0.638350000	-0.664845000	0.499060000
6	-0.674763000	-1.149944000	0.013335000
6	-1.506340000	-0.092329000	-0.123675000
1	0.923673000	-0.713323000	1.550681000
1	-1.311690000	2.063275000	0.298374000
1	-2.540601000	-0.145907000	-0.450940000
1	-0.793599000	-2.140976000	-0.409708000
1	1.449077000	1.936362000	0.322684000
1	2.439688000	-0.148011000	-0.210600000

TS 2→min

12			
6	-0.384772000	1.151787000	0.122576000
5	1.071644000	0.876803000	-0.211082000
7	1.352462000	-0.563763000	-0.443740000
6	0.339331000	-0.613362000	0.560718000
6	-1.004711000	-0.970961000	0.010987000
6	-1.496470000	0.247240000	-0.233235000
1	0.592206000	-0.743105000	1.610826000
1	-0.583500000	2.031637000	0.736628000
1	-2.446904000	0.546013000	-0.661497000
1	-1.326791000	-1.963614000	-0.279597000
1	1.936363000	1.626219000	0.124203000
1	2.282904000	-0.823052000	-0.135253000

TS 4→3

52			
6	0.405877000	3.025325000	-0.424572000
5	0.387288000	1.566194000	-0.263544000
7	-1.050289000	0.785011000	-0.107480000
6	-1.471999000	1.766045000	0.676730000
6	-1.888462000	3.063990000	0.067584000
6	-0.850208000	3.739491000	-0.458955000
1	-1.617394000	1.602321000	1.753730000
1	1.340367000	3.564181000	-0.549657000
1	-0.968858000	4.694909000	-0.963538000
1	-2.944627000	3.248805000	-0.100895000
14	-1.401927000	-0.961981000	0.209543000
6	-0.439753000	-2.050548000	-0.974424000
1	0.626358000	-2.051189000	-0.745645000
1	-0.802459000	-3.079727000	-0.890293000
1	-0.563561000	-1.737844000	-2.013392000
6	-1.005538000	-1.424622000	1.994381000
1	-1.350220000	-2.442059000	2.203024000
1	0.073508000	-1.403691000	2.163380000
1	-1.477773000	-0.766294000	2.728553000
6	-3.292971000	-1.130610000	-0.129583000
6	-3.607971000	-0.758389000	-1.593895000
1	-4.683965000	-0.858087000	-1.784181000
1	-3.321802000	0.271266000	-1.822874000
1	-3.091106000	-1.414169000	-2.300459000
6	-3.712513000	-2.599049000	0.114163000
1	-3.178382000	-3.296298000	-0.537422000
1	-3.548519000	-2.911344000	1.149767000
1	-4.782709000	-2.718616000	-0.093940000
6	-4.121363000	-0.229668000	0.807564000
1	-5.192110000	-0.385326000	0.625992000
1	-3.937900000	-0.447159000	1.864300000
1	-3.929296000	0.834311000	0.639583000
6	1.656573000	0.630873000	-0.118965000
6	2.306436000	0.418711000	1.120121000
6	2.227683000	0.069038000	-1.280632000
6	3.452800000	-0.376835000	1.178458000
6	3.381452000	-0.717110000	-1.185949000
6	4.002540000	-0.964964000	0.036420000
1	3.938439000	-0.531060000	2.138410000
1	3.804439000	-1.142632000	-2.092121000
6	1.819605000	1.085775000	2.387949000
1	0.776961000	0.844369000	2.611731000
1	2.422662000	0.781294000	3.246385000
1	1.874875000	2.174319000	2.299440000
6	5.226182000	-1.844592000	0.131381000
1	5.977137000	-1.412106000	0.798418000
1	4.971802000	-2.833587000	0.528304000
1	5.687864000	-1.991350000	-0.847565000
6	1.648998000	0.342864000	-2.652672000
1	1.888019000	-0.464103000	-3.350209000
1	0.565199000	0.468550000	-2.627471000
1	2.061408000	1.269641000	-3.065500000

TS 6→5

33			
6	-3.191285000	0.237642000	-0.613940000
5	-1.841654000	0.633992000	-0.196464000
7	-0.729055000	-0.420609000	0.167283000
6	-1.639057000	-1.201426000	0.746228000
6	-2.577687000	-1.974607000	-0.124794000
6	-3.435163000	-1.176626000	-0.788348000
1	-1.620398000	-1.376274000	1.829768000
1	-3.969336000	0.966369000	-0.812197000
1	-4.174303000	-1.560605000	-1.486084000
1	-2.330794000	-3.007580000	-0.354676000
17	-1.369071000	2.340242000	0.163020000
14	0.993486000	-0.232998000	0.723669000
6	1.265691000	1.170531000	1.944984000
1	0.478767000	1.190459000	2.703780000
1	2.220459000	1.017892000	2.458898000
1	1.284007000	2.149234000	1.465535000
6	1.339702000	-1.864145000	1.609052000
1	2.398693000	-1.930455000	1.875036000

1	0.774544000	-1.939145000	2.543577000
1	1.098125000	-2.736811000	0.996722000
6	2.058320000	-0.059293000	-0.858561000
6	1.638564000	1.173691000	-1.685697000
1	2.290403000	1.265485000	-2.563269000
1	0.610634000	1.094274000	-2.046699000
1	1.720576000	2.104199000	-1.117721000
6	3.536589000	0.100593000	-0.435831000
1	3.698878000	1.003322000	0.160429000
1	3.900431000	-0.756075000	0.140372000
1	4.170289000	0.182093000	-1.327146000
6	1.915312000	-1.321739000	-1.734754000
1	2.516707000	-1.213204000	-2.645490000
1	2.264639000	-2.222485000	-1.220953000
1	0.878810000	-1.486259000	-2.041277000

8. Catalyzed Cycloreversion Reactions

General procedure for catalyst screening:

A 0.064 M CD_2Cl_2 stock solution of substrate (**4**) and internal standard (1,3,5-trimethoxybenzene) was prepared by dissolving 0.10 g **4** and 0.054 g 1,3,5-trimethoxybenzene in a 5.0 mL volumetric flask. Another stock solution consisting of 0.010 g of catalyst in 1.0 mL CD_2Cl_2 was prepared separately. A volume of catalyst solution corresponding to 3 mol % catalyst loading was added via microliter syringe to 0.50 mL (0.032 mmol **4**) of the substrate/internal standard solution. (For dimeric catalyst precursors, a volume corresponding to 1.5 mol % precursor was added.) After allowing the reaction mixture to stir at room temperature for 3 h, the conversion was determined by ^1H NMR (Table S11).

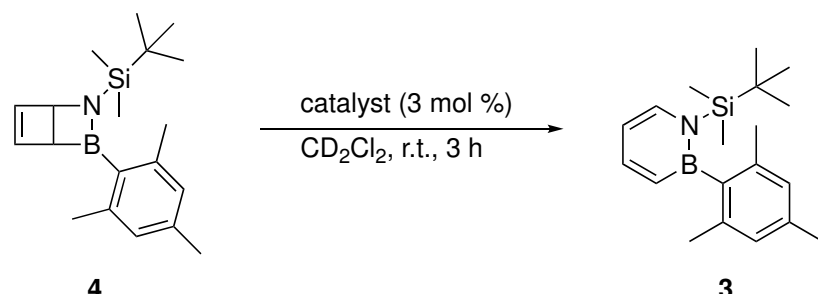


Table S11. Survey of catalysts for the cycloreversion reaction.

entry	catalyst	conversion (%) ^a
1	$(\text{Cy}_3\text{P})_2(\text{PhCH})\text{RuCl}_2$	15%
2	$[\text{Ir}(\text{cod})\text{Cl}]_2$	12%
3	$\text{Ni}(\text{CO})_2(\text{PPh}_3)_2$	0%
4	$\text{Sc}(\text{OTf})_3$	0%
5	AgOTf	2%
6	IPrAuCl	0%
7	$\text{Pt}(\text{PPh}_3)_4$	5%
8	$\text{Pd}(\text{PPh}_3)_4$	0%
9	$\text{RhCl}(\text{PPh}_3)_3$	100% ^b
10	$[\text{Rh}(\text{C}_2\text{H}_4)_2\text{Cl}]_2$	100% ^b
11	$[\text{Rh}(\text{cod})(\text{PPh}_3)_2]\text{PF}_6$	2%
12	$(\text{nbd})_2\text{RhBF}_4$	0%
13	$[\text{Rh}(\text{nbd})\text{Cl}]_2$	2%
14	$\text{Rh}(\text{nbd})(\text{PPh}_3)\text{Cl}$ Polymer	1%
15	$[\text{Rh}(\text{Cp}^*)\text{Cl}_2]_2$	0%

^a determined by ^1H NMR integration based on 1,3,5-trimethoxybenzene as internal standard.

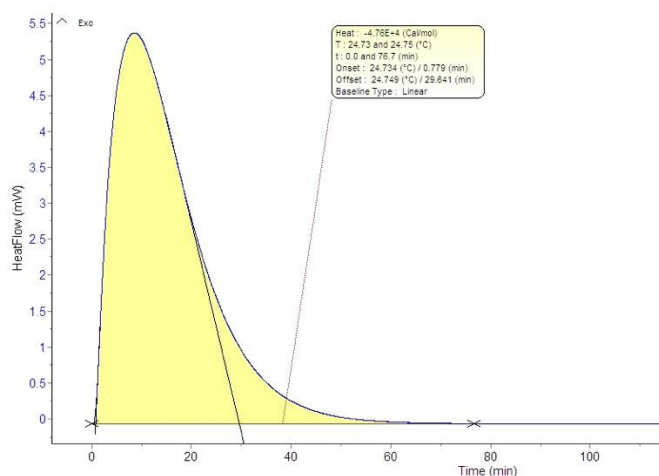
^b Full conversion to **3** was observed within 1 h.

Calorimetric Experiment :

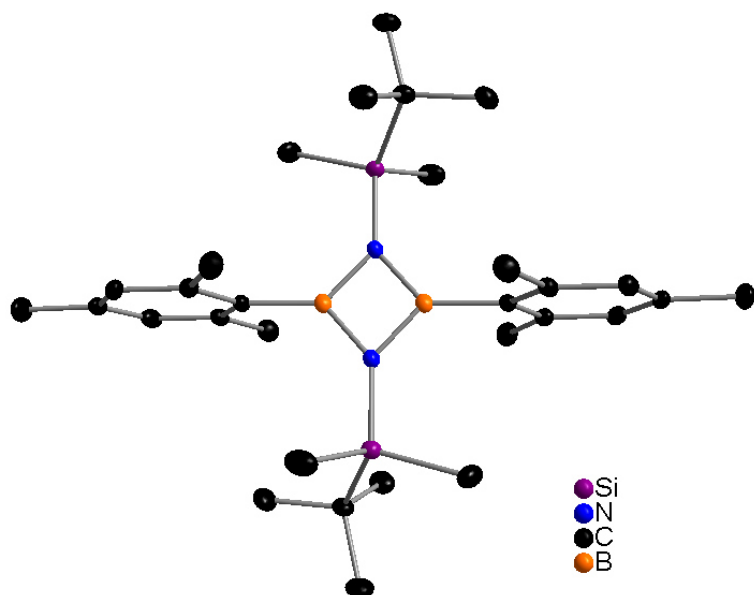
A 0.064 M CD_2Cl_2 stock solution of substrate (**4**) was prepared by dissolving 0.10 g **4** in a 5.0 mL volumetric flask. Another 0.011 M CD_2Cl_2 stock solution of Wilkinson's catalyst was also prepared by dissolving 0.020 g $\text{RhCl}(\text{PPh}_3)_3$ in a 2.0 mL volumetric flask. In a glovebox, 0.50 mL of substrate solution (0.032 mmol **4**) were added to the bottom of a Setaram-C80 calorimeter Hastelloy sample cell; the bottom half of the cell was sealed with a puncturable aluminum foil before 89 μL of catalyst solution (3 mol% catalyst) and an additional 0.30 mL CD_2Cl_2 solvent were added on top of the foil via microliter syringe. An empty reference cell was likewise prepared under N_2 . Both cells were loaded into the Setaram-C80 calorimeter and were allowed to equilibrate at 25 °C until zero heat flow was achieved (which took approximately 3 hours). Data collection was initiated just prior to puncturing the aluminum foil and was continued until the observed heat flow had returned to zero, indicating completion of the reaction. (Complete conversion of starting material **4** to 1,2-azaborinine **3** was subsequently confirmed by ^{11}B NMR and ^1H NMR). The measured heat flow trace was integrated using the Setaram software SetSoft 2000 to determine the $\Delta\text{H}_{\text{rxn}}$ of the retro-isomerization (cycloreversion) reaction. The calorimetric measurements were repeated five times and the corresponding average value of $\Delta\text{H}_{\text{rxn}}$ with standard deviation is reported.

Trial	H kcal/mol
1	-48.4
2	-48.8
3	-47.0
4	-47.6
5	-46.1

The average value of ΔH is -47.6 kcal/mol, with a standard deviation of ± 0.968 kcal/mol. A representative heat-flow trace is shown below.



9. Summary of crystallographic data for compound 8



Empirical formula	C ₃₀ H ₅₂ B ₂ N ₂ Si ₂	
Formula weight	518.53	
Temperature	100(2) K	
Wavelength	0.71073 Å	
Crystal system	Monoclinic	
Space group	P 21/c	
Unit cell dimensions	a = 10.7079(8) Å	α = 90°.
	b = 15.5938(11) Å	β = 102.6590(10)°.
	c = 9.9606(7) Å	γ = 90°.
Volume	1622.8(2) Å ³	
Z	2	
Density (calculated)	1.061 Mg/m ³	
Absorption coefficient	0.129 mm ⁻¹	
Crystal size	0.433 x 0.292 x 0.138 mm ³	
collected	36853	
Independent reflections	3569 [R(int) = 0.0294]	
Absorption correction	Numerical	
Max. and min. transmission	0.7457 and 0.7076	
Refinement method	Full-matrix least-squares on F ²	
Data / restraints / parameters	3569 / 0 / 171	
Goodness-of-fit on F ²	1.036	
Final R indices [I>2sigma(I)]	R1 = 0.0337, wR2 = 0.0925	
R indices (all data)	R1 = 0.0370, wR2 = 0.0958	

10. References

- [1] a) A. J. V. Marwitz, M. H. Matus, L. N. Zakharov, D. A. Dixon, S.-Y. Liu, *Angew. Chem. Int. Ed.* **2009**, *48*, 973; b) A. W. Baggett, M. Vasiliu, B. Li, D. A. Dixon, S.-Y. Liu, *J. Am. Chem. Soc.* **2015**, *137*, 5536.
- [2] G. R. Fulmer, A. J. M. Miller, N. H. Sherden, H. E. Gottlieb, A. Nudelman, B. M. Stoltz, J. E. Bercaw, K. I. Goldberg, *Organometallics* **2010**, *29*, 2176.
- [3] C. G. Hatchard, C. A. Parker, *Proc. R. Soc. A* **1956**, *235*, 518.
- [4] a) H. J. Kuhn, S. E. Braslavsky, R. Schmidt, *Pure Appl. Chem.*, **2004**, *76*, 2105; b) Marco Montalti, Alberto Credi, Luca Prodi, M. T. Gandolfi, *Handbook of Photochemistry*, CRC Press, Boca Raton, **2006**.
- [5] I. R. Dunkin, *Matrix-Isolation Techniques*, Oxford University Press, Oxford, **1998**.
- [6] K. Wolinski, J. F. Hinton, P. Pulay, *J. Am. Chem. Soc.* **1990**, *112*, 8251.
- [7] a) T. Helgaker, M. Watson, N. C. Handy, *J. Chem. Phys.* **2000**, *113*, 9402; b) V. Sychrovský, J. Gräfenstein, D. Cremer, *J. Chem. Phys.* **2000**, *113*, 3530.
- [8] A. D. Becke, *J. Chem. Phys.* **1993**, *98*, 5648.
- [9] C. Lee, W. Yang, R. G. Parr, *Phys. Rev. B* **1988**, *37*, 785.
- [10] P. J. Stephens, F. J. Devlin, C. F. Chabalowski, M. J. Frisch, *J. Phys. Chem.* **1994**, *98*, 11623.
- [11] M. J. Frisch, G. W. Trucks, H. B. Schlegel, G. E. Scuseria, M. A. Robb, J. R. Cheeseman, G. Scalmani, V. Barone, B. Mennucci, G. A. Petersson, H. Nakatsuji, M. Caricato, X. Li, H. P. Hratchian, A. F. Izmaylov, J. Bloino, G. Zheng, J. L. Sonnenberg, M. Hada, M. Ehara, K. Toyota, R. Fukuda, J. Hasegawa, M. Ishida, T. Nakajima, Y. Honda, O. Kitao, H. Nakai, T. Vreven, J. A. Montgomery, Jr., J. E. Peralta, F. Ogliaro, M. Bearpark, J. J. Heyd, E. Brothers, K. N. Kudin, V. N. Staroverov, R. Kobayashi, J. Normand, K. Raghavachari, A. Rendell, J. C. Burant, S. S. Iyengar, J. Tomasi, M. Cossi, N. Rega, M. J. Millam, M. Klene, J. E. Knox, J. B. Cross, V. Bakken, C. Adamo, J. Jaramillo, R. Gomperts, R. E. Stratmann, O. Yazyev, A. J. Austin, R. Cammi, C. Pomelli, J. W. Ochterski, R. L. Martin, K. Morokuma, V. G. Zakrzewski, G. A. Voth, P. Salvador, J. J. Dannenberg, S. Dapprich, A. D. Daniels, Ö. Farkas, J. B. Foresman, J. V. Ortiz, J. Cioslowski, D. J. Fox, Gaussian 09, Revision D.01, Gaussian Inc., Wallingford CT, **2009**.
- [12] R. Krishnan, J. S. Binkley, R. Seeger, J. A. Pople, *J. Chem. Phys.* **1980**, *72*, 650.
- [13] COSMO v. 1.61, Bruker AXS Inc., Madison, WI, 2012.
- [14] APEX 3 V. 2016.5-0, Bruker AXS Inc., Madison, WI, 2016.
- [15] SAINT v. 8.37A, Bruker AXS Inc., Madison, WI, 2015.
- [16] SADABS Krause, L., Herbst-Irmer, R., Sheldrick, G. M. & Stalke, D. (2015). *J. Appl. Cryst.* **48**.
- [17] SHELXTL *Acta Cryst.* **2015**, *A71*, 3-8, Shelxl *Acta Cryst.* **2015**, *C71*, 3-8.
- [18] SHELXLE, C. B. Hubschle, G. M. Sheldrick, B. Dittrich, *J. Appl. Crystallogr.* **2011**, *44*, 1281-1284.
- [19] S. A. Brough, A. N. Lamm, S.-Y. Liu, H. F. Bettinger, *Angew. Chem. Int. Ed.* **2012**, *51*, 10880.
- [20] H. F. Bettinger, O. Hauler, *Beilstein J. Org. Chem.* **2013**, *9*, 761.